# Investigating Chondroitin Sulphate Proteoglycans as a Therapeutic Target for Parkinson's disease

Fletcher, Edward Joseph Richard

*Awarding institution:*
King's College London

# Investigating Chondroitin Sulphate Proteoglycans as a Therapeutic Target for Parkinson's disease

---

Submitted for the degree of
Doctor of Philosophy

**Edward Joseph Richard Fletcher**

Wolfson Centre for Age-Related Diseases, Guy's Campus,
King's College London, SE1 1UL

# i. Abstract

Parkinson's disease (PD) is characterised by the dopaminergic cell loss within the substantia nigra pars compacta of the basal ganglia. This pathology reduces the concentration of dopamine within the striatum and results in the cardinal motor dysfunctions we associate with the disease. Currently, therapeutic treatments such as L-DOPA merely act as symptomatic relief and do not slow disease progression; new PD therapeutics targeting neurorepair and protection are therefore in demand.

In PD, remaining dopaminergic neurons possess limited capabilities for axonal regrowth and rewiring for reasons unknown. In this thesis, we suggest that the chondroitin sulphate proteoglycans (CSPGs) of the extracellular matrix may play a role in the inhibition of cellular recovery and in the aberrant plasticity associated with L-DOPA-induced dyskinesia. Previous studies have identified that the digestion of the CSPGs via the enzyme chondroitinase ABC (ChABC) permits axonal regeneration following brain injury. Here, for the first time, we investigate the efficacy of ChABC as a therapeutic strategy to aid cellular recovery in PD.

The results presented in this thesis support the ChABC-mediated digestion of CSPGs within the nigrostriatal tract as a strategy of increasing cell survival within the 6-hydroxydopamine lesioned mouse. It was discovered that ChABC treatment enhanced dopaminergic cell survival in lesioned mice; no behavioural improvements were detected however. In a subsequent study, we aimed to further increase ChABC-mediated cell survival and induce behavioural improvements by increasing the striatal levels of glial cell line-derived neurotrophic factor and brain-derived neurotrophic factor by the administration of the MAO-B inhibitor selegiline. Although ChABC alone reproduced a similar degree of cell survival as before, the addition of selegiline did not improve cell survival or behavioural outcomes despite increasing neurotrophic factor levels during the first two weeks of experimentation. Moreover, selegiline decreased the efficacy of ChABC; perhaps a potential conflict between their pathways.

Additionally, we investigated whether CSPGs and other cellular markers were upregulated in the striatum of L-DOPA-induced dyskinetic rats; a region identified to increase in volume within the dyskinetic state. Although CSPG expression did not increase, Iba1-positive microglial expression did. This suggests a role for microglia in L-DOPA-induced dyskinesia manifestation.

In conclusion, investigating the CSPGs as therapeutic targets is promising. However, identifying ways to enhance cell survival effects to induce detectable behavioural improvements is required. In order to do so, further investigations into the mechanism underlying the CSPG's inhibitory nature would be a logical next step.

## ii. Acknowledgments

I would like to thank my two supervisors Dr Susan Duty and Dr Lawrence Moon for making the completion of thesis possible. Without your guidance and expertise, I certainly would have not become the scientist I am today. I have come a long way since I first arrived to the Wolfson - conducting power calculations and keeping *all* tissue for experimentation has been learnt the hard way!

One of the biggest pleasures throughout these four years has been the Wolfson family itself. Since day one, I have loved the group of wonderful people here at the centre. Coming to work rarely felt a chore... yes, even those long surgery days! So thank you to everyone. As I may be writing another thesis just of my thanks, I would like to single out a few people. Clare - you have been my lab role model and I will never forget all the help you gave me whilst setting up. Jurassic Park! Lizzie – I knew you were the right person for the job when I first met you, your dedication and selflessness has always impressed me. You are a cracking scientist. Martin – your *inspiring positivity* has been greatly appreciated along the way! Em and Ariana – always there for support and have been the best tea/wine/Jager drinking friends I could ever ask for. Book, Mai, Dave, Talisia, Nisha (i.e. Wolfson Mum) and the rest of the Bevan/Andersson lab – thank you for your continuing support over the years.

In addition, I would like to thank Dr Anthony Vernon and his laboratory members responsible for the MRI collaboration. The wealth of knowledge you have provided to the project has been monumental.

To my housemates Merrick and Jorge, thank you both for putting up with the constant moaning over the past few months. As you are both about to enter thesis territory, I am more than willing to reflect back the emotional and drinking support! Do not forget - *everything is awesome*! I will miss you guys.

I would like to thank my parents Ann and Richard Fletcher for their continued support throughout my PhD. I know times have been tough in places but knowing you were both there for me really got me through! Finally, I would like to thank Skye. I cannot explain how much you have helped me through this tough and exhausting time. I gave this thesis the title of *Second Girlfriend*, and it certainly lived up to that name. I cannot wait to start having adventures once again. I love you.

To conclude, I would like to say *Hello to Jason Isaacs* and simply – biscuit.

## iii. Abbreviations

| | |
|---|---|
| 5-HT | 5-hydroxytryptamine; serotonin |
| 6-OHDA | 6-hydroxydopamine |
| ACh | Acetyl choline |
| AIMs | Abnormal involuntary movements |
| AP | Anteroposterior |
| α-Syn | Alpha synuclein |
| ATP | Adenosine triphosphate |
| BBB | Blood-brain barrier |
| BDNF | Brain-derived neurotrophic factor |
| BG | Basal ganglia |
| BSA | Bovine serum albumin |
| bWFA | Biotinylated Wisteria floribunda agglutinin |
| C4S | Chondroitin-4-sulphate |
| $Ca^{2+}$ | Calcium |
| cAMP | Cyclic adenosine monophosphate |
| CB | Calbindin |
| CDNF | Cerebral DA neurotrophic factor |
| ChABC | Chondroitinase ABC |
| CNS | Central nervous system |
| COMT | Catechol-O-methyltransferase |
| CS-GAG | Chondroitin sulphate glycosaminoglycans |
| CSPG | Chondroitin sulphate proteoglycans |
| DA | Dopamine |
| DAB | Diaminobenzidine tetrachloride |
| DBS | Deep-brain stimulation |
| DDC | Dopadecarboxylase |
| DJ-1 | Daisuke Junko 1 |
| DL | Dorsolateral |
| DM | Dorsomedial |
| DNSP-11 | DA neuron stimulating peptide 11 |
| DV | Dorsoventral |
| ECM | Extracellular matrix |
| ETC | Electron transport chain |
| Fe | Iron |

| | |
|---|---|
| GABA | γ-aminobutyric acid |
| GalNAc | N-acetyl galactosamine |
| GDNF | Glial-cell derived neurotrophic factor |
| GFLs | GDNF family of ligands |
| GFRα1 | GDNF-family receptor alpha 1 |
| GlcA | Glucaronic acid |
| GP | Globus pallidus |
| GPCRs | G-protein-coupled receptors |
| $H_2O_2$ | Hydrogen peroxide |
| i.p. | Intraperitoneal; administration route |
| LBs | Lewy bodies |
| L-DOPA | Levodopa; L-3,4-dihydroxyphenylalanine |
| LIDs | L-DOPA-induced dyskinesias |
| LRRK2 | Leucine-rich repeat kinase 2 |
| MANF | Mesencephalic astrocyte-derived neurotrophic factor |
| MAO-A/B | Monoamine oxidase-A/B |
| MFB | Medium forebrain bundle |
| ML | Mediolateral |
| Mn | Manganese |
| MPTP | 1-methyl-4-phenyl-1,2,3,6-tetrahydropyridine |
| MRI | Magnetic resonance imaging |
| NGS | Normal goat serum |
| NHP | Non-human primate |
| NMDA | N-methyl-D-aspartate |
| NMS | Non-motor symptoms |
| NOS | Nitric oxide synthase |
| NS | Nigrostriatal tract |
| NT | Neurotransmitter |
| $ONOO^-$ | Peroxynitrite |
| PBS | Phosphate buffered saline |
| PD | Parkinson's disease |
| PINK-1 | PTEN-induced putative kinase 1 |
| PNN | Perineuronal net |
| p.o. | per os; administration route |
| RBD | Rapid-eye movement sleep behaviour disorder |
| ROS | Reactive oxygen species |

| | |
|---|---|
| s.c. | Subcutaneous; administration route |
| SNc | Substantia nigra pars compacta |
| SNr | Substantia nigra pars reticulata |
| SOD | Superoxide dismutase |
| STN | Subthalamic nucleus |
| TBM | Tensor based morphology |
| TBS | Tris buffered saline |
| TH | Tyrosine hydroxylase |
| TSPO | 18 kDa translocator protein |
| UCH-L1 | Ubiquitin carboxy-terminal hydrolase L1 |
| VL | Ventrolateral |
| VM | Ventromedial |
| VTA | Ventral tegmental area |

# iv. Table of figures

# v. List of tables

# vi. Table of contents

# 1. General introduction

## 1.1. Parkinson's disease; the 'Shaking Palsy'

In 1817 James Parkinson published the first medical description of *paralysis agitans* within the monograph *An Essay on the Shaking Palsy* (Davie, 2008; Parkinson 2002). The condition was shown to affect the motor control of six patients in which key dysfunctions characterised the disease: bradykinesia, rigidity of the patient's trunk and a resting tremor. Works by Jean-Martin Charcot in the mid-1800s further promoted the understanding of the disease whom thereafter adopted the more common name of Parkinson's disease (PD) (Lees, 2007).

Since the work of Charcot and Parkinson of the 1800s, great advancements in PD research have paved the way for modern understandings and interventions. Despite these advancements, we are still unaware of the disease's cause or cure.

## 1.2. Prevalence of Parkinson's disease and its subtypes

PD is the second most prevalent neurodegenerative disease that affects ~2% of Europeans aged 65 to 89 (de Lau *et al.*, 2006; de Rijk *et al.*, 2000). Of these affected people, men are ~2 times more susceptible than women (Van Den Eeden *et al.*, 2003; Wirdefeldt *et al.*, 2011). The incidence is relatively low in the <50 year old demographic but rises sharply to those in the age range mentioned above, a significant concern for an ageing population (Dorsey *et al.*, 2007). PD can be broken down into two primary subtypes, idiopathic and familial. Idiopathic PD is associated with 90% of all cases (Dauer *et al.*, 2003) and arises sporadically without a known cause, whereas familial, otherwise known as hereditary PD, is associated with a much lower incidence of ~10% and has a collection of mutations associated with its prevalence.

## 1.3. Parkinson's disease pathology

The cardinal motor symptoms associated with PD are a result of cell death within the substantia nigra pars compacta (SNc); a significant component of the basal ganglia (BG). This nucleus projects to the caudate and putamen nuclei of the striatum via the nigrostriatal tract (NS) where it provides a key source of dopamine (DA) which is required for fine motor movement. A loss of this dopaminergic input leads to a severe imbalance of the two DA driven striatal pathways within the BG, the direct and indirect pathways (see 1.9.3. for further information).

Alongside the SNc cell loss, neuronal cytosolic inclusion bodies known as Lewy bodies (LBs) (Lewy, 1912) begin to accumulate within affected regions and spread in a prion-like manner according to Braak staging (Braak *et al.*, 2003; Masuda-Suzukake *et al.*, 2013). This LB-spread correlates with PD symptoms. Despite a close relationship with the disease, the role LBs have within PD has not yet been elucidated. LBs may be neurotoxic or merely a product of cellular degeneration (Goldberg *et al.*, 2000). The main constituents of LBs are ubiquitin, neurofilament protein and most prodominantly α-synuclein (α-syn) fibrils; the latter of which is most attributed to LB-related toxicity. α-syn is a 140 residue protein encoded by the SNCA gene and is abundant within the brain where it is primarily localised to the neuronal presynaptic terminals. Due to its location and interaction with membrane proteins and phospholipids (Chandra *et al.*, 2003), it is thought to have a role in neurotransmitter (NT) release (Emanuele *et al.*, 2015) and the clustering of NT vesicles at the nerve terminal (Diao *et al.*, 2013). Although α-syn and LBs are key research areas in PD research, this thesis will not tackle their role within the disease, see (Vekrellis *et al.*, 2011) for a more comprehensive review.

## 1.4. Symptomatology

The cardinal motor symptoms associated with PD, such as bradykinesia, trunk rigidity and tremor, manifest following a significant loss of SNc cells (~70%). As motor dysfunction occurs only once this threshold of cell loss is reached, PD is therefore described as a *threshold disease*. However, this is somewhat misleading as these symptoms only represent a proportion of dysfunction experienced. During the years leading to this threshold loss, known as the *prodromal phase*, a wealth of non-motor symptoms (NMS) manifest that lower quality of life.

Researchers argue that further classification of the aforementioned motor symptoms is possible but requires further characterisation. The motor features observed through clinical observations indicate two motor subtypes, tremor-dominant and non-tremor dominant. The former is associated with a slower onset and milder functional disability to that of the latter form, which presents a quick onset with a more severe functional disability (DATATOP, 1989). Although the aetiology of the two motor symptoms subtypes is unknown, further investigation may lead to better therapies more suited to the specific type of motor disturbance.

The NMS are commonly experienced well before the date of diagnosis and prolong throughout life. These range from constipation, hyposmia and sleep disorders to fatigue, mood alterations, pain and psychosis (figure 1). These symptoms manifest before motor onset and during the prodromal phase, a time in which severe SNc cell loss has not yet occurred (<70%). Therefore, these factors could be potential biomarkers in diagnosing PD well before the manifestation of motor dysfunction. The use of NMS as prodromal biomarkers for introducing neuroprotective

agents is promising. For example, a study that analysed rapid-eye movement sleep behaviour disorder (RBD) in PD patients correlated its diagnosis with a window 12 to 14 years before motor dysfunction and PD diagnosis (Postuma *et al.*, 2012); could this NMS help with therapeutic intervention? Studies such as the multicentre ONSET PD Study screened several NMS in a cohort of newly diagnosed PD patients and age matched controls (Pont-Sunyer *et al.*, 2015). It was identified that when present within the prodromal phase, certain NMS (notably, hyposmia and constipation) could discriminate PD patients from controls. Although not yet consistently predictive, studies like the ONSET PD demonstrate promise in the investigation of NMS as PD biomarkers.

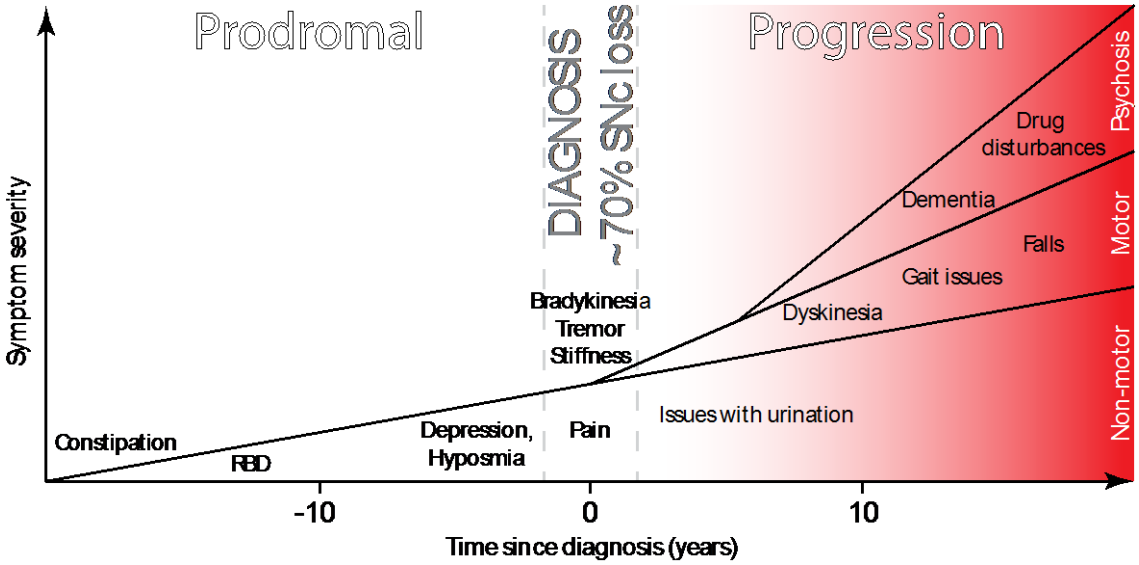


**Figure 1: Symptoms of PD during the course of disease progression.**
Within the prodromal phase (~20 years prior to diagnosis) numerous non-motor symptoms (NMS) such as constipation and depression may arise. At the time of diagnosis, typical motor dysfunctions (i.e. bradykinesia, tremor) arise and deteriorate throughout the disease. Complications involving repeated therapeutic drug use may lead to dyskinesia, psychosis and other disturbances in later stages of the disease. RBD, rapid-eye movement sleep behaviour disorder.

## 1.5. Aetiology

PD's aetiology is not fully understood but it is most likely a combination between several environmental and genetic factors. Most cases are considered idiopathic where a cause remains unclear. However, the familial form is caused at least in part by nonsense and missense mutations of certain genes. The known mutations are often described by their mistranslated proteins, these are stated below.

## 1.6. Genetic factors involved in PD

There are two key PD-associated autosomal dominant mutations, those of the PARK1 (SNCA) and PARK8 (LRRK2) genes.

### 1.6.1. α-synuclein

Gene/locus: *SNCA/PARK1*; 4q21

Function: Believed to assist neurotransmitter release, vesicle clustering and transmission

Three common mutations within the α-syn gene *SNCA* have been associated with the inherited form of PD, these are A53T, E46K and A30P (Kruger *et al.*, 1998; Spira *et al.*, 2001; Zarranz *et al.*, 2004). Each mutation causes a different manifestation of PD, A53T carriers present early onset and a response to anti-PD treatments in their forties whereas both the E46K and A30P mutations give rise to a later developing of the disease and associated dementia. Interestingly, multiplications of the wild type *SNCA* gene have shown to induce PD (Singleton *et al.*, 2003). Moreover, people with a triplication of the locus present earlier onset to those with a duplication of the *SNCA* gene, indicating a dosage effect of wild type α-syn (Cookson, 2010).

Evidence suggests that α-syn may act as a chaperone to the soluble NSF attachment protein receptor complexes required for vesicle-driven NT exocytosis (Bonini *et al.*, 2005). Therefore, it is likely that mutations or increased gene dosage of *SNCA* may alter synaptic transmission.

### 1.6.2. LRRK2 (Leucine-rich repeat kinase 2; a.k.a. Dardarin)

Gene/locus: *LRRK2/PARK8*; 12q12

Function: Signalling, kinase (many assumed functions)

The *LRRK2* gene encodes the lrrk2, or dardarin, protein that is a member of the leucine-rich repeat family. Lrrk2 is a large 286 kDa protein that has multiple domains and functions (e.g. kinase, scaffolding activity and signalling) and is located within the cytoplasm and outer mitochondrial membrane. *LRRK2* was the second gene associated with the autosomal dominant form of PD and has, potentially due to size, the highest mutation frequency of all PD associated genes. *LRRK2* mutations, namely the G2019S and R1628P, are the most common cause of familial PD (Kumari *et al.*, 2009). There are almost forty discovered variants of the gene with most of these being missense (Lesage *et al.*, 2009). However, the pathogenicity of a large proportion of these mutations is not known due to low penetrance and unidentified parental genotypes. But, the vast majority of the pathogenic forms we do know present mutations within highly conserved coding regions (Healy *et al.*, 2008).

In addition to the autosomal dominant mutations, there are also three autosomal recessive forms associated with familial PD. These are encoded by the *PARK2* (Parkin), *PARK7* (DJ-1) and *PARK6* (PINK1) genes.

### 1.6.3. Parkin

Gene/locus: *PARK2*; 6q25.2-q27

Function: E3 ligase that aids the ubiquitination of proteins targeted for the ubiquitin proteasome system

Parkin is a mitochondrially localised E3 ligase that targets dysfunctional proteins for ubiquitin proteasome system (UPS)-mediated degradation. Under stressed conditions, parkin is recruited by PTEN-induced putative kinase 1 (PINK-1) to the dysfunctional mitochondria whereby it initiates parkin-driven mitophagy via ubiquitin conjugation (Matsuda *et al.*, 2010). First discovered in Japanese patients exhibiting autosomal recessive juvenile parkinsonism (Kitada *et al.*, 1998), the mutated parkin was shown to cause dysfunctional mitochondrial mitophagy resulting in toxic effects (Rakovic *et al.*, 2011). People with these mutations were found to produce similar symptoms to sporadic forms of PD but with an earlier onset of the disease (childhood to 50 years old).

### 1.6.4. DJ-1 (Daisuke Junko-1)

Gene/locus: *PARK7*; 1p36.23

Function: Believed to protect against oxidative stress and act as a chaperone to nascent proteins

Mutations within the *PARK7* gene, which encodes the Daisuke Junko-1 (DJ-1) protein, leads to a rare autosomal recessive form of parkinsonism that exhibits early onset (~40 years old)(Bonifati *et al.*, 2003). The DJ-1 protein was discovered to be an oxidative stress sensor that protected dopaminergic cells against reactive oxygen species (ROS) toxicity (Lev *et al.*, 2013). Suggestions of DJ-1 being integral to the E3 ligase complex are still debated and its true pathogenic effects are unknown.

### 1.6.5. PINK-1 (PTEN-induced putative kinase 1)

Gene/locus: *PARK6*; 1p36

Function: Mitochondrial kinase able to protect against dysfunction

PINK-1 is involved in the quality control of the mitochondria. Being an active serine/threonine kinase, PINK-1 recruits and permits the binding of parkin to damaged mitochondria readying

the cell for mitophagy. Missense and nonsense mutations of this gene gives rise to autosomal recessive parkinsonism which, as with other autosomal recessive mutations, causes early onset parkinsonism (20 to 50 years old) (Valente *et al.*, 2004).

A close functional relationship seems apparent between the autosomal recessive mutations, Parkin, DJ-1 and PINK-1. It is therefore of no surprise that synergistic mutations between these three genes may enhance the pathogenic effects. Loss of DJ-1 function in particular may further exacerbate oxidative effects caused by poor mitochondrial quality control formed by ineffective PINK-1 protein function.

Other proteins of note are glucocerebrosidase and ubiquitin carboxy-terminal hydrolase L1 (UCH-L1). Mutations within these proteins' genes appear to not directly cause familial PD but rather enhance the risk of the disease dramatically (Aharon-Peretz *et al.*, 2004; Leroy *et al.*, 1998).

## 1.7. Environmental factors involved in Parkinson's disease

To explain the vast amount of idiopathic PD cases that, to our knowledge, are not familial, we must acknowledge the environmental factors that influence disease risk. These are commonly associated with the exposure to chemical compounds such as biocides and heavy metals.

Biocides (i.e. herbicides, fungicides and pesticides) have long been known to induce parkinsonism. Examples such as rotenone, paraquat and dichlorodiphenyltrichloroethane are inhibitors of complex I of the electron transport chain (ETC) and so disrupt the production of adenosine triphosphate (ATP) and induce oxidative stress (explained more fully in section 1.11.2.1.). These all mimic the action of the known toxin 1-methyl-4-phenyl-1,2,3,6-tetrahydropyridine (MPTP), a compound now used to induce parkinsonisms in preclinical models (see section 1.12.2.2.).

Several studies have correlated an increased risk of parkinsonism with people living rurally; people most likely to be who are exposed to biocides from well-water and crops (Ho *et al.*, 1989; Liou *et al.*, 1997; Morano *et al.*, 1994). However, a large meta analysis study has found inconsistencies identifying causal relationships between these factors and PD (Breckenridge *et al.*, 2016). Nevertheless, the use of biocides in the preclinical modelling of PD (e.g. rotenone, paraquat) have reinforced the belief that environmental toxins increase the risk of idiopathic PD (Di Monte, 2003).

Heavy metals such as manganese (Mn) and iron (Fe) have been well researched as PD risk factors (Fukushima *et al.*, 2010; Montgomery, 1995). Mn is present in low concentrations in tea, legumes and grains and is essential for a range of bodily functions (Erikson *et al.*, 2003). However, occupational exposure to Mn (e.g. mining, welding) has shown to be a significant risk factor for central nervous system (CNS) disorders, including PD (Gorell *et al.*, 1999). These disorders are collectively known as manganisms (Perl *et al.*, 2007). Manganese-induced parkinsonism differs from idiopathic PD in which the globus pallidus (GP) is the most affected region. This disorder is unresponsive to the DA replacement therapy L-3,4-dihydroxyphenylalanine (L-DOPA) (Pal *et al.*, 1999) and so is classified as parkinsonian-like rather than idiopathic PD.

Fe has long been known to have high concentrations within the brain of PD patients (Earle, 1968), particularly in the SNc (Dexter *et al.*, 1990; Dexter *et al.*, 1989b); indicating that Fe may have a role in disease progression. To further this theory, brains from PD patients have displayed reduced levels of ferritin, the intracellular protein responsible for Fe storage (Dexter *et al.*, 1990); an increase that is debated however (Farhoudi *et al.*, 2012). With increased levels

and the potentially dysfunctional homeostatic control of Fe within the BG, there may be an enhanced risk of Fe-driven toxicity in PD. Fe as a therapeutic target has led to the use of Fe chelators in models of disease with success. Desferrioxamine has been shown to increase SNc cell survival by 60% in PD toxin models (Ben-Shachar *et al.*, 1991) whereas the 8-hydroxyquinolines have been tested in the clinic (Ritchie *et al.*, 2003).

At high concentrations, Mn and Fe induce cellular toxicity through the creation of free radicals. Fe is thought to undergo the Fenton reaction when in the presence of $H_2O_2$ and ferritin to create the hazardous hydroxyl free radical (Levin *et al.*, 2011). Where on the other hand, Mn accumulates within the glia and neurones of the GP, striatum and SNc where it is believed to inhibit either complex II of the electron transport chain or the glutamate aspartate transporter whereby it ultimately disrupts ATP synthesis and induces ROS production (Gunter *et al.*, 2010; Milatovic *et al.*, 2009).

## 1.8. Why is the basal ganglia susceptible to cell death?

Multiple sources of cellular insult have been described to promote PD. But why is the SNc more vulnerable to degeneration than other regions of the BG? To understand why may allow the development of therapies which slow the progression of SNc degeneration. Several theories speculate on this susceptibility, below are two of the most discussed.

### 1.8.1. Lower expression of calbindin and $Ca^{2+}$ homeostasis

Calbindin-D28K (CB) is a calcium ($Ca^{2+}$) binding protein which regulates and buffers cellular $Ca^{2+}$. It is thought that without CB the cell accumulates toxic levels of $Ca^{2+}$ and dies. Within the non-human primate (NHP) model of PD the midbrain cells most resistant to MPTP were those expressing CB (Liang *et al.*, 1996). Studies have correlated, firstly, that different strains of mice possess differing sensitivities to MPTP (Muthane *et al.*, 1994) and, secondly, that these sensitivities can be somewhat linked to differing numbers of CB-expressing nigral neurones (Dopeso-Reyes *et al.*, 2014; Vidyadhara *et al.*, 2016). Despite this, the lower abundance of CB exists in other brain regions, so why is the SNc different to those areas? To account for this difference we must look at the physiology of the SNc neurone. The SNc A9 subset of DA neurones are, unlike the majority of brain cells, autonomous and produce regulated 2 to 4 Hz action potentials without stimuli (Chan *et al.*, 2010); a pace-making activity which requires the use of a high number of $Ca^{2+}$ channels. This increased number of channels leaves the A9 DA neurones more sensitive to $Ca^{2+}$ ions. To counter the large influx of $Ca^{2+}$ ions, $Ca^{2+}$ is actively transported out of the cell consuming a persistently high level of ATP in the process. This highlights how energy dependent the A9 neurones are even when compared to other

subtypes.

### 1.8.2. Region of high dopamine oxidation and metabolism

The oxidation of DA has been theorised to create toxic metabolites. The hazardous ROS, superoxide radicals, $H_2O_2$ and dopamine-quinone molecules have all been identified to be by-products of the catalysed oxidation of DA (Halliwell, 1992; Stokes *et al.*, 1999). Furthermore, normal monoamine oxidase (MAO) metabolism has been seen to cause the rise of a toxic metabolite known as 3,4-dihydroxyphenylacetaldehyde (DOPAL), which is later converted to 3,4-dihydroxyphenylacetic acid (DOPAC) (Marchitti *et al.*, 2007) (Figure 2). DOPAL is the main contender of the *catecholaldehyde hypothesis* that suggests that an intrinsic toxin unique to DA producing cells (i.e. DOPAL) is the cause of cell susceptibility. Several studies have tried to identify the toxic function of DOPAL within the SNc. Firstly, it has been theorised that the metabolite enhances α-syn aggregation within glial cells (Werner-Allen *et al.*, 2016). Secondly, the catechol group may auto-oxidise into two harmful products, a semiquinone radical and an ortho-quinone (Anderson *et al.*, 2011). Finally, DOPAL presents a functional aldehyde group that is well known to cause cellular damage.

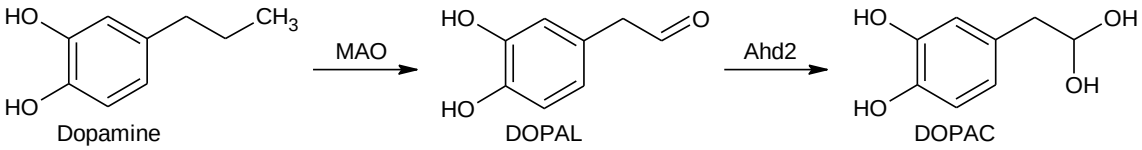


**Figure 2: The metabolism of dopamine to DOPAL.**
Dopamine is readily converted into the toxic transition metabolite DOPAL via the MAO enzyme. The intermediate is then converted into DOPAC but via Ahd2. DOPAL, 3,4-dihydroxyphenylacetaldehyde; MAO, monoamine oxidase; DOPAC, 3,4-dihydroxyphenylacetic acid, Ahd2, aldehyde dehydrogenase 2.

The MAO enzyme has been identified as a therapeutic target in an attempt to reduce intracellular production of DOPAL. However, due to the inhibition of the MAO-A subtype leading to hypertension (Sathyanarayana Rao *et al.*, 2009), pan-MAO inhibition is not conducted within the clinic. To counter this problem a recent study has assessed the use of MAO-B inhibitors, rasagiline and selegiline, on DOPAL inhibition. Although the concentration of DOPAL was reduced, the authors state that this may be due to non-selective inhibition at high doses (Goldstein *et al.*, 2016). Nevertheless, this is a promising start to a new therapeutic target.

Studies have shown that PD patients may possess lowered levels of the DOPAL dehydrogenase enzyme Ahd2 (Mandel *et al.*, 2005; Smidt, 2009). Lowered levels of Ahd2 would permit the accumulation of DOPAL and the resulting associated toxic effects. However, studies have indicated patients receiving L-DOPA treatment do not have advanced PD pathology or severity compared to patients not taking L-DOPA. Thus, indicating that an increase in DA does not correlate to increased DOPAL-induced toxicity; disproving the aforementioned catecholaldehyde hypothesis. Furthermore, the hypothesis does not explain the differing sensitivities between the A9 dopaminergic neurones of the SNc and the neighbouring A10 dopaminergic neurones of the ventral tegmental area (VTA). The mechanism behind intrinsic toxicity must therefore be more complex than first thought.

## 1.9. Pathways of the basal ganglia

The BG houses a network of nuclei found in the midbrain that orchestrates fine motor control. This process is maintained through the finely tuned balance of the BG's direct and indirect pathways; pathways primarily mediated by DA, γ-aminobutyric acid (GABA) and glutamate NTs. As the degeneration of the SNc leads to diminished striatal DA, an imbalance of these regulating NTs is formed causing the cardinal motor symptoms we associate with PD.

The nuclei which form the BG are the SNc, substantia nigra pars reticulata (SNr), putamen and caudate nucleus complex (known as the dorsal striatum within the rodent models of disease), globus pallidus externa (GPe), globus pallidus interna (GPi) and subthalamic nucleus (STN). Other key regions of the BG are the motor and sensory cortex and the thalamus. To further understand PD we must investigate the pathways between these nuclei. These pathways are discussed below and visualised in figure 3.

### 1.9.1. Corticostriatal pathway

The corticostriatal pathway links the glutamatergic pyramidal afferents of the cortex to the dendritic spines of the striatal GABAergic neurones known as the medium spiny neurones (MSNs). These MSNs feed into the downstream pathways involved in motor control. While MSNs contribute to 95% of the striatal cell populous, the fast spiking parvalbumin-positive GABAergic interneurones and the tonically active cholinergic interneurones contribute to the remaining 5%. The fast spiking interneurones receive glutamatergic input from the cortex that in turn cause the feed-forward inhibition of neighbouring MSNs cells; a circuit seen to control and suppress unwanted MSN activity (Gage *et al.*, 2010). On the other hand, the tonically active interneurones possess a burst-pause pattern of activity and are innervated by the thalamic glutamatergic afferents. When stimulated these cholinergic cells are believed to mediate learning and DA-dependent striatal plasticity (Benhamou *et al.*, 2014; Wang *et al.*, 2006).

Corticostriatal neurones can form two classes of cortical neurones, the intratelencephalic type which originate in cortical layers 2 to 6 and innervate the striatum via the external capsule and corpus callosum, or the pyramidal tract type which project from layer 5B to the thalamus and brainstem (Lei *et al.*, 2004).

### 1.9.2. Nigrostriatal pathway

The NS is the key pathway that regulates the activity of the striatal MSNs. Innervated by the dopaminergic SNc neurones, the NS projects to the striatum where the dopaminergic cells synapse onto the spines of the MSNs. The striatum possesses all five classes of DA receptor, D1 and D5 (D1-like subtype; activators of $G_s/G_{olf}$ proteins) and D2, D3 and D4 (D2-like subtype; activators of $G_o/G_i$ proteins) (Neve *et al.*, 2004); but it is the D1 and D2 receptors which dominate the striatum. MSNs cells either exclusively express D1 or D2 receptors. The MSNs that express D1 receptors (dMSNs) form the *direct pathway* whereas the MSNs that express D2 receptors (iMSNs) form the *indirect pathway*.

Following cortical coordination, DA has different downstream effects depending on the whether the dMSNs or iMSNs cells are activated. Agonism of D1 receptors causes the stimulation of the $G_s/G_{olf}$ class of G-protein coupled receptors (GPCRs), which in turn, activate adenylyl cyclase. This enzyme then catalyses the synthesis of the secondary messenger cyclic adenosine monophosphate (cAMP), which in turn, stimulates L-Type $Ca^{2+}$ channels and the resulting activation of the direct pathway. On the other hand, agonism of D2 receptors initiates the stimulation of the $G_o/G_i$ class of GPCRs that inhibits the production of cAMP. This reduces the excitability of the indirect pathway through L-Type $Ca^{2+}$ channel inhibition (Hernandez-Lopez *et al.*, 2000). Both pathways induce motor movement.

### 1.9.3. Direct, indirect and hyperdirect pathways

The direct and indirect pathways are the basis of motor control in the BG and are significantly altered in the classical model of PD. The direct pathway is a monosynaptic GABAergic link between the striatum and the GPi/SNr complex. The direct pathway is primarily driven by SNc-mediated DA agonism of the dMSN D1 receptors, although dynorphin and substance P are also utilised. The main role of the direct pathway is to induce movement through the disinhibition of the thalamocortical feedback loop.

The indirect pathway is a polysynaptic connection between the iMSNs of the striatum to the GPi/SNr complex via the GPe and STN. DA agonism of the iMSN D2 receptors causes the inactivation of the indirect pathway. Enkephalin is also utilised within this pathway. D2 receptor agonism reduces the activity of the STN, thus resulting in the lower glutamatergic activation of the GPi/SNr. This causes the disinhibition of the thalamocortical feedback loop, thereby promoting movement. In states of low DA, such as PD, the indirect pathway does not disinhibit the thalamocortical feedback loop resulting in lowered motor movement. DA is therefore the key regulator behind the balance of these two opposing pathways.

In addition to the two classical pathways there is a third known as the hyperdirect pathway. The hyperdirect pathway exhibits cortical glutamatergic afferents that directly innervate the STN. This pathway stimulates the GPi/SNr complex which ultimately deactivates the thalamocortical feedback loop; a process which reduces motor activity whilst bypassing the striatum altogether. The hyperdirect pathway is seen to control and induce a switch from impulsive to controlled movements (Bosch *et al.*, 2012; Obeso *et al.*, 2008). Furthermore, ablation of this pathway (e.g. stroke lesioning) causes impairments such as impulsivity and ballism (large involuntary movements of the limbs) (Nambu *et al.*, 2002).

### 1.9.4. Thalamic pathways

Thalamic nuclei form the key connections between both the direct and indirect pathways of the BG and specific cortical regions that act as the final part of the BG loop. In this region, glutamatergic afferents from the ventral anterior and ventral lateral thalamic nuclei innervate the cingulate, premotor and primary motor cortical regions to induce controlled motor activity.

Two glutamatergic thalamostriatal connections are present within the BG. The first links the thalamic centromedian and parafascicular nuclei to the striatal MSNs which is thought to aid striatal output (Smith *et al.*, 2014). The second is via the aforementioned tonically active interneurones (Ding *et al.*, 2010) (see figure 3).

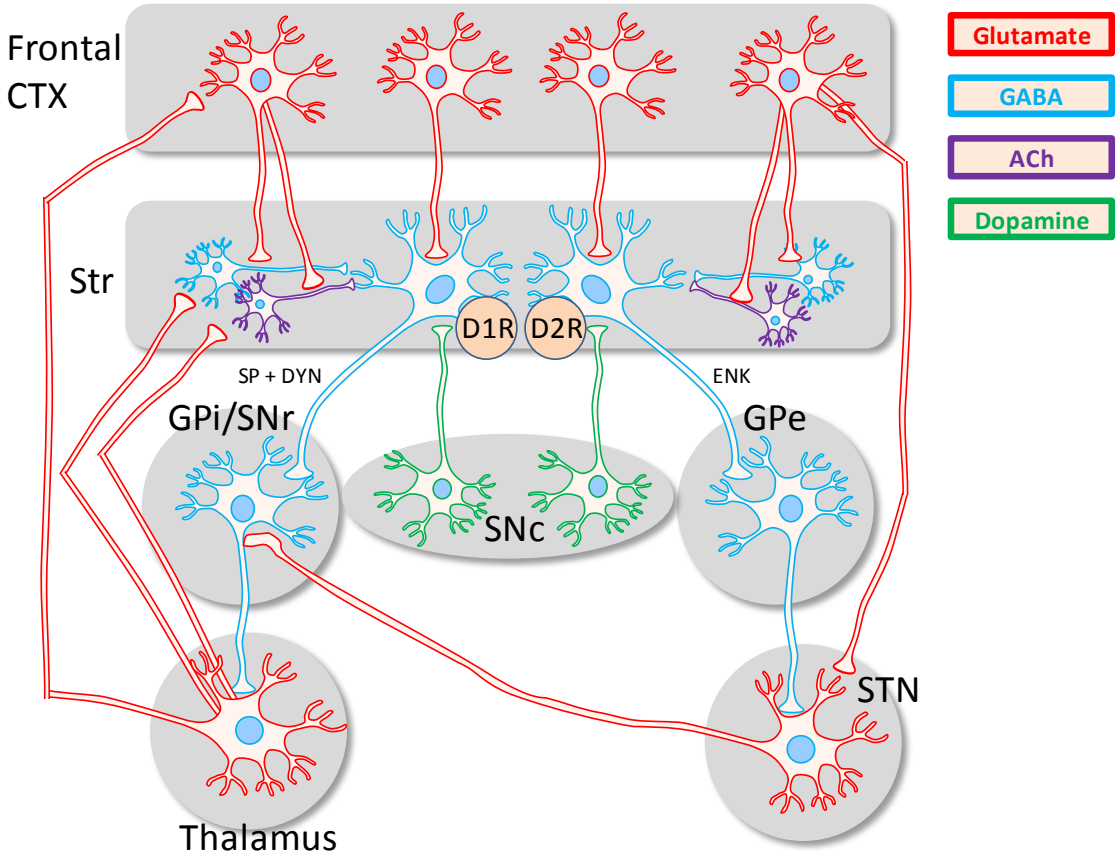


**Figure 3: Simplified overview of the basal ganglia.**
Glutamatergic (red) cortical neurons innervate the GABAergic (blue) MSNs, fast spiking interneurones and the cholinergic (purple) tonically active interneurones of the striatum. Dopaminergic (green) SNc cells release DA into the striatum and bind to D1 or D2 specific MSNs, dMSNs and iMSNs, respectively. D1 agonism leads to the activation of the direct pathway and the resulting disinhibition of the thalamocortical feedback loop. This pathway increases the thalamic release of glutamate and induces movement. Conversely, D2 agonism inactivates the indirect pathway. This pathway reduces levels of subthalamic glutamate and GPi/SNr activity. Thus causing the disinhibition of the thalamocortical pathway and inducing movement. CTX; cortex, Str; striatum, D1/2R; DA 1/2 receptors, GPi/GPe; globus pallidus interna/externa, STN; subthalamic nucleus, ENK; enkephalin, SP; substance P, DYN; dynorphin.

### 1.9.5. Alterations in the parkinsonian basal ganglia

To generate movement, the BG undergoes a series of activations and inactivations within its two key pathways. However, in PD the regulation of these is dramatically altered. Figure 4 summarises the key routes affected by the neuronal degeneration of the SNc.

The pathological loss of SNc cells reduces the DA content within the striatum, this ultimately causes aberrant glutamatergic transmission from the corticostriatal pathway (Pisani *et al.*, 2005). As a knock on effect, striatal MSNs lose both dendritic spines and arborisations in response to the plastic remodelling of the corticostriatal projections. Although a loss of MSN spines would indicate a lowering of transmission, studies analysing corticostriatal activity find the opposite in which glutamatergic receptor presence on MSNs is increased (Betarbet *et al.*, 2000a; Calabresi *et al.*, 2007). Conversely, this increase may just be a homeostatic *rebalancing* of transmission due to the altered innervation from the cortex (Jenner, 2008a).

As DA content is low, neither the D1 nor the D2 MSNs (dMSN and iMSN, respectively) are activated. As DA mediated activation of the iMSNs normally inhibits the indirect pathway ($G_i/G_o$ protein activation), a lack of DA results in the disinhibition of cAMP production causing an increase in GABA release to the GPe. Furthermore, a lack of DA mediated activation of the dMSNs leads to the inability to produce cAMP therefore inhibiting the activation of the direct pathway. This joint compounded effect results in the direct pathways lowered GABAergic transmission to the GPi/SNr and the indirect pathway's overstimulation of the STN. Together these lead to an underactive thalamocortical feedback loop that causes bradykinesia. Although not present in figure 4, the hyperdirect pathway is crucial in regulating erroneous movement and is thought to be dysregulated in PD.

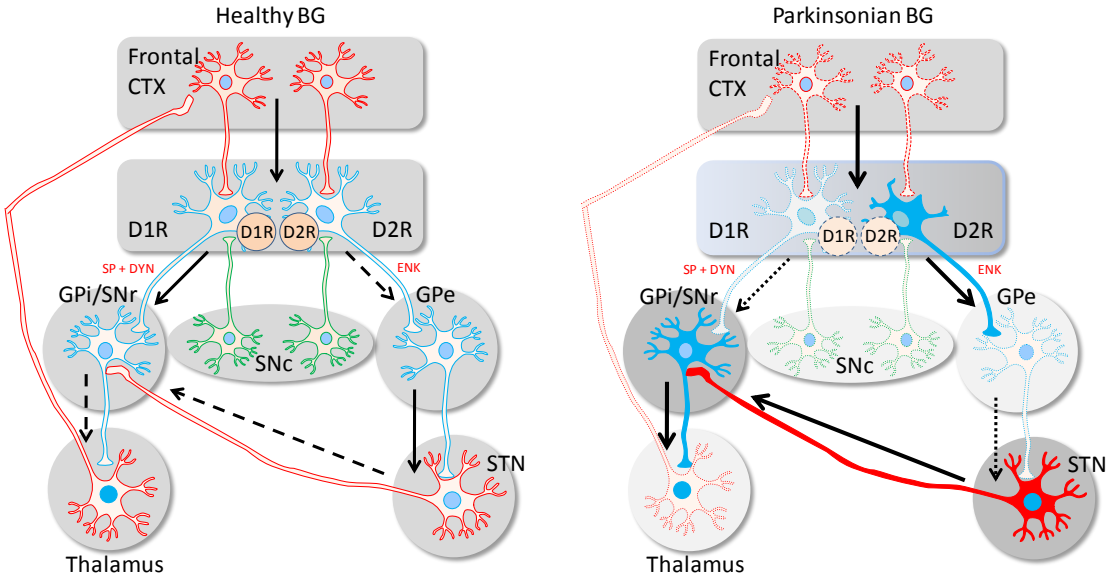


**Figure 4: Comparison of the key BG pathways affected in PD.**
In the normally functioning BG (left), DA from the SNc stimulates dMSNs and inhibits the iMSNs. This causes the generation of controlled movement through the disinhibition of the thalamocortical feedback loop. In the parkinsonian BG (right), remodelling of the corticostriatal pathway (e.g. reduction in MSN spines) alongside the diminished release of DA from the SNc leads to the overstimulation of the STN and GPi/SNr through the inactivity of dMSNs and activity of iMSNs. These alterations result in the reduced activation of the thalamocortical feedback loop which lowers motor output. In the parkinsonian BG, filled and faint neurones indicate cells of enhanced and reduced stimulation, respectively. Red; glutamatergic neurone, blue; GABAergic neurone, green; dopaminergic neurone. Thicker arrows indicate enhanced NT transmission and dashed arrows indicate reduced NT transmission.

Figure 4 presents the key overview of the dysregulated parkinsonian BG, however, the true model is far more complex. Dysfunctions in other non-BG regions such as the serotonin (5-HT), acetyl choline (ACh) and noradrenaline systems alongside alterations in the BG neuronal firing patterns are currently under investigation. By unveiling new insights behind these systems we will further our understanding of the dysregulated parkinsonian BG.

## 1.10. Current treatments for Parkinson's disease

A wide array of treatments have been developed to help rebalance the BG either by direct manipulation of the BG circuitry or through replacing striatal DA. The sites of action of these treatments are presented in figure 5.

### 1.10.1. Dopamine replacement therapies

By far the most common form of PD treatment are the DA replacement therapies. These are a broad spectrum of therapeutics that have been developed to raise the diminished level of striatal DA. These therapeutics therefore aim to lessen the symptoms associated with reduced striatal DA. Success has been found in levodopa (L-DOPA), the precursor to DA, and DA agonists, compounds that mimic DA at the molecular level. These are described below.

#### *1.10.1.1. Levodopa; L-3,4-dihydroxyphenylalanine*

Trade name: Madopar, Sinemet (as adjunct with carbidopa or benserazide)

Type: Blood brain barrier penetrable precursor to DA

Action: Metabolises into DA. Increases depleted striatal DA content

Levodopa, otherwise known as L-DOPA, is the *gold standard* of DA replacement therapies. It is the blood brain barrier (BBB) penetrable precursor to DA that, upon uptake into nerve terminals, becomes metabolised into DA by DOPA decarboxylase (DDC). As it is administered peripherally, L-DOPA exists as an adjunct therapy with the DDC inhibitors carbidopa or benserazide; compounds that enhance the bioavailability of L-DOPA by reducing its peripheral metabolism. These inhibitors do not cross the BBB and so do not interfere with intrastriatal DA synthesis. The presence of these inhibitors lowers the effective dose required for symptom relief and, whilst doing so, delays the onset of L-DOPA associated disturbances such as L-DOPA-induced dyskinesia (LID) which shall be discussed later in section 1.11.1.

Although being the most efficacious of all treatments L-DOPA can induce substantial side effects. As a result, alternative compounds are frequently prescribed to delay the use of L-DOPA and reduce its required dose (a practice commonly known as L-DOPA-sparing).

#### *1.10.1.2. Catechol-O-methyl transferase inhibitors*

Examples: Entacapone (Comtan), Tolcapone (Tasmar)

Type: Selective inhibitor of the L-DOPA metabolising enzyme, COMT

Action: Increases bioavailability of L-DOPA

To enhance the effectiveness of L-DOPA, the administration of catechol-O-methyltransferase (COMT) inhibitors can be prescribed. As an adjunct to the L-DOPA/carbidopa cocktail, COMT inhibitors have been successful in increasing the *on time* patients experience by increasing the plasma concentration of L-DOPA. Although administering COMT inhibitors alongside L-DOPA has shown to increase severity of LID, it also enhances the bioavailability of the DA precursor. This has shown to lower the effective dose by up to 25% (Jankovic *et al.*, 2008). COMT inhibitors therefore allow for L-DOPA-sparing.

Two COMT inhibitors that have been developed for clinical use are entacapone and tolcapone. Entacapone provides minor well-tolerated side effects (e.g. nausea) and is taken with great effect (Schrag, 2005). Unlike entacapone, tolcapone has been reported to induce acute liver failure which has led to questions being raised over its use (Olanow, 2000).

#### *1.10.1.3. Monoamine oxidase B inhibitors*

Examples: Rasagiline (Azilect), selegiline (L-Deprenyl), safinamide

Type: Irreversible inhibitor of the enzyme MAO-B

Action: Increases bioavailability of DA

Similar to the COMT inhibitors, MAO-B inhibitors are taken commonly as an adjunct therapy with L-DOPA in order to promote the bioavailability of DA. The MAO enzyme is bound to the outer membrane of the mitochondria within the presynaptic terminal where it catalyses the oxidation of monoamines such as DA. Its inhibition therefore leads to the increase in L-DOPA-metabolised DA present within the synaptic terminal, thus amplifying post-synaptic receptor stimulation (Sprenger *et al.*, 2013).

#### *1.10.1.4. Dopamine receptor agonists*

| | | |
|---|---|---|
| Examples: | Ergot derived: | Bromocriptine, pergolide, cabergoline |
| | Non-ergot derived: | Ropinirole, pramipexole |
| Type: | Agonists of the D2-like, and to a lesser extent the D1-like, receptor | |
| Action: | Mimics endogenous DA at the postsynaptic terminal | |

DA agonists cover a wide group of compounds that activate both the D1- and D2-like DA receptors in an attempt to restore normal BG function (Quinn, 1995). These compounds are typically favoured by newly diagnosed patients as monotherapies (Rascol *et al.*, 2000) but are also successfully used as adjunct therapies alongside L-DOPA in an act of L-DOPA-sparing (Fox *et al.*, 2011).

As DA agonists are not metabolised by the typical DA pathways, the production of DA's toxic metabolites (e.g. DOPAL) are therefore avoided. Dyskinetic motor dysfunction is also less frequent with DA agonists when compared to L-DOPA. This is thought to be due to the longer half-life these compounds possess over L-DOPA.

DA agonists are categorised into two groups, the older ergot-derived and the newer non-ergot derived compounds. Derivative compounds of the ergot fungus bind to the D2-like receptors almost selectively (many possess a weak affinity for the D1-like and 5-HT receptors). Examples of these compounds are bromocriptine, pergolide and cabergoline. The non-ergot compounds such as pramipexole and ropinirole suggest a higher affinity to the D2-like family than that of the ergoline compounds (Molho *et al.*, 1995).

Despite the significant benefits of using DA agonists, the side effects they induce can be debilitating. Typical side effects caused by both subtypes, are hallucinations, hypotension, nausea and the potential exacerbation of LID if used alongside L-DOPA (Factor *et al.*, 1995; Micieli *et al.*, 1996). Non-ergoline agonists appear to have lesser side effects than those of the ergolides (Lees *et al.*, 1997). Ergot-related erythromelalgia, retroperitoneal and pleuropulmonary fibrosis and vasospasm, although rare, have been documented as well as several behavioural dysfunctions (Reichmann *et al.*, 2006). Issues with impulse control disorders such as compulsive buying, gambling and sexual behaviour have all been related to ergot-derived DA agonists (Kaplan *et al.*, 2013). Studies have reported a 2 to 3.5 fold increase in odds of having an impulse control disorder whilst undergoing DA agonist treatment (Weintraub *et al.*, 2010).

#### *1.10.1.5. Non-dopamine replacement therapies*

Examples: Benzatropine (anti-cholinergic), amantadine (anti-glutamategic)

Type: Anti-cholinergics/anti-glutamatergic

Action: Reduces levels of cholinergic and glutamatergic activity

The anticholinergics were the first therapeutics available for PD. Despite their age, the mechanism behind these drugs remains undetermined. It is believed that they counter the increased striatal cholinergic activity caused by depleted striatal DA (Katzenschlager *et al.*, 2003). Being competitive antagonists of muscarinic receptors, anticholinergics are believed to reduce the activity of the tonically active interneurones; cells that are suggested to promote this hypercholinergic activity in the parkinsonian brain (Sanchez *et al.*, 2011). Drugs like benztropine and biperiden although successful in alleviating symptoms of tremor have proven to present significant side effects such as blurred vision, anxiety, dry mouth and cognitive impairment.

The non-selective N-methyl-D-aspartate (NMDA) antagonist amantadine has also been successful in alleviating PD symptoms (Uitti *et al.*, 1996). Similarly, amantadine's methylated analogue, memantine has also shown benefits to patients in clinical trialling (Moreau *et al.*, 2013). Currently, NMDA antagonists are being used as therapies targeting LID rather than the disease itself. This shall later be discussed in detail.

#### *1.10.1.6. Invasive methods of therapy*

Surgical intervention has long been practiced in the field of PD. During the 1950s people experiencing severe symptoms such as tremor and bradykinesia often received a thalamotomy or pallidotomy to reduce the experienced symptoms. However, after the discovery of L-DOPA the invasive and high-risk strategy was shelved for the oral therapeutic. Coincidentally, it was later discovered that pallidotomy was successful in reducing the severity of LID; an effect of long term L-DOPA use. As a result, there was a resurgence in investigating the inhibition of BG nuclei; a venture that led to the use of deep-brain stimulation (DBS).

DBS utilises brain-implanted electrodes to induce high frequency stimulation that reversibly inhibits select nuclei of interest. In effect, this is a reversible alternative to the aforementioned surgical lesioning. DBS is seen to counter the abnormal neuronal firing found within the parkinsonian BG, but why this positively affects motor control is not fully known. Electrical stimulation from DBS is thought to interrupt the aberrant anti-kinetic beta-oscillations (13-30Hz) found within key regions of the parkinsonian BG, such as the STN. These oscillations can be described as anti-kinetic as they are inhibited by voluntary movement, various drug

therapies and DBS itself (Eusebio *et al.*, 2011; Kuhn *et al.*, 2006; Levy *et al.*, 2002). Conversely, higher frequency oscillations (200-500Hz) are present during DA-dependent movement and so are associated with pro-kinesia (Foffani *et al.*, 2003).

Although the GPi, pedunculopontine nucleus and STN can be selected for DBS, the latter is most commonly chosen in reducing the rigidity, tremor and bradykinesia. Although very successful in improving quality of life, the greatest issue regarding DBS is in the eligibility of its candidates. Tight regulations prohibit people with cognitive impairment, depression or of significant age (>75) to receive DBS. This is due to the procedure possibly worsening pre-existing ailments. Younger patients who are responsive to L-DOPA and have had symptoms for at least 5 years are typically chosen for DBS (Moro *et al.*, 2006).

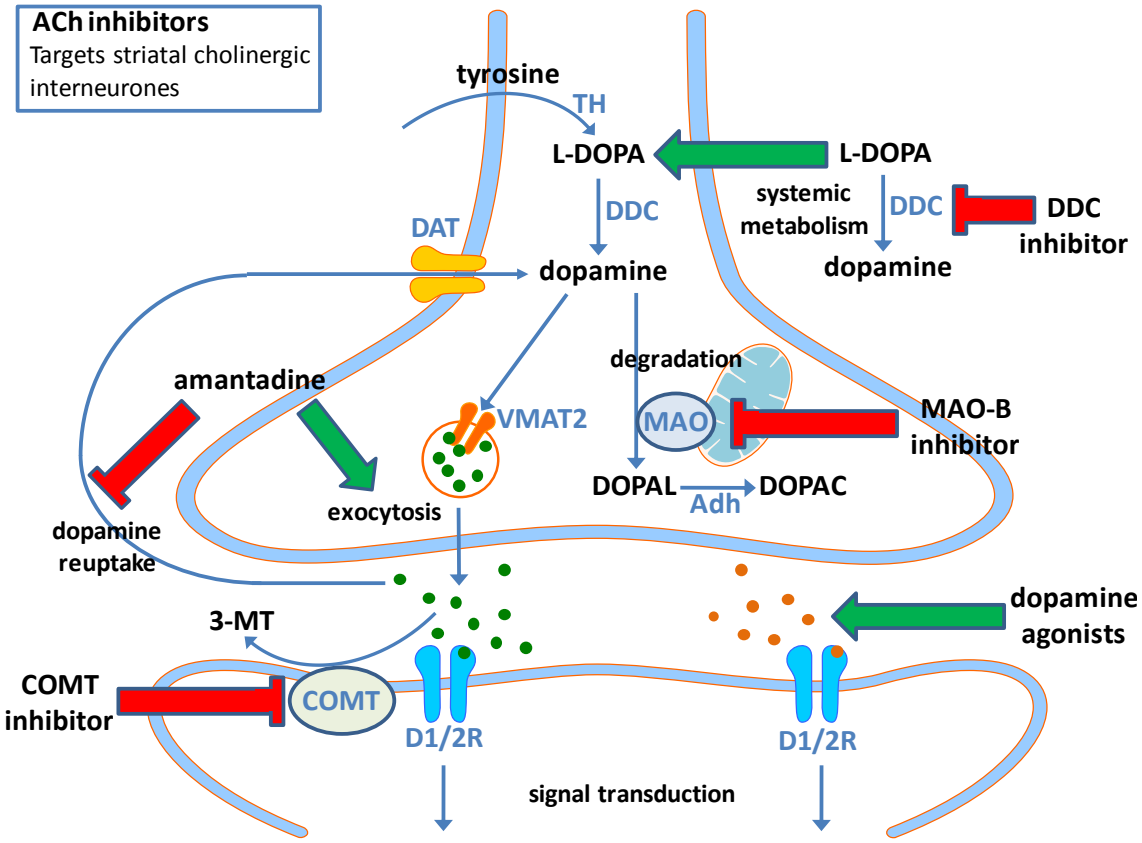


**Figure 5: Sites of action of Parkinson's disease treatments at the dopaminergic synapse**
Green arrows indicate promotion whereas red arrows indicate inhibition. Green circles are dopamine. Orange circles are dopamine agonists. TH: tyrosine hydroxylase, DDC: dopadecarboxylase, DAT: dopamine transporter, MAO: monoamine oxidase, VMAT2: vesicular monoamine transporter 2, DOPAL: 3,4-dihydroxyphenylacetaldehyde, DOPAC: 3,4-dihydroxyphenylacetic acid, Adh: aldehyde dehydrogenase, COMT: catechol-O-methyltransferase, D1/2R: dopamine 1/2 receptor, 3-MT: 3-methoxytyramine.

## 1.11. Unmet clinical needs

There are two clear unmet clinical needs in the field of PD research.

1. Understanding the mechanisms underlying LID to discover new and improved anti-dyskinetic agents.
2. Discovering novel therapeutic strategies to halt disease progression and increase SNc cell survival.

This thesis aimed to target these two clinical needs.

### 1.11.1. L-DOPA-induced dyskinesia

LID is a hyperkinetic phenomenon that affects a large proportion of PD patients globally. As its name suggests, it is caused by the aforementioned *gold standard* PD drug L-DOPA, which when administered chronically over 5-10 years (Jenner, 2008b) to a DA depleted system, induces aberrant involuntary movements.

LID can manifest in a variety of abnormal involuntary movements (AIMs), including dystonia (abnormal muscle tone), ballism (large ballistic involuntary movements of the limbs), myoclonus (jerky contraction of the muscles), and chorea (dance-like unpredictable movements), which vary upon the individual and type of LID. Depending on the manifestation of these characteristics in relation to L-DOPA dosing, the LID can be diagnosed as one of three types of dyskinesia (see figure 5 for a graphical representation of dyskinesias at varying L-DOPA plasma levels).

#### *1.11.1.1. Off-period dystonia*

Off-period dystonia is a state of abnormal muscle tone (i.e. frequent spasms and irregular postures) which manifest because of low L-DOPA plasma content within the patient. Off-peak dystonia is known to affect young-onset PD patients more than the more common idiopathic form (Mehanna *et al.*, 2014), off-period dystonia regularly occurs during the early morning or late night when L-DOPA levels are at their lowest. Off-period dystonia commonly gives rise to painful foot cramps, toe curling and leg extensions (Vidailhet *et al.*, 1999).

#### *1.11.1.2. Diphasic dyskinesia*

Diphasic dyskinesia occurs in response to both high and low plasma levels of L-DOPA. Shortly after ingestion of L-DOPA, AIMs manifest primarily within the leg and other limbs of one side of the body before subsiding and reappearing several hours later when the level of L-DOPA content declines (Encarnacion *et al.*, 2008).

#### *1.11.1.3. Peak-dose dyskinesia*

Peak-dose dyskinesia, the most common form of LID, occurs when L-DOPA reaches its peak concentration within the plasma. Typical AIMs include ballism of the arms and legs and writhing and swaying of the trunk and neck/head. Dyskinesia can also progress to the chest and cause shortness of breath and difficulties with breathing. The progressive effect of PD commonly results in a more severe peak-dose dyskinesia, as higher doses of L-DOPA must be administered to counter the motor dysfunction associated with advanced PD.

The epidemiological profile of LID varies between several large patient studies. A range of 16% to 31% of PD patients experienced LID following a year of L-DOPA exposure (CALM-PD Study 2000; Fahn *et al.*, 2004). This incidence, in another large sample study, rose to 40% following 5 years of exposure (Ahlskog *et al.*, 2001). Furthermore, 94% of patients had experience with LID after 15 years of PD diagnosis (Hely *et al.*, 2005). These data confirm that LID is an almost inevitable concern for people with PD.

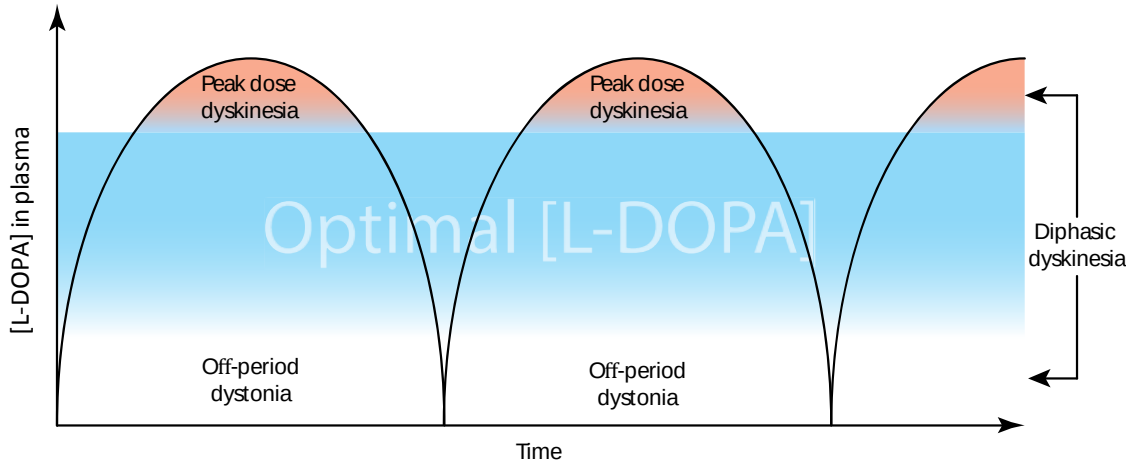


**Figure 6: Three types of dyskinesia in relation to L-DOPA plasma concentration.**
Peak dose dyskinesia manifests at the highest doses of L-DOPA whereas off-period dystonia occurs at low levels. Diphasic dyskinesia is a combination of the two.

#### *1.11.1.4. The two requirements for inducing L-DOPA induced dyskinesia*

With most PD patients guaranteed to experience LID sometime in their life, the question remains, why are PD patients predisposed to dyskinesias? The answer lies in two key prerequisites: dopaminergic cell denervation and exposure to DA replacement therapies such as L-DOPA. Despite knowing these prerequisites, the true mechanism underlying the manifestation of LID is still unknown.

Within PD, there is a degeneration of dopaminergic terminals that have key roles in recycling, releasing and buffering extrasynaptic DA. It is believed that the diminished capacity to buffer and store the acute and intermittent doses of L-DOPA leads to aberrant plasticity; an attempt to equilibrate high levels of synaptic DA (Calabresi *et al.*, 2010; Hong *et al.*, 2014). Dopaminergic cell expression, activation and tonic firing (5 Hz) is unaltered within the healthy brain. However within the DA depleted brain, the administration of L-DOPA gives rise to a fluctuating source of DA which upsets this homeostatic balance of activity (Olanow *et al.*, 2006). Although the initial terminal sprouting found in response to denervation aids in L-DOPA buffering, the brain soon becomes overwhelmed and unable to store excess L-DOPA. This reduces the experienced effect of L-DOPA and gives rise to the *wearing off* effect patients experience with L-DOPA treatment. This shortening of L-DOPA's effect becomes acute and then more closely replicates the half-life of the drug and brings about the characteristic LID AIMs. As a result, this leads to a *vicious cycle* of requiring increasingly higher doses of L-DOPA to counter motor dysfunction whilst, unfortunately, reducing its therapeutic efficacy and promoting more severe LIDs

Although it is almost certain that a PD patient receiving L-DOPA is guaranteed LID, individuals may have it manifest at varied rates and severity. These differences may be associated with individual factors that alter the risk for LID.

#### *1.11.1.5. Risk factors for L-DOPA induced dyskinesia*

Two key risk factors in LID manifestation are L-DOPA dosage and duration of its exposure, both have been found to correlate with LID severity. The DATATOP placebo-controlled clinlical trial indicated that a L-DOPA dose of 338 mg did not induce LID whereas an increase to 387 mg saw the disorder arise (DATATOP, 1989). It is also well understood that longer peak-dose dyskinesias can be seen as a result of higher L-DOPA doses (Nutt *et al.*, 1992). The duration of exposure, as previously explained in reference to LID's epidemiological profile, is directly correlated with LID susceptibility. It is because of these two factors that L-DOPA-sparing is an important strategy in tackling LID, whereby drug dosage is kept to a minimum to delay LID onset.

It is important to note that, although not L-DOPA driven, dyskinesia can be caused by other DA replacement therapies as well. However, these prove to have lower incidence when compared to L-DOPA (Nutt, 1990). DA replacement therapies are often prescribed to target motor dysfunction without a significant increase in LID risk.

There is an inverse relationship between LID and PD onset. Early onset PD (< 40 years old) sees the highest prevalence of LID, where 94% of young patients experience the disorder following 5 years of L-DOPA treatment (Quinn *et al.*, 1987). This is a dramatic increase over the 40% described for idiopathic patients. Other studies have indicated a decreased correlation with age, in which 16% of people diagnosed after 70 years old manifested LID (Kumar *et al.*, 2005). However, we must realise that the genetic factors found associated with early onset PD may play a role in LID manifestation, therefore explaining why older idiopathic PD patients may experience lower LID prevalence.

Alongside age, the gender of the patient may influence the risk of LID manifestation. It is thought that female sufferers of PD present a higher risk for LID as the lower body weight may give rise to a higher dose of L-DOPA in the plasma per kilogram. Studies have suggested that this increased plasma concentration of L-DOPA boosts the bioavailability of the L-DOPA and its dyskinetic properties (Zappia *et al.*, 2005). However, this does not incorporate other gender or hormonal factors that may differ between the sexes.

Genetic mutations other than the previously described familial factors may have a significant say in LID. Individuals possessing polymorphisms of the D2 DA receptor gene have shown a reduced risk in the induction of peak-dose dyskinesia (Oliveri *et al.*, 1999; Rieck *et al.*, 2012).

Interest in the adenosine A2 A receptor as a LID therapeutic target has led to allele discrimination assays. These assays have discovered an association between adenosine A2 A receptor polymorphisms and LID. This highlights a potentially new target for anti-dyskinetic agents (Rieck *et al.*, 2015).

#### *1.11.1.6. Current L-DOPA induced dyskinesia therapeutic interventions*

Established LID can be difficult to treat and so the prevention of the disorder is of high priority. A range of strategies can be employed to either delay LID onset, such as L-DOPA-sparing through the use of DA agonists, or to reduce severity of existing LID by administering pharmacological agents or conducting neurosurgery. As with all diseases, the approach used to treat LID should be an personalised strategy based on the patient's LID type and lifestyle.

In order to delay LID onset, a favoured approach is to reduce the intake of L-DOPA through the aforementioned L-DOPA-sparing method. By administering alternative therapies such as DA agonists and/or MAO-B inhibitors, the overall daily dose of L-DOPA can be reduced by up to 25% (Jankovic, 2008). This is certainly favourable to early-onset PD patients who not only will require far more L-DOPA over a lifetime, but also are also far more susceptible to LID than typical idiopathic patients. However, the caveat to certain DA agonists is that they provide unwanted side-effects and are less successful than L-DOPA in bettering quality of life, albeit with the development of LID (CALM-PD, 2000).

In attempts to reduce LID risk, controlled release formulations of L-DOPA (Sinemet CR) that have a longer half-life than that of the standard compound ($t_{1/2}$: 1.5 hrs) have been developed to counter the pulsatile nature associated with the standard medication. However, these have proven unsuccessful in reducing LID compared to a standard formulation of L-DOPA in a 5 year follow up study (Block *et al.*, 1997; Fox *et al.*, 2011). Nevertheless, this theory of overcoming L-DOPA's short half-life was furthered. More effective slow release strategies have now been developed, such as the intestinal extended release gel, known as L-DOPA/carbidopa intestinal gel. Randomised controlled trails found that L-DOPA/carbidopa intestinal gel applications reduced *off time* and increased *on time* without troublesome LID (Olanow *et al.*, 2014; Wirdefeldt *et al.*, 2016). Although promising, the complications associated with the surgical procedure required for the L-DOPA/carbidopa intestinal gel implantation in elderly patients has been seen as too risky; this approach is a last resort for many patients.

Amantadine is a low affinity non-selective NMDA antagonist that is commonly prescribed as an anti-dyskinetic treatment for LID. Its anti-dyskinetic effect has been proven in trials whereby double blind placebo controlled studies indicated a dramatic decrease in the duration of LID

following amantadine treatment (da Silva-Junior *et al.*, 2005; Snow *et al.*, 2000). But issues have been raised with the long term efficacy of the drug and its associated side-effects (Vijverman *et al.*, 2014). This has led researchers to assess the extended release formulation of amantadine, ADS-5102, as an improved therapeutic. Phase III clinical trials have shown promise in its anti-dyskinetic effects in which Unified Parkinson's disease rating scale (UPDRS) scores were decreased (higher scores indicate higher disease severity) whilst there was an increase in *on time* without troublesome LID (reviewed in (Lotia *et al.*, 2016; Pahwa *et al.*, 2015).

Current anti-dyskinetic approaches have proven successful in providing symptomatic relief of LID. Despite this, no current therapeutic has stopped LID from manifesting in PD patients receiving chronic L-DOPA treatment. As such, we must further investigate the mechanisms behind LID in order to discover new prophylactic therapies. Theories underlying the mechanisms are explained further in Chapter 5.

### 1.11.2. Mechanisms underlying SNc cell degeneration

In order to discover novel ways to halt disease progression and promote SNc cell survival we must further understand the processes in which cells of the NS degenerate. Key mechanisms that lead to cell death are described below.

#### *1.11.2.1. The electron transport chain and oxidative stress*

The ETC is an important process that takes place on the inner mitochondrial membrane. Its purpose is to generate ATP by a series of redox reactions involving several membrane bound electron transporters known as complexes I, II, III and IV. This process sees the sequential shuttling of electrons from complex I to complex IV by molecular donors obtained from the Kreb's cycle (e.g. nicotinamide adenine dinucleotide [NADH]). The ultimate aim of this process is to drive the transfer of protons across the membrane causing an electrochemical gradient. Once this gradient has formed, free protons drive the formation of ATP from ADP and phosphate via the ATP synthase enzyme. This is the key energy producing process in the cell. Although essential for cell survival, the mitochondria can also trigger cell death.

Disrupted ETC function through damage or mutation causes not only the cessation of ATP production but also the creation of ROS. Cells possess several biological antioxidants which buffer manageable levels of ROS (e.g. superoxide dismutase, glutathione), but continued cell stress leads to an accumulation of ROS that is beyond the cell's defence capacity. This state is known as oxidative stress. In a stressed state, ROS trigger the release of cytochrome C from the mitochondria which then facilitate the caspase cascade and finally apoptosis (Kannan *et al.*, 2000). Degenerating SNc neurones in PD brains exhibit signs of oxidative stress, such as the oxidation of proteins and cytoplasmic nucleic acid, alterations in biological antioxidants and also lipid peroxidation (Dexter *et al.*, 1989a; Riederer *et al.*, 1989; Zhang *et al.*, 1999). These pathological hallmarks all point towards the dysfunctional mitochondrion as a key component in the pathogenesis of PD (Jenner, 1996).

#### *1.11.2.2. Glutamate driven excitotoxicity*

A large unmanageable concentration of glutamate gives rise to excitotoxicity; a state which induces cell apoptosis (Olney *et al.*, 1971). Unfortunately for the BG, glutamate is a key regulator of its function which is greatly affected in PD. The two main sources of glutamatergic transmission in the BG are from corticostriatal afferents and the subthalamic projections to the GPi/SNr complex. But it is the overactivity of the subthalamic pathway which has previously been identified as a correlate for disease progression and a source of excitotoxicity (Remple *et al.*, 2011). Additionally, this excitotoxicity can be exacerbated by poor glutamate buffering.

Glutamate reuptake from the synaptic cleft has suggested to be inhibited in PD due to the dysfunctional expression of glutamate transporters in PD models (Chung *et al.*, 2008; Salvatore *et al.*, 2012).

When glutamate is in excess, it floods the synaptic cleft and overstimulates NMDA receptors on the post-synaptic membrane. Stimulation and depolarisation of these neurones leads to the influx of large quantities of $Ca^{2+}$ that then cause the activation of several pro-apoptotic pathways. $Ca^{2+}$ is known to accumulate in the mitochondria causing the depolarisation of the membrane and the opening of the permeability transition pore. In doing so, apoptotic proteins such as cytochrome C are released causing cell death (Orrenius *et al.*, 2003). Intracellular $Ca^{2+}$ can also activate the nitric oxide synthase (NOS) isozymes present in neuronal cells (nNOS) and endothelial cells (eNOS), resulting in the production of nitric oxide (NO). The highly reactive peroxynitrite ($ONOO^-$) is then formed from the reaction between NO and superoxide radicals. Both NO and $ONOO^-$ have shown to be significantly higher in PD patients and are thought to worsen disease progression (Kouti *et al.*, 2013).

#### *1.11.2.3. Dysfunction of the proteasome*

The ubiquitin-proteasome system (UPS) is an intracellular complex which ubiquitinates and degrades proteins that are destined for recycling. The aim of the UPS is to remove the hazardous build up of damaging or non-functioning proteins that may inhibit the processes within the cell. Dysfunction of the UPS underlies one of the key theories behind α-syn presence within SNc cells. Furthermore, particular forms of familial PD are associated with the mutation in UPS related proteins, such as the E3 ubiquitin ligase Parkin and the enzyme UCH-L1 (Leroy *et al.*, 1998; Um *et al.*, 2010). In idiopathic post mortem tissue, reduced expression of the core 20S proteasomal subunit has been discovered, highlighting the possible decrease in UPS activity (McNaught *et al.*, 2003). The cause of an impaired proteasome in sporadic PD is unknown.

#### *1.11.2.4. Neuroinflammation*

Neuroinflammation has been identified as a likely contributor to idiopathic PD pathology. Several inflammatory hallmarks have shown to be increased within the patient brain and various toxin models, such as activated microglia (CNS-resident macrophages) within the SNc (Hirsch *et al.*, 2009) and increases in several cytokines (IL-1, -2, -6 and tumour necrosis factor-α) within the SNc and cerebral spinal fluid (Liu *et al.*, 2003).

It has been suggested that the neuromelanin, which accumulates within the SNc cells and gives it its blackened hue, is a target for autoimmune responses (Graham, 1979). The presence of

neuromelanin was found to cause dendritic cell maturation and phagocytosis (Oberlander *et al.*, 2011). Other studies suggest autoantibodies (antibodies that target the body's own cells rather than foreign ones) are the cause of SNc cell death. In further support of this theory, injecting immunoglobulin samples from PD patients into the rat SNc induces the activation of microglia and the degeneration of dopaminergic cells (Armando *et al.*, 2016; He *et al.*, 2002).

### 1.11.3. Neurotrophic factors as therapeutics for SNc cell survival

The delivery of specific neurotrophic trophic factors (NTFs) has generated therapeutic interest in PD. NTFs are a group of neuro-active molecules that have specific neuroprotective, pro-growth or modulatory roles when interacting with neuronal cells. Several NTFs have shown promise in models of PD and even human clinical trials. NTFs, such as brain-derived neurotrophic factor (BDNF) and glial derived neurotrophic factor (GDNF), are seen as interesting alternatives to current symptomatic relief therapeutics due to their interaction with dopaminergic cells (Allen *et al.*, 2013; Howells *et al.*, 2000).

BDNF has been used in preclinical settings as a potential neuroprotective agent. Interest was first raised when its reduced concentration was detected within the SNc and VTA of PD patients (Howells *et al.*, 2000; Scalzo *et al.*, 2010). It was later discovered that an increased expression of BDNF was caused by wild-type α-syn presence but not by mutant α-syn (products of the gene point mutations A53T and A30P). This indicates a relationship between SNCA gene mutants and the abnormal expression of BDNF (Kohno *et al.*, 2004). Despite the lack of trials in humans, preclinical studies have shown positive results concerning the efficacy of BDNF. It was discovered that BDNF treatment prevented MPTP-induced (Frim *et al.*, 1994) and 6-OHDA-induced SNc degeneration (Spina *et al.*, 1992). These toxin models of PD are explained in full in section 1.12.2.

GDNF has a close relationship with dopaminergic cells, where it has shown to induce differentiation and survival of the cells from embryonic midbrain cultures (Lin *et al.*, 1993). Several GDNF delivery studies have been conducted using rodent and NHP models with great symptomatic effect but with mixed cell survival results (Martin *et al.*, 1996; Winkler *et al.*, 1996). It was the interest and promise raised from these studies that led to the investigation of GDNF administration in clinical trials.

In 2003 a phase 1 open-label clinical trial was conducted analysing the effects of intraputamenal administration of GDNF (Gill *et al.*, 2003). The study stereotaxically administered GDNF continually for 12 months to the posterodorsal putamen of five idiopathic patients via abdominal pumps. The posterodorsal putamen was selected as it was theorised

that the GDNF would be retrogradely transported back to the cell bodies, via the NS, to aid in cell survival. Patients showed a significant improvement in activities of daily living and off-medication UPDRS scores when analysed with the UPDRS. However, with a low sample size and open-label approach, the study had a significant flaw in its design. Despite this, a 12 month follow up study saw further improvements in UPDRS scores (Patel *et al.*, 2005). Later, a second open-label intraputamenal study with differing methods proved also to be successful (Slevin *et al.*, 2006). These results led the field to conduct a controlled trial. Unfortunately due to insignificant alterations in UPDRS scores, the placebo-controlled trial, which had a more robust design than that of the previous trail, was a failure (Lang *et al.*, 2006). Follow up investigations in NHPs discovered that the method of GDNF administration may have caused the low availability of GDNF to the putamen. The method was criticised for having issues with reflux and not allowing maximal spread of the NTF throughout the putamen (Salvatore *et al.*, 2006).

More recently, pre-clinical trials have been conducted to identify optimum ways of NTF delivery. Viral vector based deliveries (Wang *et al.*, 2002) and nanoparticle technology (Fletcher *et al.*, 2011) have been adopted to promote long-term expression of NTFs. In addition, approaches to promote intrinsic NTF levels within the brain have also been investigated. Enzymatically removing certain components of the extracellular matrix (ECM; regions of space in between the cells of the CNS) is thought to liberate trapped NTFs and create a more favourable milieu for synaptic plasticity and regrowth. This ECM-manipulation strategy is based on a well-described spinal cord injury model that digests the chondroitin sulphate proteoglycans (CSPGs) of the ECM to promote neuronal regrowth following injury (Bradbury *et al.*, 2002). Although not fully investigated within PD, this approach could repair and protect degenerating neurones of the SNc. Utilising the ECM as a therapeutic target for SNc cell survival will be a central theme to this thesis.

### 1.11.4. The extracellular matrix

The ECM occupies the surrounding spaces between all glia and neurones of the CNS (i.e. the interstitial space and the basement membrane) and consists of a wide array of cell-secreted molecules. The ECM is vital to the neighbouring cells of the adult and of the developing brain. In an injured state, the ECM undergoes composition alterations that are seen to be detrimental to normal cellular function. As a result, it has been a key target for cell survival therapies of the CNS.

#### *1.11.4.1. Chondroitin sulphate proteoglycans*

The ECM consists of a wide array of multifunctional molecules (see Table 1). However, it is the CSPGs that are of most interest due to their axonal repair capabilities (Bartus *et al.*, 2012; Kwok *et al.*, 2008). There are several types of CSPGs, such as phosphacan, NG2, and the lecticans; the lecticans form the largest proportion of the CSPGs. These lecticans consist of aggrecan, versican, neurocan and brevican (two smaller lecticans exist, biglycan and decorin, but these are not significant to this thesis). CSPGs consist of several constituent components, at their centre resides the structural core protein that determines the *flavour* of the CSPG (e.g. neurocan, versican). These core proteins are then bound to highly sulphated glycosaminoglycan (GAG) disaccharide chains. The degree of core protein glycosylation depends on the particular CSPG subtype; aggrecan possesses the most GAG side-chains and brevican with the least (figure 6A). Several GAG types are known, such as, keratan sulphate, heparin sulphate, dermatan sulphate and chondroitin sulphate (CS); the latter being the most abundant within neural tissue (Hascall *et al.*, 1983; Lander, 1993; Ruoslahti, 1988). The GAG disaccharide chains are formed by the alternating glucaronic acid (GlcA) and N-acetyl glucosamine (GalNAc) residues bound by glycosidic bonds.

**Table 1: Extracellular matrix components.**
Chondroitin sulphate proteoglycans are one of many extracellular matrix molecules. The table below summarises the key function of many other components. PNNs; perineuronal nets, CSPGs; condroitin sulphate proteoglycans.

| ECM components | |
|---|---|
| | **Function** |
| **Laminin** | Essential for the basement membrane, required for cell adhesion |
| **Collagen** | Structural support by providing tensile strength and scaffolding |
| **Fibronectin** | Roles associated with cell adhesion, migration and proliferation |
| **Hyaluronan** | Anionic, unsulphated GAG which provides a scaffold to CSPGs and ECM integrity |
| **Tenascin-C/R** | Glycoproteins which interact with fibronectin and aid with cell signalling |
| **Link proteins** | Join CSPG core proteins to the hyaluronan scaffolding, required for PNN formation |
| **PNNs** | Pericullular lattice structures which are comprised of CSPGs and help define developmental critical periods |
| **CSPGs** | Collection of structures comprised of a core protein and sulphated CS-GAG side-chains |

All lecticans, aside from phosphacan, possess two key domains. Firstly, the N-terminal G1 domain which has a hyaluronan and link protein binding domain. This G1 region allows the complexing of CSPGs with the hyaluronan scaffolds. Secondly, the C-terminal G3 domain which contains a lectin binding region required for ECM interactions. The G3 domain permits the binding of CSPGs to tenascin which allows the cross linking of CSPGs. In addition to these common domains, aggrecan possesses the unique G2 domain that is homologous to the G1 domain. G2's function is not fully clear, although it is known not to bind to the link protein as found with the G1 domain (Kiani *et al.*, 2002).

Two atypical CSPGs exist as membrane bound glycoproteins, NG2 and phosphacan. NG2 is found on oligodendrocyte progenitor cells whereas phopshacan is the cleaved extracellular portion of the protein tyrosine phosphatase β receptor (figure 6A). Furthermore, unlike the rest of the CSPGs, phosphacan possesses a carbonic anhydrase (CAH)-like domain that binds to contactin for cell adhesion.

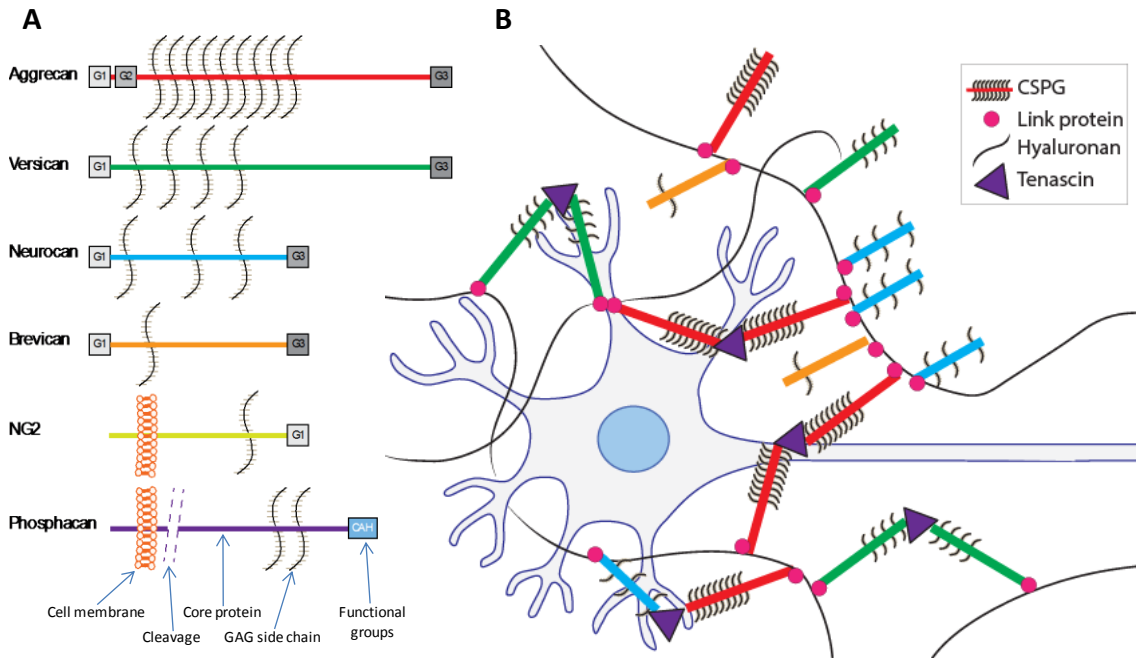


**Figure 7: Structure of the CSPGs within the extracellular matrix.**
(A) The six major CSPGs include the four lecticans, which are aggrecan, versican, neurocan and brevican, and also the transmembrane glycoproteins, NG2 and phosphacan. CSPGs bind to hyaluronan via link proteins to form the interstitial ECM structure. (B) Further cross-linking via tenascin helps form perineuronal nets that form around the cell soma and proximal dentrites.

Within the CNS, CSPGs have a significant role in the development and plasticity of neural systems during postnatal development (Pizzorusso *et al.*, 2002). However, within the adult brain their role is not known (Rhodes *et al.*, 2004). Evidence suggests that CSPGs are potentially neuroprotective in the adult brain, in which their highly sulphated-negative charge is thought to buffer divalent cations, such as $Ca^{2+}$ (Moos, 2002). An increase in $Ca^{2+}$ gives rise to ROS, so $Ca^{2+}$ buffering would therefore reduce ROS and cell death (Suttkus *et al.*, 2012). Moreover, studies examining amyloid related degeneration in Alzheimer's disease have presented a correlation between cells devoid of CSPG formations and increased AD-related neurofibrillary aggregates (Bruckner *et al.*, 1999). This reinforces the theory of CSPGs being beneficial to cell survival. However, extensive research into the upregulation of CSPGs during astroglial scar formation following spinal cord injury still suggests that CSPGs are inhibitory to neuronal growth and that their enzymatic degradation permits neuronal cell sprouting (Bradbury *et al.*, 2002). The case may be that CSPGs fulfil both roles of being a $Ca^{2+}$ buffer and a neuronal growth inhibitor within the adult CNS. It may be that the buffering effect is negligible after significant CNS damage and so CSPGs just perceive to be purely inhibitory (Rhodes *et al.*, 2004).

### *1.11.4.2. The perineuronal net*

CSPGs exist in a few forms within the ECM. A small number exist as non-aggregated units within the diffuse matrix, whereas a large majority are present in large pericellular structures known as perineuronal nets (PNNs). The PNNs are large lattice-like structures, comprised mainly of CSPGs (i.e. aggrecan) and cross-linking proteins such as tenascin that form a significant part of the ECM. Being pericellular formations, PNNs surround the neuronal cell body and extend down proximal dendrites of neuronal cells (Wang *et al.*, 2012b). The role this structure possesses differs throughout the mammalian lifecycle.

PNNs are significant to neuronal plasticity and the maturation of the CNS (Carulli *et al.*, 2006; Galtrey *et al.*, 2008), suggesting that their presence is led by neuronal activity and network development. Many regions have shown to possess PNNs, such as, the visual cortex, cerebellum, amygdala, hippocampus, spinal cord and the basal ganglia (Bruckner *et al.*, 2008; Dityatev *et al.*, 2007; Galtrey *et al.*, 2007). The plastic nature of the PNN is classically described within the developing visual system where the formation is said to close the *critical period*, a timeframe where stimulus driven neuronal activity causes the organisation of neuronal networks (Pizzorusso *et al.*, 2002; Wang *et al.*, 2011). Depleting the sensory input to these motor neurones is said to end the critical period as PNNs form and plasticity ceases (Kalb *et al.*, 1994).

Although the role of the PNN is largely associated with developmental plasticity, it is believed to still retain significance within the adult CNS, albeit an inhibitory one. Due to the high CSPG content, the PNN possesses an inhibitory role within the adult that is reversed by its removal. PNN digestion reactivates plasticity that leads to axon sprouting and repair within the CNS (Massey *et al.*, 2006). Although the exact mechanism behind this reactivation of plasticity is unclear, one theory states that as the ECM acts as a repository for many NTFs such as fibroblast growth factor-2, pleiotrophin and others (Mi *et al.*, 2007; Penc *et al.*, 1998). Its digestion therefore liberates an array of pro-growth agents creating a favourable milieu for increased cell plasticity and sprouting. It is feasible that such digestion may offer an alternative means of enhancing endogenous NTF levels in diseases that have a decline, such as PD.

## 1.12. Preclinical mammalian modelling of Parkinson's disease

Although a lot of biomarker and immunohistochemical work can be conducted on human post mortem tissue or with *in silico* modelling, the lack of behavioural and *in vivo* data can be critical. As a result, animal models of disease have been developed in order to replicate PD.

Two types of validity mark the successfulness of a model of PD these are *construct* and *face validity* (as described in (Chesselet *et al.*, 2011; Duty *et al.*, 2011). Construct validity describes how well the model replicates the pathogenesis of the disease (e.g. SNc denervation, inflammation), face validity on the other hand is a mark of how well symptomatology is represented in the model (e.g. rigidity, tremor, akinesia). No one model is considered *perfect* but some are seen as more applicable to certain studies than others. Both the pharmacological and toxin induced models are described below.

### 1.12.1. Pharmacological models of Parkinson's disease

Normally favoured for shorter and less invasive studies, the pharmacological models are typically transient and have far more face validity than construct. Nevertheless, the *quick and cheap* nature makes these models still used to this day.

#### *1.12.1.1. Reserpine*

Trade name: Raudixin, Serpasil, Serpalan

Type: alkaloid, antipsychotic, antihypertensive

Action: depletes catecholamines from nerve terminals

Reserpine irreversibly inhibits the monoamine transporter, VMAT2, the protein responsible for the transport of monoamines into vesicles at the presynaptic bulb. Inhibition of VMAT2 therefore halts the exocytosis of monoamines and the excitation of the postsynaptic neurone. Monoamines remaining in the cytoplasm of inhibited neurones are usually metabolised by COMT and MAO enzymes. A subcutaneous dose of 5 mg/kg reserpine reduces DA content in the rat striatum by 95% and the SNc by 85% within 2 hours of administration, this monoamine deprived state is maintained for ~24 hours before basal levels return (Duty *et al.*, 2011).

Reserpine reproduces good face validity in which the overall effect of DA depletion is evident by akinesia. However, the model has low construct validity as PD pathology is not present (e.g. cell loss). One of the major problems found with the model is the non-selective nature of the compound. As VMAT2 is a monoamine transporter, its inhibition affects the release of other monoamines, such as 5-HT. Despite this, some argue that this replicates the biochemistry found in PD patients whereby monamine deficiency also occurs (Duty *et al.*, 2011).

#### *1.12.1.2. Haloperidol*

Trade name: Haldol

Type: antipsychotic, antiemetic

Action: high affinity D2 receptor antagonist

As with reserpine, the overall construct validity of haloperidol is low (e.g. no SNc cell loss or other pathologies). On the other hand, face validity is replicated well with both catalepsy and rigidity exhibited. As a D2 receptor antagonist, and a D1 antagonist to a degree (Sanberg, 1980), haloperidol blocks the DA transmission in the striatum leading to aberrant firing patterns within the BG. This provides the aforementioned symptoms of catalepsy and rigidity. The behavioural phenotype of the model is short lasting and is maintained only a few hours after administration. This is considered a weak point in the construct validity of the model.

### 1.12.2. Toxin models of Parkinson's disease

Unlike the *easier* pharmacological models, toxin models require a more invasive and skilled approach to induce and reproduce. These usually present high construct and good face validity that is permanently maintained. As a result, these models are favoured for longer studies that require consistent phenotypes for the analysis of behavioural recovery over longer periods.

#### *1.12.2.1. 6-OHDA*

| | |
|---|---|
| A.k.a.: | 6-hydroxydopamine, oxidopamine |
| Type: | Toxic DA analogue |
| Action: | Reactive oxygen species generator; full mechanism not fully understood |

The 6-hydroxydopamine (6-OHDA) animal model has been one of the most commonly used in PD research since its discovery in the late sixties (Ungerstedt, 1968). As 6-OHDA does not cross the BBB, the toxin must be administered directly into the NS. Although requiring more skill to administer (i.e. stereotaxic surgical technique), this lack of BBB penetrance allows experimenters to induce hemiparkinsonian models. These animal models exhibit one lesioned hemisphere whilst the other is left unlesioned to act as an internal control. This model has been favoured by researchers assessing the functional recovery of animals following treatment by a reparative or protective agent over a long course. Any pathological improvements (e.g. cell survival, better behavioural outcomes) can then be observed in the lesioned hemisphere in comparison to the internal control. Phenotypic improvements are typically assessed by behavioural tests that distinguish the injured (a.k.a. parkinsonian) from the uninjured (a.k.a. control) sides of the body. A standard behavioural test that benefits from this unilateral model is the forelimb asymmetry test; this will be explained in detail in Chapter 3 section 3.3.4.6.

Another benefit of utilising 6-OHDA is its ability to be administered in one of three places within the NS for varying degrees of SNc denervation (Francardo *et al.*, 2011). The striatum is commonly selected to induce a partial lesion which replicates early-stage PD (~50-60% SNc cell loss) and is relatively progressive (taking several weeks to stabilise). This progression is due to the toxin being retrogradely transported back to the cell soma where toxicity is induced. Unlike the striatum, injections into the medial forebrain bundle (MFB) and SNc induce a full lesion; a model that more replicates late stage PD. Although lower doses may cause a lower cell loss, these routes are routinely used for consistent SNc ablation (>90% cell loss) and the swiftness at which they develop (<7 days). Although 6-OHDA is commonly used to induce hemiparkinsonian models, it can also be injected bilaterally for further effects (e.g. adipsia, severe akinesia).

However, mortality rates are drastically higher in these animals and therefore require much stricter post-operative care.

Upon administration, 6-OHDA is transported into the dopaminergic nerve terminals by the DA transporter (DAT). Due to the structural similarity to other catacholamines, 6-OHDA has a low affinity for other transporters such as the noradrenaline transporter which can result in off-target cell loss (Luthman *et al.*, 1989). To counter this, a noradrenaline transporter inhibitor such as desipramine can be co-administered with 6-OHDA to increase selectivity for DAT. This limits 6-OHDA's toxicity to the dopaminergic A9 and A10 neurones of the SNc and VTA, respectively. As the A10 neurones are not part of the motor circuit involved in PD, the A9 neurones are specifically targeted by stereotaxic injection to minimise A10 cell death. Pargyline, an irreversible MAO-B inhibitor, may also be administered to reduce the breakdown of 6-OHDA by MAO. This thereby lowers the required dose of 6-OHDA administered.

The mechanism of 6-OHDA's toxicity is multifaceted when compared to other toxins such as MPTP. Once 6-OHDA enters the neurone, cellular degeneration occurs through a few means. Firstly, the generation of ROS through auto-oxidation is thought to be the main cause of toxicity. Under physiological conditions, 6-OHDA can form $H_2O_2$ and the hazardous quinone molecules that, in the presence of Fe, can form harmful hydroxyl free radicals (Rodriguez-Pallares *et al.*, 2007; Soto-Otero *et al.*, 2000). Secondly, 6-OHDA has been found to directly interact and interrupt both complex I and complex IV of the ETC (Glinka *et al.*, 1997). This reduces ATP production within the cell and causes cell death. Finally, evidence suggests that 6-OHDA decreases the mRNA levels of the antioxidant enzyme SOD in the SNc (Kunikowska *et al.*, 2001).

The 6-OHDA rodent model has been a mainstay in PD research for nearly 50 years. The model, available in both the rodent and NHP, recapitulates the pathology of SNc degeneration, reduction in striatal DA, mitochondrial dysfunction and ROS production. However, it does lack key features such as LB-like inclusions or the dysfunction of other brain circuits outside of the BG. Construct validity is adequate as several factors such as ROS production and complex I inhibition are present. Face validity is high in which DA loss is significant and the resulting parkinsonian motor dysfunction is apparent. Despite some weaknesses, this toxin model is highly effective at predicting disease state (i.e. severity of lesion correlating with parkinsonism severity). This model has been solely used throughout the studies presented in this thesis.

#### *1.12.2.2. MPTP*

A.k.a.: 1-methyl-4-phenyl-1,2,3,6-tetrahydropyridine

Type: BBB penetrative proform of the 1-methyl-4-phenylpyridinium ($MPP^+$) toxin

Action: Inhibitor of Complex I of the electron transport chain

MPTP was initially discovered in the 1980s when heroin users accidentally formulated MPTP instead of the desired 1-methyl-4-phenyl-4-propionoxypiperidine opioid. Upon systemic administration to users, the damaging effects of MPTP closely resembled PD (Langston *et al.*, 1983). It was later found that MPTP's toxic metabolite $MPP^+$ specifically targeted SNc cells and resulted in the reduction of striatal DA. Since this discovery, both rodent and NHP models have been developed to reproduce parkinsonism through MPTP toxicity.

Being lipophilic, MPTP readily crosses the BBB and is therefore systemically active (Riachi *et al.*, 1989). Once within the brain MPTP is taken up by glia, namely astrocytes, and metabolised into the aforementioned toxic metabolite $MPP^+$ by MAO-B. This toxic by-product is then released from the glia into the intracellular space, before being transported into the neighbouring neurones via DAT. Once it has entered the cytosol, $MPP^+$ gathers within mitochondria and inhibits complex I of the ETC. This leads to two toxic results, the interruption of ATP synthesis and the production of ROS (Zawada *et al.*, 2011). These two factors are the primary cause of cell death. As these pathologies are present within PD this toxin model presents good construct validity.

Due to its BBB penetrative nature, systemic MPTP administration is far easier to administer than 6-OHDA which requires skilled stereotaxic surgery. The caveat to this being the inability to create a hemiparkinsonian model; removing the convenience of an internal control limb when conducting behavioural analyses. However, this bilateral denervation of the BG replicates the state of parkinsonism far better than 6-OHDA, especially within the NHP.

Although both mice and NHP are used, it is the NHP (e.g. macaque monkey), which is commonly used as the *gold-standard* MPTP PD model. This is because the NHP model recapitulates all of the main behaviours associated with PD, such as rigidity, bradykinesia and abnormal postural positioning (Bezard *et al.*, 2011) plus NMS such as sleep disturbances, cognitive impairment and LID (Barraud *et al.*, 2009; Bezard *et al.*, 2003; Schneider, 1990). The NHP MPTP model presents a wide array of PD symptoms and therefore shows strong face validity.

However, due to the expensive upkeep of the NHPs, this model is frequently exchanged for the MPTP mouse. This rodent model is considered a *trade-off* between model validity (e.g. lack of typical PD-like symptoms) and expense. Interestingly due to an innate insensitivity to MPTP, the rat model is not used. Although not fully understood, this is thought to be in part due to the higher level of VMAT2 present within rat striatal vesicles (Staal *et al.*, 2000). Recent work theorises that VMAT2 sequesters toxins into vesicles as a method of toxin removal (Lohr *et al.*, 2016). Like the rat, the mouse does retain some insensitivity to MPTP and, as a result, subchronic administrations of MPTP lead to transient phenotypes (Colotla *et al.*, 1990). These transient phenotypes are deemed of little use in testing drug efficacies, therefore to maintain a more testable phenotype a chronic dosing schedule is enforced. A common practice is to co-administer probenecid (a drug which promotes uric acid excretion) with MPTP to enhance the effects of the toxin via inhibition of urinary clearance (Lau *et al.*, 1990). In recent years the development of continuous MPTP administration through osmotic pumps has been developed. Models with a continuous delivery of MPTP present typical pathologies of PD, such as even α-syn- and ubiquitin-positive inclusions (Fornai *et al.*, 2005; Meredith *et al.*, 2008). However, this model exhibits issues with its predictive nature whereby lesion size does not always correlate with behavioural outcomes (Duty *et al.*, 2011; Gibrat *et al.*, 2009).

#### *1.12.2.3. Rotenone*

Trade name: Tubatoxin, Paraderil

Type: Pesticide

Action: Inhibitor of Complex I of the electron transport chain

Rotenone, as with MPTP, is an inhibitor of the ETC and is systemically active. Rotenone is a pesticide that was investigated in 2000 as a potential model of PD. When intravenously administered via osmotic mini pumps the neurochemical, neuropathological (including LB-like inclusions) and behavioural features of idiopathic PD were replicated (Betarbet *et al.*, 2000b). Although the model presents good face validity, the consistency of the model has been a significant issue with its use. Toxin resistance has been shown by some animals, whereby only ~50% of treated animals display PD-like symptoms seen in the original Betarbet paper.

Other ETC inhibitors of note are paraquat and maneb, both of which produce similar effects to rotenone (Saint-Pierre *et al.*, 2006; Thiruchelvam *et al.*, 2003).

#### *1.12.2.4. Lactacystin*

Trade name: n/a

Type: Bacterial (Streptomyces genus) toxin

Action: Inhibitor of the proteasome

Reduced activity of the UPS has been identified within the SNc of PD idiopathic patients (McNaught *et al.*, 2001). Alongside this observation, ubiquinated α-syn has been located within surviving SNc neurones indicating a UPS response to α-syn accumulation. This lowered ability to metabolise damaged, misfolded or accumulated proteins within cells is believed to lead to apoptosis. However, the role the dysfunctional UPS plays in the pathogenesis or manifestation of the neurodegeneration seen in PD is not certain.

In view of this finding, the lactacystin animal model of PD was established in an attempt to replicate both the proteasomal dysfunction and SNc cell death associated with PD. The bacterial toxin lactacystin was found to induce not only cell death but also the accumulation and aggregation of α-syn-positive inclusion bodies within the rodent. Similarly, administration of other proteasome inhibitors such as PSI and epoximycin induce typical parkinsonian effects (McNaught *et al.*, 2002; Xie *et al.*, 2010). In the rodent this model induces bradykinesia and rigidity which is reversed by L-DOPA administration (McNaught *et al.*, 2004). Due to the SNc cell loss, inclusion presence and motor dysfunction, this model retains good construct and face validity. Despite robust validity, the use of this model has been limited. This is in part due to the inconsistent reproduction of the model, whereby several labs were not able to recreate the motor dysfunction or cell loss first described (Kadoguchi *et al.*, 2008; Kordower *et al.*, 2006; Manning-Bog *et al.*, 2006). Although promising, this model requires further validation.

### 1.12.3. Genetic models of Parkinson's disease

Identifying the genes responsible for familial PD has led to the creation of transgenic models of disease.

#### *1.12.3.1. α-synuclein*

Action: A30P and A53T mutations in drosophila and mouse; A53T in rat

The identification of the autosomal-dominant α-syn mutation led to the generation of the α-syn transgenic model (Chesselet *et al.*, 2011). This model has been developed in mouse, rat and drosophila, each with varying results. Mouse models have shown, quite surprisingly, no loss in DA and no responsiveness to L-DOPA. An opposite result to the rat which has L-DOPA responsiveness whilst displaying LB-like inclusions. Furthermore, drosophila models possess not only DA loss and LB-like inclusions but are responsive to L-DOPA despite having no mitochondrial dysfunction (Dawson *et al.*, 2010). These models report inconsistency in SNc cell loss and as a result have not established a significant role in PD modelling as of yet.

#### *1.12.3.2. MitoPark*

Action: Cre-loxP conditional knockout of TFAM; DA cell targeted

The MitoPark mouse is a dopaminergic conditional knockout model of the mitochondrial transcription factor TFAM. It was first established to replicate the many familial forms of PD which present mitochondrial dysfunction. The knockout is generated by crossing knock-in Cre recombinase (DAT promoter driven) mice with mice expressing a loxP flanked TFAM gene. This allows the conditional deletion of the TFAM gene in cells expressing DAT, resulting in the inhibition of the respiratory chain (Ekstrand *et al.*, 2009). The phenotype presents a slow progressive loss of BG dopaminergic neurones resulting in reduced striatal DA content and typical motor impairments. Intraneuronal LB-like inclusions can also be found. Moreover, a recent study found MitoPark mice recapitulating typical MRI alterations found within the PD patient, such as ventricular volume and Fe accumulation (Cong *et al.*, 2016). The construct and face validity of the model is significant as both PD pathogenesis and symptomatology are well represented. Despite this model not being widely available yet, it shows promise as a genetic model of disease.

## 1.13. General aims of this thesis

As previously described there are two key unmet clinical needs in PD research, these are: facilitating the neurorepair and/or protection of the vulnerable SNc cells and understanding the mechanisms behind the LID phenomenon.

This thesis has attempted to, firstly, investigate novel ways of providing neuroprotection and repair of the degenenerating SNc cells and, secondly, further identify the mechanism underlying LID. The broad aims and their reasoning are described below.

### 1.13.1. Aims

The CSPGs and PNNs have been considered inhibitory to cellular plasticity and regrowth following injury for many years in the spinal cord injury field. Since the early 2000's, investigators in the field have utilised the ECM as a therapeutic target to induce motor recovery. Here we suggest that the CSPGs and PPNs may have significance in PD.

*Aim of Chapter 2: Examine the expression of CSPGs in the NS*

CSPGs may play a role in the NS and may therefore be responsible for the inhibition of axonal repair. However, little is known about these molecules in context of PD. In Chapter 2 of this thesis, we aimed to perform preliminary studies to examine the expression of CSPGs in the NS in order to establish whether these molecules are likely to be useful targets in the treatment of PD.

*Aim of Chapter 3: Investigate the potential of ECM manipulation in the repair or protection of the SNc cells in a rodent model of PD*

Having confirmed their presence in relevant mouse brain regions, we aimed to investigate whether enzymatic digestion of the CSPGs and PNNs can induce restoration of the injured NS. A venture explored in the spinal cord injury field but not extensively within PD research. It would be of great interest to determine the efficacy of the strategy in both late stage (full) and early stage (partial) 6-OHDA lesion models of disease.

*Aim of Chapter 4: Identify a method of enhancing NTF levels within the BG, and also whether enhanced NTF levels could induce repair or protection of the SNc cells in a rodent model of PD*

As described in 1.11.3., increasing the level and/or expression of NTFs, such as GDNF, in patients with PD has been of significant interest. Be it in animal or Man, no method has attempted to increase *endogenous* release of NTF within the damaged NS without the use of viral vector delivery; a technique which provides many safety considerations. We therefore aimed to identify whether the treatment of systemic NTF-release agents in the unilateral lesion 6-OHDA model increases cell survival.

*Aim of Chapter 5: Investigate the mechanism behind LID by identifying any cellular changes which occur within the dyskinetic striatum*

The mechanism behind LID has not yet been identified. Current theories indicate aberrant plastic changes that occur in the striatum and the corticostriatal pathway. In order to attempt to counter the effects of LID, further investigations into its manifestation are required. We therefore aimed to identify any gross striatal changes via neuroimaging and then focus on any cellular alterations that may unravel the mechanism of LID.

# 2. Investigating the distribution of chondroitin sulphate proteoglycans in the mouse basal ganglia

## 2.1. Introduction

### 2.1.1. Chondroitin sulphate proteoglycans as therapeutic targets

The chondroitin sulphate proteoglycans (CSPGs) are a key focus of this thesis. As these extracellular matrix (ECM) molecules have been described as modulators of plasticity, we wished to target the CSPGs for cellular repair and protection strategies.

As briefly described in the general introduction, CSPGs are considered inhibitory to axonal growth through means not fully known (see Chapter 3 for two main theories). Despite this, their removal is well established as being beneficial to growth following injury to the CNS (Bradbury *et al.*, 2002). These CSPGs can crosslink around the cell soma to form perineuronal nets (PNNs); pericellular formations which have been described as key regulators of plasticity within the neonate and developing systems (Wang *et al.*, 2012a). CNS injury has been identified to induce CSPG deposition in an attempt to, presumably, limit damage to the surrounding tissues. This process has been seen to inhibit any recovery in the long term (Fitch *et al.*, 1997; Moon *et al.*, 2002).

CSPGs are interesting targets for novel PD therapeutic strategies, as they are considered inhibitory to growth as well as regulators of plasticity. However, before assessing the efficacy of CSPG removal in a model of PD, we must first characterise the CSPGs within the mouse through immunohistochemical means. This will help identify which CSPGs may have relevance to PD through their expression in the BG.

### 2.1.2. The distribution of CSPGs in the mammalian CNS

Certain CSPGs have been identified as being localised to particular CNS tissues in the past. Although not specific to the mouse BG, these studies have aided our understanding of CSPGs within the brain. The distribution and characteristics of several CSPGs in the mammalian CNS are described below.

#### *Aggrecan*

Aggrecan is the most glycosylated member of the lectican family. It is expressed within both connective and neural tissues whilst also being an essential component in cartilage. However, its most interesting role in the ECM is within the PNN where it is required for the formation and function of its structure; aggrecan is required more than other CSPGs (Morawski *et al.*, 2012). Aggrecan and the PNN are therefore in concert in controlling neuronal plasticity. As with the PNN, it is likely that aggrecan manipulation would be required for the reopening of the *critical period* (i.e. the period where stimulus driven neuronal plasticity causes the organisation of neuronal networks) to induce neuronal rewiring and growth.

#### *Versican*

Versican remains a unique lectican as it has several core protein splice variants. Versican's GAG binding region is encoded by two genes, GAGα and GAGβ. With these, versican can form four different isoforms depending on the presence of these domains (see Table 2).

**Table 2: Isoforms of versican.**
Differential splicing of the two GAG region genes dictate the final isoform of that specific versican. Four isoforms exist.

| Versican isoforms | |
|---|---|
| | **GAG domains present** |
| **$V_0$** | Both GAGα and GAGβ in core; the largest versican isoform |
| **$V_1$** | Only the larger GAGβ in core |
| **$V_2$** | Only the smaller GAGα in core |
| **$V_3$** | Neither in core; smallest versican isoform |

Versican is expressed in both the CNS and other regions, with the $V_2$ variant being the most plentiful in neuronal tissues (Paulus *et al.*, 1996). Interestingly, $V_2$ versican has been found expressed by immature oligodendrocytes during development (Asher *et al.*, 2002). This presents an interesting link between the inhibitory nature of both CSPGs and oligodendrocytes (which are recruited to CNS injury).

#### *Brevican*

Brevican is the smallest and least glycosylated lectican CSPG and is widely prevalent throughout the adult CNS. Brevican is expressed by immature oligodendrocytes and by astrocytic cells (Yamada *et al.*, 1997a). Once again, this links the CSPGs to the glial cells of the CNS.

#### *Neurocan*

Neurocan is another lectican CSPG that is brain specific in its expression. Produced by oligodendrocyte progenitors, astrocytes and neurones (Asher *et al.*, 2000; Meyer-Puttlitz *et al.*, 1996; Oohira *et al.*, 1994), neurocan appears to have a relationship with glial and neuronal cells alike.

#### *NG2*

Although not a member of the lectican family as the others before, NG2 is of interest due to its close relationship with the immune system. As described in the General Introduction (section 1.11.4.1.), NG2 are transmembrane CSPGs which are predominantly expressed on the surface of oligodendrocyte progenitor cells. Interestingly, NG2 has been suggested to also associate with microglia whereby the colocalisation of microglial-specific markers and NG2 has been identified (Pouly *et al.*, 1999). However, this is debated as a distinct difference in localisation has also been found (Levine, 1994).

### 2.1.3. The ECM and the lectican CSPGs following birth

It has been previously discussed that CSPGs and PNNs have significance in early development. However, their role in later life has not been fully identified. As idiopathic PD is an age-related disease, we must not forget that the distribution of CSPGs in the elderly may be different to the young adult used in many of these experiments. Therefore, it is of importance to understand the nature of CSPG expression (namely the lecticans) at this stage.

In the days following birth, the ECM undergoes several changes in which CSPGs that are high in the neonate are slowly exchanged for an array of CSPGs found in the adult CNS. CSPGs in high expression during the neonate period are neurocan and the $V_0/V_1$ versican isoforms. These are then replaced by more typical adult CSPGs such as $V_2$ versican, aggrecan and brevican (Milev *et al.*, 1998). $V_2$ versican and brevican presence is mostly found in white matter due to their association with oligodendrocytes and myelinated axons (Ogawa *et al.*, 2001) and aggrecan presence is mostly associated with PNNs (Morawski *et al.*, 2012).

This switch from neonatal to adult CSPG subsets can be associated with the closing of critical

periods and the reduction in axonal plasticity as an attempt to *lock down* neuronal pathways. To further understand this switch, Milev *et al.* took whole brain extracts of rats of varying ages ranging from neonate (day 0) to adult (day 250) in order to assess the levels of lectican CSPGs present. Figure 7 adapts the data from that study to clearly show the changes occurring at different ages of the rodent brain.

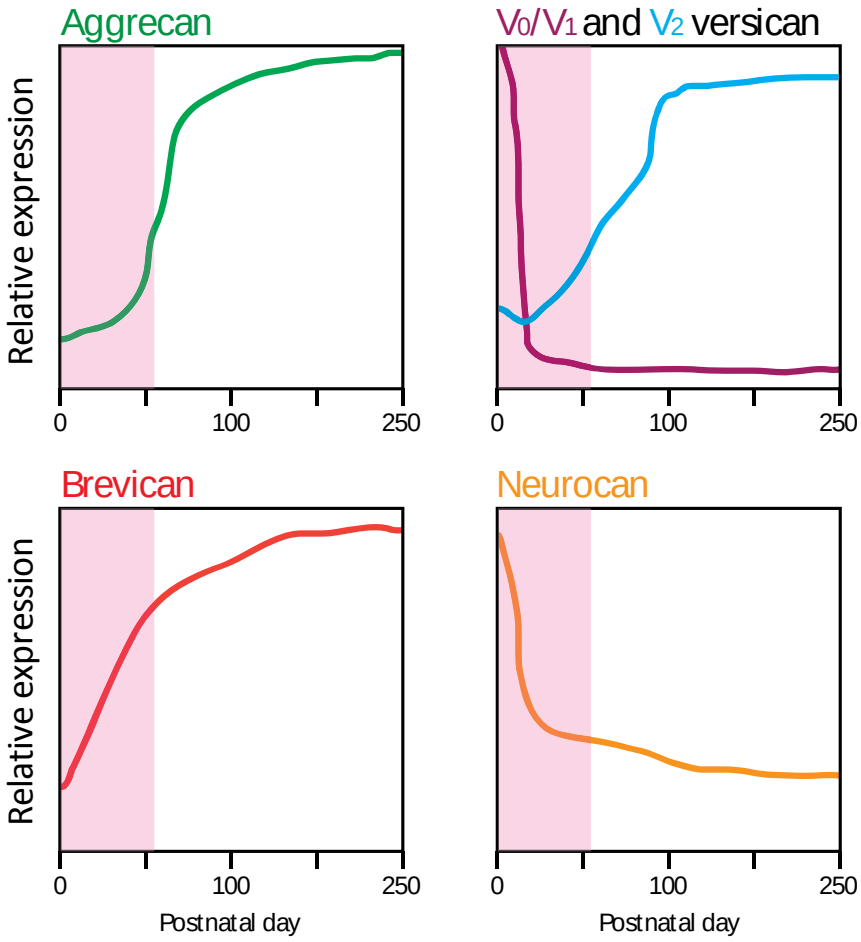


**Figure 8: Time course of CSPG expression in the rat from birth to adult.**
Neurocan and $V_0/V_1$ versican are both expressed to a high degree in neonatal rats. These levels start to decline as other lecticans are expressed more highly in the brain, such as aggrecan, $V_2$ versican and brevican. Pink regions highlight postnatal day 56 (8 weeks old); the common age of young adult animals used throughout this thesis. Plots are estimations based on data from (Milev *et al.*, 1998).

With these data clearly presenting alterations in ECM composition in the postnatal versus adult rodent brain it may be of benefit to look beyond 250 days. As PD is age-related, investigations of CSPG distributions in aged animals may reveal new insights in ECM-targeted therapies; novel agents may work differently in young adult and aged brains. Such differences would then need to be taken into account when either designing or interpreting the studies aimed towards the investigation of the therapeutic target potential of CSPGs in PD rodent models.

### 2.1.4. Study rationale

Although aggrecan-associated PNN expression has been previously mapped in the human BG (Bruckner *et al.*, 2008), there has been no characterisation of PNNs and CSPGs within the mouse BG, specifically the SNc and striatum. Therefore, before proceeding with large investigative studies that manipulate the ECM, we first set out to confirm the presence of at least one type of CSPG within the mouse BG. In particular, we were keen to identify which CSPGs were present in the mouse SNc. Preliminary investigations saw very weak staining for both brevican and neurocan in the adult mouse BG (which was not possible to image in thin paraffin embedded sections), for these reasons, these two CSPGs were not investigated further. However, the expression of aggrecan, versican and NG2 were examined.

In addition to identifying specific CSPGs, we wished to investigate the localisation of PNNs within the mouse SNc. PNN expression has been shown to be devoid in the dopaminergic systems of the human BG (Bruckner *et al.*, 2008). We wished to investigate whether this was also the case within the naive mouse. If so, a lack of PNNs within the SNc region may explain the enhanced neuronal susceptibility the cells possess to ROS and other means of degeneration.

Finally, as PD is an age-related disease we wished to investigate the expression of certain CSPGs within the young adult and aged mouse brain. Such comparisons may explain the pathophysiology of ageing. It would also determine whether CSPGs are appropriate targets in PD. If they were not present in the aged BG, CSPG-related interventions may be ineffective in PD.

## 2.2. Aims and Hypotheses

This chapter presents two brief investigations into the distribution of CSPGs within the naive mouse BG. The first study was a qualitative investigation of aggrecan, versican (all isotypes due to selectivity of the antibody used), NG2 and PNN expression within the naive mouse SNc.

The final study, investigated the expression of aggrecan, CS56 (pan intact CS-GAG antibody) and tyrosine hydroxylase (TH) in the young adult (8 weeks old) compared to the aged mouse (18 months old). The aims and hypotheses for these studies are described below.

Study aims:

1. *Investigate whether there is expression of aggrecan, versican and NG2 in the adult mouse SNc and surrounding regions. Which CSPGs may be worthwhile investigating in later studies?*

2. *Determine whether PNNs are found associated with the dopaminergic cells of the mouse SNc*

3. *Investigate whether age is a factor in the expression of aggrecan, CS56 and/or TH in the naive aged (18 months old) and young adult (8 weeks old) mouse*

Study hypotheses:

1. *The adult mouse expresses aggrecan, versican and NG2 in the SNc and surrounding regions. All three CSPGs are worth investigating in later investigations.*

2. *PNNs are found not to be associated with the dopaminergic cells of the SNc*

3. *The expression of aggrecan, CS56 and TH is not different in the naive aged (18 months old) compared to the young adult (8 weeks old) mouse*

## 2.3. Materials and Methods

### 2.3.1. Investigative study 1: Identifying CSPGs and perineuronal nets within the naive mouse SNc

#### *2.3.1.1. Naive mouse tissue used*

6 formalin perfused fixed brains from eight-week-old male C57Bl/6 mice (Harlan, UK) were used in this study; courtesy of Dr Martin Broadstock.

3 formalin perfused fixed brains were used for CSPG identification, these were previously embedded in paraffin wax and ready to be sectioned. The remaining 3 perfused fixed brains were to be embedded in gelatin and sectioned for PNN identification. Gelatin embedding was conducted on these 3 brains to obtain thicker sections which were required to identify the diffuse PNN structure.

#### *2.3.1.2. Sectioning of the paraffin embedded brains*

The 3 paraffin embedded brains containing the SNc were sectioned (7 µm thick sections) with a microtome (Thermo Scientific) at three rostrocaudal levels of the SNc (rostral: -2.92 mm, medial: -3.16 mm and caudal: -3.52 anteroposterior [AP] mm; relative to bregma). Sections were then mounted on Poly-L-lysine coated slides (VWR Int.; 4 sections per slide) before being stored at 60°C over night.

#### *2.3.1.3. CSPG staining in paraffin embedded naive SNc sections*

Coronal sections were deparaffinised (2x 5 minutes in xylene before 4x 2 minutes in 100% methanol immersions). 3% $H_2O_2$ (10 minutes) immersion allowed the quenching of endogenous peroxidases before sections were boiled within a 1 mM citric acid antigen retrieval solution (pH 6) for 10 minutes. Blocking solution (1% bovine serum albumin [BSA] in 0.05M Tris buffered saline (TBS) with 1% sodium azide, pH 7.6) was applied to the sections (10 minutes) prior to the 24 hour incubation with either aggrecan, NG2 or versican primary antibody (see Table 3 for dilutions). A biotinylated anti-rabbit IgG secondary antibody (see Table 3) was applied before a final incubation with the streptavidin-biotinylated horseradish peroxidase conjugate (VectorLabs PK6100 Vectastain Elite ABC kit) for 30 minutes at room temperature. Slides were immersed in diaminobenzidine tetrachloride (DAB) developing buffer (10% DAB in 200 ml 0.1M TBS with 0.03% $H_2O_2$, pH 7.6) for 10 minutes. Finally, sections were rinsed thoroughly in distilled $H_2O$ for 10 minutes to remove any traces of DAB, dehydrated in 100% methanol (4x 2 minutes immersions) and cleared in xylene (2x 5 minute immersions). Sections were mounted with coverslips using the solvent based plastic mountant, DPX.

### 2.3.1.4. Gelatin embedding

The 3 remaining perfused fixed brains were submerged within cryoprotectant (30% sucrose, 0.01% Sodium Azide in PBS) until sunk. Tissue was then set within gelatin (10% porcine skin type A gelatin in 0.1 M PBS) then further post fixed in 10% buffered (pH 7.4) formalin for 8 hours. The set gelatin block was trimmed and frozen on a freezing sledge microtome. A series of 40 µm parasagittal sections of the SNc were then taken and stored as free-floating sections within PBS at 4°C.

### 2.3.1.5. bWFA and TH fluorescence staining of PNNs and SNc cells on free floating sections

Parasaggital sections (which contained the SNc: +0.96 mm mediolateral [ML]; relative to bregma) were washed in TBS (3x 5 minutes) before a blocking solution (3% normal goat serum (NGS)) was added for 1 hour at room temperature. The TH primary antibody and biotinylated WFA (see Table 3) were left to incubate with the sections overnight at room temperature. After TBS washes (3x 5 minutes) Alexa Fluor 546 (see Table 3) was applied for 3 hours at room temperature. ExtrAvidin-FITC (see Table 3) was then administered with DAPI (1 µg/ml) for 2 hours. Vectorshield (VectorLabs) was then used to mount coverslips onto the sections; nail polish was used around the edges of the slide to stop the section from drying out.

**Table 3: Investigative Study 1: Antibodies used for immunohistochemistry.**
The following antibodies were used at their described dilutions and according to the histology protocol described above.

| Immunohistochemistry antibodies | | | | | |
|---|---|---|---|---|---|
| **Antibody** | **Type** | **Antigen** | **Host** | **Dilution** | **Supplier** |
| Aggrecan | Primary | CSPG core protein | Rabbit; polyclonal | 1 in 200 | ab36861; Abcam |
| Versican | Primary | CSPG core protein | Rabbit; monoclonal | 1 in 200 | ab177480; Abcam |
| TH | Primary | Tyrosine hydroxylase | Rabbit; polyclonal | 1 in 500 | AB152; Millipore |
| NG2 | Primary | CSPG core protein | Rabbit; polyclonal | 1 in 200 | ab5320; Abcam |
| biotinylated *Wisteria floribunda* agglutinin | Primary | PNNs | Plant agglutinin | 1 in 500 | L1516; Sigma Aldrich |
| Alexa Fluor 546 | Secondary | rabbit primary ABs | Goat IgG (H + L) | 1 in 200 | A-11035; Invitrogen |
| ExtrAvidin-FITC | Secondary | conjugates with biotin | Egg white avidin | 1 in 200 | E2761; Sigma Aldrich |
| biotinylated anti-rabbit | Secondary | rabbit primary ABs | Goat IgG (H + L) | 1 in 200 | BA1000; Vector Labs |

### 2.3.1.6. Image analysis

CSPG expression images of the SNc were imaged at 5X magnification (Axioskop, light-field compact microscope). TH and bWFA fluorescently labelled parasaggital SNc sections were imaged using a wide field fluorescence microscope (Zeiss) and Axiovision software at 20X magnification.

Digital TIFF format images were equilibrated in Adobe Photoshop CS5 in order to create the background uniform in terms of brightness and contrast.

No analysis was performed in the first investigative study, as this was purely a qualitative venture to identify whether particular CSPGs were present in the mouse SNc.

### 2.3.2. Investigative study 2: Comparing TH and CSPG distribution within the young and aged mouse

#### *2.3.2.1. Naive young adult and aged mouse tissue*

5 perfused fixed brains from eight-week-old and 5 perfused fixed brains from eighteen-month-old male C57Bl/6 mice (Harlan, UK) were used; courtesy of Dr Martin Broadstock.

The perfused fixed brains were previously embedded in paraffin wax and were ready to be sectioned. Sectioning was conducted as described in section 2.3.1.2. Sections of the three rostrocaudal levels of the SNc (rostral: -2.92 mm, medial: -3.16 mm and caudal: -3.52 AP mm; relative to bregma) and the striatum (rostral: +1.0 mm, medial: +0.5 mm and caudal: -0.22 AP mm; relative to bregma) were taken.

#### *2.3.2.2. Tyrosine hydroxylase and CSPG staining in the young adult and aged mouse SNc and striatum*

Coronal sections were deparaffinised (2x 5 minutes in xylene before 4x 2 minutes in 100% methanol immersions). 3% $H_2O_2$ (10 minutes) immersion allowed the quenching of endogenous peroxidises before sections were boiled within a 1 mM citric acid antigen retrieval solution (pH 6) for 10 minutes. Blocking solution (1% bovine serum albumin [BSA] in 0.05M Tris buffered saline (TBS) with 1% sodium azide, pH 7.6) was applied to the sections (10 minutes) prior to the 24 hour incubation with either aggrecan, CS56 or TH primary antibody (see Table 4 for dilutions). A biotinylated anti-rabbit IgG or biotinylated anti-mouse IgG secondary antibody (see Table 4) was applied (depending on the host of the primary antibody) before a final incubation with the streptavidin-biotinylated horseradish peroxidase conjugate (VectorLabs PK6100 Vectastain Elite ABC kit) for 30 minutes at room temperature. Slides were immersed in diaminobenzidine tetrachloride (DAB) developing buffer (10% DAB in 200 ml 0.1M TBS with 0.03% $H_2O_2$, pH 7.6) for 10 minutes. Finally, sections were rinsed thoroughly in distilled $H_2O$ for 10 minutes to remove any traces of DAB, dehydrated in 100% methanol (4x 2 minutes immersions) and cleared in xylene (2x 5 minute immersions). Sections were mounted with coverslips using the solvent based plastic mountant, DPX.

**Table 4: Investigative Study 2: Antibodies used for immunohistochemistry.**
The following antibodies were used at their described dilutions and according to the histology protocol described above.

| Immunohistochemistry antibodies | | | | | |
|---|---|---|---|---|---|
| **Antibody** | **Type** | **Antigen** | **Host** | **Dilution** | **Supplier** |
| Aggrecan | Primary | Protein core protein | Rabbit; polyclonal | 1 in 200 | ab36861; Sigma Aldrich |
| CS56 | Primary | Intact CS-GAGs | Mouse; monoclonal | 1 in 1000 | ab11570; Sigma Aldrich |
| TH | Primary | Tyrosine hydroxylase | Rabbit; polyclonal | 1 in 500 | AB152; Millipore |
| biotinylated anti-rabbit | Secondary | rabbit primary ABs | Goat IgG (H + L) | 1 in 200 | BA1000; Vector Labs |
| biotinylated anti-mouse | Secondary | mouse primary ABs | Goat IgG (H + L) | 1 in 200 | BA9200; Vector Labs |

#### *2.3.2.3. Image analysis of CSPG and TH presence in young adult and aged striatum*

Densitometry images for the immunohistochemistry markers were acquired with a Canon DSLR camera with a macro lens. Digital TIFF format images from all treatment groups were equilibrated in Adobe Photoshop CS5 in order to create the background uniform in terms of brightness and contrast. ImageJ (publically available: National Institutes of Health) was used to measure the optical densities of CSPG and TH stain within the striatum.

6 sections per marker were used across the rostrocaudal axis per animal (two caudal, two medial and two rostral striatum). Using the freehand tool in ImageJ, the dorsal or ventral striata were selected and their optical densities obtained (both the left and right hemispheres were analysed and averaged). Each optical density at each rostrocaudal level was then averaged to create a representative degree of expression throughout either the dorsal or the ventral striatum. These results were then averaged across all animals in their respective groups. This gave a representative optical density for the marker in either the dorsal or ventral striatum of either the young adult or aged mice.

#### *2.3.2.4. Image analysis of CSPG presence in young adult and aged SNc*

SNc densitometry images for the immunohistochemistry markers were obtained as described above in section 2.3.2.3.

6 sections per marker were used across the rostrocaudal axis per animal (two caudal, two medial and two rostral SNc). Using the freehand tool in ImageJ, the SNc was selected and its optical density obtained (both the left and right hemispheres were analysed and averaged). Each optical density at each rostrocaudal level was then averaged to create a representative degree of expression throughout the SNc. These results were then averaged across all animals in their respective groups. This gave a representative optical density for the marker in the SNc of either the young adult or aged mice.

#### *2.3.2.5. Assessment of the number of TH-positive SNc cells within the aged and young adult naive mouse brain*

TH-positive cells were imaged at 10X magnification (Axioskop, light-field compact microscope). Digital TIFF format images from all treatment groups were equilibrated in Adobe Photoshop CS5 in order to create the background uniform in terms of brightness and contrast. ImageJ (publically available: National Institutes of Health) was used to count the TH-positive cells.

Triplicate sections (three sequential sections) were taken at each of three different levels of the SNc (rostral: -2.92 mm, medial: -3.16 mm and caudal: -3.52 mm; AP axis relative to bregma) for each animal. SNc cell counts from the two hemispheres were then averaged. Only TH-positive cells from the SNc were counted, VTA TH-positive cells were omitted as these do not form part of the basal ganglia motor circuitry. Counts for the triplicate sections were further averaged to give an average count of SNc cells within a hemisphere for each SNc level. A final mean for each animal was obtained by averaging the values of the three levels. Mean SNc counts for the aged and young adult mice were then calculated.

### 2.3.3. Statistical analyses

All statistical analyses within this chapter were conducted with the SigmaPlot 12 package; statistical tests used are displayed within the figure legends. Graphpad Prism 5 was used to plot all graphs. GPower 3.1 was utilised for power calculations.

For all immunohistochemical density comparisons within the striatum the Two-way ANOVA and Bonferroni post hoc test was used. For all immunohistochemical density comparisons within the SNc the Student's *t*-test was used. The Student's *t*-test was also used for the SNc cell count analysis.

## 2.4. Results

### 2.4.1. CSPGs are expressed within the mouse SNc

To investigate the expression of CSPGs within the mouse SNc, we immunohistochemically stained for the CSPG core proteins aggrecan, NG2 and versican. Analyses were those of a qualitative nature, therefore, we only wished to confirm the presence of these CSPGs whilst observing regions of high expression. No statistical testing was conducted. All patterns found were consistent across all three animals.

Aggrecan presented high levels of expression in the SNc when compared to the expression of NG2 (figure 8A). The stain represented the disperse nature of CSPGs within the diffuse matrix. No distinct PNN formations can be seen (the PNN structure will be explained more fully in figure 9). Expression seems uniform across the section with a slight increase in the ventral midbrain and cortical regions (i.e. visual cortex [V1]) and lowered expression in white matter regions such as the cingulate cortex (Cg).

NG2 presented very little expression within the SNc and surrounding areas (figure 8B). Imaging for this CSPG core protein proved very difficult to image due to the highly diffuse staining. Although higher expression can be found in the medial mammillary nucleus (MM), NG2 is not greatly expressed in the naive mouse BG.

Versican, as with aggrecan, presented high levels of expression within the mouse SNc (figure 8C). Regions of most positivity were in the cortex, such as the visual and the neighbouring retrosplenial granular cortex (RSG), and the ventral midbrain regions, such as the SNc and SNr. No PNN formations were stained with the versican antibody.

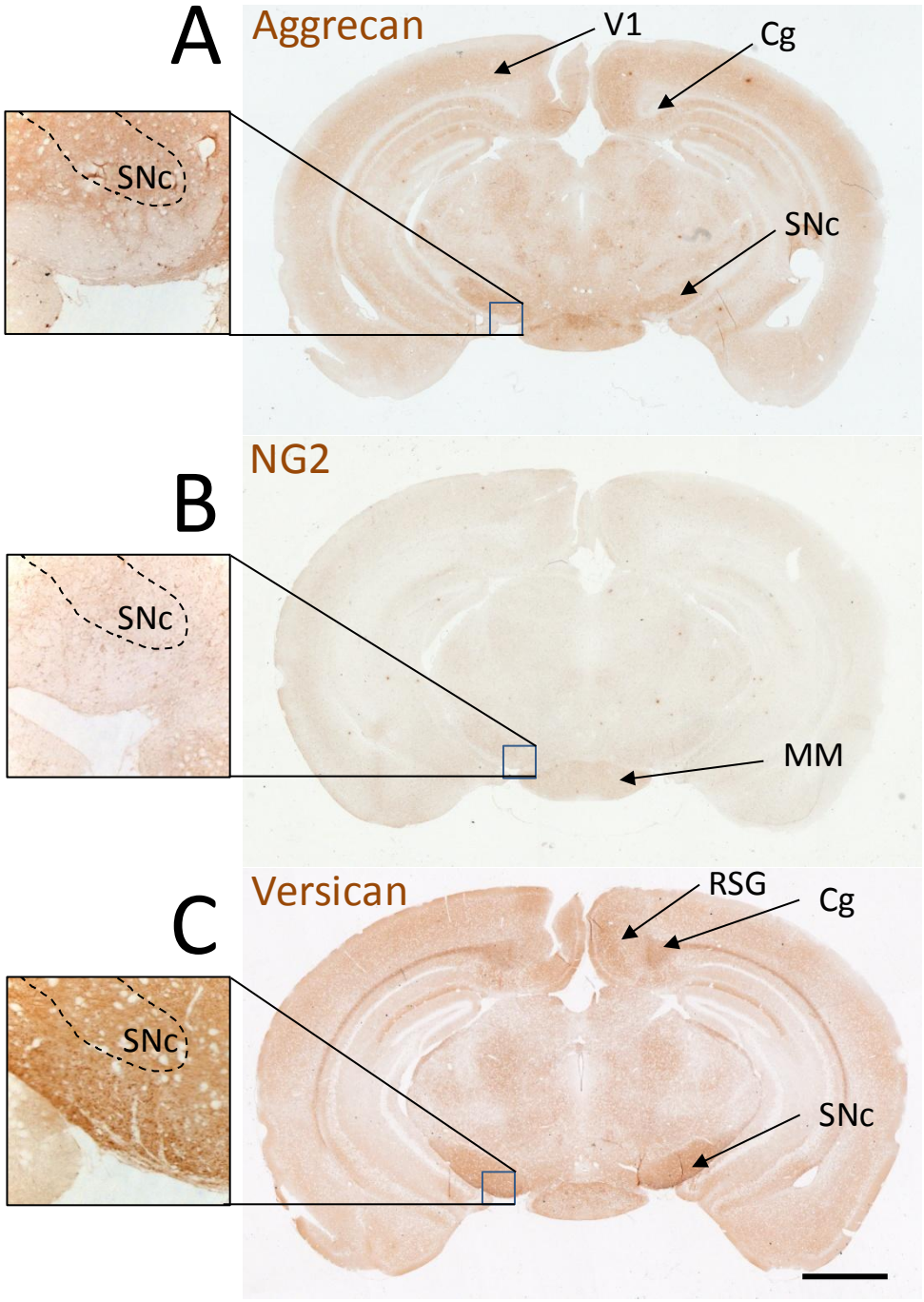


**Figure 9: CSPG expression within the naive mouse SNc.**
Images taken at 5X magnification from coronal sections of the mouse SNc indicate the presence of aggrecan, NG2 and versican. Images are representative of all three animals. 20X magnification insert images focus on the region of the SNc itself (black dashed line)(A) Aggrecan expression within the SNc is high. (B) NG2 is not highly expressed within the mouse SNc. (C) Versican expresses highly within the mouse SNc. Cg = cingulate cortex, MM = medial mammillary nucleus, RSG = retrosplenial granular cortex, SNc = substantia nigra pars compacta, V1 = primary visual cortex. Scale bar = 1 mm.

### 2.4.2. Perineuronal nets do not surround cells of the mouse SNc

Although previous investigations have confirmed the absence of PNNs within the human SNc, we wished to use immunofluorescent techniques to determine whether this was conserved in the mouse as well. A similar result would support the translatability from the mouse ECM to the human. Representative images of the PNN distributions in the SNc are shown below. These patterns were seen across all three mice.

Parasaggital sections, containing the SNc of naive mice, were stained for TH and PNN presence using the anti-TH antibody and biotinylated *Wisteria floribunda* agglutinin (bWFA; a classical marker for PNNs). bWFA staining alone indicated a channel of PNN absence within the SNc (figure 9A). PNNs, as depicted by the higher magnification inset image in Panel A, can be clearly found in the regions surrounding the SNc such as the SNr (ventral to the SNc) and the VTA (dorsal to the SNc). The channel of PNN absence can be found to house the dopaminergic TH-positive cells of the SNc (figure 9B)

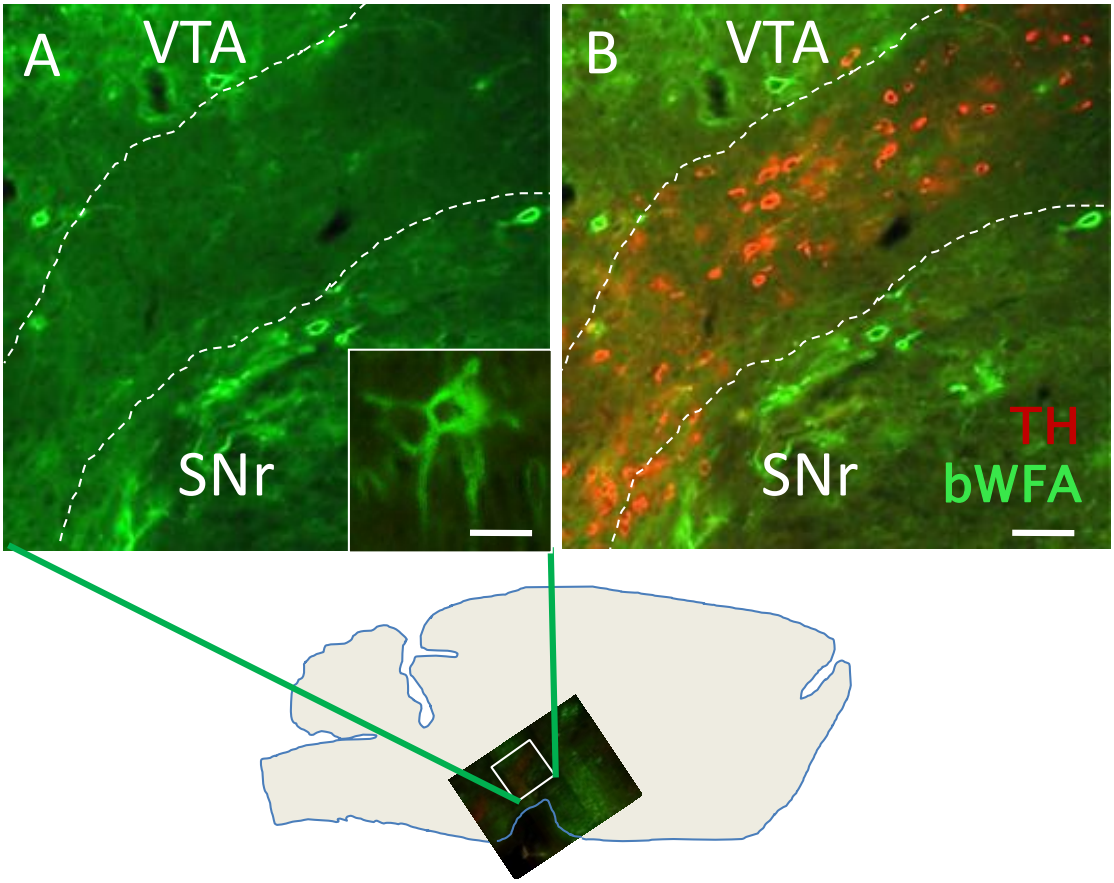


**Figure 10: PNNs are absent within the SNc.**
(A) Representative fluorescent images taken from parasagittal sections of the mouse SNc indicate the absence of PNNs (green; biotinylated *Wisteria floribunda* agglutinin antibody [bWFA]) in the SNc (red; tyrosine hydroxylase). Inset image displays the typical structure of a PNN; inset scale bar = 25 µm. (B) TH clearly marks the SNc that resides within the PNN-absent channel. Scale bar in panel B = 100 µm.

### 2.4.3. Aggrecan and CS56 distribution is enhanced within the SNc and striatum of the aged mouse

To examine whether young adult mice (8 weeks old) possessed different CSPG expressions to that of the aged mice (18 months old), we stained for aggrecan and the pan-marker for CS-GAGs, CS56. All images below are taken from the medial SNc (-3.16 mm AP; relative to bregma) or medial striatum (+0.5 mm AP; relative to bregma). Quantification is shown for all rostrocaudal levels combined as there were no differences in expression patterns at the three rostrocaudal levels.

Overall, aggrecan had a diffuse staining pattern throughout regions of the rostrocaudal axis. In particular, the SNc appeared to have higher staining in the aged animals compared to the young adults, as evident in figure 10A + B. Quantification confirmed this difference as significant. Aggrecan had a higher degree of optical density within the aged SNc (0.184 ± 0.0008) than the young adult mouse SNc (0.178 ± 0.0007; $p<0.001$; Student's *t-test*) (Figure 10 C).

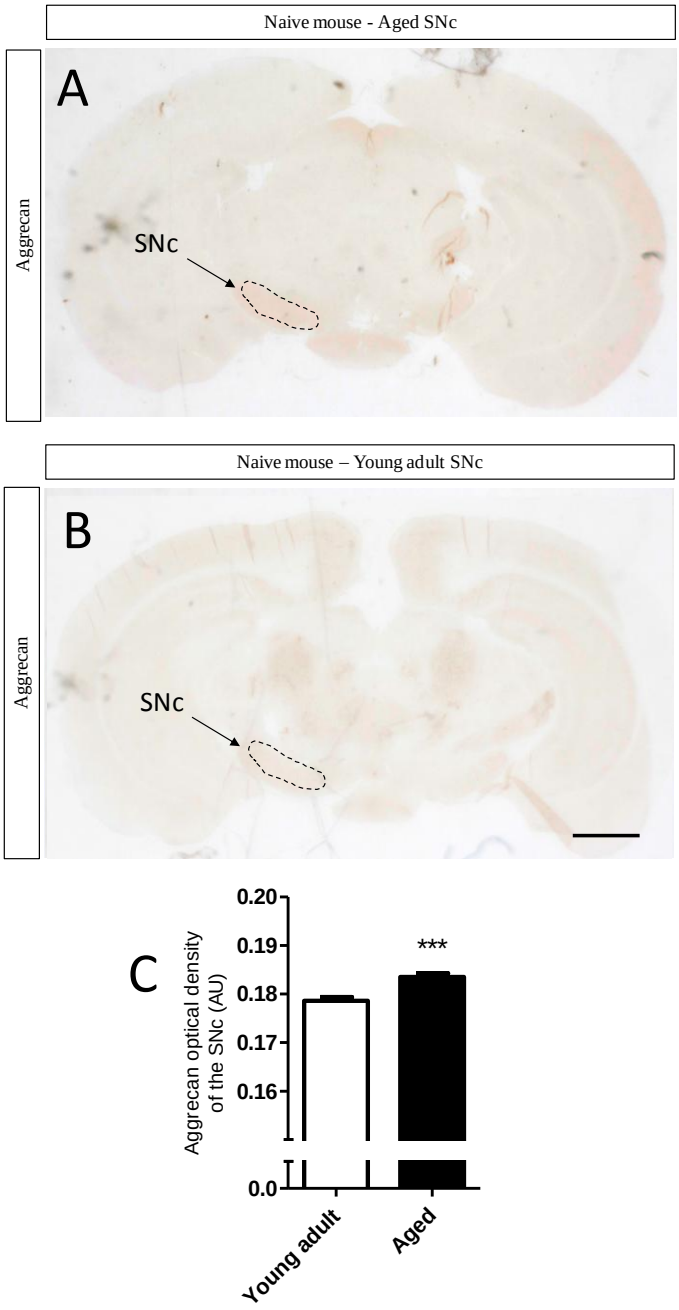


**Figure 11: Aggrecan expression within the aged and young adult mouse SNc.**
(A + B) Representative coronal medial SNc sections stained for aggrecan from an aged and young adult mouse, respectively. Dashed line corresponds to the area of SNc taken for optical density readings. Scale bar = 1 mm. (C) Data represent the averaged optical densities of the SNc across all three levels. Student's *t*-test; *** denotes $p<0.001$. Scale bar = 1 mm. Young adult: n=5, aged: n=5. Data are mean ± S.E.M. AU = arbitrary units.

As with the previous SNc stain, the diffuse staining of aggrecan was apparent throughout the rostrocaudal axis of the striatum. Although difficult to see by eye in figure 11A + B below, aggrecan was also found to be significantly higher in the dorsal striatum of the aged mouse (0.18 ± 0.0003) when compared to the equivalent striatal hemisphere in the young adult mouse (0.172 ± 0.004; $p<0.05$; Two-way ANOVA with Bonferroni post hoc; figure 11C). There was no significance between the ventral regions of the aged or young adult animals.

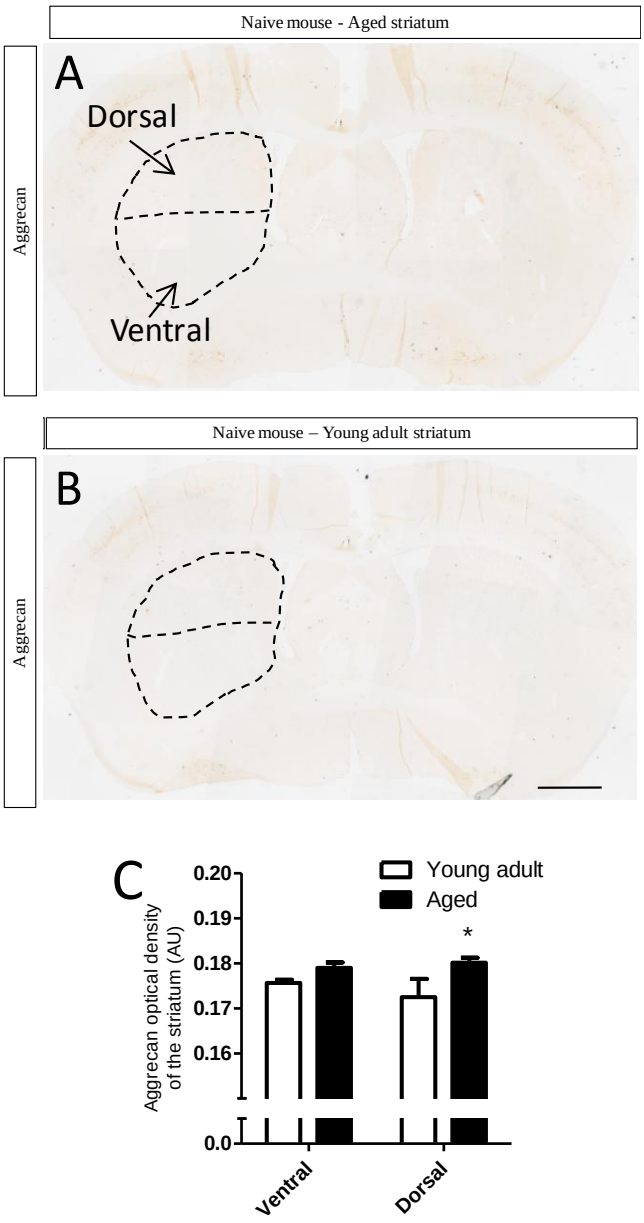


**Figure 12: Aggrecan expression within the aged and young adult mouse striatum.**
(A + B) Representative coronal medial striatal sections stained for aggrecan from an aged and young adult mouse, respectively. Dashed line corresponds to the striatum taken for optical density readings. The top region of the striatum is the dorsal striatum whereas the bottom region of the striatum is the ventral striatum. Scale bar = 1 mm. (C) Data represent the averaged optical densities of the dorsal and ventral striatum across all three levels. Two-way ANOVA with Bonferroni post hoc test; * denotes $p<0.05$ between the dorsal striata of the aged and young adult treated groups. Young adult: n=5, aged: n=5. Data are mean ± S.E.M. AU = arbitrary units.

The pan-marker for intact CS-GAGs, CS56, was diffusely stained throughout the rostrocaudal axis. However, unlike aggrecan, CS56 expression was topographical. Darker staining was apparent in regions of white matter and the ventral midbrain. It was apparent that CS56 expression was enhanced in the retrosplenial granular cortex (RSG) in the aged animals when visually compared to the young adult (no statistical testing was conducted; figure 12A + B).

CS56 was expressed at a significantly higher level in the aged mouse SNc (0.226 ± 0.002) to that of the young adult (0.22 ± 0.002; p=0.049; Student's *t*-test; figure 12 C).

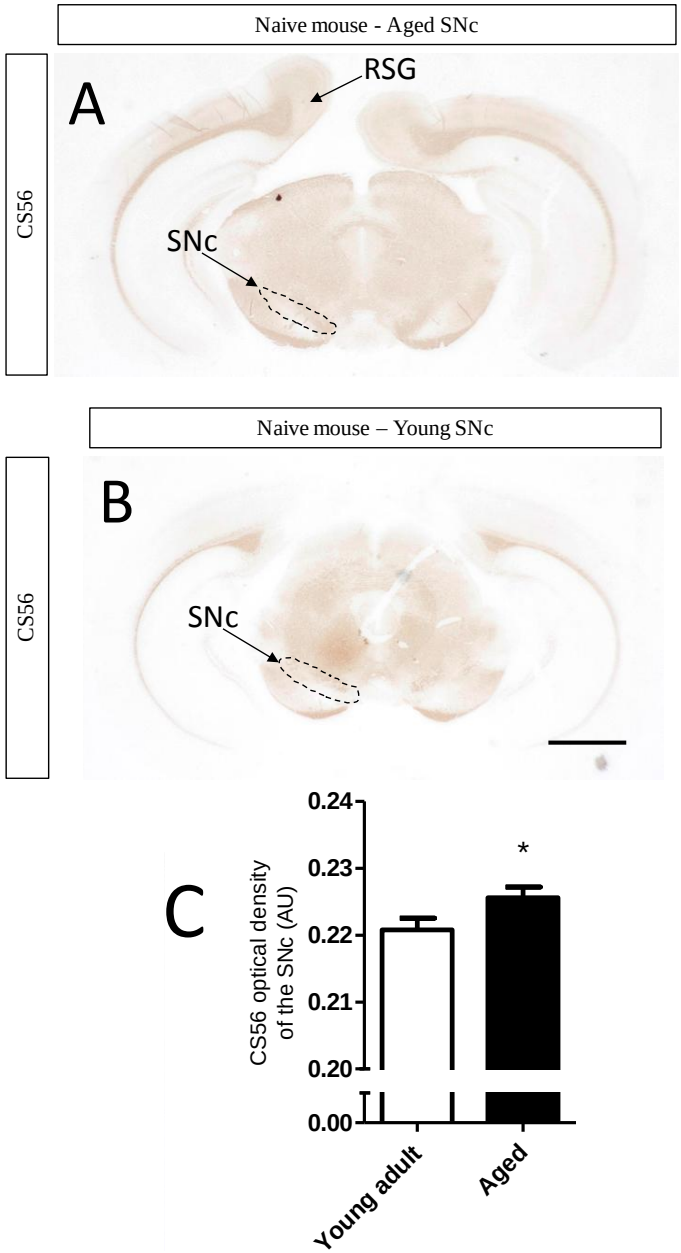


**Figure 13: CS56 expression within the aged and young adult mouse SNc.**
(A + B) Representative coronal medial SNc sections stained for CS56 from an aged and young adult mouse, respectively. Dashed line corresponds to the area of SNc taken for optical density readings. RSG = retrosplenial granular cortex. (C) Data represent the averaged optical densities of the SNc across all three levels. Student's *t-test*; * denotes p<0.05. Scale bar = 1 mm. Young adult: n=5, aged: n=5. Data are mean ± S.E.M. AU = arbitrary units.

Striatal expression of CS56 was topographical, with some regions of the rostrocaudal striatum being more stained than others. CS56 was specific to striosomes and white matter tracts within the sections (no statistical testing was conducted). CS56 expression within the cortex appeared to be raised in the aged mouse when compared to the young adult (no statistical testing was conducted) (figure 13A + B).

The degree of CS56 expression was not significantly different within either the dorsal or ventral striatum of the aged (dorsal: 0.203 ± 0.004, ventral: 0.199 ± 0.004) or young adult mice (dorsal: 0.206 ± 0.004, ventral: 0.194 ± 0.003; Two-Way ANOVA with Bonferroni post hoc test; figure 13C).

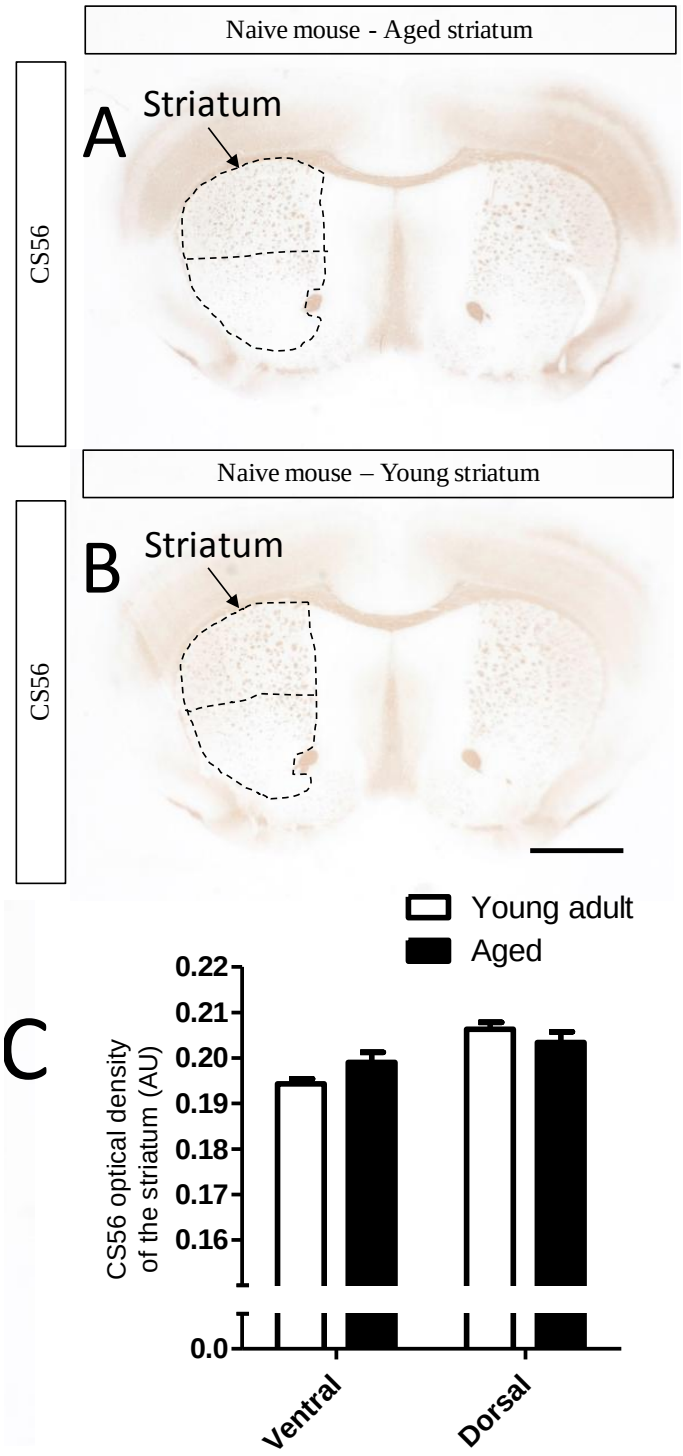


**Figure 14: CS56 expression within the aged and young adult mouse striatum.**
(A + B) Representative coronal medial striatal sections stained for CS56 from an aged and young adult mouse, respectively. Dashed line corresponds to the striatum taken for optical density readings. The top region of the striatum is the dorsal striatum whereas the bottom region of the striatum is the ventral striatum. (C) Data represent the averaged optical densities of the dorsal and ventral striatum across all three levels. Scale bar = 1 mm. Young adult: n=5, aged: n=5. Data are mean ± S.E.M. AU = arbitrary units.

### 2.4.4. TH-positive SNc cells were seen to decrease whereas striatal TH-positive fibres were found to increase

TH staining was found to mark the cells of both the SNc and the VTA. Only the TH-positive SNc cells were counted, these cells are ringed in figure 14A + B. Data in figure 14C display the average count of TH-positive cells in one hemisphere of SNc across all rostrocaudal levels.

The average number of TH-positive cells in one hemisphere of the aged mouse SNc (57 ± 4.5 cells; figure 14C) was significantly lower to that found in the young adult (92.5 ± 4.6 cells; $p<0.05$; Student *t*-test).

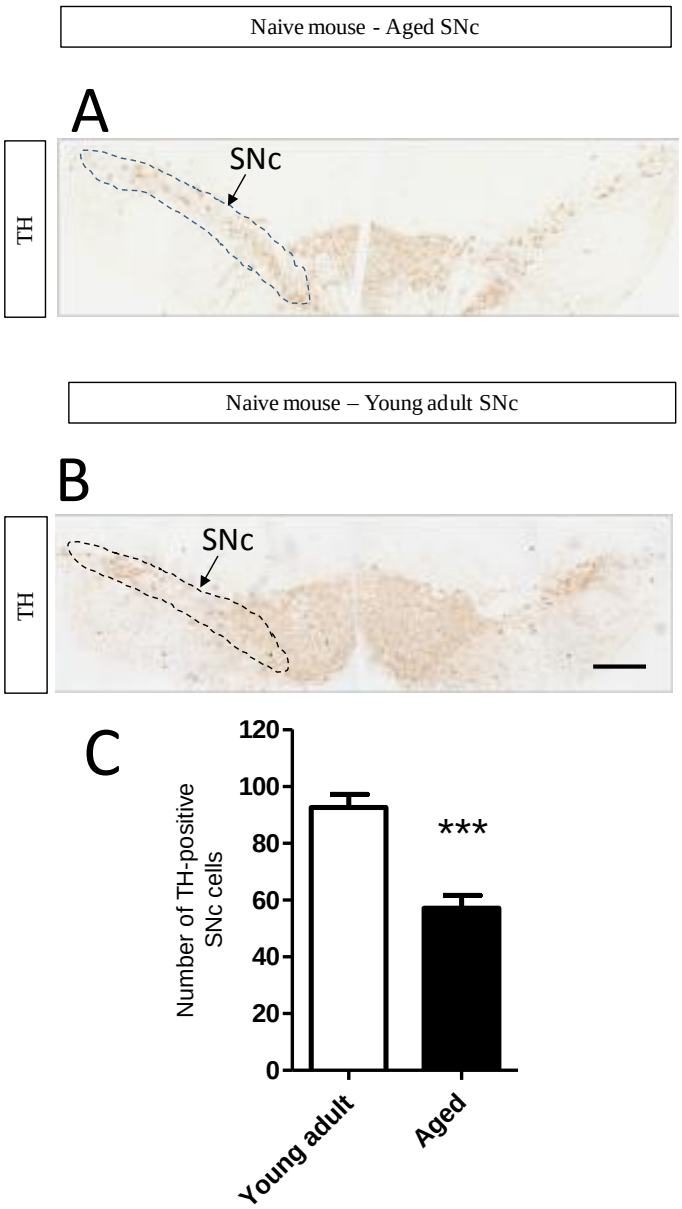


**Figure 15: TH-positive SNc cells in the aged and young adult mouse.**
(A + B) Representative coronal medial SNc sections stained for TH from an aged and young adult mouse, respectively. Dashed line corresponds to the SNc in which only the A9 dopaminergic cells were counted. (C) Data represent the averaged number of TH-positive cells within one hemisphere of SNc across all three levels. Student's *t*-test; *** denotes $p<0.001$. Scale bar = 250 µm. Young adult: n=5, aged: n=5. Data are mean ± S.E.M.

TH density was significantly elavated within the aged striatum compared to the young adult in both the dorsal (young adult: 0.024 ± 0.0001 and aged: 0.032 ± 0.0001; $p<0.001$; Two-way ANOVA with Bonferroni post hoc test) and ventral (young adult: 0.024 ± 0.0001 and aged: 0.032 ± 0.0001; $p<0.001$; Two-way ANOVA with Bonferroni post hoc test) hemispheres.

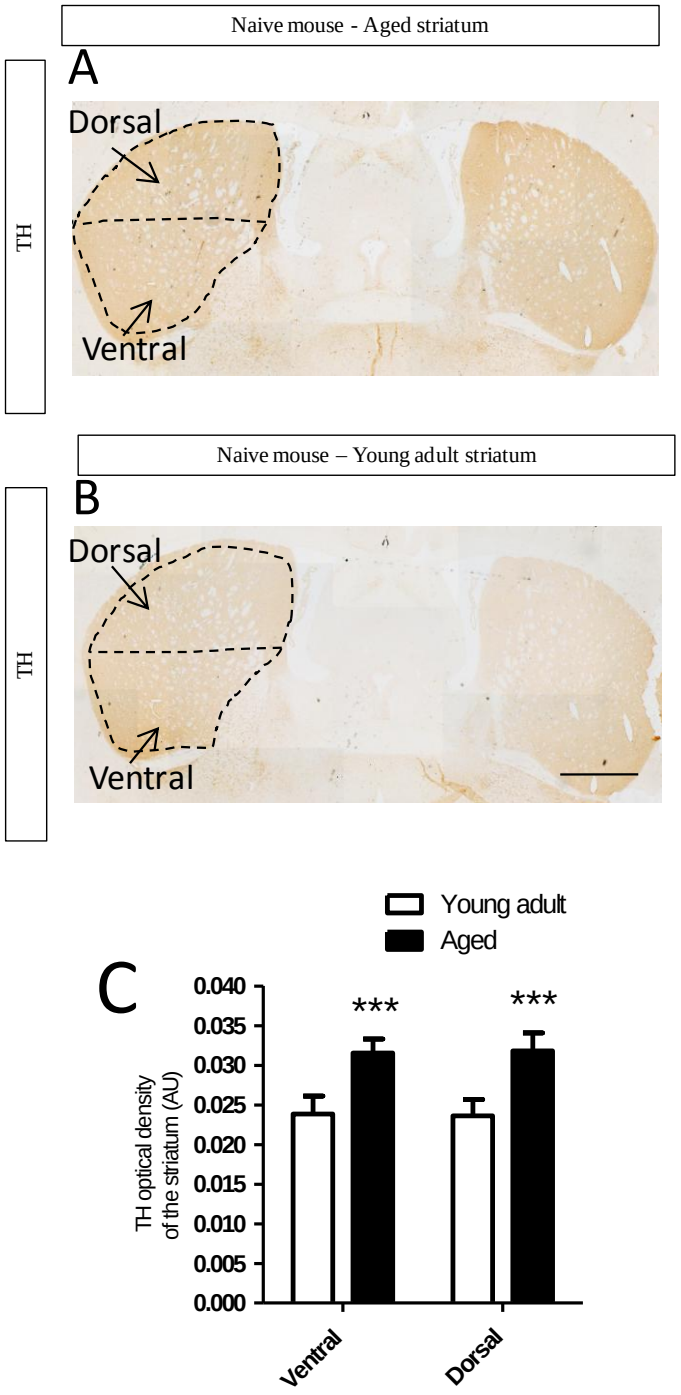


**Figure 16: TH-positive striatal fibres within the aged and young adult mouse striatum.**
(A + B) Representative coronal medial striatal sections stained for TH from an aged and young adult mouse, respectively. Dashed line corresponds to the striatum taken for optical density readings. The top region of the striatum is the dorsal striatum whereas the bottom region of the striatum is the ventral striatum. (C) Data represent the averaged optical densities of the dorsal and ventral striatum across all three levels. Two-way ANOVA with Bonferroni post hoc test; *** denotes $p<0.001$ Scale bar = 1 mm. Young adult: n=5, aged: n=5. Data are mean ± S.E.M. AU = arbitrary units.

## 2.5. Discussion

### 2.5.1. Aggrecan and versican were found expressed highly in the naive mouse SNc

The purpose of this small investigative study was to determine whether the naive mouse would express particular CSPGs within the SNc. Unfortunately, due to the availability of certain brain sections, only the SNc was tested and not other PD relevant regions such as the striatum.

Aggrecan and versican were both found to have high positivity within the ventral regions of the midbrain where the SNc could be found. When comparing the expression of these lecticans to the data by Milev et *al* (Milev *et al.*, 1998) (see figure 7 for graphical representations), we see a close relationship with aggrecan and versican expression increasing 8 weeks postnatally. It is likely that our versican stain depicts the increase in $V_2$ versican and not the neonatal $V_1$ and $V_0$, as depicted by the aforemention plots in figure 7. We cannot distinguish between isoforms as the antibody used was a pan-versican marker.

Unfortunately, unlike aggrecan and versican, NG2 did not express highly in any region of these sections; the MM being the only exception. Nevertheless, there is some global diffuse staining within the mouse brain. As the CSPG NG2 is strongly associated with resident glia of the brain (i.e. oligodendrocyte progenitors and potentially microglia), this CSPG is most likely at a low level of expression due to no local injury or region of neuroinflammation. Perhaps NG2 optical density would increase significantly if it were investigated in tissue from toxin mouse models (possessing regions of inflammation and injury). However, NG2 has been described as transient even in these injured states (Morgenstern *et al.*, 2002). This transient nature may be due to the expression of NG2 correlating with the oligodendrocyte progenitors recruited to the site of injury and not with the glia they eventually mature into.

Since we could not detect any notable staining of neurocan or brevican positivity within the adult mouse, these two lecticans were not included in this chapter. The absence of neurocan positivity can be explained by the decreased presence of this CSPG following birth (figure 7). However the absence of brevican does not follow the work by Milev *et al.* According to the study, brevican expression should increase following birth. This may be a fault of the antibodies used or, more likely, it is because brevican is closely associated with oligodendrocytes (Niederost *et al.*, 1999) and therefore displayed a similar low expression to that of NG2.

As only aggrecan and versican were detected within the SNc in high levels, only these two CSPGs shall be used in the future to detect levels of CSPG expression within the mouse BG. However, this does not support our initial hypotheses as these were the only CSPGs robustly expressed within the SNc.

### 2.5.2. Perineuronal nets were not associated with the SNc dopaminergic neurones

The PNN staining indicated that the pericellular formations were specific to particular cell types and that no association between PNN and TH-positive SNc cells were found; supporting our hypothesis. The presence of PNNs in anatomically neighbouring regions to the SNc, such as the GABAergic SNr, suggests that, as found by Bruckner *et al*., 2008, PNNs may exclusively associate with GABAergic regions. Furthermore, according to that study's data, PNNs were not found associated with glutamatergic cells of the pedunculopontine nucleus or the ventral lateral nucleus. This indicated that PNNs might only associate with the inhibitory nuclei of the BG.

The absence of PNNs in the SNc raises the question of whether these pericellular formations are actually protective. It has been suggested that alterations in the ECM may help protect neurones against oxidative stress, environmental stress and ageing (Cabungcal *et al.*, 2013; Morawski *et al.*, 2004; Suttkus *et al.*, 2014). Furthermore, there is evidence suggesting that regions of numerous PNN-associated neurones present low/no tau pathology in tissue from patients with Alzheimer's disease (Bruckner *et al.*, 1999), furthering this theory that CSPGs enforce a protective state. However, the obvious question arises - If CSPGs are protective, why does their digestion give rise to axonal sprouting and growth? This conflict between the *pro-growth versus inhibitory* argument is not yet understood. Perhaps their absence in the SNc is a contributor to cell vulnerability. On the other hand, it is possible that as PNNs are in neighbouring regions they are still able to protect and secrete beneficial molecules to the SNc cells.

### 2.5.3. Age may be a significant factor of CSPG distribution in the naive mouse

As aggrecan was detected within the human BG (Bruckner *et al.*, 2008), it was of interest to investigate whether age was a factor to its distribution. Additionally, to understand the degree of CS-GAG expression within these tissues, the CS56 marker was also used. We were also interested to analyse any alterations in TH-positive SNc cell or striatal fibre presence between the different ages of these animals.

Our results suggest that the aged mouse presented higher levels of aggrecan in both the SNc and striatum to that of the young adult mouse. This correlated to an increase in CS56

expression in the aged SNc but not the striatum. Although thought to stabilise following birth, both aggrecan and CS-GAG presence is enhanced beyond the level seen in the young adult. But this increase is predictable when taking the work of Milev *et al*. into account. As the degree of aggrecan expression in the young adult mouse (see figure 7; pink region) is found on the exponential rise of the sigmoidal curve, the final stabilised expression of the CSPG is likely to be higher in the aged animals. Although not investigated by Milev *et al.*, CS56 would likely follow the same expression to aggrecan as the CS-GAGs would be expressed most prevalently on the aggrecan core proteins (aggrecan is the most glycosylated lectican).

This indicates a potential issue with many models used in ECM-targeted therapies for age-related diseases. As many studies utilise animals that are young adults, the results obtained may not translate well to the elderly patient, as age may be a factor in the success of that therapy. Thus, using an aged model of disease may produce results that reflect those found in an aged ECM environment, such as those in age-related diseases. Despite this, these changes in expression were still considerably small and would likely not affect ECM-targeted therapies. In fact, these data show that CSPG expression is still present to a similar, albeit slightly higher, degree to those of the young adult. This result is positive and validates the use of the younger mice. If CSPGs were not expressed within the aged tissue then their use as a therapeutic target in an age-related disease would be lost.

### 2.5.4. In the aged naive mouse the number of TH-positive SNc cells declined but TH-positive fibre density in the striatum increased

It was also of interest to investigate whether age was a factor in total SNc cell number and total TH-positive fibres in the striatum; these are both factors suggested to decrease with age. Perhaps a loss in cells or fibres could correlate to CSPG upregulation.

Within our small sample it was apparent that the number of cells drastically declined with age, with the young adult revealing a similar count of SNc cells (80 – 100 cells per hemisphere) to previously published data (Heuer *et al.*, 2012). This result followed previous beliefs that age reduced SNc cell numbers within mammalian models (Surmeier *et al.*, 2010). Age-related cell loss is thought to be due to several factors, reduced UPS activity (Tai *et al.*, 2008), toxin susceptibility (McCormack *et al.*, 2004) and ROS accumulation from the enhanced metabolic rate of the SNc cell (Wallace, 2005). Perhaps in subsequent studies investigating markers of these age-related factors in the aged mouse would be of interest.

On the other hand, TH-positive fibre optical densities were found to be significantly higher in the age mouse striatum to that of the young adult. This result was somewhat surprising, as a decrease in SNc cell counts would usually be predictive of a loss in striatal TH-positive

terminals; a similar pattern to what is found in PD itself and its related toxin models. This phenomenon has not been documented before and is possibly a false positive due to a low sample size. However if true, this suggests that the remaining cells in the aged SNc are inducing compensatory TH-positive terminal sprouting. This plasticity could be an attempt to output a similar concentration of striatal DA to that of a young adult. Perhaps this is a form of repair countering the effects of natural SNc cell loss in aged mice. This deserves future investigation, whereby an increased sample size alongside assessments of DAT expression would be required. However, the effects of ageing are outwith the main aims of this thesis.

### 2.5.5. Chapter conclusions

Overall, the investigative studies in this chapter have answered several important questions. The mouse BG does express aggrecan and versican but other CSPGs such as NG2, brevican and neurocan display little to no positivity. With brevican as the only exception, these expressions were expected when taking the work of Milev *et al.* into consideration.

As described within the human BG, PNNs are not associated with the SNc. This raises more questions about the function of the PNN. Is their absence an additional reason to the SNc's susceptibility of cell degeneration?

Finally, age may be a significant factor in the expression of aggrecan and therefore potentially the rest of the lectican family. Although it is well known that CSPGs express differently in the neonate and during development to the adult, it was not clear whether this was found within the aged animal as well. We discovered that both aggrecan and CS56 were expressed within the aged mouse striatum and that they were slightly raised above the levels detected in the young adult. This ultimately justified the use of young adult mice in future studies as similar CSPG expressions between the ages were found.

# 3. Investigating the effect of CSPG digestion within the nigrostriatal tract of the partial and fully lesioned hemiparkinsonian mouse model

## 3.1. Introduction

### 3.1.1. CSPGs and perineuronal nets within the human basal ganglia

CSPGs are conserved in the mammalian CNS where they reside in the PNN and diffuse ECM surrounding a range of varying neuronal networks, one of which being the BG (Bruckner *et al.*, 2008; Deepa *et al.*, 2006). In Chapter 2, we showed how CSPGs are expressed in key mouse brain regions affected in PD and how in aged tissue certain CSPGs were not only present but also increased beyond what was found in the young adult mice. ECM-related therapies have been investigated as methods of neuronal repair, primarily in the spinal cord injury field. This chapter investigates whether an ECM-related therapy can be developed for PD.

The aforementioned Bruckner *et al.,* 2008 paper analysed ECM components within various areas of the BG. It was found that PNNs, key regulators of neuronal plasticity, surrounded the GABAergic projection neurons of the GPi/SNr and the GABAergic fast spiking interneurones of the striatum but not of the dopaminergic cells of the SNc. This finding was confirmed in the histological studies of Chapter 2. This cell selectivity raised several questions in regards to the PNN's true function within the BG. Firstly, are PNNs beneficial for cation buffering? If so, does their absence in the SNc increase cell vulnerability? Secondly, are PNNs, which are in close proximity to the SNc, somehow inhibitory towards intrinsic recovery methods in PD? It is interesting to note that only healthy human brains have been analysed for PNN presence, therefore it is possible that PD patients possess altered PNN and CSPG distributions or structures that could affect disease state. Although we tried to investigate this in Chapter 2, the quality of tissue led to inadequate staining therefore this shall remain unclear.

Although there is evidence indicating the presence of CSPGs in the human BG, there is little data to suggest that CSPGs have a role in the disease. Only one study suggests that CSPGs may have a function within PD. Utilising an antibody for CS-GAGs it was discovered that CSPGs were retained in high concentrations within LBs (DeWitt *et al.*, 1994). The specific role of these LB-bound CSPGs is not understood, but it is theorised that they affect protein aggregation.

### 3.1.2. The inhibitory nature of CSPGs and perineuronal nets

CSPGs within the PNN have been widely accepted as inhibitory to axon growth and neuronal repair; as of yet there is no agreed upon mechanism of inhibition. Multiple theories have attempted to explain the inhibitory nature of the PNN and to why its digestion leads to axon sprouting within injured models. Two of the most significant theories have been described below (see (Wang *et al.*, 2012a) for a comprehensive review):

- The PNN may simply act as a physical barrier to growth, in which new cellular contacts and advancing filopodia are inhibited (Asher *et al.*, 2000; Oohira *et al.*, 1991). Being a dense ECM lattice, the digestion of the CS-GAGs may enable the forming of new cell contacts and reduce inhibitory CSPG-receptor interactions. To date, three receptors have been discovered to interact with CSPGs, these are: receptor protein tyrosine phosphatase sigma (Shen *et al.*, 2009), contactin-1 (Mikami *et al.*, 2009) and leukocyte common antigen-related phophatase (Fisher *et al.*, 2011). Genetic and pharmacological inhibition of the Rho/ROCK and PKC signalling pathways have overturned the inhibitory nature of the CSPGs, indicating the role these cascades may have in blocking axonal regeneration (Monnier *et al.*, 2003) (Sivasankaran *et al.*, 2004). Genetic knockouts of these receptors have led to neuronal regeneration following spinal cord injury, indicating an inhibitory function. Despite this, the role these receptors may play in PNN-related plasticity is still not known.

- The PNN may be a source of molecules that affect neuronal plasticity. Molecules such as the semaphorin 3A have shown to bind to the PNN (de Winter *et al.*, 2016; De Wit *et al.*, 2005). Semaphorin 3A is a known growth cone collapser which inhibits lamellapodia in advancing cells. Their presence in the PNN is thought to cause inhibition towards lamellapodia through chemorepulsion. Moreover, PNNs are thought to harbour pro-growth molecules such as NTFs which are liberated when digested. NTFs such as fibroblast growth factor 2, vascular endothelial growth factor, hepatocyte growth factor and BDNF have all shown affinity for GAG side-chains (Karumbaiah *et al.*, 2015; Takada *et al.*, 2013). Therefore, PNNs potentially trap NTFs and limit their exposure to the enwrapped neurone.

### 3.1.3. Removing the perineuronal nets

The enabling of axonal regrowth by the removal or digestion of CSPGs has been frequently mentioned in previous sections. Removing CSPGs can be done in one of a few ways.

The most prominent method of removing CSPGs is via the administration of the *Proteus vulgaris* bacterial enzyme known as chondroitinase ABC (ChABC). ChABC is a lyase with the capability to degrade CS-GAG chains via the hydrolysis of the GlcA/GalNAc glycosidic bond. This in effect *prunes* the GAG side-chains off the attached CSPG core protein. Pruned side chains reveal residual stub epitopes attached to the core protein which are then effective binding sites for the chondroitin-4-sulphate (C4S) antibody; a common marker used to visualise tissue digested by ChABC (see figure 16). Digested CSPGs lose their inhibitory nature and permit repair to occur. As CSPGs are removed, PNNs lose their dense lattice structure, their inhibitory mechanisms and their potential trapping of NTFs. The administration of ChABC *in vivo* has been the basis of the *ChABC spinal cord injury recovery model*, a paradigm model that promotes functional recovery post injury (Barritt *et al.*, 2006; Bradbury *et al.*, 2002).

Although sometimes used interchangeably in terms of plasticity and therapeutic target, the diffuse matrix CSPGs and PNNs are different structures. These two locations of CSPG are impossible to individually target when using ChABC. As a result, any beneficial plastic effects caused by CS-GAG digestion cannot be attributed to PNN removal alone. However, a genetic approach has been developed to knockout the formation of the PNN. The Crtl1 gene has been identified as one of the most important genes required for effective PNN formation (Carulli *et al.*, 2006; Wang *et al.*, 2011). Crtl1 encodes the link protein that binds the core protein to the CS-GAG side chains. Disruption of this gene leads to the inability to form normal PNNs and, as a result, leaves the brain open for plasticity. Animals with this genotype have presented significant motor recovery following spinal cord injury, which has been comparable to that of ChABC-mediated recovery (Carulli *et al.*, 2010). This genetic approach has proven that the recovery seen with ChABC administration can be largely, if not solely, caused by the digestion of the PNN in spinal cord injury models. This does not rule out the possibility of the CSPGs of the diffuse matrix being inhibitory, rather PNNs are most likely more inhibitory due to their sheer number of CSPG components.

Methods of CSPG removal have not been investigated extensively in other areas of neurodegeneration such as PD. As the degeneration of SNc cells and their inability for repair are significant factors in PD, novel methods of promoting restoration are of major interest.

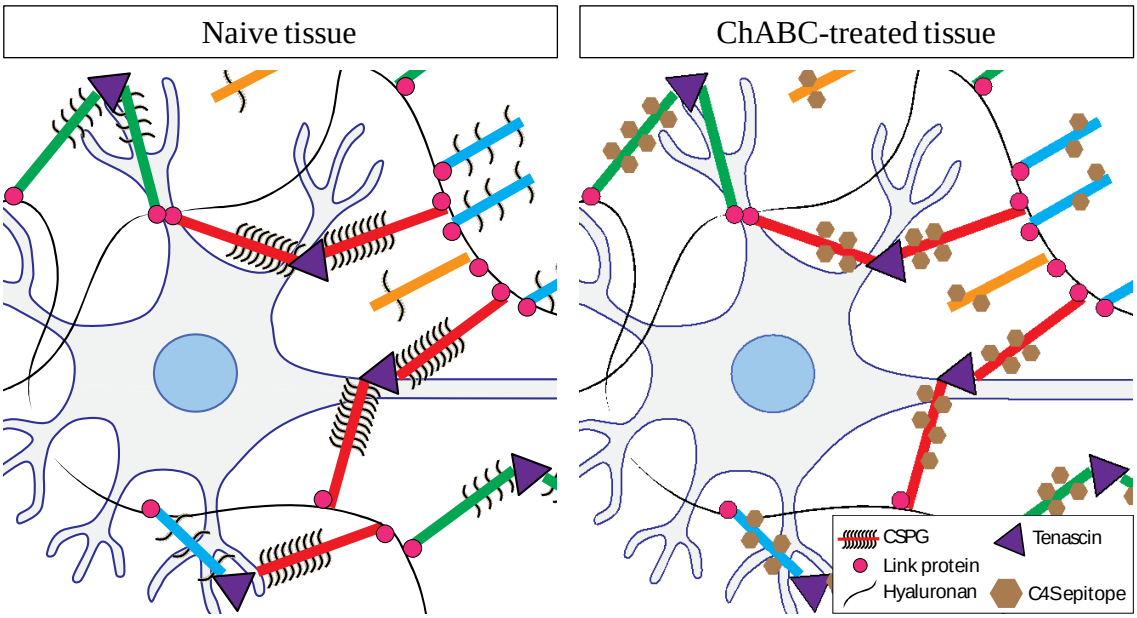


**Figure 17: PNNs in naive and ChABC-treated tissue.**
As shown in Chapter 1, the CSPGs of the PNN are bound to the scaffolding protein hyaluronan by link proteins. The net-like structure is formed by the complexing of several CSPGs via the binding to tenascin. CSPGs in the naive tissue (left cartoon) possess many CS-GAG side-chains that are believed to cause axonal inhibition. However, ChABC administration induces the digestion of the CS-GAGs (right cartoon) and the unveiling of chondroitin-4-sulphate (C4S) epitopes. These sites allow the binding of C4S antibodies to the digested CSPGs and highlight regions of successful digestion.

### 3.1.4. ChABC administration as a Parkinson's disease therapeutic venture

To date, ChABC has been utilised in few studies regarding PD. One relevant study administered ChABC to rats bearing a damaged nigrostriatal pathway (NS) whereby an axotomy was made to the MFB by a Scouten wire-knife incision (AP: -3.0 mm, ML: ± 2.5 mm and DV: -7.5 mm; relative to bregma and dura mater surface) (Moon *et al.*, 2001). These injured rats were administered ChABC perilesionally via implanted cannulae on days 0, 3, 7 and 10 and later killed on days 11, 18 or 100 post-axotomy. ChABC administration elicited the regrowth of TH-positive NS fibres when compared to those of the control group; no significance was found between any of the days post-lesion in the number TH-positive processes. Unfortunately, no behaviour was conducted so determining whether functional recovery was induced by ChABC is impossible. This study suggests that ChABC administration induces plasticity and repair in the rodent BG as seen in ChABC spinal cord injury recovery model. As the axotomy model does not replicate the mechanism or pathology associated with the disease, construct validity is nonexistent. Nonetheless, this proof-of-concept investigation suggests that applying ChABC in a more conventional model of PD could give rise to a novel repair approach.

Homotopic grafting has proven difficult in restoring the dopaminergic function of the BG due to

issues with long distance rewiring and potentially the CSPG-rich inhibitory environment. CSPGs have been found to proliferate significantly in the glial scar surrounding graft sites and so therefore can been seen as a barrier to growth (Barker *et al.*, 1996). With this in mind, studies investigated the effect of ChABC administration on graft success rate and discovered CSPG digestion aided graft growth (Diaz-Martinez *et al.*, 2013; Kauhausen *et al.*, 2015). This further confirms the inhibitory nature of CSPGs within the BG and their potential as a therapeutic target in PD.

### 3.1.5. Study rationale

The brief use of ChABC in the injured rodent BG has provided the proof-of-concept for ECM-targeted therapeutics in PD. So far, there has been no investigation into the effects of ChABC on either SNc cell protection/repair or behavioural recovery in a face-and-construct-valid toxin model of disease. In this chapter, we investigate for the first time the potential of ChABC administration as a method of recovery in the injured BG of the 6-OHDA mouse model. The unilateral 6-OHDA model was chosen, as each animal possessed its own control hemisphere to which it could compare lesion severity. These data then permitted the comparison of SNc cell survival between the saline- and ChABC-treated animals. Additionally, this toxin model was used as it could recreate both early and late stage pathology of PD through either a full or a partial lesion, respectively. Both the early and late stage models were of interest, as it would indicate whether digestion of the CSPGs could help protect susceptible SNc cells in the early stages or repair dying SNc cells in the late stages of disease. As this mouse model was new to the Duty laboratory, both the 6-OHDA mouse models had to be established prior to the two main studies.

## 3.2. Aims and Hypotheses

A wealth of data supports the inhibitory role of CSPGs within the mammalian CNS. To date, several spinal cord injury models have targeted the CSPGs of the ECM as a method of repair. Nonetheless, only one study suggests the possibility of ChABC-mediated axonal repair within the BG. Moon *et al*. presented increased TH-positive fibre sprouting following ChABC treatment in the damaged NS, a study that paved way for the possibility of ChABC as a novel agent in the treatment of PD. However, the axotomy model used in the Moon *et al.* 2001 paper was not a model of PD, therefore the next step was to administer ChABC within a validated model of PD (i.e. the unilateral 6-OHDA mouse). This chapter describes for the first time the effects of ChABC in both a full and partial unilateral 6-OHDA lesion model. To assess the effect of ChABC, both behaviour and SNc cell survival rates were recorded and analysed.

This chapter is subdivided into five studies. The initial three are pilot studies that establish the full lesion model, the partial lesion model and the method of ChABC administration. The final two studies present the effects of ChABC within these full and partial lesion models. The aims and hypotheses for the latter two studies are described below.

Study aims:

1. *Determine whether ChABC has a beneficial effect on cellular and motor recovery in the full lesion 6-OHDA hemiparkinsonian mouse model*

2. *Determine whether ChABC has a beneficial effect on cellular and motor recovery in the partial lesion 6-OHDA hemiparkinsonian mouse model*

Study hypotheses:

1. *Entire digestion of CSPGs in the NS by ChABC administration will act as a neuroprotective/repair strategy in the full hemiparkinsonian mouse model of PD*

2. *Entire digestion of CSPGs in the NS by ChABC administration will act as a neuroprotective/repair strategy in the partial hemiparkinsonian mouse model of PD*

## 3.3. Materials and Methods

Several methods have been repeated throughout this experimental chapter. In these cases, the method will be described in full in the first instance and then referenced to as *section x.x.x.* in the later instances.

### 3.3.1. Pilot study 1: Establishing the 6-OHDA full lesion mouse model

#### *3.3.1.1. Animal subjects*

18 eight-week-old male C57Bl/6 mice (Harlan, UK) were maintained on a 12:12 hour light/dark cycle (07:00am lights on) with food and water *ad libitum*. Room temperature and humidity were kept at 22 ± 2°C and 55 ± 2% respectively. All surgical, behavioural and histological procedures were performed whilst blinded to the experimental groups.

#### *3.3.1.2. Experimental design*

The timeline for the study is described below in figure 17. A week prior to lesioning (d-7) a 7 day habituation period was implemented to ensure animals were non-responsive to non-biologically relevant stimuli. On day 0, 6-OHDA lesioning was conducted in a randomised block design whilst blind to 6-OHDA dose. A recovery period of 19 days was then enforced post-lesion whereby daily rehydration and health checks were conducted until the animals had returned to pre-surgical weight. Necropsy was conducted at midday on day 21. Animals were killed by anaesthetic overdose and brains were removed for histological analysis.

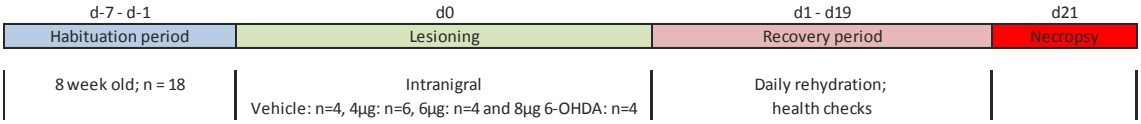


**Figure 18: Experimental design: Pilot study 1: Establishing the 6-OHDA full lesion model.**
All procedures of the study were conducted on certain days pre- or post-lesion as described in the figure. Further details are found either below the time line or in subsequent sections.

### 3.3.1.3. Surgery

Surgeries conducted were based around a randomised block design to reduce variability between the blinded treatment groups. All animal procedures were conducted in accordance with the Animal Scientific Procedures Act 1986. Anaesthesia was induced in mice using a 5% isofluorane/oxygen mixture within an induction chamber and maintained at 3% isofluorane/oxygen. Body temperature was monitored and maintained at 37°C with a homeothermic heating blanket (Harvard Apparatus). The surgical site was sterilised with 0.4% chlorhexidine (Hibiscrub) and eye-drops (Viscotears) were applied to the animal's eyes to avoid drying out and ulceration during surgery and post-recovery. An incision was made from eye to ear level along the AP axis before the surface of the skull was then cleaned and dried.

### 3.3.1.4. 6-OHDA full lesion model

In this model, varying concentrations of 6-OHDA were injected *supranigrally* to identify the dose which would induce a consistent full lesion.

Fine-bore holes (Ø 0.5 mm) were drilled at coordinates AP: -3.0 mm and ML: +1.2 mm (relative to bregma and skull surface). A blunt-ended 30 gauge needle was then inserted supranigrally to dorsovetral [DV]: -4.5 mm (relative to bregma and skull surface) before either saline, 4, 6 or 8 µg 6-OHDA.HBr (Sigma-Aldrich) in 1 µl ice-cold 0.02% ascorbate/saline (Vehicle: n=4; 4 µg: n=6; 6 µg: n=4; 8 µg 6-OHDA.HBr: n=4) was administered at a rate of 0.5 µl/min. The injection needle was left in place for 5 minutes after toxin administration to ensure the full diffusion of the compound.

### 3.3.1.5. Post-operative procedure

After the suturing and sterilisation of the surgical site, animals were administered 0.1 ml buprenorphine (Vetergesic; 0.1 mg/kg; subcutaneous [s.c.]) and 1 ml Hartmann's solution (Aqupharm 11; s.c.) for analgesia and rehydration purposes, respectively. Animals were then left to recover for the rest of the surgical day in a clean cage resting on a heat mat set to 37°C (Harvard Apparatus) with food and tap water *ad libitum*. Lesioned mice suffer from extensive heat loss and so it was important to ensure all animals had sufficient warmth during recovery. Morning and afternoon checks of all the animals were conducted daily to ensure that weight was gained in the days following surgery; 1 ml of warmed Hartmann's solution was administered if >10% body weight had been lost from the previous weigh-in. Unwell animals were placed back on heat mats in a clean cage to ensure body temperature was stabilised. Rigorous post-operative care reduced the mortality rate to ~10%.

### 3.3.1.6. Immunohistochemical assessment of lesion size

On day 21, animals were killed by an anaesthetic overdose (4 ml/kg IP, sodium pentobarbital, Sigma-Aldrich) and perfusion-fixed with PBS, followed by 10% formalin (Sigma-Aldrich) at room temperature. Brains were then removed and postfixed within 10% formalin overnight at room temperature.

### 3.3.1.7. Paraffin embedding and sectioning

Post-fixed brains were readied for paraffin wax embedding by firstly removing the cerebellum and forebrain in the coronal axis. Tissue was then set in paraffin wax using a Leica TP1020 processing machine. A 120 min/station protocol was adopted (complete cycle: 20 hours). Tissue embedded paraffin wax blocks containing the entire SNc were then sectioned (7 µm thick sections) with a microtome (Thermo Scientific) at three rostrocaudal levels of the SNc (rostral: -2.92 mm, medial: -3.16 mm and caudal: -3.52 AP mm; relative to bregma). Sections were then mounted on poly-L-lysine coated slides (VWR Int.) before being stored at 60°C over night. Note, in this initial study the striatum was not analysed.

### 3.3.1.8. Tyrosine hydroxylase staining in paraffin embedded 6-OHDA unilaterally lesioned brain sections

The same paraffin wax immunohistochemical protocol was used to that found in Chapter 2 section 2.3.1.3. The key difference was in the primary antibody used (anti-tyrosine hydroxylase; 1:500 dilution; AB152; rabbit host; Millipore).

### 3.3.1.9. Assessment of lesion severity via percentage SNc cell loss

Triplicate sections (three sequential sections) were taken at each of three different levels of the SNc (rostral: -2.92 mm, medial: -3.16 mm and caudal: -3.52 mm; AP axis relative to bregma) for each animal (nine sections in all per animal). To highlight SNc cells, sections were stained for TH-positivity, as explained in section 2.3.2.2. Cells of the SNc, in both the lesioned and unlesioned hemispheres, were imaged at 10X magnification (Axioskop, light-field compact microscope). TH-positive cells from both hemispheres were counted via ImageJ software. Only TH-positive cells from the SNc were counted, VTA TH-positive cells were omitted as these do not form part of the basal ganglia motor circuitry.

TH-positive SNc cells in the lesioned and intact SNc were then counted for each triplicate. The number of TH-positive cells remaining in the lesion hemisphere as a percentage of the intact was then calculated. Triplicate sections were then averaged to give a final value of *SNc cells remaining* for each SNc level (three final values for each animal). A final mean for the *SNc cells remaining* at each level in an experimental group was then obtained by averaging those values

from all animals in that group. If no difference was found between the three SNc levels in an experimental group then the values for the three levels were averaged. This then gave an overall *SNc cells remaining* value across the three SNc levels analysed (caudal, medial and rostral).

.

## 3.3.2. Pilot Study 2: Characterising the 6-OHDA partial lesion mouse Parkinson's disease model

### *3.3.2.1. Animal subjects*

7 eight-week-old male C57Bl/6 mice (Harlan, UK) were used and treated according to conditions in section 3.3.1.1.

### *3.3.2.2. Experimental design*

The timeline for the study is described below in figure 18. A week prior to lesioning (d-7) a 7 day habituation period was implemented to ensure animals were non-responsive to non-biologically relevant stimuli. On day 0, 6-OHDA lesioning was conducted in a randomised block design whilst blind to 6-OHDA dose. A recovery period of 14 days was then enforced post-lesion whereby daily rehydration and health checks were conducted until the animals had returned to pre-surgical weight. Necropsy was conducted at midday on day 15. Animals were killed by anaesthetic overdose and brains were removed for histological analysis.

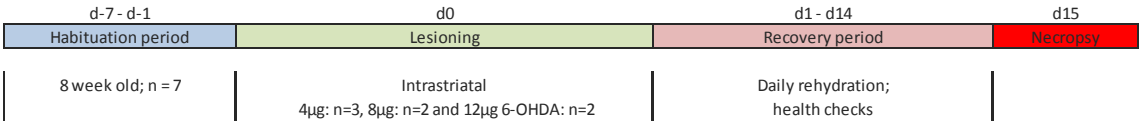


**Figure 19: Experimental design: Pilot study 2: Establishing the 6-OHDA partial lesion model.** All procedures of the study were conducted on certain days pre- or post-lesion as described in the figure. Further details are found either below the time line or in subsequent sections.

### *3.3.2.3. Surgery*

All surgical (apart from the lesioning protocol) and post-operative care techniques were identical to sections 3.3.1.3. and 3.3.1.5., respectively.

### *3.3.2.4. 6-OHDA partial lesion model*

In this model, varying concentrations of 6-OHDA were injected *intrastriatally* to identify the dose which would induce a consistent partial lesion.

Fine-bore holes (Ø 0.5 mm) were drilled at coordinates AP: +0.5 mm, ML: +2.2 mm (relative to bregma and skull surface). A blunt-ended 30 G needle was then inserted intrastriatally at DV: -3.5 mm (relative to bregma and skull surface) before 4, 8 or 12 µg 6-OHDA.HBr (Sigma-Aldrich) in 1 µl ice-cold 0.02% ascorbate/saline (4 µg: n=3; 8 µg: n=2; 12 µg: n=2) was administered at a rate of 0.5 µl/min. The injection needle was left in place for 5 minutes after toxin administration to ensure the full diffusion of the compound.

### *3.3.2.5. Assessment of lesion severity via percentage striatal TH-positive fibres remaining and TH-positive SNc cells remaining*

On post-lesion day 15, all animals were killed, perfuse fixed and their brains removed. Brains were embedded in paraffin wax, as according to section 3.3.1.7. Immunohistochemical staining of TH, as described in Chapter 2 section 2.3.1.3., was conducted on both SNc and striatal sections to detect the number of TH-positive cells within the SNc and also TH-positive fibres within the striatum. The key difference was in the primary antibody used (anti-tyrosine hydroxylase; 1:500 dilution; AB152; rabbit host; Millipore).

SNc cell counts were conducted according to the protocol in section 3.3.1.9.

Triplicate sections (three sequential sections) were taken at three different levels of the striatum (rostral: + 1.0 mm, medial: + 0.5 mm and caudal: - 0.22mm; AP axis relative to bregma) for each animal (nine sections in all per animal). Sections were stained for TH-positivity to highlight striatal TH-positive dopaminergic terminals. TH-positivity in both the lesioned and unlesioned striatal hemispheres, were imaged at 10X magnification (Axioskop, light-field compact microscope) and analysed via ImageJ software. Striatal images were divided into quadrants, these being the dorsolateral (DL), dorsomedial (DM), ventrolateral (VL) and ventromedial (VM) as depicted in figure 28. The TH-positivity in each quadrant was determined by grey mean value assessment in ImageJ using the freehand tool.

The TH-positive fibre optical densities of the four striatal quadrants in the lesioned and intact hemispheres were then assessed for each section. The density of TH-positive fibres remaining in each quadrant in the lesion hemisphere as a percentage of the respective quadrant in the intact was then calculated for all nine sections. Triplicate sections were then averaged to give a final *TH-positive fibres remaining* value for each quadrant at each striatal level (twelve final values for each animal). A final mean for *TH-positive fibres remaining* in each quadrant at each level in a experimental group was then obtained by averaging that quadrant's *TH-positive fibres remaining* value across all animals in that group.

## 3.3.3. Pilot Study 3: Identifying two coordinates for ChABC administration to cause the digestion of CSPGs along the entire nigrostriatal tract

### *3.3.3.1. Animal subjects*

5 eight-week-old male C57Bl/6 mice (Harlan, UK) were used in both the first set of coordinates tested and second set. Animals were treated according to conditions in section 3.3.1.1.

### *3.3.3.2. Experimental design*

The timeline for the study is described below in figure 19. A week prior to lesioning (d-7) a 7 day habituation period was implemented to ensure animals were non-responsive to non-biologically relevant stimuli. On day 0, ChABC administration was conducted in either the rostral SNc and caudal striatum or supranigral and intrastriatal regions. A recovery period of 6 days was then enforced post-lesion whereby daily rehydration and health checks were conducted until the animals had returned to pre-surgical weight. Necropsy was conducted at midday on day 7. Animals were killed by anaesthetic overdose and brains were removed for histological analysis.

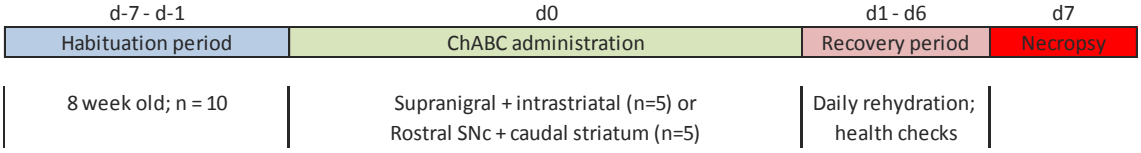


**Figure 20: Experimental design: Pilot Study 3: Identifying the sites for ChABC administration.** All procedures of the study were conducted on certain days pre- or post-lesion as described in the figure. Further details are found either below the time line or in subsequent sections.

### *3.3.3.3. Surgery*

All surgical and post-operative care techniques were identical to sections 3.3.1.3. and 3.3.1.5., respectively.

### *3.3.3.4. Stereotaxic injections of ChABC into the SNc and striatum*

Fine-bore holes (Ø 0.5 mm) were drilled at AP: +0.5 mm and ML: ±2.0 mm (relative to bregma and skull surface; intrastriatal site) and AP: -3.0 mm and ML: ±1.2 mm (relative to bregma and skull surface; supranigral site). All five animals received two single 1 µl intracerebral injections of ChABC (10 U/ml; Seikagaku) into the left hemisphere. One dose was administered intrastriatally (DV: -3.5 mm; relative to bregma and skull surface) and the other supranigrally (DV: -3.5 mm; relative to bregma and skull surface) (as determined by Paxinos and Watson Mouse Brain Atlas). The injection needle was left in place for a further 5 minutes to avoid reflux.

#### *3.3.3.5. Stereotaxic injections of ChABC into the rostral SNc and caudal striatum*

Fine-bore holes (Ø 0.5 mm) were drilled at AP: -2.3 mm and ML: ± 1.0 mm (relative to bregma and skull surface; rostral SNc site) and AP: +0.02 mm; ML: ±2.2 mm (relative to bregma and skull surface; caudal striatum site). All five animals received two single 1 µl intracerebral injections of ChABC (10 U/ml; Seikagaku) into the left hemisphere. One dose was administered into the rostral SNc (DV: -4.2 mm; relative to bregma and skull surface) and the caudal striatum (DV: -3.5 mm; relative to bregma and skull surface) (as determined by Paxinos and Watson Mouse Brain Atlas). The injection needle was left in place for a further 5 minutes to avoid reflux.

#### *3.3.3.6. C4S staining of digested CS-GAG stub epitopes in paraffin embedded mouse brain sections*

Apart from the use of the C4S primary antibody (mouse monoclonal; 1:500; MPBio #636511), the immunohistochemical procedures for detecting C4S immunoreactivity were otherwise identical to those described in Chapter 2 section 2.3.1.3.

C4S staining was visualised and imaged at 10X magnification (Axioskop, light-field compact microscope). No quantification was conducted. Sections were instead used to confirm the pattern of CSPG digestion in BG regions.

## 3.3.4. Investigating the effect of ChABC administration on cellular and behavioural recovery in a full 6-OHDA lesion mouse model

### *3.3.4.1. Animal subjects*

27 eight-week-old male C57Bl/6 mice (Harlan, UK) were used and treated according to conditions in section 3.3.1.1.

### *3.3.4.2. Experimental design*

The timeline for the study is described below in figure 20. A week prior to lesioning (d-7) a 7 day habituation period was implemented to ensure animals were non-responsive to non-biologically relevant stimuli. During this period, baseline recordings for the cylinder test (see section 3.3.4.6.) were conducted (days -4 and -1). 6-OHDA and ChABC administration was conducted on day 0 in a randomised block design whilst blind to the treatment. All animals received 8 µg of supranigral 6-OHDA and either ChABC or saline (rostral SNc and caudal striatum). A recovery period of 31 days was enforced whereby daily rehydration and health checks were conducted until the animals had returned to pre-surgical weight. During this period the cylinder test was conducted on all animals at weekly intervals. On day 35 and 38 animals undertook the amphetamine and apomorphine-induced rotation tests, respectively. On day 42 post-lesion animals were killed by anaesthetic overdose and brains were removed for histological analysis.

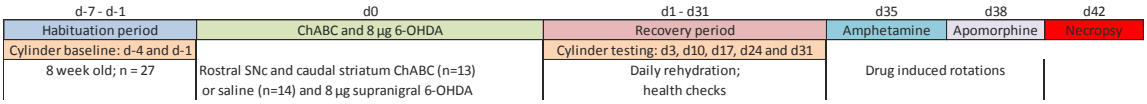


**Figure 21: Experimental design: Investigating the effect of ChABC administration on cellular and behavioural recovery in a full 6-OHDA lesion mouse model.**
All procedures of the study were conducted on certain days pre- or post-lesion as described in the figure. Further details are found either below the time line or in subsequent sections.

### *3.3.4.3. 6-OHDA and ChABC administration*

All methods of surgery and post operative care were identical to those previously described in sections 3.3.1.3 and 3.3.1.5., respectively. The 6-OHDA lesioning protocol (8 µg 6-OHDA; supranigral) was identical to those used in section 3.3.1.4.

Animals received two 1 µl intracerebral injections of either saline (n=14) or ChABC (n=13; 10 U/ml; Seikagaku) into the 6-OHDA injected hemisphere. In accordance with data obtained from Pilot Study 3 to derive optimum CSPG digestion, one dose was administered into the rostral SNc (AP: -2.3 mm; ML: +1.0 mm and DV: -4.2 mm; relative to bregma and skull surface) and the other into the caudal striatum (AP: +0.02 mm; ML: + 2.2 mm and DV: -3.5 mm; relative to

bregma and skull surface). The injections of ChABC were administered sequentially 5 minutes after the injection of the 6-OHDA and were left in place for a further 5 minutes to avoid toxin reflux.

#### *3.3.4.4. Quantifying and assessing the effect of ChABC in the full lesion model*

Behavioural, immunohistochemical and analytical methods were similar to those in the pilot studies. As the techniques have been previously mentioned, brief descriptions of the methods conducting in this study are described below.

#### *3.3.4.5. Behavioural assessment of parkinsonian phenotype*

At set time points pre- or post-6-OHDA lesioning (see subsequent tests for specific days), behavioural assessments of hemiparkinsonian phenotype was conducted via the cylinder test, amphetamine-induced rotation and apomorphine-induced rotation tests.

#### *3.3.4.6. Cylinder test*

The cylinder test exploits the natural rearing behaviour rodents exhibit in novel environments in order to identify bias in forepaw use following a unilateral lesion (Schallert *et al.*, 2000). As the forepaw contralateral-to-the-lesion is weakened, the ipsilateral paw will therefore be favoured in the majority of weight-bearing touches. This test, through a calculated *asymmetry score*, can identify whether an animal recovers the mobility of its contralateral forepaw by disease modifying pharmacological agents or cell survival strategies. The cylinder test can correlate SNc lesion severity to the calculated asymmetry score (Lundblad *et al.*, 2002).

On days -4, -1, 3, 10, 17, 24 and 31, mice were placed individually within 2 litre glass beakers (Ø 12 cm) in which the forepaw preference was monitored during rearing behaviour (figure 21). Mirrors were placed behind the beakers to ensure a 360° view of the animal during its rears. 5 minute video recordings of the cylinder test were taken; only cases where the animal had not yet made the required 10 touches did the experiment run for additional time. Weight bearing touches by only the forepaw ipsilateral-to-the-lesion, contralateral-to-the-lesion or both forepaws simultaneously were measured. An *asymmetry score* was then calculated to indicate the proportional use of each forepaw.

The score equation is as follows:

$$AsymmetryScore = \left( \frac{(½\,Both) + Contra}{Total} \right) \times 100$$

Where: *Both* is the weight-bearing touch of both the ipsi- and contralateral-to-the-lesion forepaws simultaneously, *Contra* is the weight-bearing touch of only the contralateral-to-the-lesion forepaw and *Total* is the total number of weight-bearing touches (the sum of *Both*, *Contra* and the ipsilateral-to-the-lesion touches).

A score of 50% would indicate no bias whereas a lower score would denote a loss of injured (contralateral) forepaw ability. Any behavioural recovery would be represented by a rise in asymmetry score back to 50%. A minimum of 10 touches were required before the experimental run was judged complete. In order to maintain consistency with activity levels, testing was always carried out at midday. Representative images of the cylinder test in progress can be seen in figure 21.

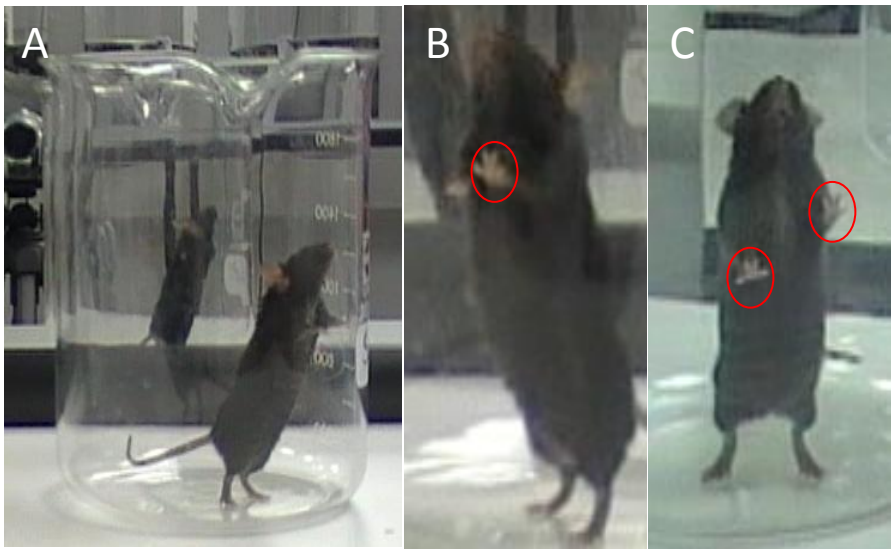


**Figure 22: Performance of the cylinder test.**
(A) Mice were individually placed in 2 litre beakers for 10 minutes. Specific forepaws used for weight-bearing touches were recorded. (B) A unilaterally lesioned mouse will favour the ipsilateral-to-the-lesion paw over the contralateral. Asymmetry scores typically drop to 20-30%. Red circle highlights the weight-bearing touch of the ipsilateral paw. (C) Saline administered animals present no bias in paw preference. Non-lesioned animals typically present an asymmetry score of ~50%. Red circles highlight weight-bearing forepaw touches. This would be recorded as a *Both*.

### *3.3.4.7. Amphetamine and apomorphine-induced rotations*

Lesioned mice were administered with either D-amphetamine hemisulphate (Tocris; 5 mg/kg, i.p.) in saline or apomorphine (Sigma-Aldrich; 0.5 mg/kg, s.c.) in saline. Animals were placed within cylindrical arenas (Ø 40 cm) immediately after drug administration in which the motion tracking tool Ethovision XT6 was used for recording. A custom optimised calibration file was loaded, which allowed the recording of full 360° rotations about the animal's midpoint (figure 22C + D). Ipsiversive and contraversive rotations were then individually measured. The lesioned animals expected response to amphetamine and apomorphine is shown in figure 22A + B respectively. A 20 minute habituation period prior to drug administration was conducted; rotations were recorded for 120 minutes thereafter.

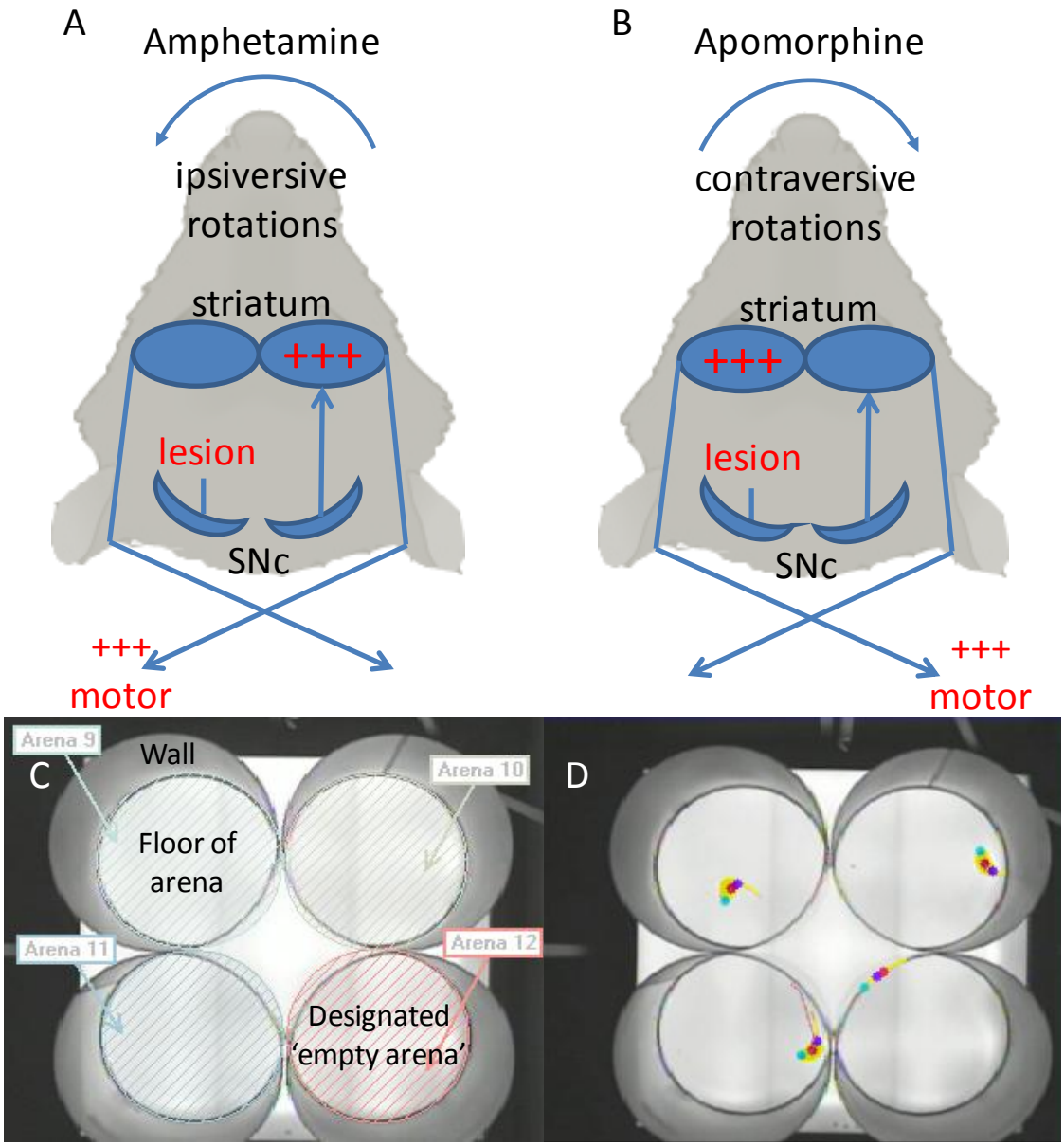


**Figure 23: Typical rotational behaviour of amphetamine- and apomorphine-induced rotations as measured by Noldus Ethovision XT6 tracking software.**
(A) Amphetamine increases striatal DA by upregulating vesicular DA release. As a result, motor output is increased (+++) from the unlesioned hemisphere causing ipsiversive rotations towards the lesion. (B) In contrast, as toxin driven denervation upregulates D1/D2 receptor expression at the post-synaptic nerve terminal, apomorphine (non-selective DA receptor agonist) has a more marked action in the lesioned hemisphere (+++). This therefore causes contraversive rotations (away from the lesion) in the hemiparkisonian rodent (C) The Noldus Ethovision XT6 apparatus distinguished the animal's body from the arena via the *dynamic subtraction* method of detection, in which animals placed into the defined arena were considered novel when compared to an empty reference arena. A typical arena set up is shown in panel C. (D) Nose, midpoint and tail-base markers were assigned (blue, red and purple dots, respectively) by the program. 360° rotations about the animal's midpoint were recorded as a single rotation in either the ipsiversive or contraversive direction.

### *Immunohistochemical assessments*

On post-lesion day 42, all animals were killed, perfuse fixed and their brains removed. Brains were embedded in paraffin wax, as according to section 3.3.1.7. Immunohistochemical staining of TH, as described in Chapter 2 section 2.3.2.2., was conducted on both SNc sections (rostral: -2.92 mm, medial: -3.16 mm and caudal: -3.52 mm AP; relative to bregma) and striatal sections (rostral: +1.00 mm, medial: +0.5 mm and caudal: -0.22 mm AP; relative to bregma) to detect the number of TH-positive cells within the SNc and TH-positive fibres within the striatum. The assessment of lesion severity by the cells remaining in the SNc and TH content within the striatum was conducted as per section 3.3.1.9. and 3.3.2.5., respectively.

As no significance was detected between the two dorsal striatal (between DL and DM) or two ventral striatal quadrants (between VL and VM), the striatal optical densities for the DL and DM were averaged to form the *dorsal striatum* and the striatal optical densities for the VL and VM were averaged to form the *ventral striatum.*

## 3.3.5. Investigating the effect of ChABC administration on cellular and behavioural recovery in a partial 6-OHDA lesion mouse model

### *3.3.5.1. Animal subjects*

34 eight-week-old male C57Bl/6 mice (Harlan, UK) were used and treated according to conditions in section 3.3.1.1.

### *3.3.5.2. Experimental design*

The timeline for the study is described below in figure 23. A week prior to lesioning (d-7) a 7 day habituation period was implemented to ensure animals were non-responsive to non-biologically relevant stimuli. During this period, baseline recordings for the cylinder test were conducted (days -3 and -1). 6-OHDA and ChABC administration was conducted on day 0 in a randomised block design whilst blind to the treatment. All animals received 4 µg of intrastriatal 6-OHDA and either ChABC or saline (rostral SNc and caudal striatum). A recovery period of 35 days was enforced whereby daily rehydration and health checks were conducted until the animals had returned to pre-surgical weight. During this period the cylinder test was conducted on all animals at weekly intervals. On day 37 animals undertook the amphetamine-induced rotation test. This study did not require the apomorphine-induced rotation test as this behavioural assay responds only to fully lesioned animals. On day 39 post-lesion animals were killed by anaesthetic overdose and brains were removed for histological analysis.

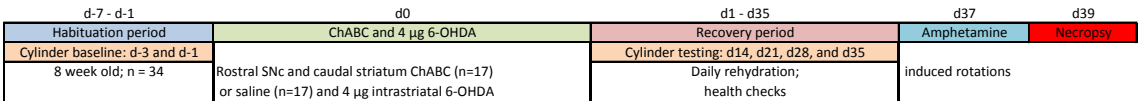


**Figure 24: Experimental design: Investigating the effect of ChABC administration on cellular and behavioural recovery in a partial 6-OHDA lesion mouse model.**
All procedures of the study were conducted on certain days pre- or post-lesion as described in the figure. Further details are found either below the time line or in subsequent sections.

### *3.3.5.3. Quantifying and assessing the effect of ChABC in the partial lesion model*

Behavioural, immunohistochemical and analytical methods were similar to those in the pilot studies. As the techniques have been previously mentioned, brief descriptions of the methods conducting in this study are described below.

### *Behavioural assessments*

The cylinder test was conducted to assess the degree of forelimb asymmetry as described in section 3.3.4.6. Cylinder tests were conducted during the habituation period on days -3 and -1 and on days 14, 21, 28 and 35 post-lesion. On post-lesion day 37 the amphetamine-induced rotation test was conducted as per section 3.3.4.7.

### *Immunohistochemical assessments*

On post-lesion day 39, all animals were killed, perfuse fixed and their brains removed. Brains were embedded in paraffin wax, as according to section 3.3.1.7. Immunohistochemical staining of TH, as described in Chapter 2 section 2.3.1.3., was conducted on both SNc and striatal sections to detect the number of TH-positive cells within the SNc and also TH-positive fibres remaining within the striatum. The assessment of lesion severity by the cells remaining in the SNc and TH content within the striatum was conducted as per section 3.3.1.9. and 3.3.2.5., respectively.

As no significance was detected between the two dorsal striatal (between DL and DM) or two ventral striatal quadrants (between VL and VM), the striatal optical densities for the DL and DM were averaged to form the *dorsal striatum* and the striatal optical densities for the VL and VM were averaged to form the *ventral striatum.*

## 3.3.6. Statistical analysis

All statistical analyses within this chapter were conducted with the SigmaPlot 12 package; statistical tests used are displayed within the figure legends. Graphpad Prism 5 was used to plot all graphs. GPower 3.1 was utilised for power calculations.

## 3.4. Results

### 3.4.1. Pilot Study 1: supranigral administration of 8 µg 6-OHDA induced the full ablation of the mouse SNc

To assess the efficacy of ChABC as a PD therapeutic we wished to apply the enzyme to both a partial and full unilateral 6-OHDA lesion model. However, due to the novelty of the mouse model within the Duty laboratory these models were required to be characterised.

This *dose finding* pilot focussed on identifying the correct dose of supranigral 6-OHDA required to induce a consistent full lesion in the SNc; a lesion model that attempts to recapitulate the pathology of late-stage PD (>85% SNc cell loss). To determine which dose of 6-OHDA was most successful in producing the correct lesion size, immunohistological approaches were conducted to permit the counting of the remaining cells in both the intact and lesioned SNc. These values would then be used to determine the total cells remaining in the lesioned SNc as a percentage of the total cells in the intact. Unfortunately, due to damage, no striatal tissue was obtained for TH-positive fibre assessment.

With this full lesion model established, it would then be possible to assess the effects of ChABC in a model of late-stage PD.

### *TH immunohistochemistry of the SNc*

To gather the relevant data required for correct 6-OHDA dose assessment, images of the SNc were first obtained. Photomicrographs (10X magnification), shown below in figure 24, depict the increased loss in SNc cells in the parkinsonian hemisphere in a dose dependent manner. The A10 dopaminergic cells of the VTA (black dotted line) were avoided when counting the SNc's A9 dopaminergic cells (black dashed line; vehicle section). The medial lemniscus (ml) was used as *spirit level* throughout the SNc as it allowed myself to determine whether the sections were perpendicular to the central midline of the brain.

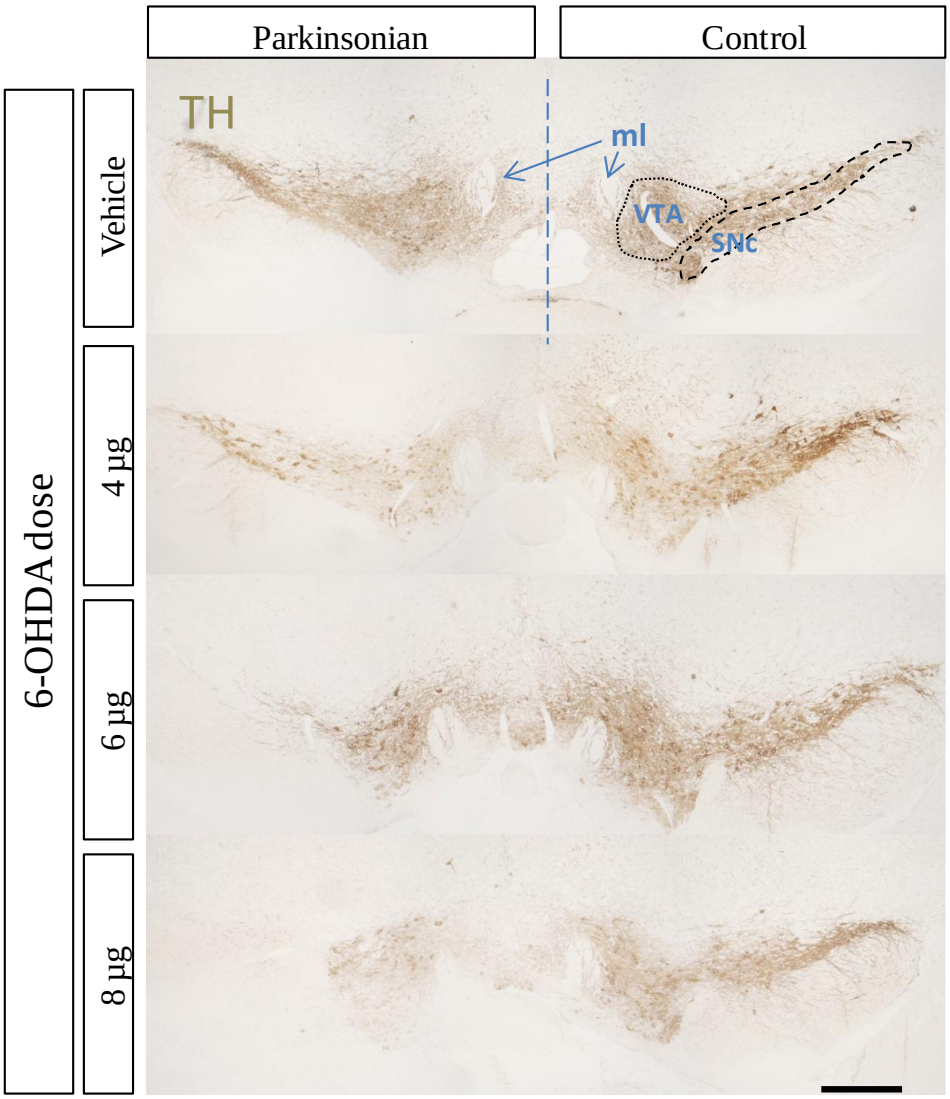


**Figure 25: Photomicrographs highlighting a 6-OHDA dose dependent increase in SNc pathology severity.**
Coronal TH-positive SNc cell sections taken at the medial level (-3.16 mm AP; relative to bregma). Top to bottom: vehicle, 4 µg, 6 µg and 8 µg 6-OHDA. The lesioned SNc is shown on the left of each section. The SNc (black dashed line) and ventral tegmental area (VTA; black dotted line shown) have been highlighted on the vehicle section above. The medial lemniscus (ml) acted as a *spirit level* to aid cutting a perpendicular section for accurate cell counts. Scale bar represents 250 µm.

### *Assessment of cells remaining in the SNc as a result of 6-OHDA lesioning*

TH-positive cells of the rostral, medial and caudal SNc sections were counted in the lesioned and intact hemispheres of each animal. Counts from the three levels were then averaged. Raw cell count data is presented in figure 25A. All doses of 6-OHDA induced a significant loss in TH-positive SNc cells in the lesioned hemisphere ($p<0.001$ for all groups; Two-Way ANOVA with Bonferroni post hoc test). Loss in total cell numbers in the lesioned SNc compared to the intact SNc were as follows: 79 to 31, 69 to 20 and 75 to 17 for the 4, 6 and 8 µg 6-OHDA groups, respectively. The saline vehicle did not see a significant loss in cell number in the injected hemisphere (Lesioned: 68 SNc cells and Intact: 69 SNc cells). The number of SNc cells in the uninjured SNc was equivalent to those found in published data (Heuer *et al.*, 2012).

To help standardise these results with other published lesion models, final means of the TH-positive cells in the lesioned SNc as a percentage of the intact SNc were calculated. These values were an average of the three SNc levels. Intranigral 6-OHDA produced significant SNc cell loss across all 6-OHDA doses compared to the vehicle administered animals ($p<0.001$ for all groups; One-Way ANOVA with Bonferroni post hoc test). The mean percentage of TH-positive cells remaining in the lesioned SNc (to those of the intact SNc) of animals in the 4, 6 and 8 µg groups were 40.6 ± 11.5 %, 27.6 ± 11.9% and 23.6 ± 5% respectively (figure 25B).

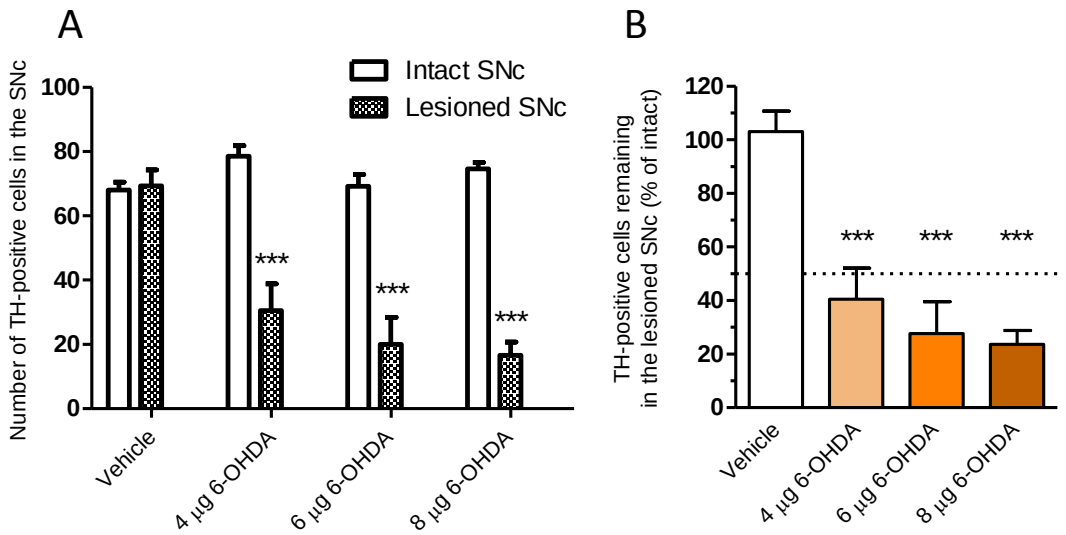


**Figure 26: Increased concentrations of 6-OHDA induced higher severity in SNc pathology.** (A) Averaged TH-positive cell counts across the caudal, medial and rostral levels of the intact and lesioned SNc. (B) TH-positive cells in the lesioned SNc as a percentage of the intact SNc across the caudal, medial and rostral levels. Lesion severity increased with 6-OHDA dose. Panel A: Two-way ANOVA with Bonferroni post hoc test; *** denotes $p<0.001$ between lesioned hemisphere and group's intact hemisphere. Panel B: One-way ANOVA with Dunnett's post hoc test; *** denotes $p<0.001$ between 6-OHDA dose and vehicle control. Saline: n=4, 4 µg: n=6, 6

### 3.4.2. Pilot Study 2: Intrastriatal administration of 4 µg 6-OHDA induced the partial ablation of the mouse SNc

This second *dose finding* pilot study focussed on identifying the correct dose of intrastriatal 6-OHDA required to induce a consistent partial lesion in the SNc. This lesion model would attempt to recapitulate the pathology of early-stage PD (~50-60% SNc cell loss). To determine which dose of 6-OHDA was most successful in producing the correct lesion size, immunohistological approaches were conducted to permit the counting of the remaining cells in both the intact and lesioned SNc. These values were then used to determine the total cells remaining in the lesioned SNc as a percentage of the total cells in the intact. Additionally, optical densities of the TH-positive fibres in the lesioned striatum were obtained to calculate dopaminergic terminal loss as a percentage of the intact.

With this full lesion model established, it would then be possible to assess the effects of ChABC in a model of early-stage PD.

### *TH immunohistochemistry of the SNc*

To gather the relevant data required for correct 6-OHDA dose assessment, images of the SNc were first obtained. Photomicrographs, shown in figure 26, depict the increased loss in SNc cells in the parkinsonian hemisphere (black dashed line; vehicle section).

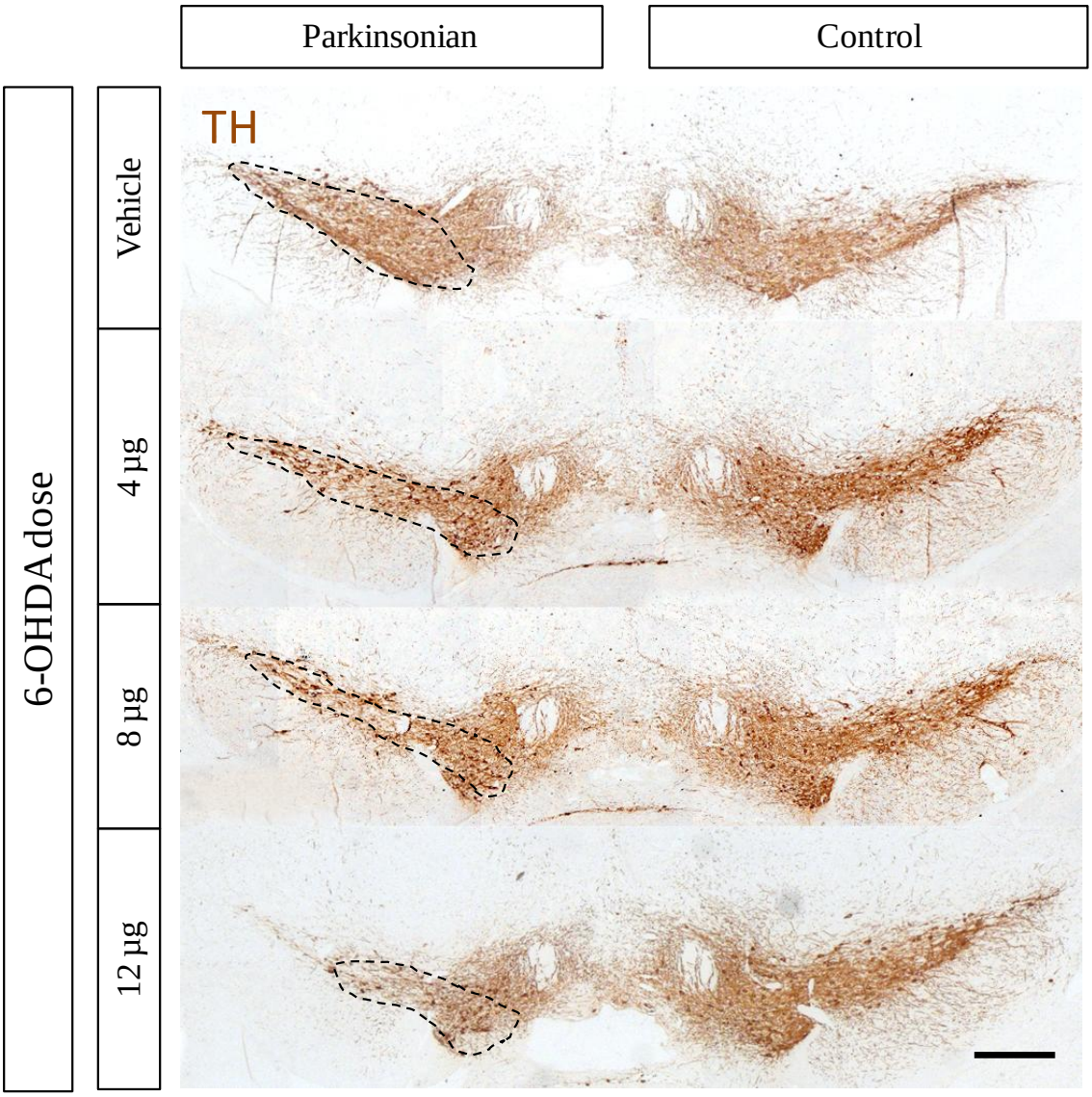


**Figure 27: Photomicrographs highlighting a 6-OHDA dose dependent increase in SNc pathology severity.**
Photomicrographs of coronal TH-positive SNc cell sections taken at 10X magnification. Top to bottom: Vehicle, 4 µg, 8 µg and 12 µg 6-OHDA. The unilaterally lesioned SNc is shown on the left of each section. All sections were cut at the medial level (-3.16 mm AP; relative to bregma). Black dashed line indicates the SNc. Scale bar represents 250 µm.

### *Assessment of cells remaining in the SNc as a result of 6-OHDA lesioning*

TH-positive cells of the SNc were counted in the lesioned and intact hemispheres of each animal. Raw data is presented below in figure 27A. Only the 12 µg dose of 6-OHDA induced a significant loss in TH-positive SNc cells in the lesioned hemisphere ($p<0.05$; Two-Way ANOVA with Bonferroni post hoc test). Loss in total cell numbers in the lesioned SNc compared to the intact SNc were as follows: 58 to 37, 69 to 34 and 85 to 36 for the 4, 8 and 12 µg 6-OHDA groups, respectively. The saline vehicle did not see a significant loss in cell number in the injected hemisphere (Lesioned: 69 SNc cells and Intact: 65 SNc cells). The number of SNc cells in the uninjured SNc was equivalent to those found in published data (Heuer *et al.*, 2012).

To help standardise these results with other published lesion models, final means of the TH-positive cells in the lesioned SNc as a percentage of the intact SNc were calculated. These values were an average of the three SNc levels. Intrastriatal 6-OHDA produced significant SNc cell loss across all 6-OHDA doses compared to the vehicle administered animals (4 µg and 8 µg: $p<0.05$ and 12 µg: $p<0.01$; One-Way ANOVA with Bonferroni post hoc test). The 4 µg 6-OHDA group induced a partial lesion which left almost half of the SNc cells alive (56.7 ± 8.9%). The 8 and 12 µg 6-OHDA groups induce a fuller lesion that left 43.9 ± 20.8% and 36.3 ± 16.1% of the lesioned SNc alive, respectively; figure 27B. The 4 µg 6-OHDA dose produced the closest lesion size to that of the ideal partial lesion (~50-60% cell and TH-positive fibre content loss).

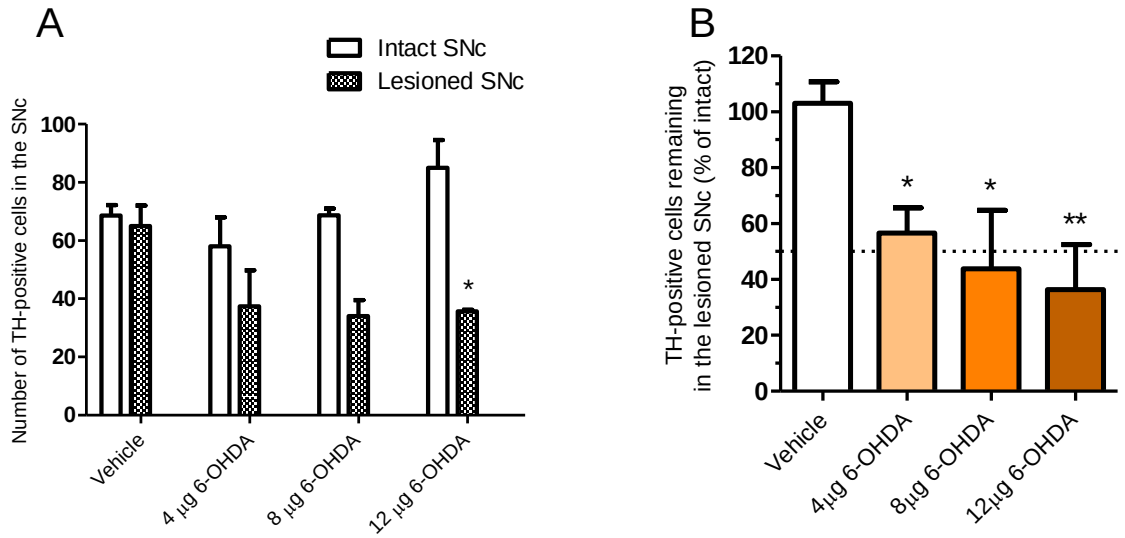


**Figure 28: Increased concentrations of 6-OHDA induced higher severity in SNc pathology.** (A) TH-positive cell counts in the intact and lesioned SNc. (B) TH-positive cells in the lesioned SNc as a percentage of the intact SNc. Lesion severity increased with 6-OHDA dose. Panel A: Two-way ANOVA with Bonferroni post hoc test; * denotes $p<0.05$ between the group's lesioned hemisphere and intact hemisphere. Panel B: One-Way ANOVA with Dunnett's post hoc test; * denotes $p<0.05$ and ** denotes $p<0.01$ between 6-OHDA dose and vehicle control. Saline: n=3, 4 µg: n=3, 6 µg: n=2 and 8 µg: n=2. Data are mean ± S.E.M.

### *TH immunohistochemistry of the striatum*

Photomicrographs (10X magnification) of the striatum were taken to assess the degree of dopaminergic denervation caused by the varying doses of 6-OHDA (figure 28). The remaining levels of TH-positive fibres in the parkinsonian striatum (black line; 4 µg 6-OHDA section) were seen to decline with an increasing dosage of 6-OHDA. In figure 29, analysis of TH-positive denervation was assessed by optical density measurements of the subdivided quadrants of both striata (which were DM, DL, VM, and VL).

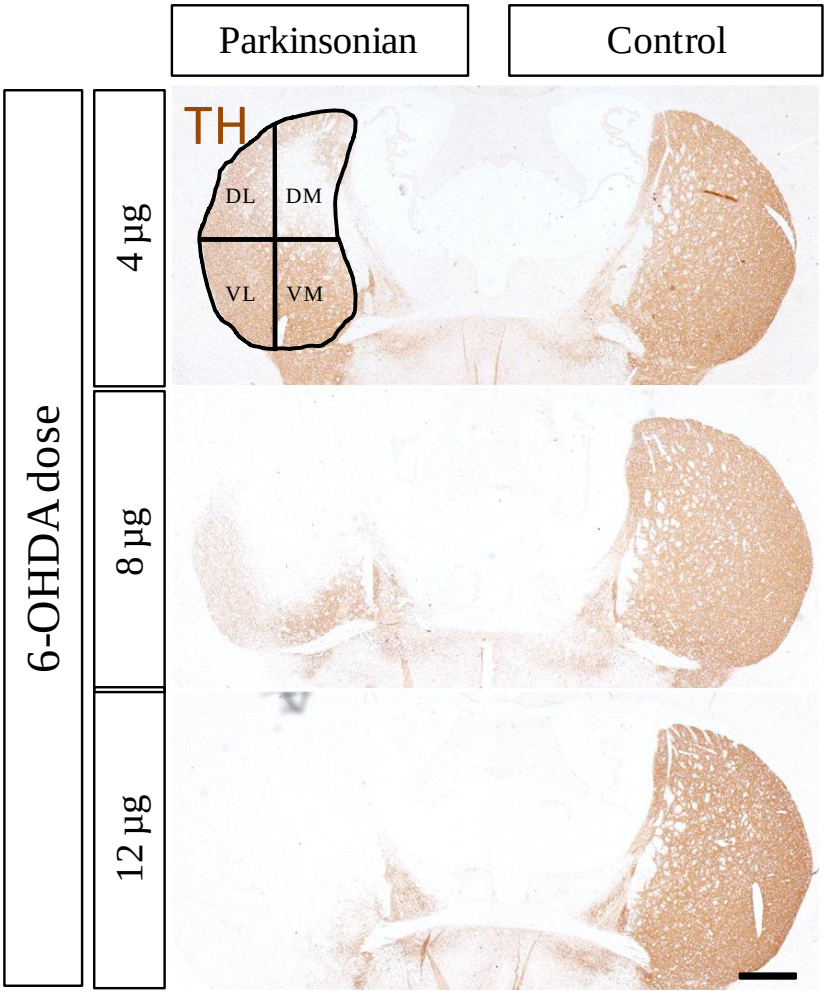


**Figure 29: Photomicrographs highlighting a 6-OHDA dose dependent increase in striatal pathology severity**

(A) Photomicrographs of the TH-positive dopaminergic terminals in the mouse striatum taken at 10X magnification. Top to bottom: 4 µg, 8 µg and 12 µg 6-OHDA. Striata were divided into quadrants for analysis, these were dorsomedial (DM), dorsolateral (DL), ventromedial (VM), and ventrolateral (VL). All sections were cut at the medial level (+1.00 mm AP; relative to bregma and skull surface). Scale bar represents 500 µm.

### *Assessment of TH-positive fibres remaining in the striatum as a result of 6-OHDA lesioning*

Optical densities of the TH-positive fibres within the four quadrants of the lesioned and intact striata were obtained. Means representing the TH-positive fibres in the quadrants of the lesioned striatum as a percentage of the equivalent quadrants in the intact striatum were then calculated. These were calculated for the caudal, medial and rostral levels (figure 29A - C).

The 4 µg 6-OHDA dose produced the closest lesion size to that of the ideal partial lesion (~50-60% TH-positive fibre content loss). The 4 µg dose induced the smallest lesion size across all four quadrants which left a significant amount of TH-positive fibres within the lesioned striatum (Mean TH-positive fibres remaining across all four quadrants - Caudal: 35.0 ± 11.4%, Medial: 56.2 ± 6.1%, Rostral: 59.8 ± 4.9). However, the 8 µg and 12 µg doses ablated the striatum almost entirely across all quadrants (TH-positive fibres remaining across all four quadrants - Caudal: 9.1 ± 4.9%, Medial: 20.0 ± 14.3%, Rostral: 33.1 ± 19.5 and Caudal: 11.7 ± 6.1%, Medial: 14.5 ± 9.6%, Rostral: 25.5 ± 14.5, respectively). The dashed line at 50% cell loss indicates the ideal partial lesion for each quadrant at each level.

No specific statistical tests were performed as the purpose of these data was to qualitatively identify the 6-OHDA dose that could provide a consistent partial lesion. The 4 µg 6-OHDA dose produced the closest lesion size to that of the ideal partial lesion across the striatum (~50-60% TH-positive fibre content loss), whereas the 8 and 12 µg 6-OHDA doses induced a more full ablation of the SNc.

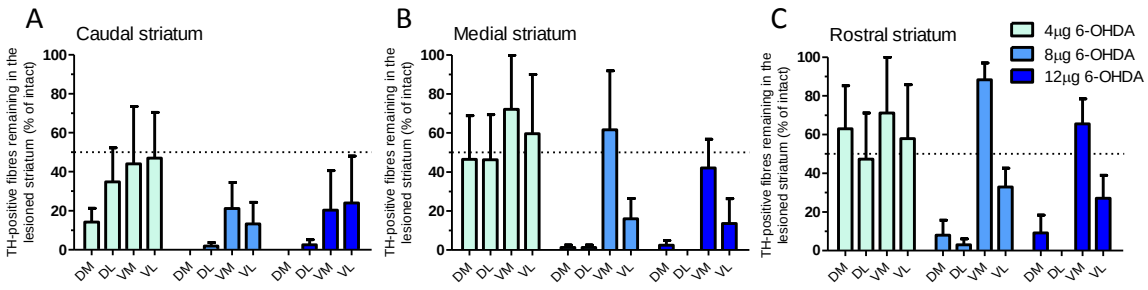


**Figure 30: Increased concentrations of 6-OHDA induced higher severity in striatal pathology.** (A - C) The three levels of the striatum at which analysis of TH content was taken. Data represent the measured optical densities of the TH-positivity in a striatal quadrant within the lesioned striatum as a percentage of the equivalent quadrant within the intact striatum. Black dashed line denotes an ideal partial lesion size of ~50%. 4 µg: n=3, 8 µg: n=2 and 12 µg: n=2. Data are mean ± S.E.M. Scale bar represents 250 µm.

### 3.4.3. Pilot Study 3: ChABC digests CSPGs along the nigrostriatal tract when administered to the caudal striatum and dorsal SNc

Injecting ChABC both intrastriatally and supranigrally (see methods for coordinates; section 3.3.3.4.) saw the digestion of the CSPGs along the rostro-caudal axis of the mouse brain (figure 30). Brown stain indicates immunoreactivity for the C4S CS-GAG stub epitope; an epitope highlighting regions of ChABC digestion. Only the left hand hemisphere was injected with ChABC, the right hand side was left as a control. Not all regions of the NS, such as the MFB, were digested (yellow ovals).

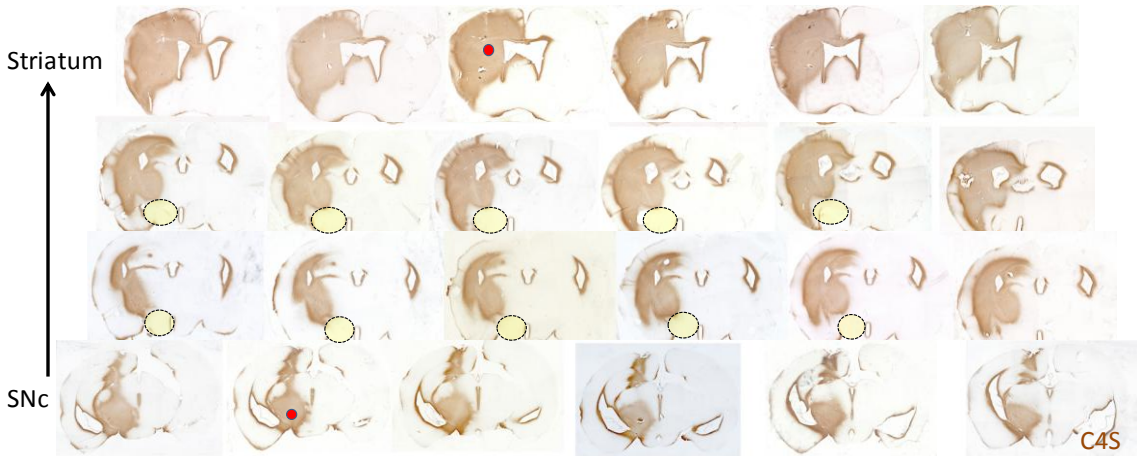


**Figure 31: C4S immunoreactivity displaying the ChABC digestion pattern following the intrastriatal and supranigral administration of ChABC.**
Displayed are 6 consecutive sections of the striatum (top row), rostral and caudal NS (two centre rows) and the SNc (bottom row) presenting the pattern of CSPG digestion. ChABC was injected into the striatum (injection site: red dot, top row) and the SNc (injection site: red dot, bottom row). Yellow circles indicate regions of the NS which were not digested by ChABC.

Readjusting the location of the striatal ChABC injection site to a more caudal region and the SNc injection site to a more rostral region (see methods for coordinates; section 3.3.3.5.) compared to the previous pilot enhanced ChABC digestion in the NS. Along the rostro-caudal axis the entire NS was found immunoreactive for the C4S stub epitope (figure 31).

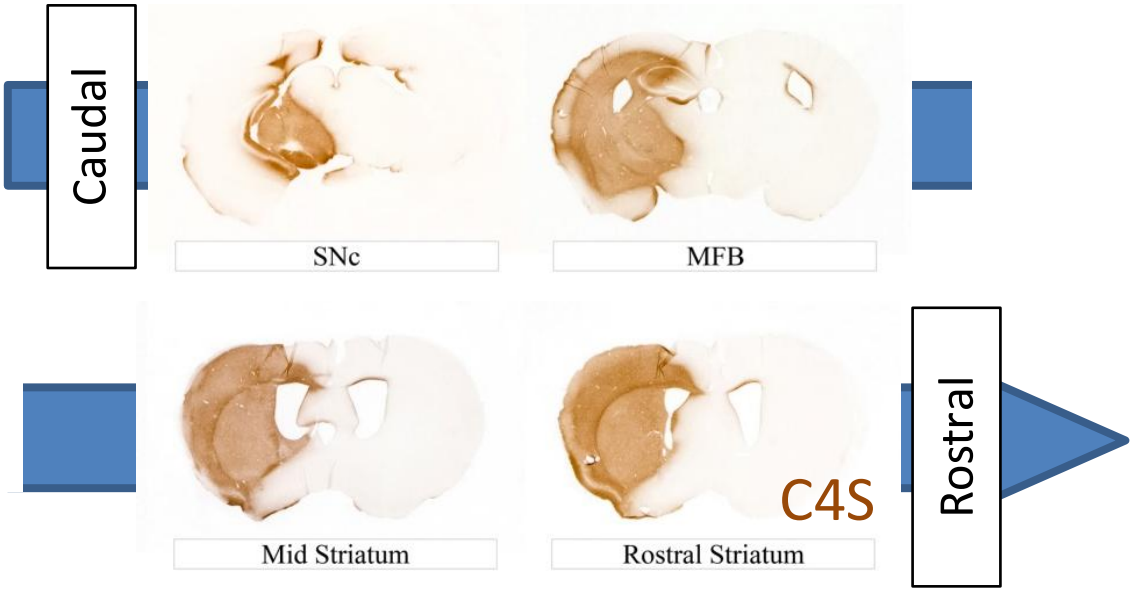


**Figure 32: C4S immunoreactivity displaying the ChABC digestion pattern following the caudal striatal and rostral SNc administration of ChABC.**
Displayed are 4 representative images of the SNc, MFB, mid striatum and rostral striatum. The entire NS was found to have immunoreactivity for the C4S epitope.

### 3.4.4. ChABC administration does not increase SNc cell survival in a full lesion 6-OHDA model of Parkinson's disease

This study used the parameters derived in Pilot Study 1 and 3 (i.e. dose of 6-OHDA required for a consistent full lesion and the location of ChABC administration for full digestion of the NS) to determine the effect of ChABC's digestion of CSPGs within the NS of a full lesion model.

#### *Confirmation of CSPG digestion along the nigrostriatal tract*

Using the coordinates determined by Pilot Study 3, unilateral ChABC administration brought about the full digestion of the entire NS in the lesioned left hemisphere (figure 32A; bottom panel). The ChABC digested the CSPGs surrounding the fully ablated SNc and neighbouring regions, whereas vehicle administration presented no C4S-positivity and thus no digestion. At other levels of the NS, C4S digestion was also apparent (figure 32). Due to the success of the CSPG digestion, these results now validate the rest of the data in this study.

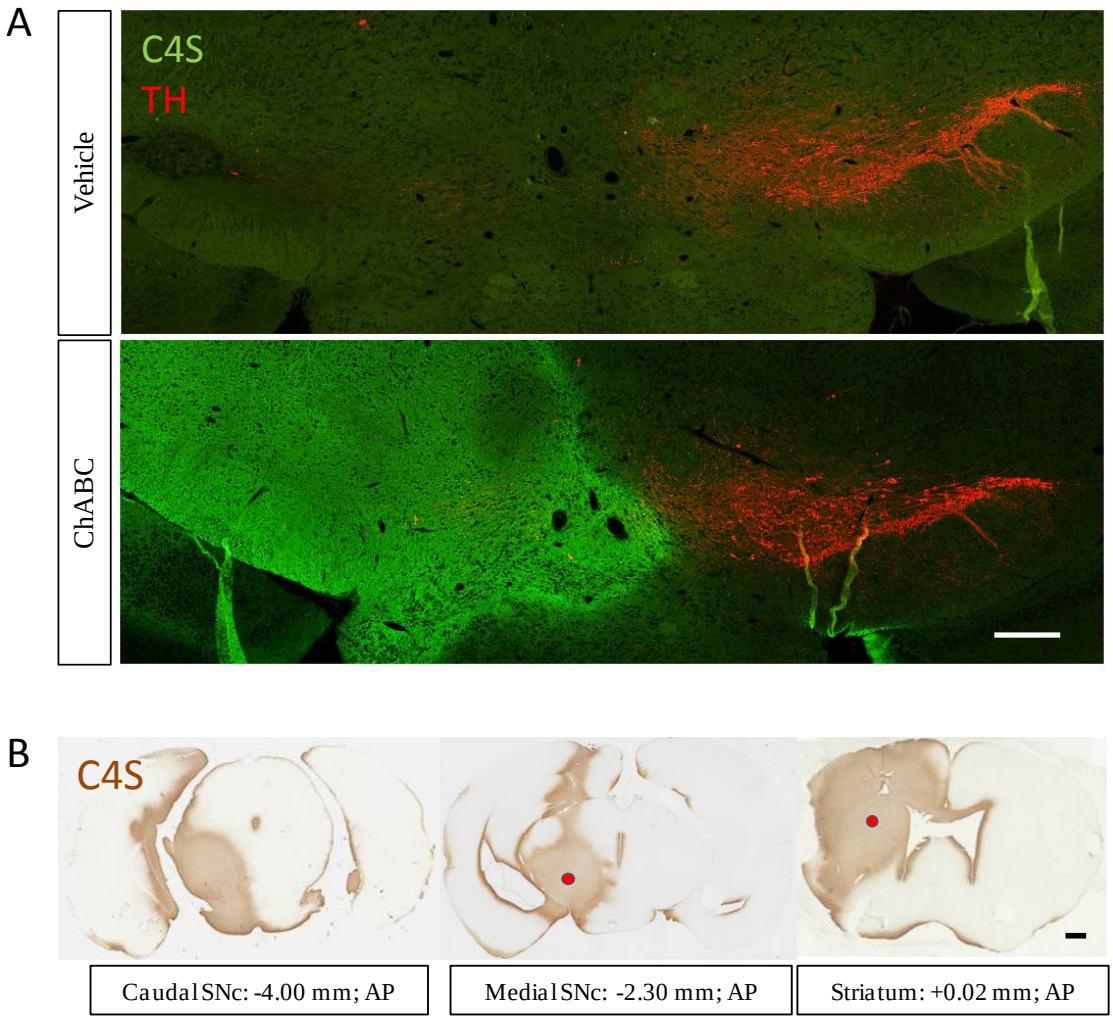


**Figure 33: Two bolus injections of ChABC digests the entire NS in the full lesion model.**
(A) Immunofluorescent photomicrographs of the SNc indicating area of CSPG digestion. The ChABC-digestion epitope, C4S (green), was not detected in the saline-treated animals but only the ChABC-treated. TH immunoreactivity (red) indicates SNc cells. Full lesioning of the SNc in the left hand hemisphere removes any TH-positivity. (B) Three levels of the NS (Caudal and medial SNC and striatum) highlighting the regions of C4S-positivity and thus CSPG digestion (brown). Red dots indicate the location of ChABC administration. Scale bar: 500 µm.

### *TH immunohistochemistry of the SNc and striatum*

To gather the relevant data required for correct 6-OHDA dose assessment, images of the SNc and striatum were first obtained. Photomicrographs, shown in figure 33A + B, depict the increased loss in SNc cells and TH-positive striatal fibres in the parkinsonian hemisphere (left), respectively.

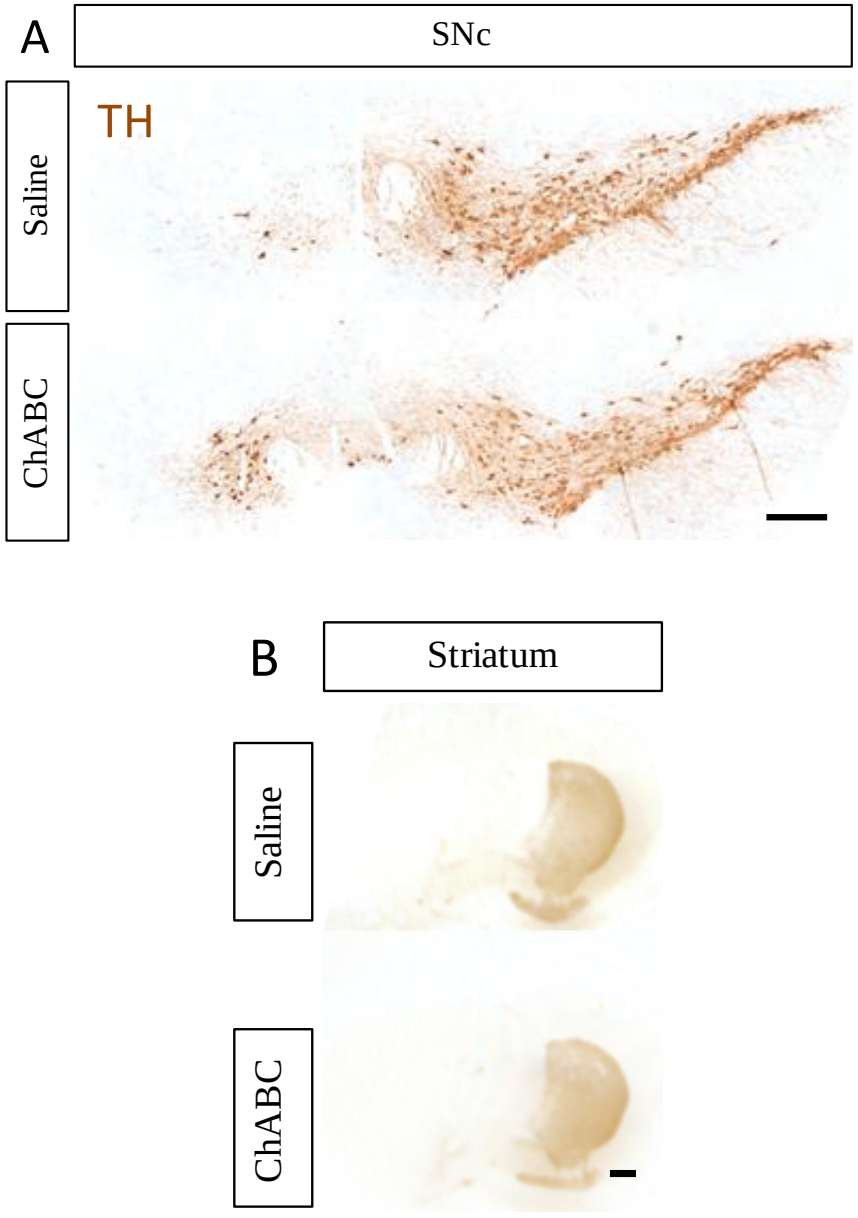


**Figure 34: Photomicrographs highlighting ChABC's inability to increase TH-positive cell and fibre survival in the full lesion model.**
(A) Photomicrographs of the coronal TH-positive SNc cell sections taken at 10X magnification. Top: saline-treated SNc, Bottom: ChABC-treated SNc. The unilaterally lesioned SNc is shown on the left of each section. All sections were cut at the medial level (-3.16 mm AP; relative to bregma and skull surface) Scale bar represents 250 µm. (B) Photomicrographs of the TH-positive dopaminergic fibres taken at 5X magnification. All sections were cut at the medial level (+1.00 mm AP; relative to bregma and skull surface). Scale bar represents 500 µm.

### *Assessment of TH-positive cells remaining in the SNc and TH-positive fibres remaining in the striatum as a result of saline and ChABC treatment*

TH-positive cells of the SNc were counted in the lesioned and intact hemispheres of each animal (data not shown). These data were then used to produce values that represent the TH-positive cells in the lesioned SNc as a percentage of the intact SNc. There was no significant difference between treatment groups in the percentage of SNc cells remaining in the fully lesioned hemisphere. Animals that received saline had 6.2 ± 3.1% cells remaining compared to animals that received ChABC (6.7 ± 3.7%; Student's *t*-test; figure 34A). A similar pattern was observed in the levels of striatal TH-positive dopaminergic terminals (figure 34B), whereby levels of TH-positivity across the dorsal striatum or ventral striatum in the ChABC group (6.1 ± 5.4% and 9.5 ± 2.7%, respectively) showed no difference compared to the dorsal striatum or ventral striatum in the vehicle control animals (3.4 ± 3.5% and 10.9 ± 4.8%, respectively; Two-Way ANOVA with Bonferroni post hoc test).

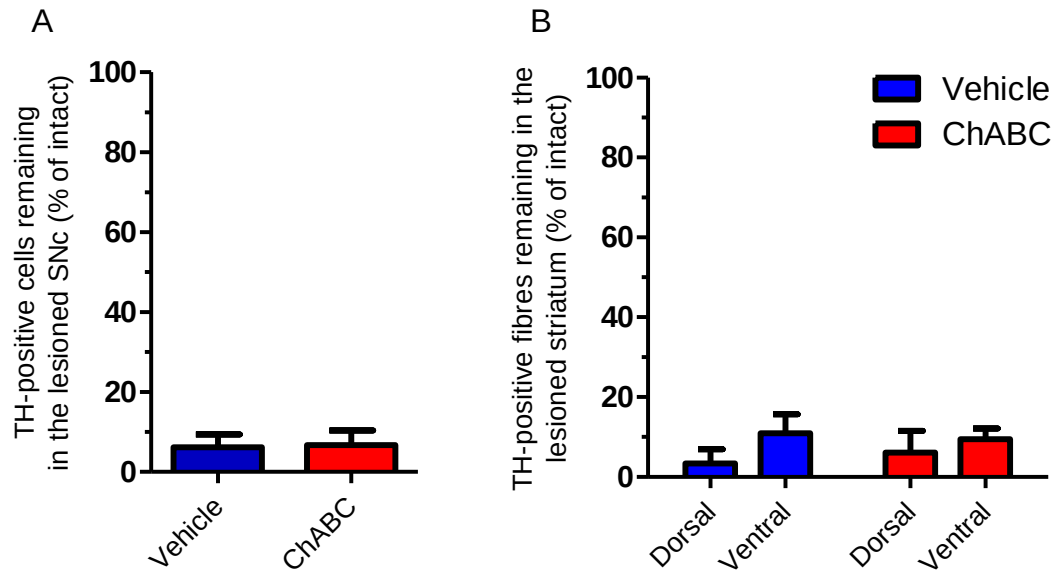


**Figure 35: Effects of ChABC on cell and terminal pathology in the full lesion model.**
(A) Percentage number of TH-positive SNc cells remaining in the lesioned hemisphere as a percentage of the intact for both the saline- and ChABC-treated groups. Total cell counts were averaged across the three levels of SNc analysed. (B) Percentage TH-positive dopaminergic fibres in the lesioned striatum for both the saline- and ChABC-treated group. Panel represents averaged data for the dorsal quadrants (DL and DM) and ventral quadrants (VL and VM) across all three levels of the striatum. Saline: n=17 and ChABC: n=17. Data are mean ± S.E.M.

### *Assessment of behavioural outcomes as a result of saline and ChABC treatment*

In order to determine whether ChABC improved behavioural outcomes, three tests were enforced. These were the cylinder and the two drug-induced rotation tests. Two-Way repeat measures ANOVA with Bonferroni post hoc tests were used for all three.

No significant differences between treatment groups were seen in asymmetry score on any day (figure 35A). Both groups presented similar average base line asymmetry scores (mean values for days -4 and -1; Saline: 48.1 ± 1%; ChABC: 48.8 ± 0.7%). Scores declined from day 3 until the end of experimentation for both the groups (values on day 31; Saline: 30.6 ± 3%; ChABC: 33.7 ± 3.7%).

Results from the drug-induced rotation tests were not significant. Amphetamine did not induce a difference in net ipsiversive rotations between saline- and ChABC-treated animals. Both the saline- and ChABC-treated animals peaked at ~60 minutes (51.6 ± 12.6% and 54.9 ± 8.4%, respectively) (figure 35B). Similarly, apomorphine did not induce a difference in net contraversive rotations between saline- and ChABC-treated animals Both the saline- and ChABC-treated animals peaked at ~40 minutes (10.5 ± 3.9% and 8.2 ± 4.1%, respectively) (figure 35C). Due to timing complications, both drug-induced rotation tests were limited to 90 minutes.

From the three tests used in this study, ChABC did not elicit better behavioural outcomes when compared to the vehicle control group.

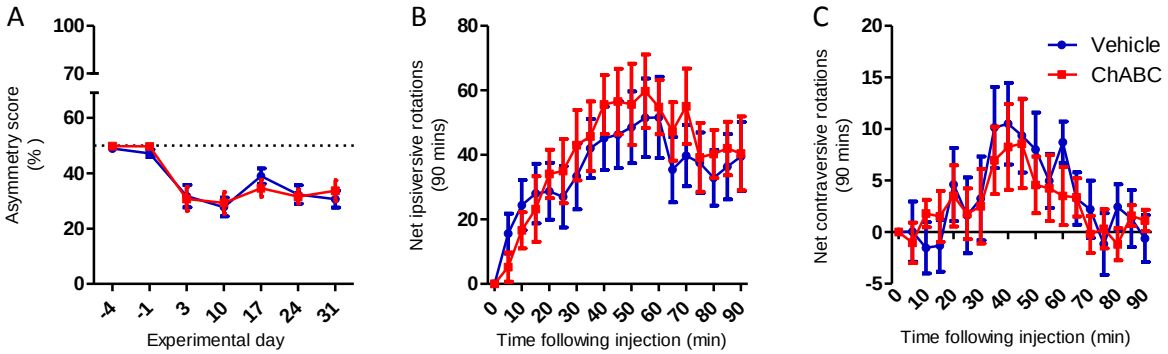


**Figure 36: Effects of ChABC on behaviour in a full lesion hemiparkinsonian model of PD.**
(A) Asymmetry score of animals in the saline and ChABC-treated group determined by the cylinder test. (B) Amphetamine-induced net ipsiversive rotations of animals in the saline- or ChABC-treated groups. Mice were tested over 90 minutes. (C) Apomorphine-induced net contraversive rotations of animals in the saline- or ChABC-treated groups. Mice were tested over 90 minutes. Saline: n=17 and ChABC: n=17. Data are mean ± S.E.M.

### 3.4.5. ChABC-treatment increases cell survival in the rostral SNc of the partial lesion model

Despite ChABC not producing a beneficial effect in the full lesion model, we believed that it could still possess efficacy in the partial lesion model. This study utilised the parameters derived in Pilot Study 2 and 3 (i.e. dose of 6-OHDA required for a consistent partial lesion and the location of ChABC administration for full digestion of the NS) to determine the effect of ChABC's digestion of CSPGs within the NS of a partial lesion model.

#### *Confirmation of CSPG digestion along the nigrostriatal*

As with the previous full lesion investigation, this partial lesion study used the coordinates determined by Pilot Study 3. As before, unilateral ChABC administration brought about the full digestion of the entire NS in the lesioned left hemisphere (figure 36). The ChABC digested the CSPGs surrounding the SNc, striatum and NS regions. Although not shown below due to difficulty of imaging, vehicle administration presented no C4S-positivity and thus no digestion. Due to the success of the CSPG digestion, these results now validate the rest of the data in this study.

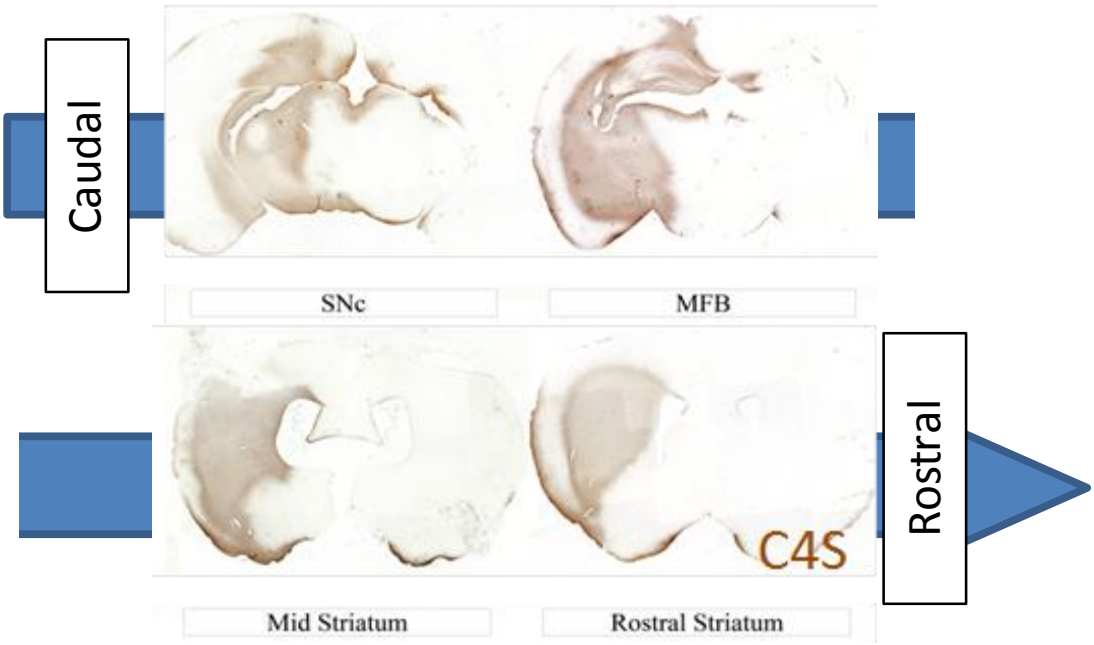


**Figure 37: Two bolus injections of ChABC digest the entire NS in the partial lesion model.** Photomicrographs of four levels of the NS highlighting the regions of C4S-positivity and thus CSPG digestion (brown). ChABC was administered unilaterally into the 6-OHDA lesioned hemisphere (left hand side).

### *TH immunohistochemistry of the SNc and striatum*

To gather the relevant data required for the assessment of ChABC's cell survival effects, images of the SNc and striatum were obtained. Photomicrographs, shown in figure 37A + B, depict increased SNc cell and TH-positive striatal fibre survival in the ChABC group (left hemisphere). It is evident that ChABC helps either protect or repair neurones of the NS.

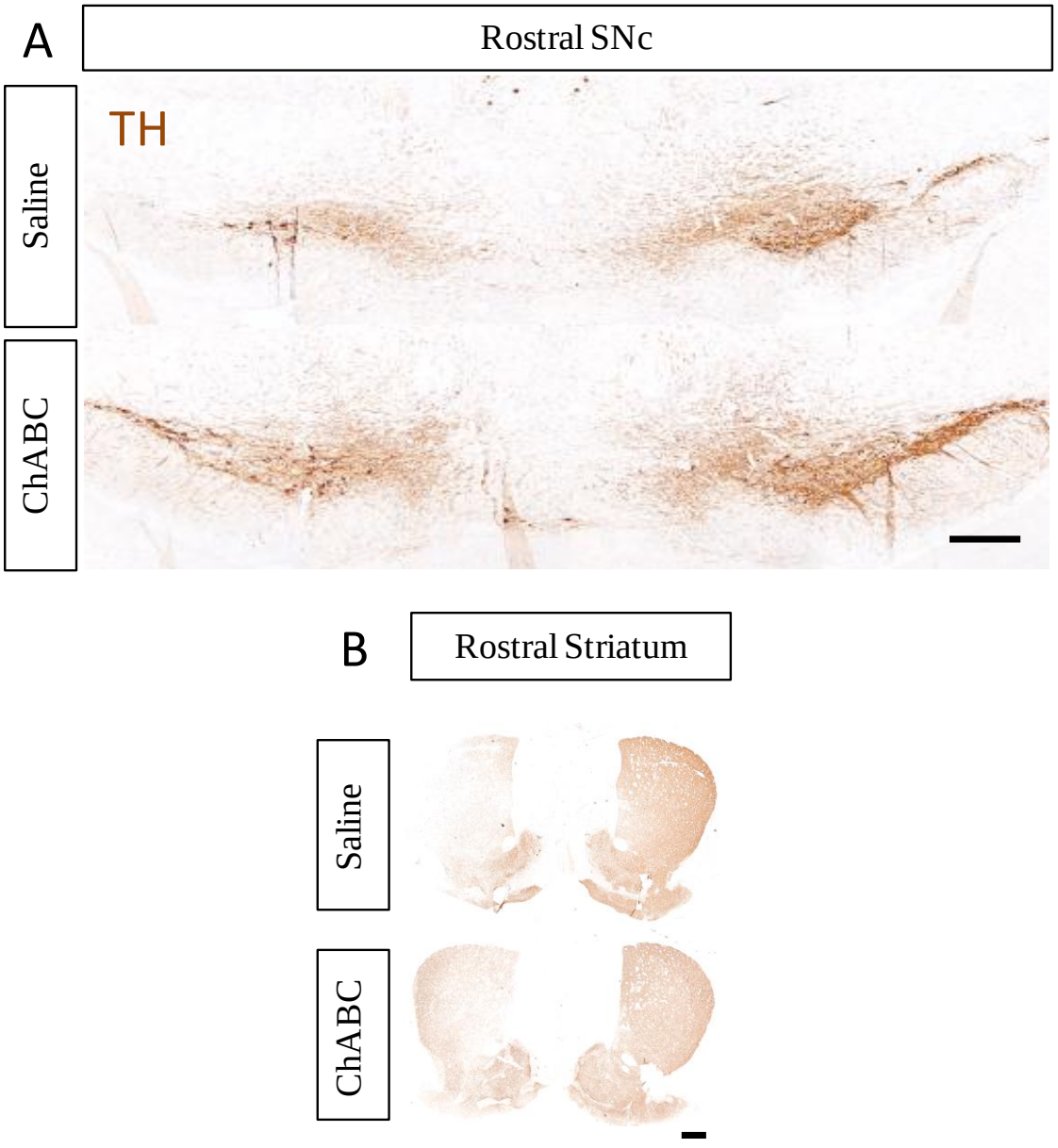


**Figure 38: Photomicrographs highlighting ChABC's effect of increasing TH-positive cell and fibre survival in the partial lesion model.**
(A) Rostral coronal TH-positive SNc cell sections. Top: saline-treated SNc, Bottom: ChABC-treated SNc. The unilaterally lesioned SNc is shown on the left of each section. All sections were cut at the rostral level (-2.92 mm AP; relative to bregma and skull surface) Scale bar represents 250 µm. (B) Rostral coronal sections of the TH-positive dopaminergic fibres of the mouse striatum. All sections were cut at the rostral level (+1.0 mm AP; relative to bregma and skull surface). Scale bar represents 500 µm.

### *Assessment of cells remaining in the SNc and TH-positive fibres remaining in the striatum as a result of saline and ChABC treatment*

TH-positive cells of the SNc were counted in the lesioned and intact hemispheres of each animal (data not shown). These data were then used to produce values that represent the TH-positive cells in the lesioned SNc as a percentage of the intact SNc. Unlike the previous study, the three levels of the SNc were not averaged as significance was found between them.

When kept split into the three different levels of the SNc, a significant difference between the saline- (24.8 ± 6.1%) and ChABC-treated animals (51.6 ± 8.5%) was found at the rostral level ($p=0.022$; Student *t*-test; figure 38C). Both the caudal and medial levels of the SNc saw a consistent partial lesion equivalent to the degree of severity seen in Pilot Study 2 (Percentage TH-positive cells remaining: Saline: 44.6 ± 4%, ChABC: 49 ± 6% and Saline: 37 ± 6%, ChABC: 43 ± 6%, respectively). However, no difference was found between the saline- and ChABC-treated groups at either level (figure 38A + B). Despite this, these data indicate that the ideal lesion size (~50 - 60%) was obtained.

Similarly, when kept split into the three different levels of the striatum, a significant difference in TH-positivity between the saline- and ChABC-treated animals was found in the dorsal half (averaged DM and DL quadrants) of the rostral striatum (Saline: 15.3 ± 3.5%; ChABC: 36.3 ± 6.5%; $p=0.014$; Two-Way ANOVA with Bonferroni post hoc test; figure 38F). As with the SNc, neither the caudal or medial levels presented any significance in ChABC-mediated cell terminal survival (figure 38D + E). However, the size and consistency of the lesion in these areas do further emphasise the success of the lesioning.

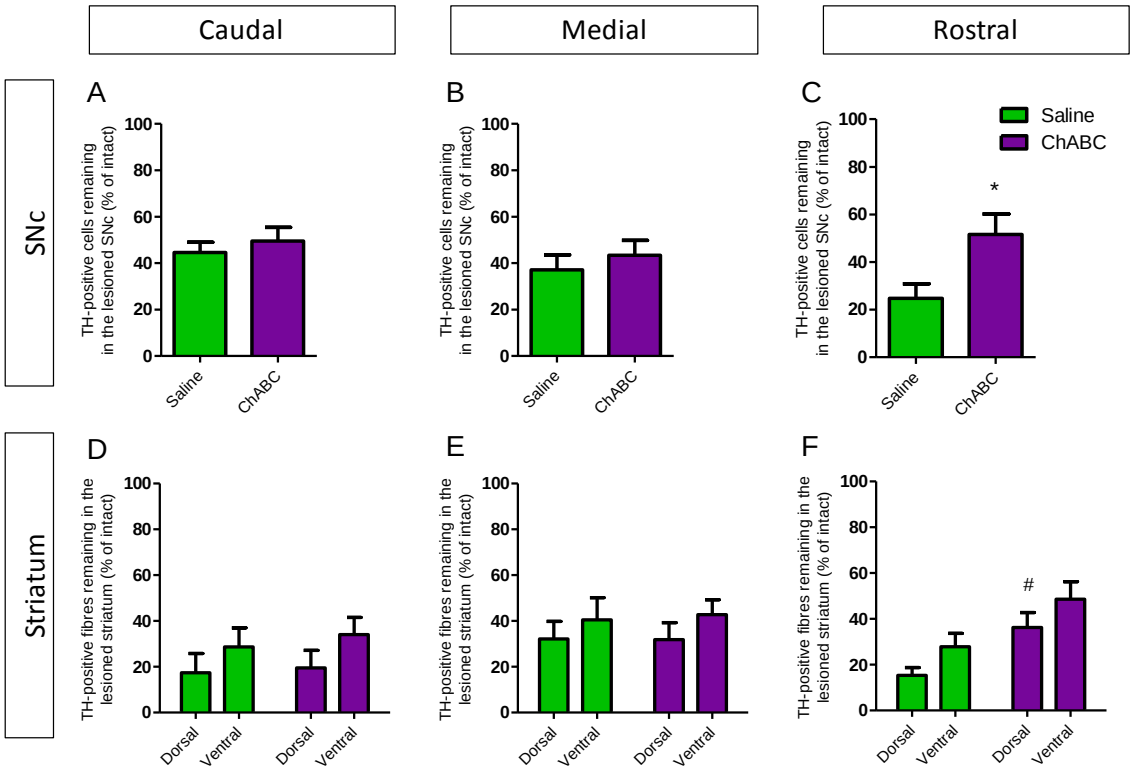


**Figure 39: Effects of ChABC on cell and terminal pathology in the partial lesion model.**
(A - C) Percentage of TH-positive SNc cells remaining in the lesioned hemisphere as compared to the intact for both saline- and ChABC-treated groups. Panels represent the percentage at the caudal (A), medial (B) and rostral (C) levels of the SNc. (D-F) Percentage TH-positive dopaminergic terminals in the lesioned striatum as compared to the intact for both the saline- and ChABC-treated groups. Panels represent the percentage at the caudal (D), medial (E) and rostral (F) levels of the striatum analysed. Data are split into the dorsal (Average of the DM and DL quadrants) and ventral regions (Average of the VM and VL quadrants). Panels A-C: Student's *t*-test; * denotes $p<0.05$; Panels D-F: Two-way ANOVA with Bonferroni post hoc test $^{\#}$ denotes $p<0.05$ between the dorsal striata of the saline- and ChABC-treated groups. Saline: n=17 and ChABC: n=17. Data are mean ± S.E.M.

### *Assessment of behavioural outcomes as a result of saline and ChABC treatment*

In order to determine whether ChABC improves behavioural outcomes, two tests were enforced. These were the cylinder and the amphetamine-induced rotation tests. The apomorphine-induced rotations test was not used as it only induces rotations in fully lesioned animals (i.e. ~85% SNc cell loss).

No significant differences between treatment groups were seen in asymmetry score on any day (figure 39A). Both groups presented similar average base line asymmetry scores (mean scores for days -3 and -1; Saline: 41.2 ± 1.2%; ChABC: 48.2 ± 1.4%). Scores declined from day 14 until the end of experimentation for both the groups (scores on day 35; Saline: 28.1 ± 4.6%; ChABC: 36.5 ± 3.9%; ns; Two-Way repeat measures ANOVA with Bonferroni post hoc test).

Amphetamine did not induce a difference in net ipsiversive rotations between saline- and ChABC-treated animals (figure 39B). Both groups peaked at ~70 minutes where mean scores of 33.1 ± 8.1% and 28.6 ± 5.9 for saline and ChABC treatment, respectively. A similar number of net rotations were seen between the two groups for the entire 120 minutes.

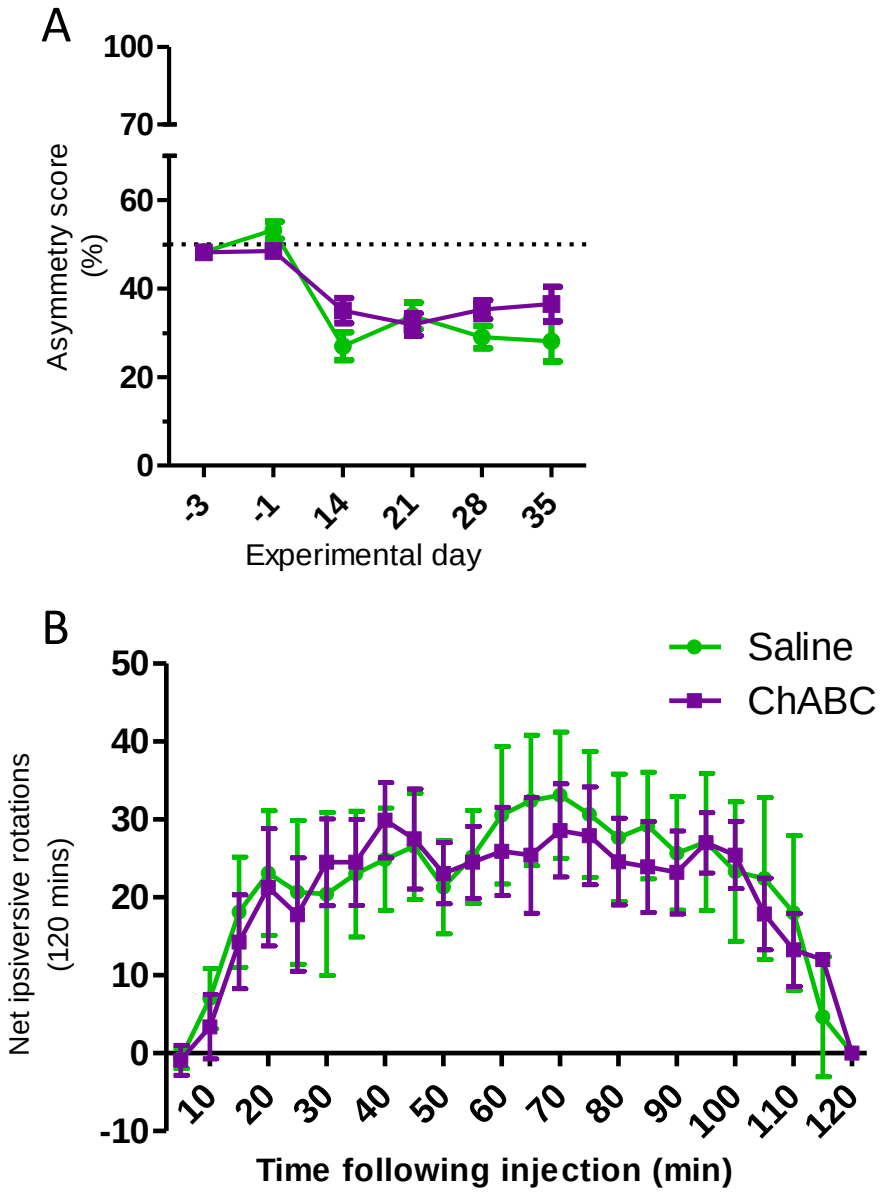


**Figure 40: Effects of ChABC on behavioural outcomes in a partial lesion hemiparkinsonian model of PD.**

(A) Asymmetry scores of animals in the saline and ChABC groups determined by the cylinder test. Animals were tested prior to lesioning and weekly for 35 days post lesion. (B) Amphetamine-induced net ipsiversive rotations of animals in the saline or ChABC groups. Mice were tested over 120 minutes. Saline: n=17 and ChABC: n=17. Data are mean ± S.E.M.

## 3.5. Discussion

The two main studies within this chapter set out to test two hypotheses. These were, firstly, whether ChABC administration would act as a strategy of increasing cell survival in the full hemiparkinsonian mouse model of PD. Secondly, whether ChABC administration would act as a strategy of increasing cell survival in the partial hemiparkinsonian mouse model of PD.

### 3.5.1. Characterising the 6-OHDA full and partial lesion models

In order to establish the model, a range of 6-OHDA neurotoxin doses was used to characterise the full lesion 6-OHDA model. Doses of 4, 6 and 8 µg 6-OHDA, chosen on the basis of similar previous mouse lesioning studies (Francardo *et al.*, 2011; Glajch *et al.*, 2012; Heuer *et al.*, 2012; Iancu *et al.*, 2005), were administered locally to the SNc. Both the 6 and 8 µg doses of 6-OHDA could have been chosen to ablate the SNc as both produced the desired size lesion. The 4 µg dose induced a near partial lesion and so was not taken into consideration. A significant weakness of this pilot study was the absence of striatal TH-positive dopaminergic terminal analysis. Due to a misfortunate loss of striatal tissue, this analysis was not possible. Nevertheless, the SNc pathology and behavioural analyses were conclusive enough for the 8 µg 6-OHDA dose to be used for the full lesion model.

Similar to the characterisation of the full lesion model, a range of 6-OHDA doses were chosen based on previously published mouse lesioning studies (Francardo *et al.*, 2011; Heuer *et al.*, 2012; Iancu *et al.*, 2005). Of the concentrations chosen, the 4 µg 6-OHDA dose induced a consistent partial lesion across all levels of the SNc and striatum; a comparable size to that found by others (Francardo *et al.*, 2011; Heuer *et al.*, 2012). Unfortunately, behaviour was not conducted in this pilot due to time constriants. However, the pathology the dose induced was ideal for the partial lesion study and so behavioural data was not essential for reaching this decision.

### 3.5.2. ChABC digestion patterns

As the use of ChABC in the parkinsonian BG was novel, the mechanism behind any beneficial effects were not known. To induce any restorative effect it was not known whether CSPG digestion would be required at the injured cell bodies (SNc), at their terminals (striatum) or between the two (MFB region). Therefore, it was logical to digest the entire NS in order to explore for any effect before focusing on one of three of the stated areas. When injected directly to the two sites (striatum and SNc), ChABC did not digest CSPGs along the entire NS, with ventral regions of the brain not being digested. The two relocated injection sites (caudal striatum and rostral SNc) were found to cause the full digestion required for the two lesion

model studies. This digestion was evident by the exposure of the C4S stub epitopes following ChABC treatment. This method of C4S staining has been frequently used in the spinal cord injury field as a method of detecting digested CS-GAGs. Although other epitopes can be detected (e.g. 2B6), they all produce the same pattern correlating to CS-GAG digestion.

It is important to stress the significance of a single bolus injection being able to maintain digestion of CSPGs after a month. In the spinal cord field, ChABC's efficacy is considerably lower in long term studies and therefore methods of prolonging ChABC exposure have been investigated. Here we present data showing single administrations of ChABC providing the desired effect. Discussion regarding ChABC's efficacy and stability is further mentioned in section 3.5.7.

### 3.5.3. ChABC does not improve cell survival or behavioural outcomes in a fully lesioned model of Parkinson's disease

Despite the entire and sustained digestion of the NS (as shown in Pilot Study 3), ChABC did not provide a cell survival effect to either the state of cellular pathology or behavioural outcomes; disproving our first hypothesis. This lack of effect may be attributed to the severity and speed of the developed full lesion. Although ChABC-mediated digestion of the CSPGs occurs rapidly (within 24 hours; data not shown), it seems that no degree of NTF liberation or barrier removal can counter the effects of the cell death. Although a negative result, this does however highlight an important point behind the mechanism of ChABC's beneficial nature. Any cellular repair or protection, if present, would most likely occur to slowly degenerating neurones rather than quickly ablated ones as seen in this model. This therefore highlights the importance of analysing the effects of ChABC within the partial lesion model where this slower degeneration occurs.

### 3.5.4. ChABC successfully improves cell survival but not behavioural outcomes in a partially lesioned model of Parkinson's disease

Digestion of the CSPGs along the entire NS proved to be beneficial to the rostral regions of the SNc and dorsal striatum, where cell number and TH-positive terminals were preserved respectively; adding support to our second hypothesis. However, these effects did not translate to an improved behavioural outcome. This is most likely due to the behavioural tests not being sensitive enough to detect such a subtle phenotype. To counter this, other behavioural tests would have to be investigated or a further promotion of detectable ChABC-mediated cell survival would be required. To note, the cell loss seen in the rostral SNc of the saline-treated animals was greater than the desired ~50% lesion. This was believed to be an effect of the close proximity between the rostral level analysed and the injection site of the ChABC. Despite

this, ChABC still demonstrated an increase in cellular protection against cell degeneration.

Unfortunately, due to the preparation of the tissue from these studies (formalin fixed and embedded in paraffin wax) we could not test for increases in NTF or other potentially liberated factors that would help elucidate the beneficial mechanism behind CSPG digestion. Although this was not the main aim behind this study, it would have been of interest to investigate this further in this model of disease. Thus while we have evidence for some improvement, we cannot deduce whether this is down to the liberation of NTFs and other chemorepellents/attractants (i.e. semaphorin 3A) or through physical barrier degradation and the formation of cellular contacts (i.e. receptor protein tyrosine phosphatase sigma).

### 3.5.5. Dissecting the mechanism of ChABC-mediated cell survival

Throughout this chapter, ChABC has been discussed as an agent of improving *cell survival*. This is a loose term that has been used to describe either SNc cell neuroprotection or neurorepair. As was not clear whether ChABC was inducing one or the other, the term cell survival was used. Nevertheless, by altering the timing of the ChABC we may be able to dissect the neuroprotection potential from the neurorepair. As our current design administers ChABC during the same lesioning surgery, cell protection can occur during the early stages of lesion development and neurorepair can occur once the partial lesion has been established. This could be avoided by instead injecting ChABC in a separate surgery after the lesion has stabilised. Any increase in cell survival would then therefore be a result of neurorepair of the remaining cells in the injured SNc. See figure 40 for visualisation.

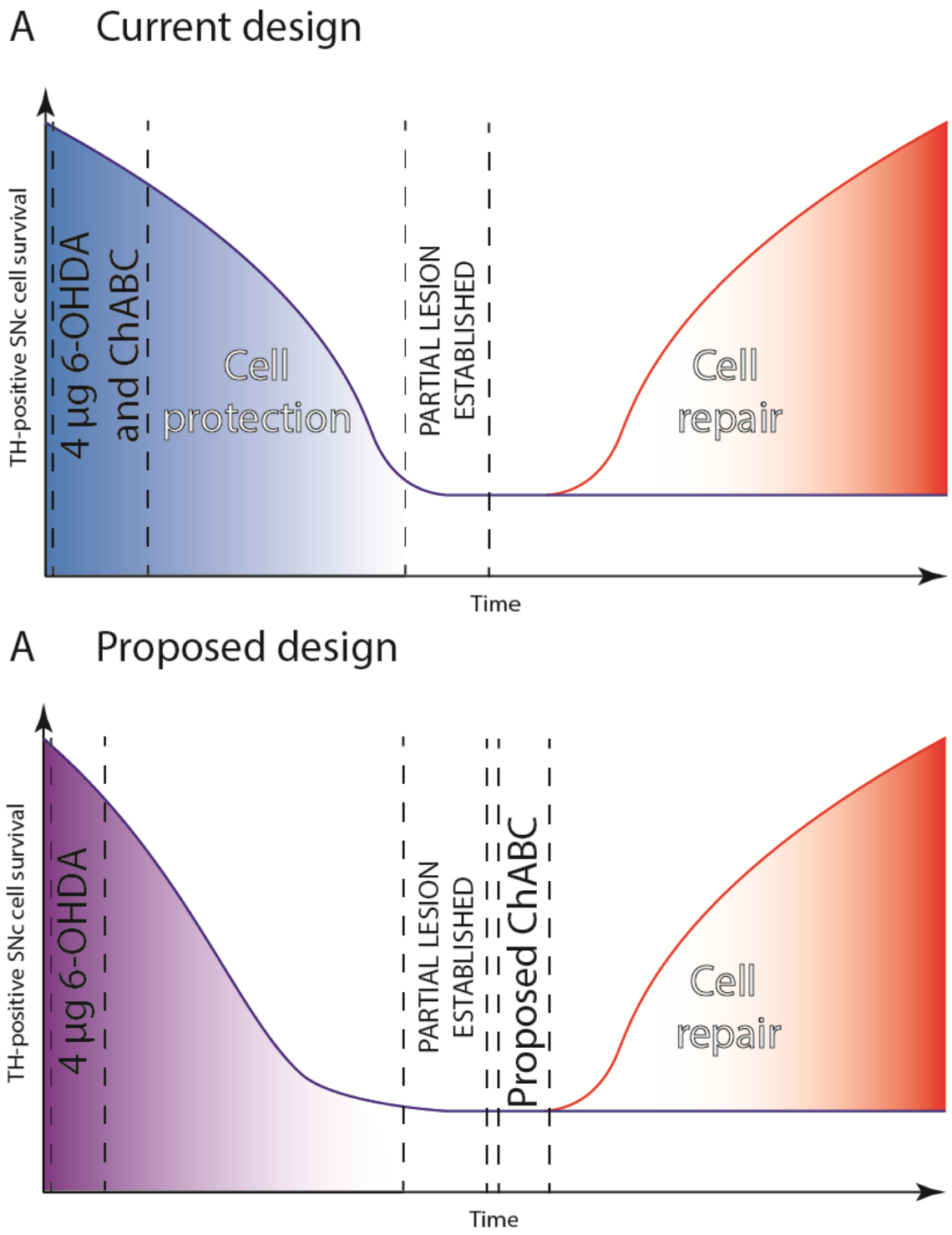


**Figure 41: ChABC treatment timing could highlight whether neuroprotection or neurorepair is elicited.**

(A) Current design of ChABC administration. As ChABC is given to the NS whilst undergoing lesioning, it is unclear whether the enzyme is providing a protective effect during this stage or a repair effect once the lesion has established. (B) The proposed design of ChABC administration. This alters the time of ChABC treatment to when the lesion has developed. Any benefits seen by the enzyme will surely be the cause of cellular repair.

### 3.5.6. Issues regarding pan-CS-GAG digestion

Although CSPGs have their own separate subtypes, so do the CS-GAG side-chains. As previously mentioned, the CS-GAGs are formed by the disaccharide subunits comprised of GlcA and GalNAc. These moieties are sulphated by sulphotransferase enzymes at different carbon sites resulting in altered structures (see Table 5). By slightly altering the CS-GAG's structure, and thus molecule binding affinities, the subtypes of CS-GAGs can bind to either beneficial or inhibitory growth molecules. The CS-GAG subtype most associated with inhibition is CS-E. CS-E has been shown to have high affinity for the axon-repulsive guidance molecule semaphorin 3A, and is therefore thought to account for the inhibitory nature of the PNN (Dick *et al.*, 2013; Gilbert *et al.*, 2005; Vo *et al.*, 2013). In addition, neurotrophins (BDNF, NGF and NT-3 -4/5) have showed preferential binding for CS-E (Gama *et al.*, 2005; Rogers *et al.*, 2011) and therefore potentially trap growth promoting compounds to inhibit axonal growth. Other CS-GAG isotypes such as CS-A have been shown to be growth inhibitory (Wang *et al.*, 2008), presumably due to inhibitors and guidance molecules being bound to that subtype.

Fourth-carbon sulphated CS-GAGs (i.e. CS-E, CS-A) are considered inhibitory, whereas conversely, sixth-carbon sulphated CS-GAGs (i.e. CS-D, CS-C) are seen as growth permissive (Clement *et al.*, 1998; Lin *et al.*, 2011). It has been suggested that CSPGs with a higher ratio of sixth-carbon to fourth-carbon sulphated CS-GAGs give rise to a pro-plastic environment; lower ratios were associated with the inhibition of plasticity and the closure of the critical period (Miyata *et al.*, 2012). It seems likely that this *sulphation code* may determine the fate of axonal regeneration following injury.

**Table 5: Differing CS-GAG sulphation patterns give rise to different isoforms.**
Four CS-GAG subtypes exist within the mammalian brain. These are dependent on the location of the sulphate groups. CS-B is not included as it is dermatan sulphate and not of the chondroitin family.

| CS-GAG subtype | | Location of sulphation |
|---|---|---|
| Chondroitin sulphate A | CS-A | GalNAc, fourth carbon |
| Chondroitin sulphate C | CS-C | GalNAc, sixth carbon |
| Chondroitin sulphate D | CS-D | GalNAc, sixth carbon; GlcA second carbon |
| Chondroitin sulphate E | CS-E | GalNAc, fourth and sixth carbon |

With this in mind, a significant drawback to the use of ChABC has been its pan-CS-GAG digestive property. Pan ChABC-digestion removes not only the inhibitory CS-GAGs, such as CS-E, but also the proposed growth permissive ones, namely CS-D. To promote the ChABC effect seen in the partial lesion study, it may be possible to selectively digest or block the inhibitory CS-GAGs whilst leaving the beneficial isoforms in order to maximise ChABC's effect. Genetic

approaches, pharmacological agents and inhibitory antibodies selective for certain sulphated CS-GAGs would be the next stage in manipulating the ECM for axonal recovery. To date, such a strategy is not yet possible at least in terms of pharmacological agents or blocking antibodies.

### 3.5.7. Further considerations concerning ChABC

Concern regarding ChABC's proposed short-lived efficacy has been raised (a proposed 8 day half life (Mountney *et al.*, 2013)). Studies in the spinal cord injury field have questioned the stability of ChABC over long periods (Tester *et al.*, 2007). The enzyme is believed to become denatured/inactive quickly under physiological conditions and that prolonged exposure of the enzyme requires frequently repeated intrathecal administration (two week intervals) (Huang *et al.*, 2006), gene therapy (Curinga *et al.*, 2007) or trehalose-thermostabilising (Lee *et al.*, 2010). Despite these concerns, the studies within this chapter have shown C4S immunoreactivity to be evident after a month, an extended timeframe to the aforementioned spinal cord injury investigations that saw CSPG turnover after two weeks. It is quite possible that the expression of CSPGs and their *de novo* synthesis following digestion is different in the brain to that of the spinal cord. The efficacy of a single bolus treatment of ChABC is of great importance to these studies, so investigating the degree of CSPG digestion following an additional month or two of recovery should be considered. This would indicate whether further administrations of ChABC would be required to maintain an increased effect of cell survival in a more chronic model of recovery.

### 3.5.8. Chapter conclusions

Overall, the studies in the Chapter have revealed for the first time that ChABC has cell survival benefits in a toxin model of PD. Although ChABC elicited no pathological recovery in the full lesion model, the lesion was believed to be too severe and fast acting for the benefits of ChABC to initiate. Thus, ChABC's benefits were only present in the slower and less severe partial lesion model. As of yet, no improved behavioural outcomes have been caused by ChABC administration. However, this may be due to the sensitivity of the tests used and the small increase in cell survival induced.

ChABC has proven to be a worthwhile venture in the discovery of new therapeutic agents. Identifying methods of increasing ChABC's potency in cell survival would be a logical next step. This shall be pursued in Chapter 4.

# 4. Enhancing the cell survival effects of ChABC with selegiline treatment

## 4.1. Introduction

As shown in Chapter 3, ChABC presents potential as a therapeutic agent in promoting neuroprotection or repair in the partial 6-OHDA lesion model. However as the degree of increased cell survival was modest, no changes in behavioural outcomes were observed. We propose that in order to achieve better behavioural phenotypes we must increase the degree of ChABC-mediated neuroprotection or repair. One of the main theories of why CSPG digestion leads to axonal regrowth and repair is that CS-GAG digestion causes the liberation of neurotrophic factors (NTFs) which then bind to neighbouring neurones. Therefore, in addition to ChABC administration we wish to promote NTFs within the injured NS; primarily GDNF and BDNF due to their significance in PD. This would test whether it is possible to enhance the level of cell survival previously shown in Chapter 3 to a degree that is detectable by behavioural tests.

### 4.1.1. The Neurotrophic factor families

NTFs were mentioned briefly in Chapter 1 as potential agents to improve cell survival in neurodegenerative diseases such as PD. Although only two NTFs were previously mentioned (GDNF and BDNF), there are many more which belong to four distinct families. These families are the GDNF family of ligands (GFLs), neurotrophins, neurokines and the mesencephalic astrocyte-derived neurotrophic factor/cerebral DA neurotrophic factor (MANF/CDNF) family (see Table 6).

**Table 6: The four families of NTFs.**
There are four families of NTFs within the CNS, the neurotrophins, GFLs, neurokines and the CDNF/MANF family. The former two are most referred to in this thesis.

| **NTFs** | |
|---|---|
| **Family** | **Members** |
| Neurotrophins | BDNF, NT-3, -4, NGF |
| GDNF family of ligands (GFLs) | GDNF, neurturin, artemin, persephin |
| Neurokines | CNTF, LIF, IL-6, IL-11, CT-1, CLC, OSM |
| CDNF/MANF family | CDNF, MANF |

NTFs are required for both neuronal development and maintenance in particular systems of the CNS. But only the NTFs that affect the midbrain DA neurones of the SNc are of importance to our work. Although studies have shown promise for the more recently discovered MANF (Petrova *et al.*, 2003) and CDNF (Lindholm *et al.*, 2010) NTFs in protecting dopaminergic cells, for the purpose of this chapter we shall focus on the two most well-described NTFs in relation

to PD – the GDNF and BDNF molecules.

### 4.1.2. Signalling mechanisms of GDNF and BDNF

#### *GDNF*

The signalling cascades for GDNF are illustrated in figure 41. GDNF, like other members of the GFL family, initiate dopaminegic cell signalling through the activation of the transmembrane receptor tyrosine kinase known as Ret. Unlike other tyrosine kinases, GDNF does not bind to Ret directly. Instead GDNF binds to the membrane bound co-receptor GDNF-family receptor alpha 1 (GFRα1) before it then complexes with Ret. Four subtypes of this co-receptor exist, each with varying affinities for GFL molecules; GFRα1 possesses the highest affinity for GDNF. Ret phosphorylation occurs following the binding of the ligand to GFRα1, whereby several downstream pro-survival cascades are activated, such as the MAPK/ERK and PI3K/Akt pathways (d'Anglemont de Tassigny *et al.*, 2015; Onyango *et al.*, 2005; Ugarte *et al.*, 2003).

Interestingly, transgenic models displaying the heterozygous loss or a conditional knockout of the GFRα1 gene displayed degeneration of dopaminergic SNc cells and striatal dopaminergic terminals. Additionally, the heterogenous mouse was seen to possess an increased sensitivity to MPTP (Boger *et al.*, 2008), whereas the conditional knockout saw pronounced glial activation within the SNc and striatum (Kramer *et al.*, 2007). These data reinforce the notion that GDNF has a key supportive and protective role in the BG and in PD.

In addition to the phosphorylation of Ret inducing pro-survival pathways (e.g. MAPK/ERK), GDNF has been shown to inhibit apoptosis by activating bcl-2 and bcl-xl whilst also inhibiting caspase-3 (Sawada *et al.*, 2000). Addtionally, GDNF has shown to increase levels of the antioxidants glutathione peroxidise, SOD and catalase that are instrumental in countering ROS activity (Chao *et al.*, 1999) (figure 41). Moreover, there is evidence suggesting that the anti-apoptotic signalling pathway involving casein kinase 2 contributes to the protective effect of GDNF (Chao *et al.*, 2006). Casein kinase 2 has been found to protect proteins from caspase-related mechanisms (Litchfield, 2003).

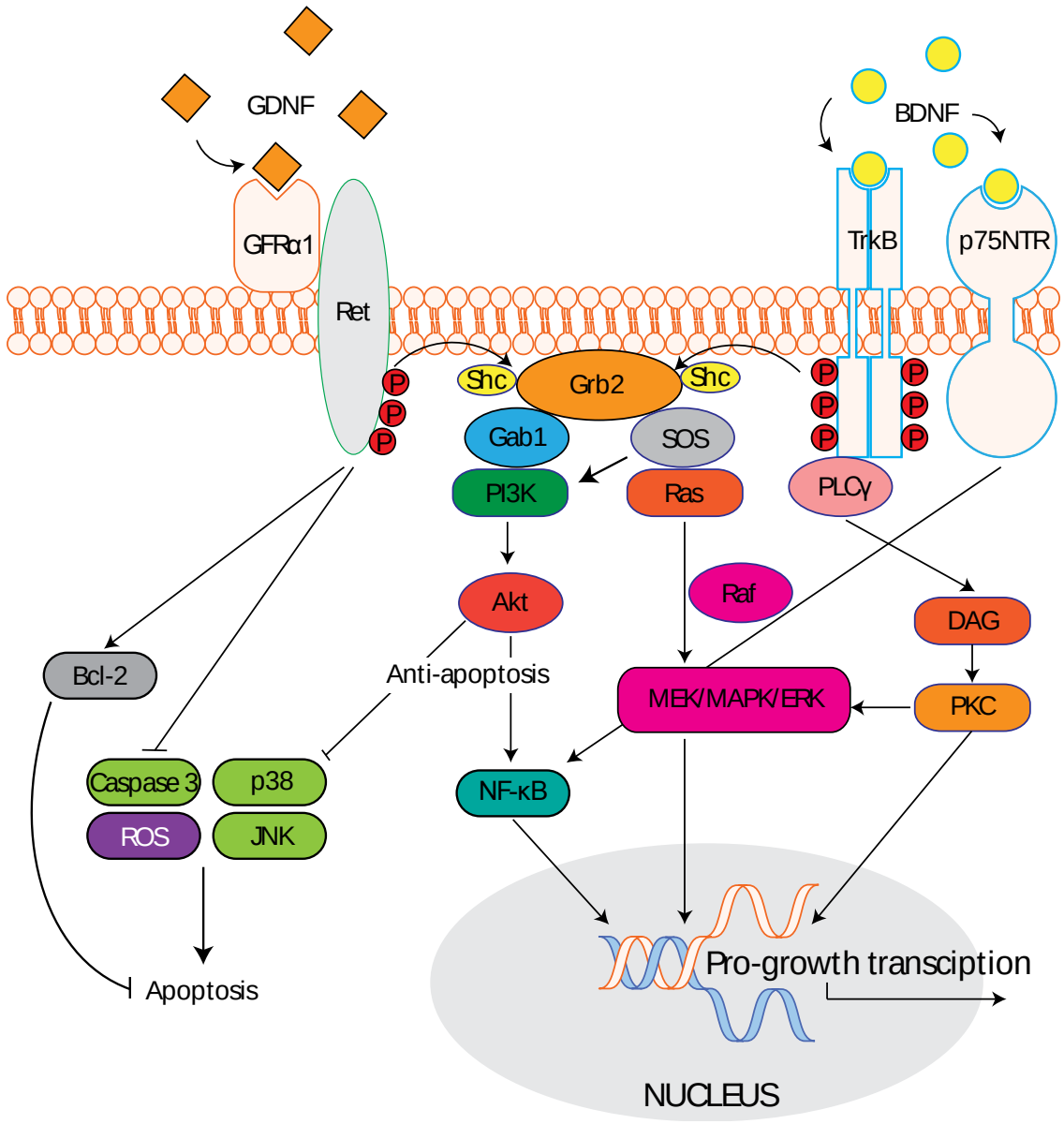


**Figure 42: Pro-survival intracellular signalling of GDNF and BDNF.**
The pro-survival and anti-apoptotic pathways involved in GDNF and BDNF signalling overlap significantly. Upon binding of GDNF and BDNF, the GFRα1/Ret complex and TrkB receptors autophosphorylate and activate common pathways. Shc has high affinity for the phosphorylated tyrosine sites found on the Ret and TrkB intracellular domains. The binding of Src to the adapter protein growth factor receptor-bound protein 2 (Grb2) leads to the activation of Ras. Ras then activates both the MAPK/ERK cascade (through the activation of the Raf kinase) and the PI3K/Akt pathway (though SOS binding to PI3K); PI3K can also be activated through the Grb2 associated binder 1 (Gab1). The PI3K/Akt pathway leads the inhibition of the pro-apoptotic proteins p38 and c-Jun N-terminal kinases (JNK), it is also known to activate the transcription factor NF-κB that has a role in cell survival and the inflammatory response. Activated Ret is known to cause the activation of the B-cell lymphoma 2 oncoprotein (Bcl-2) and the inhibition of caspase 3 and other downstream effects that lead to the reduction in ROS. BDNF is also a ligand for p75NTR that is known to have downstream interactions with NF-κB.

### *BDNF*

Being a member of the neurotrophins, BDNF binds and activates TrkB; a tyrosine kinase receptor of the tropomysin-related kinase (Trk) family (Barbacid, 1994). Upon the binding of BDNF, the TrkB receptor dimerises which causes the autophosphorylation of its intracellular domain and the exposure of docking sites for phospholipase C-γ (PLC-γ) and src homology 2 domain containing adapter protein (Shc). These proteins are integral to the pro-survival and anti-apoptotic intracellular cascades such as MAPK/ERK, PI3K/Akt and PLC-γ (Kaplan *et al.*, 1997; Yamada *et al.*, 1997b); a similar signalling transduction pattern to that of GDNF. Addtionally, BDNF has affinity for the p75 neurotrophin receptor (p75NTR)(Dougherty *et al.*, 1999), a receptor essential in aiding Trk binding affinities (Segal, 2003) but also the activation of nuclear factor κB (NF-κB); a key transcription factor which has a multitude of effects including cytokine production and controlling neuronal survival (Reichardt, 2006).

Both GFRα1/Ret and TrkB receptors are located at the terminals of dopaminergic cells. GDNF and BDNF, which are both secreted by neurones and glia (Chiu *et al.*, 2009; Liu *et al.*, 2001), signal primarily in a retrograde fashion whereby signal transduction starts at the cell terminal and proceeds down the axon to the cell soma. It is well established that axonal transection of neurones greatly inhibits cell growth and initiates cell degeneration (Hendry, 1975). This can be in part due to the cessation of this retrograde NTF signalling that is essential for cell survival and maintenance (Rich, 1992).

Unfortunately, for many degenerative diseases axonopathy precedes neuronal death. It is thought that axonopathy results in NTF signalling not being able to reach the cell soma in order to promote pro-survival gene transcription; leading to a degenerative cycle. When discussing the application of NTFs as a therapeutic target this highlights the importance of timing (ensuring some cells undergoing axonopathy are alive and can respond to NTFs) and location of NTF delivery (NTF infusion at the cell terminals is more effective than at the cell soma (Ito *et al.*, 2016)). In the case of the partial 6-OHDA lesion established in Chapter 3, the timing of NTF application would be throughout the development of the lesion and after it has been stabilised; causing both neuroprotection and neurorepair of the injured neurones. The location of NTF application would be the striatum as this is where the terminals of the injured SNc neurones reside.

### 4.1.3. Promoting brain GDNF and BDNF levels with MAO-B Inhibitors

The importance of GDNF and BDNF presence within the CNS is clear. Although the evidence supporting BDNF's therapeutic capabilities is far less than that of GDNF, it is apparent that many of the downstream signalling cascades overlap. Therefore, BDNF may act in a very similar manner in lesion models of disease. As a result, these NTFs have been the target of many preclinical and clinical investigations to help promote neuronal repair. As described in Chapter 1, both BDNF and GDNF have been researched in preclinical models of PD as agents of increased SNc cell survival (Martin *et al.*, 1996; Singh *et al.*, 2006; Winkler *et al.*, 1996). Unlike BDNF, GDNF has reached the clinic multiple times with varying results (Gill *et al.*, 2003; Patel *et al.*, 2005) (see Chapter 1 section 1.11.3. for further details). Although promising in increasing SNc cell survival and potentially improving UPDRS scores, both BDNF and GDNF cannot penetrate the BBB. Alongside the direct intraputamenal GDNF infusions seen in the Gill *et al* clinical trial, multiple methods of delivering these NTFs have been suggested to counter their BBB-impenetrable nature. A recent study investigated the *in vivo* application of the synthetic BBB-penetrable GDNF-derived 11 amino acid neuropeptide, DA neuron stimulating peptide-11 (DNSP-11), on the pathological and behavioural responses of hemiparkinsonian rodents. DNSP-

11 elicited both the sparing of TH-positive cells and striatal dopaminergic terminals (Stenslik *et al.*, 2015). Others have utilised nanoparticles to deliver NTFs across the BBB with some effect in increasing the striatal exposure to GDNF (Fletcher *et al.*, 2011). These studies indicate the promise GDNF and its derivatives have on neuroprotection. Viral delivery of both BDNF and GDNF has shown success in PD models. Adeno-associated virus and herpes simplex virus delivery of GDNF and BDNF presented modest improvements in rat models of PD (Klein *et al.*, 1999; Sun *et al.*, 2005). Herpes simplex virus delivery of BDNF and GDNF in the unilaterally lesioned 6-OHDA rat, as shown by Sun *et al*., increased the number of cells in the 6-OHDA lesioned SNc as a percentage of the intact from 22% in the lesion control to 34% and 54%, for BDNF and GDNF respectively. Although successful in promoting cell survival, these methods of NTF delivery have not been ideal. Methods of increasing intrinsic levels of NTFs through means other than exogenous administration have therefore been of interest.

When exploring ways of potentially enhancing the degree of survival offered by ChABC treatment we have been keen to explore more translatable mechanisms to boost BDNF and GDNF levels. To date the one with most promise has been the treatment of MAO-B inhibitors. The MAO-B inhibitors rasagiline and selegiline have been suggested to promote the synthesis of neurotrophins and GFLs, such as GDNF and BDNF (Maruyama *et al.*, 2013; Maruyama *et al.*, 2004; Mizuta *et al.*, 2000) and also MAPK/ERK-mediated neuroprotective effects (Bar-Am *et al.*, 2010; Naoi *et al.*, 2010; Riederer *et al.*, 2011; Weinreb *et al.*, 2009). Evidence has shown that the systemic administration of selegiline enhanced the levels of GDNF and BDNF in the striatum and ventral midbrain of MPTP-treated mice. These increased levels were suggested to reduce the MPTP-induced loss of SNc cells and TH-positive striatal fibres whilst also improving gait dysfunction (Zhao *et al.*, 2013).

As both MAO-B inhibitors are approved by the Food and Drug Administration, the drug repositioning potential of rasagiline and selegiline is attractive. With all of these aforementioned factors in mind, utilising a MAO-B inhibitor as a systemic inducer of GDNF and BDNF release to enhance the already observed neuroprotection caused by ChABC was of significant interest.

### 4.1.4. Study rationale

We have previously shown that ChABC digestion of the CSPGs within the hemiparkinsonian BG produces an increase in cell survival. Although not yet proven, we theorise that this digestion leads to the liberation of NTFs from the ECM resulting in cell survival. If true, this could highlight the importance of intrinsic NTF release in providing restorative benefits within the damaged BG. Ultimately, the mechanism in which digestion works is not of importance other than that it results in the increased survival of SNc cells and dopaminergic nerve terminals. However, ChABC treatment does not give rise to a better behavioural phenotype when compared to controls; arguably an effect of the minor increase in cell survival.

In this study, we investigated whether administration of the MAO-B inhibitor, selegiline, would increase NTF presence, namely GDNF and BDNF, within the mouse BG. Furthermore, we believe that this increase would enhance the cell survival induced by CSPG digestion in the partial 6-OHDA lesion mouse model to a degree beyond what was found in our previous study. This would result in an improved and detectable behavioural phenotype. Due to the aforementioned studies indicating NTF signalling being retrogradely transmitted, we believe that the primary region of enhanced GDNF and BDNF levels should be the dopaminergic nerve terminals within the dorsal striatum. Therefore, we focused our attention of GDNF and BDNF levels to this region.

## 4.2. Aims and Hypotheses

This chapter incorporates two studies. The first, to identify whether systemic treatment of the MAO-B inhibitor, selegiline, would increase GDNF and BDNF levels within the mouse BG. The second, investigate whether the incorporation of selegiline treatment in the previously established ChABC model would potentiate the cell survival effect seen by the digestion of the CSPGs in the lesioned murine BG. The main aims and hypotheses for this chapter are described below.

Study aims:

1. *Identify whether the systemic treatment of selegiline increases GDNF and BDNF concentrations in the ventral midbrain and striatum of naive mice*

2. *Investigate whether selegiline increases the cell survival promoted by ChABC through enhancing BDNF and GDNF levels in the 6-OHDA partial lesion mouse model*

Study hypotheses:

1. *Selegiline will increase the levels of both GDNF and BDNF within the ventral midbrain and striatum of naive mice*

2. *Selegiline-enhanced concentrations of GDNF and BDNF will enhance the cell survival induced by ChABC in the 6-OHDA partial lesion mouse model*

## 4.3. Materials and Methods

### 4.3.1. Pilot study: Investigating the effects of systemic selegiline on GDNF and BDNF levels within the SNc and striatum of naive mice

#### *4.3.1.1. Animal subjects*

15 eight-week-old male C57Bl/6 mice (Harlan, UK) were maintained on a 12:12 hour light/dark cycle (07:00am lights on) with food and water *ad libitum*. Room temperature and humidity were kept at 22 ± 2°C and 55 ± 2% respectively. All surgical, behavioural and histological procedures were performed whilst blinded to the experimental groups.

#### *4.3.1.2. Experimental design*

The study timeline is described below in figure 42. A week prior to the initiation of selegiline treatment, a 7 day habituation period was implemented to ensure animals were non-responsive to non-biologically relevant stimuli. On day 0, selegiline (n=12) or saline (n=3) was orally gavaged daily at midday for the remaining 2 weeks. On days 1, 3, 7 and 14 following the initiation of selegiline treatment, three animals were culled to assess GDNF and BDNF levels in the striatum. On day 14 the three saline control animals were also killed. Animals were killed by cervical dislocation and brains were removed for biochemical analysis.

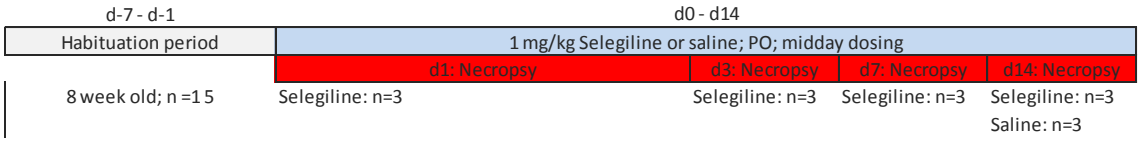


**Figure 43: Experimental design for Pilot Study: Investigating the effects of systemic selegiline on GDNF and BDNF levels within the SNc and striatum of naive mice.**
All procedures of the study were conducted on certain days pre- and post- selegiline treatment as described in the figure. Further details are found either below the timeline or in subsequent sections.

#### *4.3.1.3. Selegiline treatment*

Mice were dosed either selegiline (n=12; 1 mg/kg; per os (p.o.); Sigma-Aldrich) or saline (n=3; PO) daily for 2 weeks. Dosing sessions were conducted every day at midday and directly before any culls on days 1, 3, 7 and 14.

#### 4.3.1.4. Western blotting procedure

##### Tissue extraction and preparation

Upon the designated day of necropsy, mice were killed by dislocation of the neck and heads were removed. The ventral midbrain and striata, from both the left and right hemispheres, were dissected from the rest of the brain and individually stored on dry ice until homogenised. The ventral midbrain was removed instead of the SNc as it was difficult to accurately dissect the SNc from the rest of the ventral midbrain; previous studies had done the same (Zhao *et al.*, 2013). Four samples from each animal were thus obtained. Each sample was homogenised in 500 µl RIPA buffer (see table 7 for recipe) on ice at pH 7.4 using a Ultra-Turrax tissue homogeniser (KIA Werke, Germany) to provide crude homogenates. The homogenates were then stored at -80°C.

**Table 7: RIPA homogenisation buffer recipe.**
In order to homogenise striatal and SNc samples the tissue was mixed in a solution of salts, detergent and enzyme inhibitors. The recipe for this RIPA buffer is given below.

| **RIPA buffer recipe (for 1L)** | | |
|---|---|---|
| Concentration | Ingredient | Provider |
| 50 mM | Tris HCl | Sigma |
| 150 mM | NaCl | Sigma |
| 1% | NP-40 | Sigma |
| 0.1% | SDS | Sigma |
| 0.5% | Na Deoxycholate | Sigma |
| 0.1 mM | EDTA | Sigma |
| 1 tablet per 10 ml | Protease cocktail inhibitor | Roche |
| 1 tablet per 10 ml | Phosphatase cocktail inhibitor | Merck |
| | pH to 7.4 | |

##### Protein quantification assay

In order to determine the concentration of total protein within each sample the bicinchoninic acid assay was conducted. Firstly, a set of standards were prepared using BSA (Sigma-Aldrich, USA) in RIPA buffer. These standards were serially diluted to the following concentrations: 2, 1.5, 1, 0.75, 0.5, 0.25, 0.125, 0.0625 mg/ml and the crude homogenates to sample dilutions of 1:2, 1:4, 1:8 and 1:16 in RIPA. 5 µl of either standard or samples was added to a well of a 96-well plate (Nunc A/S, Denmark) in triplicate. Bicinchoninic acid reagents A (5 ml) and B (100 µl) were well mixed before 100 µl of the solution was added to each of the 96-wells. Any bubbles were popped with a fine sterile needle. Using a plate reader (Molecular Devices, Spectramax 340PC), the absorbance readings for the standards (read at 562 nm) were used to create a standard curve. The standard curve was used to determine the concentration of the diluted unknown sample by comparing absorbance values.

### *Western blotting*

With the concentration of the samples determined, appropriate volumes of crude sample, 5x Laemmli sample buffer (GenScript, USA) and $dH_2O$ were added to receive a final volume of 100 µl with a final sample protein concentration of 1 µg/µl. Samples were then boiled at 95°C for 5 minutes. Samples were stored at -20°C once cooled.

24-well 10% SDS-polyacrylamide gels were used to run the samples. A cortex control standard (20 µg) was always run in the first lane and full-range molecular weight marker (2.5 µl; RPN800E; Amersham) in the second and centre lanes. 20 µg of total protein (thus 20 µl) was loaded into the remaining lanes, one for each sample. Gels were run at 160 volts until the molecular weight marker was visualised at the bottom of the gel.

Individual gels were then sandwiched between a nitrocellulose membrane (Amersham Biosciences), blotting paper and fibre pads. Gels were transferred at 60 volts for 90 minutes. Post transfer, nitrocellulose membranes were blocked with 5% powdered milk in 0.1% tween-20/PBS (PBST-milk) to ensure non-specific binding was kept to a minimum. After the blocking stage, the membranes were incubated in the desired primary antibody in PBST-milk overnight at 4°C (see table 8 for specific primary antibody concentrations). The following day, PBST washes (3x 5 minutes) were performed to remove excess antibody. The appropriate secondary antibodies (Table 8) were then incubated in PBST-milk for 1 hour. Final PBS washes (3x 5 minutes) were then performed to remove excess secondary antibody. To ensure that the results were consistent, a total of three gels (3 results for each sample) were performed to increase the number of technical replicates.

**Table 8: Antibodies used for Western blotting.**
The following antibodies were used at their described dilution and according to the protocol described above.

| Western Blotting Antibodies | | | | |
|---|---|---|---|---|
| **Antibody** | **Type** | **Host** | **Dilution** | **Supplier** |
| Tyrosine hydroxylase | Primary | Rabbit; polyclonal | 1 in 5000 | AB152; Millipore |
| GDNF | Primary | Rabbit; polyclonal | 1 in 5000 | ab18956; Abcam |
| BDNF | Primary | Rabbit; polyclonal | 1 in 5000 | ab108319; Abcam |
| βIII-Tubulin | Primary | Rabbit; polyclonal | 1 in 10000 | ab6046; Abcam |
| IRDye 800CW | Secondary | Goat anti-rabbit | 1 in 10000 | 925-32211; Li-Cor |

### *Re-probing nitrocellulose membranes*

The nitrocellulose membranes were reprobed for different markers after use. Due to the molecular weight of GDNF and BDNF being similar, a membrane stripping process was required to remove the first round of antibodies. A mild stripping buffer (see Table 9 for formulation) was used to cover the membrane for 5 - 10 minutes at room temperature. The buffer was discarded before fresh mild stripping buffer was again applied to the membrane for a further 5 - 10 minutes. The buffer was then discarded before PBS washes were performed (2x 10 minutes). PBS-T washes were then finally performed (2x 5 minutes) to ready the membrane for primary antibody incubation once again.

**Table 9: Mild stripping buffer recipe.**
The following amounts and volumes of ingredients were used to formulate the mild stripping buffer.

| **Mild stripping buffer (for 1 L)** | | |
|---|---|---|
| Amount | Ingredient | Provider |
| 15 g | Glycine | Sigma |
| 1 g | SDS | Sigma |
| 10 ml | Tween20 | Sigma |
| | pH to 2.2; bring to 1 L with $dH_20$ | |

### *Membrane image analysis*

Membranes were imaged using the Odyssey infrared scanner (Li-cor; version 3.0.16). Wavelength selection (i.e. 800 nm to be used), size of scan and scan intensity were tailored to the antibodies used within the Western blot. The intensity of the rat cortex control was calculated and used to express all other band intensities against it as a standardised ratio. The standardised values for the samples were then compared to the standardised samples from control mice (i.e. mice which received no selegiline) in order to determine whether NTF protein levels had been significantly increased following selegiline treatment. ImageJ was used to determine band intensities.

## 4.3.2. Investigating the effect of selegiline in the established ChABC-treated 6-OHDA partial lesion mouse model

### *4.3.2.1. Animal subjects*

40 eight-week-old male C57Bl/6 mice (Harlan, UK) were used and treated according to conditions in section 4.3.1.1.

### *4.3.2.2. Experimental design*

The time line for the study is described below in figure 43. A week prior to the initiation of selegiline treatment, a 7 day habituation period was implemented to ensure animals were non-responsive to non-biologically relevant stimuli. Selegiline (n=20) or saline (n=20) was administered daily for a week before surgery (the required time for significant increases in GDNF and BDNF levels as discovered by the pilot study [see figure 44]) and up until necropsy. During the habituation period, baseline recordings for the cylinder test were conducted on days -3 and -1. All animals received 4 µg of intrastriatal 6-OHDA and either ChABC or saline (rostral SNc and caudal striatum) on day 0 in a randomised block design whilst blind to the treatment. A recovery period of 35 days was enforced whereby daily rehydration and health checks were conducted until the animals had returned to pre-surgical weight. During this period the cylinder test was conducted on all animals at weekly intervals (days 14, 21, 28 and 35). On day 39 post-lesion animals were killed by anaesthetic overdose and brains were removed for biochemical and histological analysis.

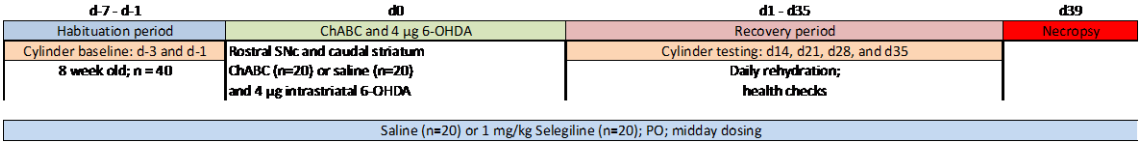


**Figure 44: Experimental design for the study: Investigating the effect of selegiline in the established ChABC-treated 6-OHDA partial lesion mouse model.**
All procedures of the study were conducted on certain days pre- and post- ChABC and 6-OHDA treatment as described in the figure. Further details are found either below the timeline or in subsequent sections.

### *4.3.2.3. Selegiline treatment*

Mice were dosed either selegiline (n=20; 1 mg/kg in saline; p.o.; Sigma-Aldrich) or saline (n=20; p.o.) daily for the entirety of the study. An 18 G stainless steel bent feeding needle (Harvard Apparatus) was used to administer selegiline or saline. A week of treatment was provided before lesioning to ensure significant increases in GDNF and BDNF were present, as discovered by the pilot study. Dosing sessions were conducted every day at midday and directly before any cylinder testing or culls.

#### 4.3.2.3. Surgery

All surgical and post-operative care techniques were identical to the partial lesion study; described in sections 3.3.1.3. and 3.3.1.5. of Chapter 3, respectively.

#### 4.3.2.4. Stereotaxic 6-OHDA and ChABC injections

One week after the initiation of selegiline or vehicle treatment, all 40 mice underwent partial 4 µg 6-OHDA lesioning, as described in Chapter 3 section 3.3.2.4. Five minutes post 6-OHDA injection mice received two single 1 µl injections of 10U/ml ChABC (n=19) or saline (n=19) at the two sites previously described in Chapter 3 section 3.3.3.5. These were in the rostral SNc: AP: -2.3 mm, ML: ± 1.0 mm and DV: -4.2 mm (relative to bregma and skull surface) and the caudal striatum: AP: +0.02 mm, ML: ±2.2 mm and DV: -3.5 mm (relative to bregma and skull surface).

Two animals were culled during the recovery period due to ill health. This resulted in four experimental groups: Saline/Saline (n=10), Saline/Selegiline (n=9), ChABC/Selegiline (n=9) and ChABC/Saline (n=10).

#### 4.3.2.5. Behavioural assessment of parkinsonian phenotype

The cylinder test was performed on pre- or post-lesion days -3, -1, 14, 21, 28 and 35. The cylinder test was conducted as described in sections 3.3.4.6. of Chapter 3.

#### 4.3.2.6. Striatum and SNc extraction

On day 39, mice were killed by dislocation of the neck and heads were removed. The whole brain was coronally bisected leaving the striatal and nigral regions separate. The striata from both the lesioned (left) and intact (right) hemispheres were removed from the brain and separately stored on dry ice ready for Western blotting. The remainder of the brain containing the SNc was submerged and postfixed in 10% formalin overnight ready for paraffin embedding and sectioning.

#### 4.3.2.7. Western blotting procedure

Striatal samples were prepped for Western Blotting as described in section 4.3.1.4. In addition to using antibodies directed against GDNF and BDNF, these samples were also probed for striatal TH levels (dilutions of antibodies found in Table 8). This was because all of the striatal tissue had been used for Western blotting and none for paraffin wax embedding and immunohistochemistry.

##### *Membrane image analysis*

As described in section 4.3.1.4., membranes were scanned at 800 nm. Size of scan and scan intensity were tailored to the antibodies used within the Western blot. The intensity of the rat cortex control was calculated and used to express all other band intensities against it as a standardised ratio. The standardised values for the samples were then compared to the standardised samples from saline/saline control mice (i.e. mice which received saline instead of selegiline and saline instead of ChABC) in order to determine whether protein levels had been significantly increased following selegiline or ChABC treatment. ImageJ was used to determine band intensities.

#### 4.3.2.8. Immunohistochemical assessment of lesion size

Once the tissues containing the SNc had been post-fixed, they were embedded in paraffin wax and then sectioned (7 µm thick sections) with a microtome (Thermo Scientific) at three rostrocaudal levels of the SNc (rostral: -2.92 mm, medial: -3.16 mm and caudal: -3.52 AP mm; relative to bregma). Slide mounted sections were then stained for TH-positive SNc cells as described in Chapter 2 section 2.3.2.2. Cell counts were then conducted on imaged tissue to give the number of TH-positive cells in both the lesioned and intact SNc, as per Chapter 2 section 2.3.2.5.

### 4.3.3. Statistical analysis

All statistical analyses were conducted with the Graphpad Prism 5; statistical tests used are displayed within the figure legends. Graphpad Prism 5 was used to plot all graphs. GPower 3.1 was utilised for power calculations.

## 4.4. Results

### 4.4.1. Pilot study: Daily treatment of selegiline enhances striatal GDNF and BDNF levels in naive mice

Work by Zhao *et al*., has previously shown that administration of the MAO-B inhibitor selegiline promotes the endogenous release of both BDNF and GDNF within the BG of MPTP-lesioned mice. As we wished to finally use this finding as a method of enhancing GDNF and BDNF levels beyond what was seen with our ChABC model (see Chapter 3), we wanted to first validate the results seen by Zhao *et al*.

A time dependent increase in GDNF and BDNF levels was observed in the Western blot analysis following 14 days of daily selegiline administration (figure 44A). This reached significance after 7 days of selegiline treatment (GDNF: 1.9 ± 0.06 and BDNF: 2.3 ± 0.24 compared to saline control; Two-Way ANOVA with Bonferroni post hoc test; $P<0.001$) and maintained for another week when the study finished (GDNF: 1.3 ± 0.14; $p<0.01$ and BDNF: 1.8 ± 0.21; $p<0.05$ compared to saline controls; Two-Way ANOVA with Bonferroni post hoc test). Interestingly this significant increase was only apparent in the striatal tissue (figure 44B + C). Although the ventral midbrain tissue saw a similar dose dependent increase in BDNF and GDNF, neither NTFs were significantly raised beyond the saline control.

A decline was apparent in both GDNF and BDNF levels on day 14 when compared to day 7 of daily selegiline treatment. This was observed in both the striatal and ventral midbrain tissue. Nevertheless, NTF levels remained significant in the striatum.

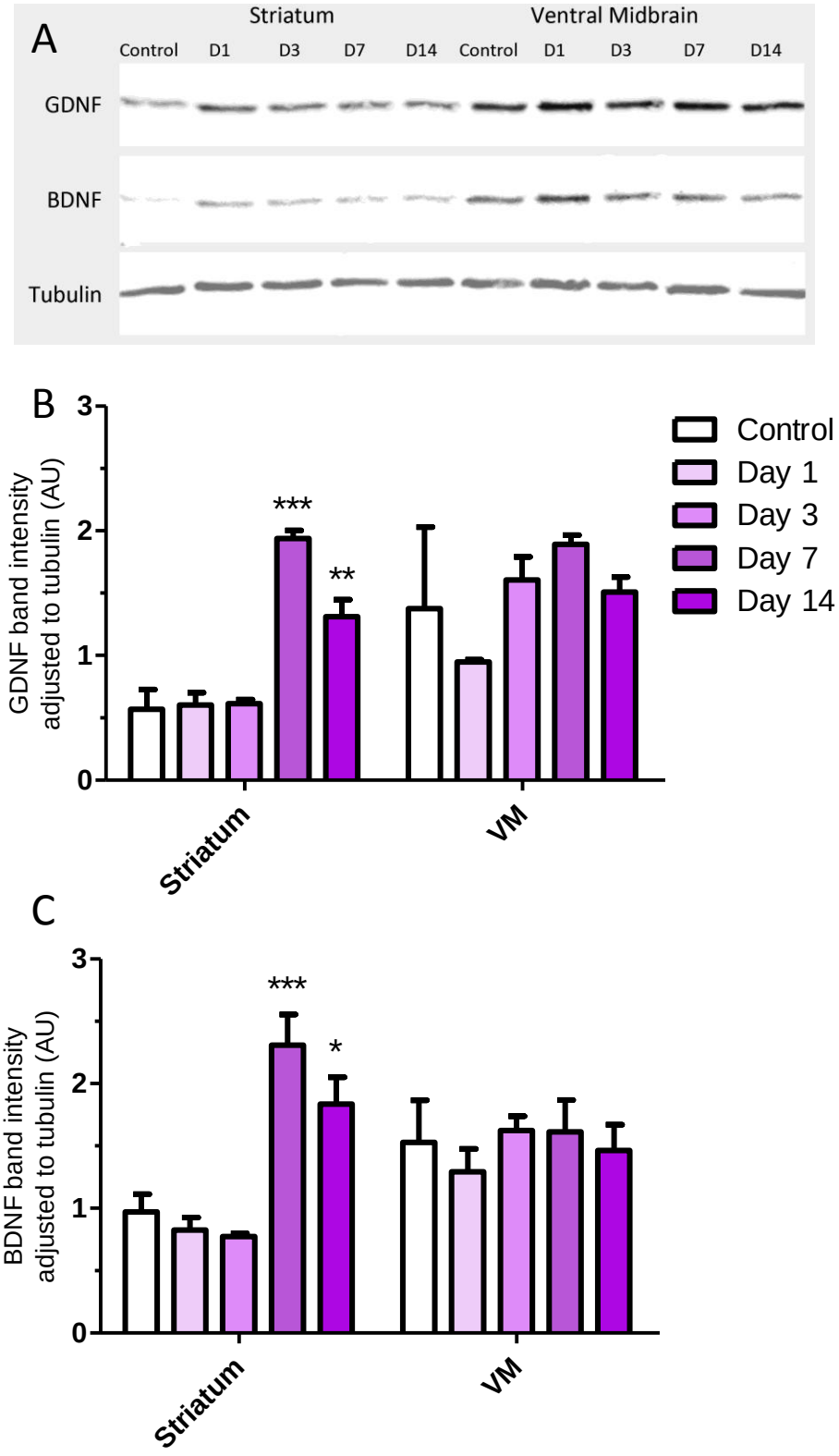


**Figure 45: Semi-quantitative Western blot analysis of GDNF and BDNF levels within the BG following selegiline treatment.**

(A) Representative immunoreactive bands for GDNF, BDNF and βIII-Tubulin loading control. Each band represents one of three animals culled at that specific day (D1, D3, D7 or D14). Control (saline-treated) mice were culled on day 14 (D14). (B + C) Percentage intensity of control indicates the degree of GDNF and BDNF presence relative to the saline control animals. Two-way ANOVA with Bonferroni post hoc test. ***, ** and * denote $p<0.001$, $p<0.01$ and $p<0.05$, respectively, between experimental day and saline control. Each experimental group and BG region: n=3. Data are mean ± S.E.M.

### 4.4.2. Investigating the effect of selegiline in the established ChABC-treated 6-OHDA partial lesion mouse model

As daily treatment of selegiline was considered successful in enhancing striatal GDNF and BDNF levels in naive mice, we wished to test whether this increase would further the beneficial effects seen by ChABC in the previous chapter. As the results in section 4.4.1. indicated that a week of selegiline treatment was required to maintain increased levels of GDNF and BDNF, a week of dosing was conducted before lesioning and ChABC administration.

#### *Confirmation of CSPG digestion along the NS*

To validate the study in regards to CSPG digestion, the pattern of C4S immunoreactivity was firstly investigated. This study study used the coordinates determined by Pilot Study 3 in Chapter 3. As before, unilateral ChABC administration brought about the full digestion of the entire NS in the lesioned left hemisphere (figure 45). The ChABC digested the CSPGs surrounding the SNc, striatum and NS regions. Although not shown below, vehicle administration presented no C4S-positivity and thus no digestion. The degree of CSPG digestion by ChABC treatment was considered successful.

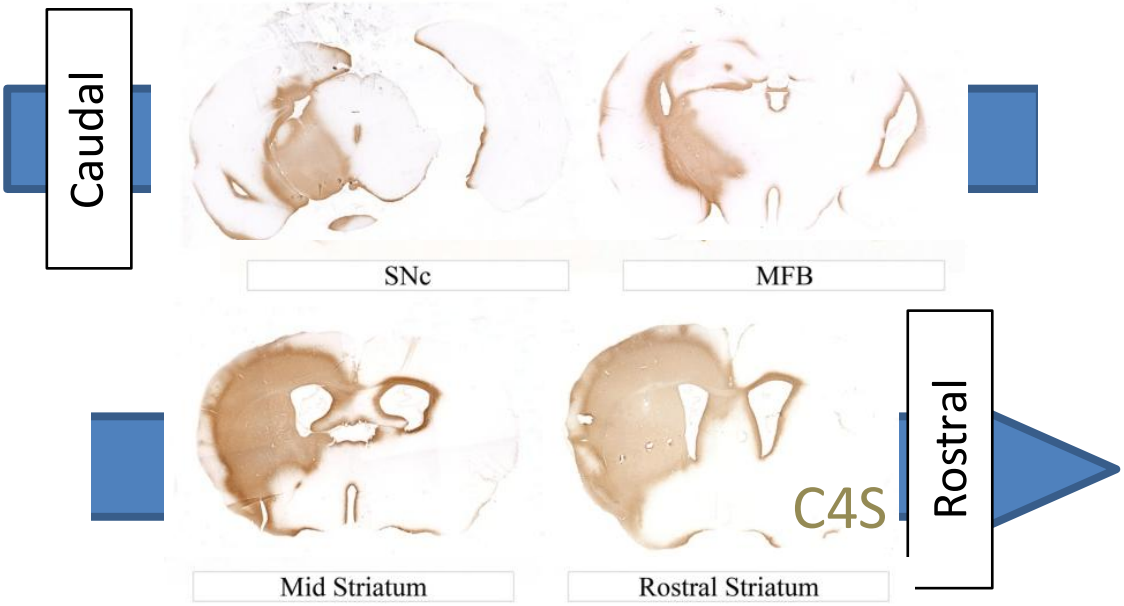


**Figure 46: Two bolus injections of ChABC digest the entire NS.**
Photomicrographs of four levels of the NS highlighting the regions of C4S-positivity and thus CSPG digestion (brown). ChABC was administered unilaterally into the 6-OHDA lesioned hemisphere (left hand).

### *TH immunohistochemistry of the SNc and striatum*

To assess the therapeutic benefit of both selegiline and ChABC on cell survival, images of the SNc were obtained. Photomicrographs, shown in figure 46, depict only an increase in cell survival in the ChABC-only experimental group (bottom panel). No TH-positive striatal fibre photomicrographs were obtained as the tissue was used for Western blotting.

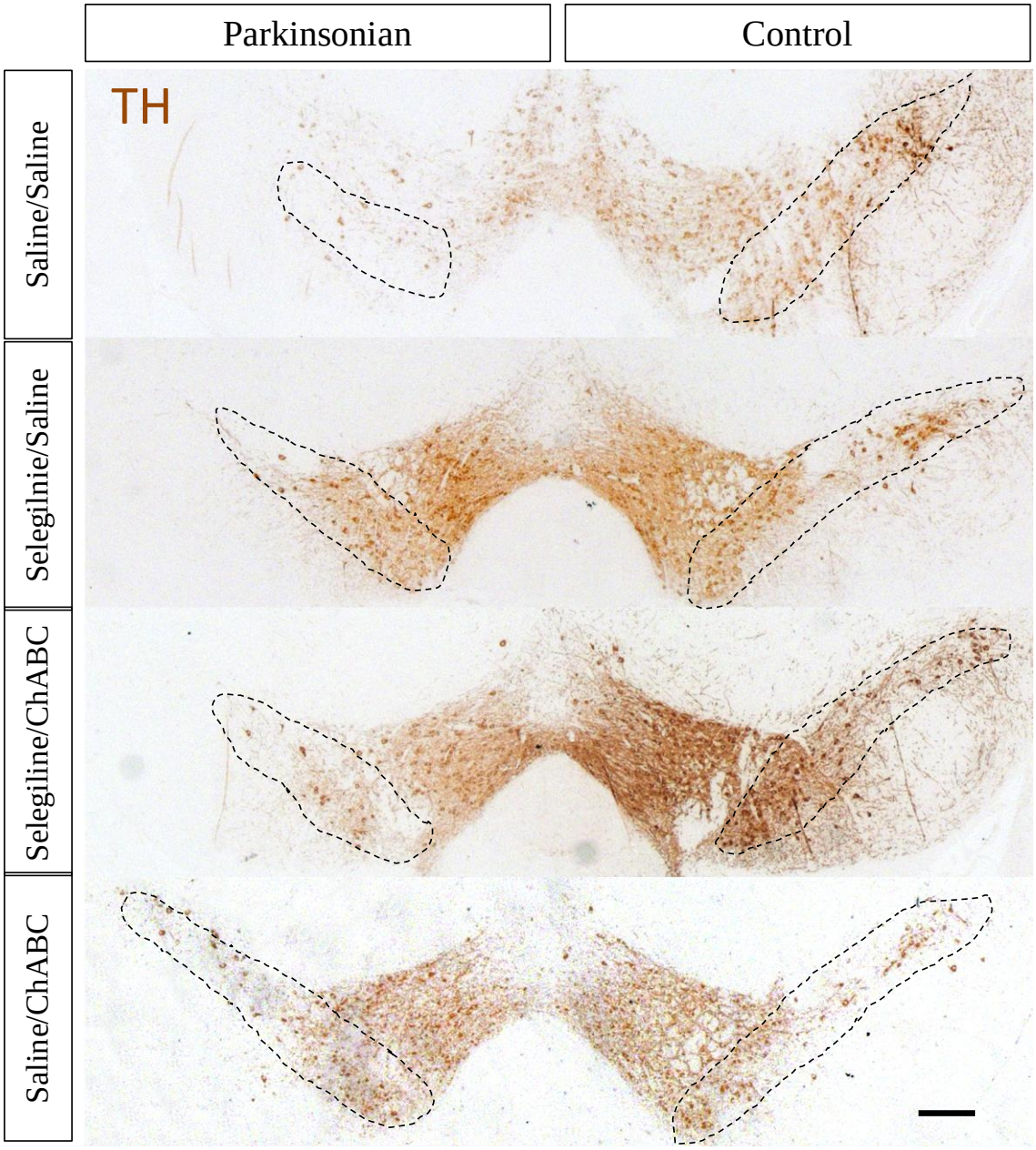


**Figure 47: Photomicrographs highlighting the TH-positive SNc cells remaining following selegiline or saline and ChABC or saline treatments.**
Coronal TH-positive SNc cell sections. Top to bottom: Saline/Saline control, Saline/ChABC, Selegiline/ChABC and Saline/ChABC. The unilaterally lesioned SNc is shown on the left of each section. All sections were cut at the rostral level (-2.92 mm AP; relative to bregma and skull surface). Black dashed line indicates the SNc. Scale bar represents 250 µm.

### *Assessment of TH-positive cells remaining in the SNc as a result of ChABC and selegiline treatment*

Using the data obtained from the photomicrographs, TH-positive cells of the SNc were counted in the lesioned and intact hemispheres of each animal (data not shown). These data were then used to produce values that represent the TH-positive cells in the lesioned SNc as a percentage of the intact SNc. As with Chapter 3's study, the three levels of the SNc were not averaged as significance was found between them.

There was no significant difference in the percentage of SNc cells remaining in the partially lesioned hemisphere between the saline- and selegiline-only treatment groups (blue versus white bars). This was consistent across all three levels of the SNc analysed. However, animals of the ChABC-only group displayed a higher percentage of cells remaining in the rostral SNc level to that of the saline control (Control: 23.5 ± 3.5% and ChABC only: 42.1 ± 10.5%; p=0.027; One-Way ANOVA with Bonferroni post hoc test) (figure 47C; orange versus white bars). This increase in the rostral level was significantly higher than the combined treatment of selegiline and ChABC (selegiline/ChABC: 15.9 ± 2.9% and ChABC only: 42.1 ± 10.5%; p<0.05; One-Way ANOVA with Bonferroni post hoc test). Furthermore, the degree of cell survival ChABC-only induced matched the results from the ChABC partial lesion study in Chapter 3 (Chapter 3 rostral SNc: 51.6 ± 8.5%).

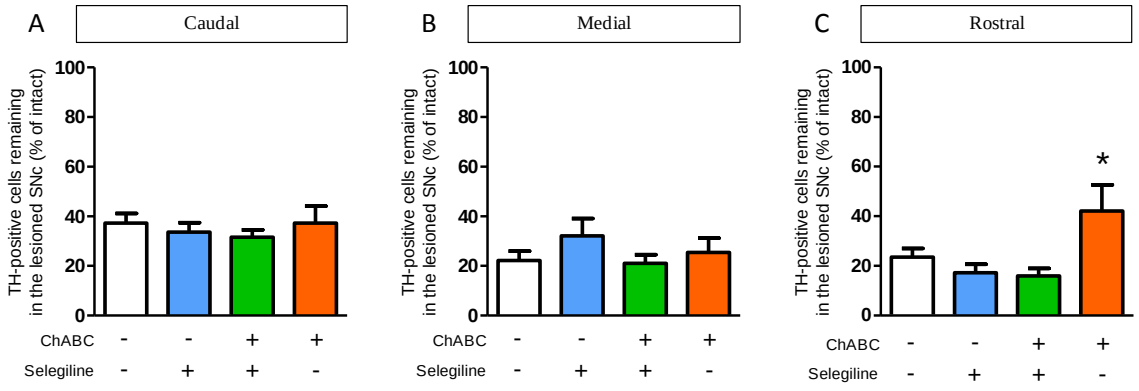


**Figure 48: Analyses of SNc cells, striatal TH-positive fibres and striatal GDNF and BDNF levels following the treatment of ChABC and selegiline.**
(A - C) Percentage number of TH-positive SNc cells remaining in the lesioned hemisphere as compared to control of all four experimental groups. All three levels of the SNc were left separated. One-way ANOVA with Dunnett's post hoc test; * denotes p<0.05 between group and saline/saline control (white bar). Saline/saline (white bar): n=10, selegiline/saline (blue bar): n=9, selegiline/ChABC (green bar): n=10 and saline/ChABC (orange bar): n=9. Data are mean ± S.E.M.

### *Semi-quantitative Western blot analysis of GDNF and BDNF levels following ChABC and selegiline treatment*

Western blot analysis was conducted to identify whether striatal protein levels had been affected by ChABC or selegiline administration in an individual or synergistic manner. Although both the lesioned (ChABC/6-OHDA) and intact (control) striata were taken for GDNF and BDNF measurement, no difference was found between any experimental group. Results were therefore averaged for analysis. Western blotting revealed no statistical significance in GDNF and BDNF levels in the striatum between any groups at the end of the study (figure 48A - C).

No improvements were found in the percentage of TH-positive fibres remaining in the lesioned striatum (as percentage of saline/saline control; ns; One-Way ANOVA with Bonferroni post hoc test).

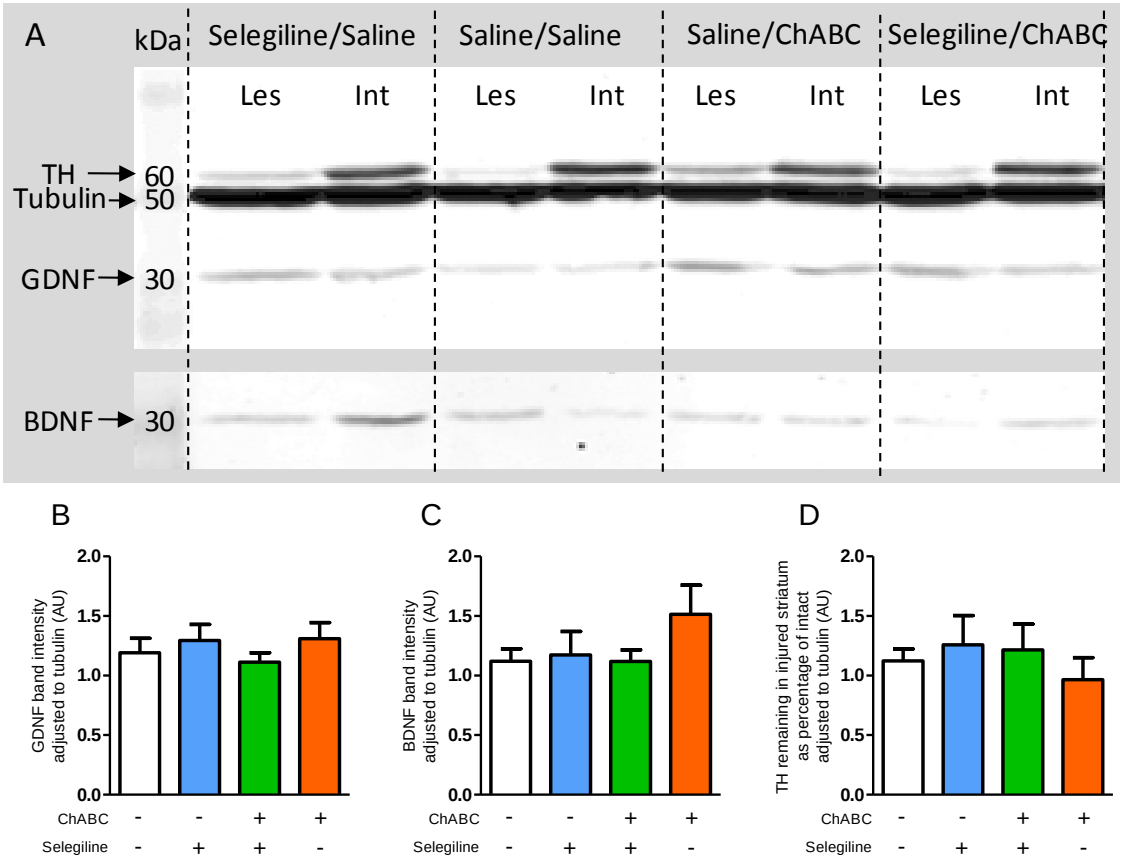


**Figure 49: Analyses of striatal GDNF, BDNF and TH-positive fibre levels following the treatment of ChABC and selegiline.**
(A) Representative immunoreactive bands for GDNF, BDNF, TH and βIII-Tubulin loading control. (B + C) Western blot analysis of striatal GDNF and BDNF concentrations in both hemispheres, respectively. (D) Western blot analysis of striatal TH remaining in the lesioned hemisphere as a percentage of the intact. Saline/saline (white bar): n=10, Selegiline/Saline (blue bar): n=9, Selegiline/ChABC (green bar): n=10 and Saline/ChABC (orange bar): n=9. Data are mean ± S.E.M.

### *Assessment of behavioural outcomes as a result of ChABC and selegiline treatment*

No significant differences between treatment groups were seen in asymmetry score on any day (figure 49). All four groups presented similar average base line asymmetry scores (averaged for days -3 and -1: Saline/saline: 49.8 ± 0.8%, selegiline/Saline: 48.9 ± 1.7%, selegiline/ChABC, 49.5 ± 0.9% and Saline/ChABC: 48.0 ± 1.5%; ns; Two-Way repeat measures ANOVA with Bonferroni post hoc test). A score of 50% represents an unbiased and therefore unlesioned phenotype. Following lesioning on day 0, scores declined from day 3 until the end of experimentation for all the groups (Score on day 35; Saline/saline: 34.5 ± 3.9%; selegiline/Saline: 40.2 ± 2.5%; selegiline/ChABC: 33.9 ± 3.5% and Saline/ChABC: 32.4 ± 2.3%; ns; Two-Way ANOVA with Bonferroni post hoc test). No significance was observed between any group receiving either ChABC or selegiline.

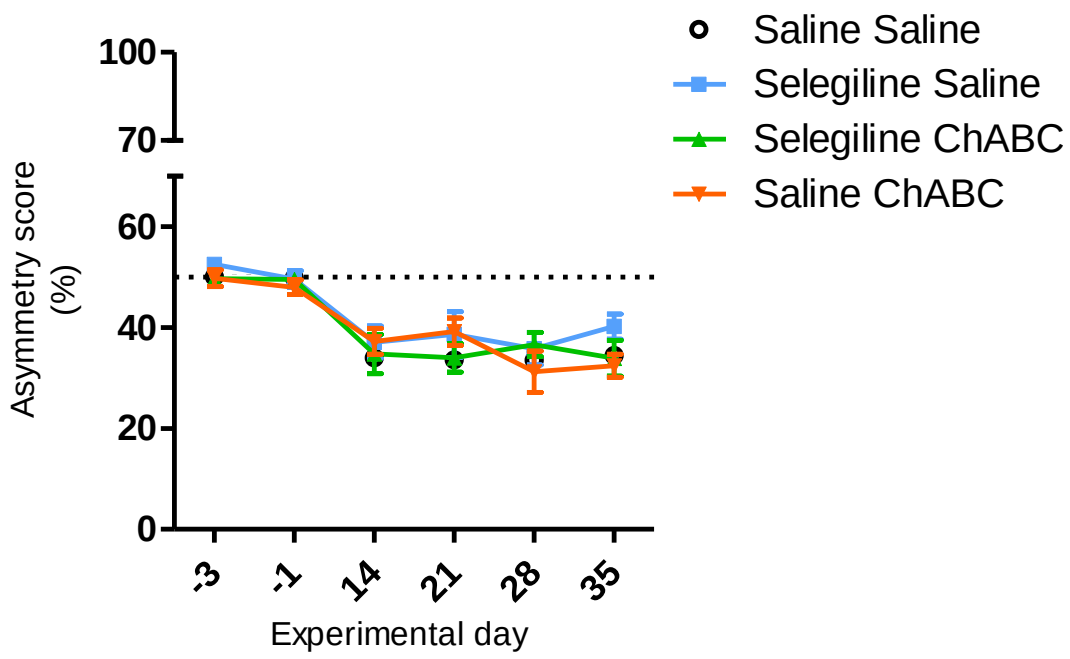


**Figure 50: Cylinder test.**
Asymmetry scores of animals from the four experimental groups (ChABC and selegiline treatment with saline controls). Mice were tested prior to lesioning and weekly for 35 days post lesion. Saline/saline: n=10, Selegiline/Saline: n=9, Selegiline/ChABC: n=10 and Saline/ChABC: n=9. Data are mean ± S.E.M.

## 4.5. Discussion

### 4.5.1. Systemically administered selegiline significantly enhanced GDNF and BDNF levels within the striatum of naive mice

The studies in this chapter set out to test the hypothesis that the MAO-B inhibitor, selegiline, would enhance the degree of cell survival beyond what was discovered by ChABC alone in Chapter 3. This would ideally result in a favourable and detectable functional phenotype. Selegiline was theorised to enhance cell survival by increasing striatal GDNF and BDNF presence, a finding also found by others (Zhao *et al.*, 2013).

Initial studies sought to confirm that use of selegiline would be an effective way to boost GDNF and BDNF levels. Following 7 days of selegiline treatment it was found that both GDNF and BDNF protein levels were enhanced in the striatum of treated animals; supporting the use of selegiline as a pharmacological means to boost these NTF levels. Our results differed to those found in the Zhao study who not only found an increase in GDNF and BDNF within the striatum but also the ventral midbrain. However, due to the size of the dissected ventral midbrain, this difference could be attributed to an error in dissection. Being a small region to dissect, our ventral midbrain homogenates may have possessed different tissues not associated with the ventral midbrain, therefore diluting the results. However, variations in tissue content would be associated with a large degree of error, which was not found in our results.

Although both the D7 and D14 time points saw the increased levels in GDNF and BDNF, the mean levels declined in concentration during the second week of daily selegiline treatment. Although we did not expand this pilot study beyond fourteen days, it may be wise in future to investigate whether an additional week of treatment would induce a significant fall in protein concentrations. If so, this may confound the outcome of chronic studies beyond fourteen days using daily selegiline treatment.

### 4.5.2. Selegiline does not enhance the effect of ChABC treatment in the partial lesion mouse model

This study was a success as not only were the NS CSPGs effectively digested by ChABC, but also because the CSPG-only group elicited an increase in survival of the rostral SNc cells. The degree of survival seen in the ChABC-only group was equivalent to that observed in Chapter 3's ChABC partial lesion investigation. However, contrary to our hypothesis, this survival was not further enhanced by selegiline and did not provide an improved and detectable behavioural phenotype. While disappointing, this study did however replicate our previous results obtained from Chapter 3 and therefore reinforced the validity of our findings.

At the end of the study, Western blot analysis indicated selegiline to be ineffective at increasing GDNF and BDNF protein levels within the mouse striatum. This is despite the promising effects seen in the previous 14 day pilot study which saw a robust increase in striatal GDNF and BDNF after 7 and 14 days. It is likely that the trend in GDNF and BDNF decline has continued to a significantly lower level in the additional weeks this study ran. As we do not know the specific mechanism in which selegiline promotes GDNF and BDNF release, it is difficult to understand whether some form of desensitisation is occurring between the inhibitor and its target or through other means. It may be worth while exploring how frequently selegiline has to be administered to maintain heightened GDNF and BDNF levels once peak concentration at D7 has been reached. This may halt the possibility of desensitisation to the compound.

Although we are confident that GDNF and BDNF levels were elevated following 14 days of selegiline administration, the treatment of the MAO-B inhibitor did not enhance the levels of GDNF and BDNF after 39 days of daily treatment. This indicated that the 14 day window of increased striatal GDNF and BDNF content was not sufficient to enhance cell survival in this 2 month study. This highlights a few points, firstly, that increased striatal levels of GDNF and BDNF (a result of selegiline treatment) within the *neuroprotection window* (initial 14 days post-lesion) do not enhance neuroprotection. Secondly, as GDNF and BDNF levels were enhanced only within this early window of the study, we cannot conclude whether these increased NTF levels would affect neurorepair (figure 50).

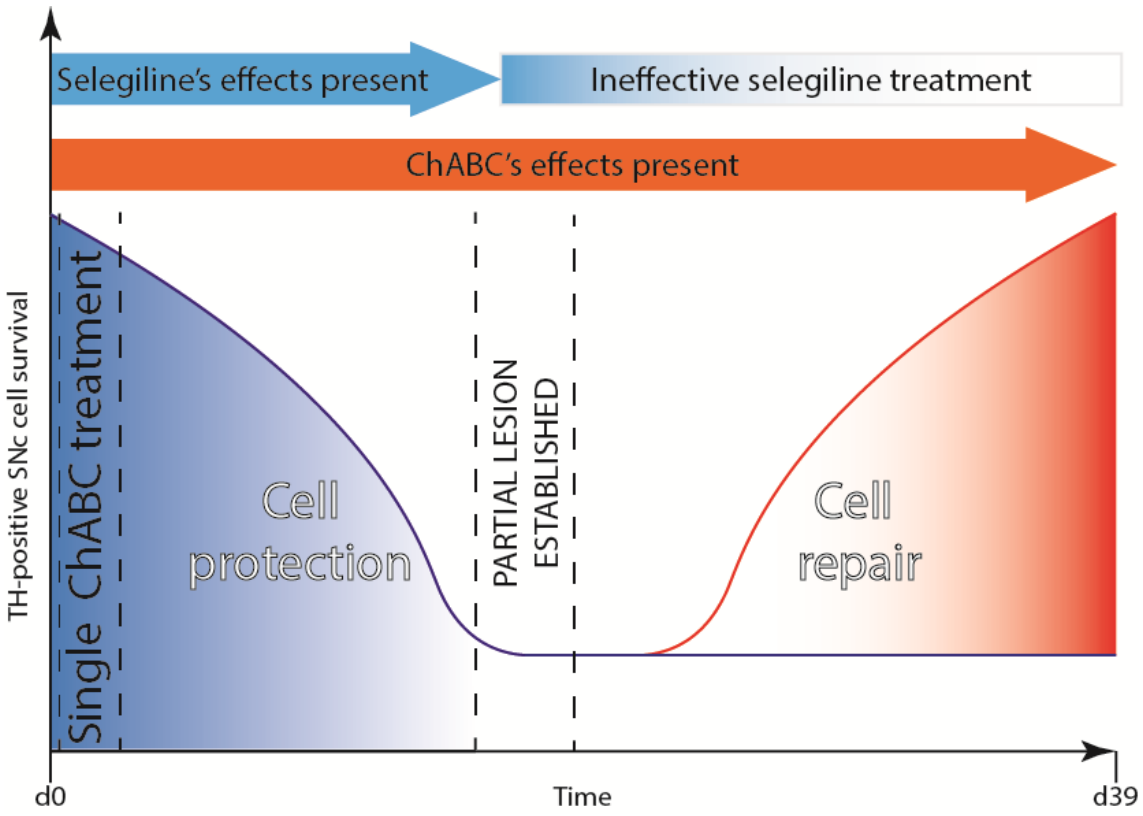


**Figure 51: Time course of study following 6-OHDA lesioning.**
Single bolus treatment of ChABC induced cell survival when dosed alone (Chapter 3). This may have been attributed to either neuroprotection or repair as it was administered before 6-OHDA lesioning. Selegiline increased GDNF and BDNF levels during 14 days of daily treatment (as described in pilot study, figure 44) but was not found to maintain these levels at the end of the study (d39). This indicated that, although GDNF and BDNF levels were enhanced during the early protection window, no significance was found. Therefore, selegiline's assumed beneficial effect is likely to not work via neuroprotection.

In addition, the co-treatment of selegiline and ChABC was, unexpectedly, equivalent to the saline control group and not the ChABC-only group. This result indicated a possible negating effect of selegiline on the ChABC-induced digestion of the CSPGs. Due to the unknown mechanisms underlying both CSPG digestion and selegiline's promotion of NTFs, it is difficult to pinpoint any conflicting protein interactions. Despite this, several studies have utilised both GDNF and ChABC treatment to promote recovery in spinal cord injury models with success (Tom *et al.*, 2009; Zhang *et al.*, 2013) or at least with no *cancelling-out* effect (Sivak *et al.*, 2014). Thus, any conflicting interactions between selegiline and ChABC must be either in a GDNF/BDNF-dependent pathway or directly between the two enzymes. This latter point has been resolved within this study, as the activity of ChABC was not inhibited by daily selegiline treatment; this was made evident by the digestion of CSPGs (C4S presence) within the NS.

A significant flaw in this study was the use of selegiline during the 6-OHDA lesion induction stages of the study (D0-D14). The MAO inhibitor, pargyline, is commonly pre-treated before 6-

OHDA surgery to reduce the metabolism of the toxin and enhance its effects (Thiele *et al.*, 2012). With selegiline working in a similar fashion to pargyline, selegiline would have increased the efficacy of 6-OHDA in all the animals treated. This would have caused more severe lesions in mice receiving selegiline. In future studies it may be advisable to pre-treat all animals with pargyline to ensure all animals receive the same exposure to 6-OHDA with or without selegiline. Of course, direct infusion of GDNF and/or BDNF would have circumvented this problem, but we were keen to explore novel systemic strategies that have an easier translation to patients.

Unfortunately, an improved behavioural phenotype was not found following ChABC and/or selegiline treatment. No significance was detected between the asymmetry scores in animals in any group. These are simply attributed to the lack of cellular and TH-positive fibre recovery provided by selegiline. The ChABC-only group did provide an increase in SNc cell survival, but as with the previous investigation in Chapter 3, the cylinder test was not sensitive enough to detect the modest improvement.

### 4.5.3. Further considerations regarding selegiline

Selegiline has shown in other works to be important in MAO-B inhibition but also in providing a degree of cell survival. We, and many others, believe that these two processes are mutually exclusive for the reasons below. As the inhibition of MAO-B is irreversible, the rate of MAO-B turnover is dependent on *de novo* synthesis. Studies have identified that the time taken for MAO-B levels to return back to basal activity following selegiline administration (0.25 mg/kg) to be 7 days in the rat (Timar, 1989). In humans, selegiline (5 mg/kg; twice daily) was found to have a persistent half life of 40 days (Fowler *et al.*, 1994). However, in our studies and in other's (Zhao *et al.*, 2013), data suggest that daily administration of selegiline is required to promote and maintain the increase in GDNF and BDNF levels. This need for frequent treatment supports a non-MAO-B inhibition driven mechanism underlying this increase in GDNF and BDNF release.

### 4.5.4. Future investigations

Several areas of further investigation could be undertaken in regards of this study. In order to identify whether selegiline possesses any neuroreparative efficacy in this model of disease, alterations can be made to the dosing regimen. It is clear that selegiline has no neuroprotective role but it may possess effects of neurorepair. These effects were not apparent in this study as the increase in GDNF and BDNF levels would have declined after 2 weeks of daily administration and therefore selegiline would have been ineffective during this *neurorepair window* (i.e. after the lesion had developed). With this in mind, it may be of interest to administer selegiline 2 weeks post-lesion until the end of the investigation. Any increases in cell

survival would then be associated with neurorepair.

Other NTFs to investigate would be neurturin, MANF and CDNF; candidates with promise in the dopaminergic system. Neurturin has been implemented in effective gene therapy strategies in both rodent and NHP models (Kordower *et al.*, 2013) which have translated into the clinic. However, the efficacy of neurturin has yet to be proved in double-blinded trials (Domanskyi *et al.*, 2015). Intranigral lentiviral expression of CDNF and MANF in the 6-OHDA lesioned mouse has proved beneficial. CDNF overexpression lowered the amphetamine-induced rotations and increased TH-positive terminals in the striatum, whilst MANF provided significant protection of the SNc neurones (Cordero-Llana *et al.*, 2015). The same study saw the combined intranigral treatment of CDNF and MANF provide a synergistic combination of the two behavioural and pathological benefits (Lindahl *et al.*, 2016). These investigations highlight the importance of detecting other NTFs that have proven to have neuroprotective results in both the human and animal models of PD.

The expression of the GFRα1/Ret receptors, TrkB and p75NTR receptors on striatal dopaminergic terminals would be important to identify through both histological and biochemical means. Long-term exposure to selegiline may induce receptor plasticity that gives rise to more NTF receptors being trafficked to the cell membrane, ultimately increasing cell sensitivity to GDNF and BDNF. On the other hand, chronic exposure may cause receptor downregulation which may explain the dampening of any neuroprotective effect.

It is possible that the increase in NTF release by selegiline is specific to only naive and MPTP lesioned mice (Zhao *et al.*, 2013). Although highly unlikely, it is possible that the mechanism in which 6-OHDA causes toxicity inhibits the interaction between the MAO inhibitor and its target. To confirm whether this were true, a small pilot analysing the striatal NTF content and SNc cell pathology within MPTP- and 6-OHDA-lesioned mice treated with selegiline would be suggested. This study would follow the same protocol as described in section 4.3.2. but would also include MPTP treatment as a method of lesioning for an additional group. No ChABC would be administered, as this is purely an investigation into selegiline's ability to enhance NTF levels in the 6-OHDA model.

### 4.5.5. Chapter conclusions

Overall, the studies in this chapter have revealed that the daily administration of selegiline does not enhance the degree of ChABC-mediated cell survival but it may in fact inhibit it. The reasons for this are unknown, but we assume it to be due to interactions between their two pathways rather than directly between the proteins. Surprisingly, the selegiline-only group did not promote the levels of striatal GDNF and BDNF as seen in the 2 week pilot study. This indicated that selegiline can only promote these levels for ~2 weeks before they return to baseline and that an altered dosing regimen may be required for longer studies such as this one. We suggest that, as selegiline does not induce neuroprotection during the initial 2 weeks, delaying the treatment to a later time point would target the *neurorepair window.*

# 5. Identifying striatal changes in a rodent model of L-DOPA-induced dyskinesia

## 5.1. Introduction

As mentioned in Chapter 1, L-DOPA-induced dyskinesia (LID) is one of the greatest drawbacks to L-DOPA use in the treatment of PD. Arising following the long-term pulsatile exposure to L-DOPA, LID brings about abnormal involuntary movements (AIMs) that drastically lower quality of life. LID therefore remains a key unmet clinical need for people with PD. In the absence of a complication-free effective anti-dyskinetic treatment, further understanding of the mechanisms that underlie LID is required to unveil new therapeutic targets.

### 5.1.1. Mechanisms underlying L-DOPA-induced diskinesia

The pulsatile stimulation of the postsynaptic dopaminergic receptors in the striatum alongside severe SNc denervation gives rise to LID. However, the mechanisms behind its manifestation have not been fully elucidated.

The pathogenesis of LID is thought to combine several pre- and post-synaptic alterations within the many pathways of the BG. Therefore, the phenomenon is likely not to be confined to a single mechanism. A previously accepted theory of LID states that L-DOPA exposure leads to a hyperactive direct pathway and a hypoactive indirect pathway through D1 and D2 receptor agonism (Jenner 2008). The culmination of the two leads to the lowered activity of the GPi/SNr complex that in turn causes the aberrant disinhibition of the thalamocortical feedback loop and the induction of involuntary movements. Although nicely simplistic and somewhat true, this theory is outdated. Contradictory evidence, such as an unaffected indirect pathway in NHP models of LID (Herrero *et al.*, 1996) and pallidotomies reducing LID (not increasing LID as suggested by the theory) (Parkin *et al.*, 2002) indicates a far more complex mechanism, or combination of mechanisms, at work.

On balance, it would appear that stimulation of D1 and D2 receptors have a significant role in the induction of dyskinesia. Studies utilising genetic knockout mice demonstrated that the deletion of D1 receptors led to a lowered expression of dyskinetic associated markers, such as FosB and dynorphin, whilst also inhibiting the manifestation of LID. Furthermore, the same experimenters saw persistence of the typical manifestation of LID and the associated molecular markers in D2 receptor deficient mice (Darmopil *et al.*, 2009). This suggested that D1 receptors, but not D2, were an absolute requirement for LID manifestation. D2 on the other hand may play a more modulatory role.

Interestingly, studies show a role for the D2-like D3 receptor in the modulation of LID (Bezard *et al.*, 2003). Mainly expressed within the nucleus accumbens and other ventral striatum regions (Xu *et al.*, 1997), D3 receptors become overexpressed within the dorsal striatum after L-DOPA treatment in PD models (Guillin *et al.*, 2001). Studies have produced conflicting results when using D3 antagonists as anti-dyskinetic agents (Kumar *et al.*, 2009; Mela *et al.*, 2010; Visanji *et al.*, 2009). These varied results may be explained by the lack of selectivity the D3 antagonists may have for other receptors of the D2-like family. To investigate the role of D3 receptors in LID, recent studies utilised a knockout D3 receptor mouse and determined LID susceptibility. These transgenic mice presented lower dyskinesia scores whilst retaining the efficacy of L-DOPA as a DA replacement therapy (Solis *et al.*, 2015). D3 receptor antagonism may therefore be an interesting move in the treatment of LID.

Increasing evidence suggests 5-HT has a significant role in the maintenance of LID. The DA from L-DOPA metabolism is not only formed, stored and released within the dopaminergic neuronal terminals but also in the serotonergic neurones (Maeda *et al.*, 2005; Tanaka *et al.*, 1999). In response to L-DOPA treatment and the insufficient DA regulation caused by the extensive dopaminergic denervation, 5-HT fibres release DA as a *false NT* (Carta *et al.*, 2007). This is possible due to their similarity to dopaminergic terminals (i.e. VMAT2 and the DDC enzyme expression (Carta *et al.*, 2008)). In support of this, 5-$HT_{1A}$ and 5-$HT_{1B}$ agonists have been shown to ameliorate LID (Gil *et al.*, 2011), whereby, these agonists dampened the activity of the presynaptic 5-HT neurones that were releasing DA (Carlsson *et al.*, 2007).

Altered glutamatergic transmission within the corticostriatal pathway has long been associated with the manifestation of LID. Evidence suggests that this pathway is overactive within animal models of LID resulting from the enhanced expression and phosphorylation of glutamate receptors (Ba *et al.*, 2011; Chase *et al.*, 2000; Ouattara *et al.*, 2010). The NMDA receptor, more specifically the striatal concentrated NR2B-subunit containing NMDA receptor (Calon *et al.*, 2003), has been pharmacologically investigated in LID. Selective NR2B NMDA receptor antagonists, such as dextromethorphan, have shown to reduce dyskinetic effects in both Man and NHPs, whereby abnormal movements were reduced (Morissette *et al.*, 2006; Verhagen Metman *et al.*, 1998). Further evidence suggests that in rodent and NHPs LID models antagonists of the glutamatergic amino-3-hydroxy-5-methyl-4-isoxazole proprionic acid (AMPA) receptor also inhibit the progression of LID (Bibbiani *et al.*, 2005). Alongside the already prescribed anti-dyskinetic NMDA antagonist amantadine (detailed in Chapter 1), these data further emphasise the importance of the glutamatergic corticostriatal pathway in LID pathogenesis and also the complexity of the mechanisms underpinning LID.

This putative aberrant plasticity in the corticostriatal pathway (e.g. altered transmission, false transmitter release) has been researched extensively. However, CSPGs have not yet been investigated as potential mediators of this plasticity. We understand that throughout development and into adulthood, CSPGs shape axonal sprouting and growth through controlling cellular plasticity. It is because of this strong relationship with cellular plasticity that we were interested in identifying whether CSPGs played a role in LID.

### 5.1.2. CSPGs in L-DOPA-induced diskinesia

To date, there has been no direct link between the CSPGs of the ECM and LID. CSPG-related plasticity has been associated with the early development of the corticostriatal pathway and other striatal connections (Lee *et al.*, 2008). Therefore, CSPGs may play a role in striatal alterations found later in life or in disease states such as LID.

The CSPG neurocan was expressed within the rat neostriatum during early development. Within the first postnatal week dopaminergic terminals increase within the striatum, correlating to a rise in neurocan expression in the same striatal compartments (Charvet *et al.*, 1998). Similarly, PNN development occurs a week later (second postnatal week) within the striatum, whereby their presence is associated with the closing of the critical period and the dampening of neuroplasticity (Pizzorusso *et al.*, 2002). It is therefore clear that CSPGs and PNNs are involved in the development and wiring of dopaminergic systems, but their involvement in the aberrant plasticity of LID manifestation is yet to be revealed.

### 5.1.3. Preclinical models of L-DOPA-induced diskinesia

Two well established models of LID are the hemiparkinsonian 6-OHDA rodent and the MPTP NHP. After varying durations of daily L-DOPA and DDC inhibitor (e.g. benserazide) administration, hemiparkinsonian rodents develop AIMs. In rodents, these AIMs are described as aberrant axial (trunk twisting), limb (dystonic or ballistic movements) and orolingual (repetitive tongue protrusions, chewing) (ALO) movements; AIMs are the rodent equivalent of human dyskinesias. Although AIMs do not resemble true dyskinetic movements, they are countered by anti-dyskinetic agents. This presents good predictive validity of this LID model. As with the 6-OHDA lesion model, the key advantage of using a hemiparkinsonian model of LID is its ability to compare between the lesioned and intact hemispheres of the dyskinetic animals. However this leads to a major flaw when analysing the results (as seen within this chapter's study), as effects from L-DOPA treatment cannot be separated from the potential effects caused by dyskinesia. This is as AIMs will usually manifest in denervated animals following L-DOPA treatment. The inability to create non-dyskinetic L-DOPA-treated hemiparkinsonian animals is a weakness that is observed in the interpretation of all results received from LID

studies.

The NHP dyskinesia model more closely replicates human dyskinesia. The MPTP-driven dopaminergic denervation primes the brain for quick-onset dyskinesias following L-DOPA treatment. As with the hemiparkinsonian rodent, the same anti-dyskinetic agents (i.e. amantadine) also reduce the dyskinesia found in the NHP model. Unfortunately, the same problem exists regarding an effective control group, whereby MPTP lesioned NHPs will exhibit dyskinesia to a degree following L-DOPA treatment and so no non-dyskinetic control can be replicated.

In recent years there has been a current interest in developing a genetic model of LID which presents slow dopaminergic degeneration. Initial strategies of using known genetic models of PD to induce LID were unsuccessful due to the low denervation caused by the mutation (Francardo *et al.*, 2014). The most successful genetic model of LID has been the unconventional pentraxin 3 knockout, otherwise known as the aphakia mouse (Francardo *et al.*, 2014). Pentraxin 3 is a transcription factor required for dopaminergic cell differentiation. Aphakia mice have been shown to have an age-degenerative decline in dopaminergic cells alongside LID manifestation following L-DOPA treatment. Although possessing differing AIMs (known as *three paw dyskinesias*) to those of the 6-OHDA LID model, the aphakia mouse presents pharmacologically reversible involuntary movements together with increased levels of dyskinetic associated markers such as ΔFosB/FosB (Ding *et al.*, 2007; Ding *et al.*, 2011). Despite this promise, the aphakia mouse also suffers from the same inability to create non-dyskinetic controls.

As the hemiparkinsonian rodent is the most accessible, most economical and less ethically impacting model, it is frequently chosen for LID investigations. Unlike other models in this thesis, the rat model was used. This was because of the accessibility for neuroimaging (a key part of this chapter) and for the previously described reasons.

### 5.1.4. Structural and functional assessments of the striatum in a dyskinetic rat

In order to unravel the complexities underlying LID, methods of detecting alterations within key BG regions of patients have been explored extensively using neuroimaging techniques such as magnetic resonance imaging (MRI) and positron emission tomography (PET). To date, functional MRI (fMRI) investigations have highlighted brain network and metabolic activity changes relating to dyskinesia and its pathophysiology (Brooks *et al.*, 2000; Cerasa *et al.*, 2012). However, the link between these biological mechanisms and known correlates of brain functional activity such as the structure and volume of the basal ganglia and other areas of

grey matter (Fauvel *et al.*, 2014; Ilg *et al.*, 2008), have yet to be extensively investigated. Therefore, investigating potential neuroanatomical correlates with LID in the dyskinetic 6-OHDA rodent model would be of great scientific interest.

### 5.1.5. Study rationale

As there is a gap in our understanding of LID and any associated neuroanatomical changes, this chapter attempted to identify any alterations in the striatum of the dyskinetic rat. By combining the well-established rodent model of LID with structural neuroimaging, specifically structural MRI, it was thought possible to elucidate any potential underlying structural changes within the striatum associated with LID. As the corticostriatal pathway is considered one of the key signalling pathways involved in the pathophysiology of LID, the striatum was targeted for neuroimaging.

Investigations were then undertaken to identify whether CSPGs, known modulators of plasticity, were altered within the striatum of the dyskinetic rat. Alterations in CSPG expression were thought to underlie the changes found within the striatum that lead to LID. As aggrecan and versican had been successful in previous immunohistochemical studies (Chapter 2), these were chosen for this chapter.

Finally, changes in striatal volume were correlated to CSPG expression along with cellular markers (e.g. vasculature, microglia). Finding correlates of striatal shape and volumetric alterations may highlight new aspects not yet investigated in LID research. Each marker is described below.

#### *Aggrecan and versican*

As CSPGs are associated with the plasticity and rewiring of the striatum during development, aggrecan and versican were theorised to affect LID manifestation. Furthermore, it was believed that their decreased expression could give rise to an increased ECM volume and therefore may explain the expansion of the dorsal striatum.

#### *GFAP*

Astrocytes (GFAP) were stained for within the striatum due to the believed association of neuroinflammation existing within patients experiencing LID (Bartels *et al.*, 2007). Neuroinflammation and swelling may explain any increases in striatal volume detected by TBM MRI.

### *RECA1*

Endothelial cells (RECA1) were stained for within the striatum due to its believed association with dyskinesia, in which angiogenesis and BBB permeability are potential hallmarks of LID (Faucheux *et al.*, 1999; Ohlin *et al.*, 2011). Angiogenesis in particular may explain any increases in striatal volume.

## 5.2. Aims and Hypotheses

This study was a collaborative effort between the laboratories of Dr Susan Duty and Dr Anthony Vernon. The former was responsible for establishing the rodent model of LID, scoring AIM severity and conducting immunohistochemistry, whereas the latter was responsible for the neuroimaging. Reference to individuals responsible for any results included herein will be made. The aims and hypotheses for the study are described below.

Study aims:

1. *Using T2-weighted MRI, investigate any structural alterations that correlate with dyskinesia in a rodent model of LID*

2. *Analyse aggrecan and versican expression within the striatum of dyskinetic and non-dyskinetic animals to identify whether CSPGs underlie LID manifestation*

3. *If any MRI alterations have been detected, identify any changes in cellular (GFAP, RECA1 and Iba1) and extracellular markers (versican and aggrecan) that could account for these structural changes*

Study hypotheses:

1. *T2-weighted MRI will detect significant alterations in striatal volume and structure of dyskinetic animals*

2. *Aggrecan and versican expression will alter within the striatum of dyskinetic animals*

3. *Immunohistochemical techniques will detect changes in extracellular and cellular markers that will correlate with the structural changes seen in the MRI*

## 5.3. Materials and Methods

### 5.3.1. Animals

20 adult male Sprague-Dawley rats (270-300g, Harlan Laboratories, UK) maintained on a 12:12 hour light/dark cycle (07:00am lights on) with food and water *ad libitum*. Room temperature and humidity were kept at 22 ± 2°C and 55 ± 2% respectively. All AIMs testing, MRI and histological procedures were performed whilst blinded to the treatment groups.

### 5.3.2. Experimental design

The timeline for the study is described below in figure 51 and fuller destails given in subsequent materials and methods sections. A week prior to lesioning (d-7) a 7 day habituation period was implemented to ensure animals were non-responsive to non-biologically relevant stimuli. During this habituation period, baseline recordings for the cylinder test were conducted on day -1. On day 0, all animals received a full 6-OHDA lesion of the MFB. A recovery period of 13 days was then given post-lesion whereby daily rehydration and health checks were conducted until the animals had returned to pre-surgical weight. On day 14 following the recovery period, baseline cylinder tests were conducted. The *LID priming phase* was then conducted between days 21 and 42, whereby L-DOPA (n=9) or saline (n=10) was administered (whilst blind to the treatment group) alongside AIMs testing on alternate days. The AIMS reversal test was conducted on day 56. On day 63, animals were killed by anaesthetic overdose and brains were left in their heads ready for MRI scanning. A month later, the brains were removed from the heads and stored at 4°C for immunohistochemistry.

All procedures up to and including the removal of the heads (sections 5.3.3. to 5.3.10.) were conducted by Dr Clare Finlay, Duty laboratory.

| d-7 - d-1 | d0 | d1 - d13 | d14 | d21 - d42 | d56 | d63 |
|---|---|---|---|---|---|---|
| Habituation period | MFB Lesioning | Recovery period | Behaviour | L-DOPA treatment and AIMs testing | Amantadine | Necropsy |
| Cylinder baseline: d-1 | 30 min pre-treat: pargyline and desipramine 12.5 µg MFB 6-OHDA | Daily rehydration; health checks | Cylinder test; Apomorphine-induced rotations | L-DOPA (or saline) treatment and AIMs testing on alternate days | LID reversal test | Whole heads for MRI. Brains then removed for histology |
| 270-300 g rats; n = 19 | | | | | | |

**Figure 52: Experimental design for the dyskinesia study.**
All procedures of the study were conducted on certain days pre- and post-lesioning as described in the figure. Further details are found either below the timeline or in subsequent sections.

### 5.3.3. Pargyline and desipramine pretreatment

30 minutes before MFB lesioning, all 20 rats were pre-treated with 5 mg/kg pargyline (i.p.) to inhibit the MAO-B-mediated peripheral metabolism of 6-OHDA and also 25 mg/kg desipramine (i.p.) to block the noradrenaline transporter and increase selectivity of 6-OHDA for dopaminergic cells.

### 5.3.4. Surgery

Even though this study utilised rats instead of mice, surgical (apart from the lesioning protocol) and post-operative care techniques were identical to sections 3.3.1.3. and 3.3.1.5., respectively, of Chapter 3.

### 5.3.5. Full 6-OHDA lesioning of the rat median forebrain bundle

Unlike previous lesioning studies described, this study induced a full lesion by injecting 6-OHDA into the MFB.

Fine-bore holes (Ø 1 mm) were drilled at coordinates AP: -2.6 mm and ML: ±2.0 mm (relative to intraural line and skull surface). A blunt-ended 30 G needle was then inserted above the MFB to DV: -8.8 mm (relative to intraural line and skull surface) before all animals were infused with 12.5 µg 6-OHDA.HBr (Sigma-Aldrich) in 2.5 µl ice-cold 0.02% ascorbate/saline. The injection needle was left in place for 5 minutes after toxin administration to ensure the full diffusion of the compound.

### 5.3.6. Behavioural assessment of parkinsonian phenotype

To ensure that all the animals entering the LID priming phase had a complete lesion, the cylinder and apomorphine-induced rotation tests were conducted.

### 5.3.7. Cylinder test

The cylinder test, as described in section 3.3.4.6. of Chapter 3, was conducted to assess whether animals had attained the fully ablated SNc and parkinsonian phenotype required for LID induction post-lesioning. As rats were utilised within this chapter, the only difference in testing to other chapters was that the testing environment was a Perspex cylinder 21 cm in diameter and 34 cm in height. Cylinder tests were conducted during the habituation period on day -1 and also on day 14 post-lesion.

### 5.3.8. Apomorphine-induced rotations

On day 14, the apomorphine-induced rotation test was conducted to ensure a full lesion had developed. Following 30 min acclimatisation in rotometers, rats were injected with apomorphine (0.5 mg/kg, s.c.) and the total net contraversive rotations were then recorded over 90 minutes using Rotorat software (MedAssociates Inc.). Rats bearing a successful full lesion (19 of the 20; one failed to produce any rotations and so was removed from the study for not having a full lesion) were then randomly assigned to saline or L-DOPA treatment groups.

### 5.3.9. Induction, measurement and confirmation of L-DOPA-induced abnormal involuntary movements

Starting three weeks post lesioning (d21), successfully lesioned animals were injected daily for a further 21 days with either L-DOPA (6.25 mg/kg; s.c.) and benserazide (15 mg/kg; s.c.) (n=9) or saline (s.c.; n=10). The severity and durations of axial, forelimb and orolingual AIMs were assessed on days 21, 23, 25, 27, 29, 31, 33, 37 and 41 of post-lesion using the established scoring criteria (Cenci *et al.*, 1998; Winkler *et al.*, 2002).

Rats were placed in a 40 cm diameter clear acrylic cylinder for 30 minutes acclimatisation and scored for baseline AIMs. Following injection of L-DOPA or saline, rats were scored for a one minute period every 20 minutes for up to 180 minutes (or until baseline was finally reached). Each animal was scored for severity and duration of individual ALO AIMs.

On day 56 to confirm that dyskinesia was established, rats were treated with the known anti-dyskinetic compound, amantadine HCl (Sigma Aldrich; 40 mg/kg; s.c.), or saline 30 minutes prior to L-DOPA-treatment (or saline-treatment in control rats). This was conducted in a randomised, crossover design allowing a wash out between treatments. AIMs were scored as above by an experimenter blinded to the treatment received.

### 5.3.10. Animal necropsy

On day 63 rats were terminally anaesthetised with sodium pentobarbital (600 mg/kg; i.p.) and transcardially perfused with saline then 10% formalin. The heads were removed and, with the brain left *in situ,* were placed in 10% formalin for a further 24 hours. Residual 10% formalin was then removed by immersing the heads in PBS with 0.05% sodium azide at 4°C for four weeks to ready the brains for MRI. Regular changes of the wash solution were performed twice-weekly.

### 5.3.11. Neuroimaging

The following neuroimaging techniques and procedures were carried out by the Vernon laboratory based at the Institute of Psychiatry, Psychology and Neuroscience (King's College London) based at Denmark Hill, London. The methods are included here for completeness.

#### *5.3.11.1. Magnetic resonance imaging*

A 7T small-bore horizontal magnet MRI scanner (Agilent Technologies Inc. Santa Clara, USA) equipped with a custom-made quadrature volume radiofrequency coil (43 mm inner diameter, Magnetic Resonance Laboratory, Oxford) was used for all *ex vivo* MR acquisition. Anatomical MRI were acquired using a Fast Spin Echo sequence: repetition time/effective echo time = 4000/60 ms, averages=8, field of view = 30 x 30 mm, matrix size 128 x 128, 45 contiguous coronal slices, 0.6 mm thick, giving an in-plane resolution of 125 µm. Scans were acquired blinded to treatment status in a random order, interspersed with phantoms to ensure consistent operation of the magnet. Post-acquisition, anatomical MR images were converted offline to NIFTI file format and visually inspected for motion or intensity artifacts prior to analysis. No scans were excluded on this basis.

The volume of the corpus striatum in each hemisphere was calculated by multiplying the sum of the striatum surface area on all slices measured by the slice thickness (0.5 mm). Intra-rater and inter-rater reliability were assessed following repeated measurements using the intraclass correlation coefficient as previously described with values <0.9 rejected (Wolf *et al.*, 2002). An index of striatal asymmetry was also computed by calculating the ratio of the volume of the striatum in the left (ipsilateral) and right (contralateral) hemispheres for each animal in each treatment group.

#### *5.3.11.2. Tensor based morphometry MRI*

A mean image of the entire dataset (n=19 scans) was generated using rigid-body registration (6 degrees of freedom) using a population-based registration method based on FSL-FLIRT (Crum *et al.*, 2013; Jenkinson *et al.*, 2002; Jenkinson *et al.*, 2001). Using this mean image, the external and internal borders of the left and right corpus striatum from approximately X to Y mm from bregma based on the rat stereotaxic atlas (Watson 2007 atlas) were manually defined using the polygon tool in ITK-SNAP (http://www.itksnap.org) (Yushkevich *et al.*, 2006) by two expert raters (Miss Ana Lopez and Dr Anthony Vernon, IoPPN, KCL) using previously published criteria (Vernon *et al.*, 2011; Wolf *et al.*, 2002). Segmentation performance was assessed using intra-class correlation co-efficient with values <0.95 rejected. This segmentation was used to create a binary mask for implementation in our tensor based morphometry (TBM) pipeline to assess

anatomical differences related to L-DOPA treatment in the striatum. Maps of localized volume difference at each voxel relative to the reference brain for the striatum were computed from the log of the Jacobian determinant of this non-rigid transformation for each scan. In addition, we then performed an exploratory brain-wide TBM analysis to identify potential anatomical changes beyond our a priori driven interest in the striatum. Data are shown at both an exploratory uncorrected threshold ($p<0.01$ uncorrected) and corrected for multiple comparisons using the false discovery rate ($q=0.1$; 10%) (Genovese *et al.*, 2002).

### 5.3.12. Tissue preparation and immunohistochemistry for aggrecan, versican, GFAP, Iba1 and RECA1

The following procedures were all performed by me as part of this thesis work. One month following MRI analysis, brains were removed from the skulls and submerged in 30% sucrose/PBS with 0.05% sodium azide for three days then post-fixed in 10% formalin for a further 24 hours. Brains were then embedded in 10% porcine gelatin and again post-fixed in 10% formalin for 24 hours before a final immersion in 30% sucrose/PBS with 0.05% sodium azide. 40µm thick coronal sections were cut through the striatum (AP: +1.70 mm to -2.50 mm relative to bregma; Paxinos and Watson 2007) using a freezing sledge microtome and stored as free-floating sections in PBS with 0.05% sodium azide.

Sections were incubated for 10 minutes with 3% $H_2O_2$ and 10% methanol in $dH_2O$, washed thrice in TBS (pH 7.4) and then incubated for 60 minutes in 0.2% triton-X100 in TBS (TXTBS) containing 3% normal goat serum (NGS) or, in the case of anti-Iba1, 1% BSA. Next, sections were incubated overnight at room temperature in rabbit polyclonal anti-TH (1:2500; Millipore AB152), rabbit polyclonal anti-GFAP (1:10000; Abcam ab7260), goat polyclonal anti-Iba1 (1:2000; Abcam ab5076) or mouse polyclonal anti-RECA1 (1:2000; Abcam ab9774). Sections were then washed in TBS before a one hour incubation in 1% BSA or 3% NGS containing the appropriate biotinylated secondary antibody - goat anti-rabbit (1:1000; Vector BA-1000), horse anti-goat (1:1000; Vector BA-9500) or horse anti-mouse (1:1000; Vector BA-2001). Next, sections were incubated in streptavidin horseradish peroxidise binding complex (Vector Labs; SA-5004) for 30 minutes before a final TBS wash and immersion in developing solution (0.05% DAB in TBS with 0.01% $H_2O_2$) for 10 minutes. Sections were mounted onto Superfrost plus® slides (VWR International) and left to dry overnight and dehydrated in industrialised methylated spirit before being coverslipped with DPX mountant.

### 5.3.13. Image analysis

Densitometry images for the aggrecan and versican markers were acquired with a Canon DSLR camera with a macro lens. High magnification images used for Iba1-positive, GFAP-positive and

RECA1-positive analysis were obtained using a Zeiss Axioskop brightfield microscope and a 20X objective (Zeiss). A 63X oil immersion objective (Zeiss) was also adopted for further detailed images of Iba1-positive microglia. Axiovision 4.6 software (Zeiss) was used to capture the images.

Digital TIFF format images from all treatment groups were equilibrated in Adobe Photoshop CS5 in order to create the background uniform in terms of brightness and contrast. ImageJ was used to measure the optical densities of each striatum. To correct for background staining the density of the medial corpus callosum, a region not known to be associated with dyskinesia, was subtracted from the striatal density measurements.

Aggrecan, versican, RECA1, GFAP and Iba1 background corrected density measurements were obtained from both the dorsal and ventral striatum of the lesioned and intact hemispheres. An average of nine sections across the rostrocaudal axis was obtained per animal. For Iba1 cell number, counts were obtained from dorsal striatum alone, in the lesioned and intact hemispheres. For all markers, three sections (section 3: AP: +0.26 mm, section 5: AP: -0.7 mm and section 7 AP: -1.66 mm; relative to bregma) of each nine-section rostrocaudal series were taken.

For measures of Iba1 density per soma, density was obtained from microglia resident to the dorsal striatum in lesioned and intact hemispheres. An average of 3 sections per rat (sections 3, 5 and 7 as above) were taken. To calculate the grey mean density of just the soma, the freehand selection tool was used to mask density calculations to just the cell bodies.

All densitometry and microglial cell count figures present data averaged across the three sections of the rostrocaudal axis. This was to obtain an average of the entirety of the striatum.

### 5.3.14. Statistical analyses

All statistical analyses within this chapter were conducted with the SigmaPlot 12 package; statistical tests used are displayed within the figure legends. Graphpad Prism 5 was used to plot all graphs.

## 5.4. Results

### 5.4.1. Medial forebrain lesioning induced a full ablation of the SNc in all animals as determined by behavioural testing

In order for effective LID development, behavioural tests were conducted to ensure that a parkinsonian phenotype was present in all animals. As animals were to be kept alive on this experimental day (d14), SNc cell counts were not possible and so the use of the cylinder and apomorphine-induce rotation test was required.

A day before lesioning (d-1), all animals conducted the cylinder test to establish baseline readings. A typical asymmetry score of ~50% (indicative of no paw preference) was detected for the to-be 6-OHDA lesioned animals (48.9 ± 0.99%; baseline value). This highlighted that the animal cohort was not naturally biased to preferring one paw. Post-lesion (d14) (figure 52A), unilaterally lesioned animals produced asymmetry scores of 6.0 ± 1.5% ($p<0.001$ versus baseline; Student's *t*-test) indicating that the animal cohort had been significantly unilaterally lesioned since contralateral paw use had markedly fell.

To confirm that the unilateral lesion expressed was not partial but full (as required for sufficient LID development), animals conducted the apomorphine-induced rotation test. A test, as previously described to induce rotations only in fully unilaterally lesioned animals.

On day 14 post-lesion, the apomorphine-induced rotation test was conducted (figure 52B). Animals assigned to the saline- or L-DOPA-treatment groups were separated *post hoc* to assess whether each group had equally lesioned animals. When dosed with apomorphine, to-be saline-treated animals produced high counts of contraversive rotations (386 ± 44). These counts were similar to those of the to-be L-DOPA-treated animals, which displayed 377 ± 50 rotations; no significance was found between the groups (Student *t*-test). Due to the large number of contraversive rotations, both groups were considered to have fully lesioned NS. One animal was removed from the study as it produced no net contraversive rotations, it was therefore considered unlesioned. The rat's data was not included in figure 52B.

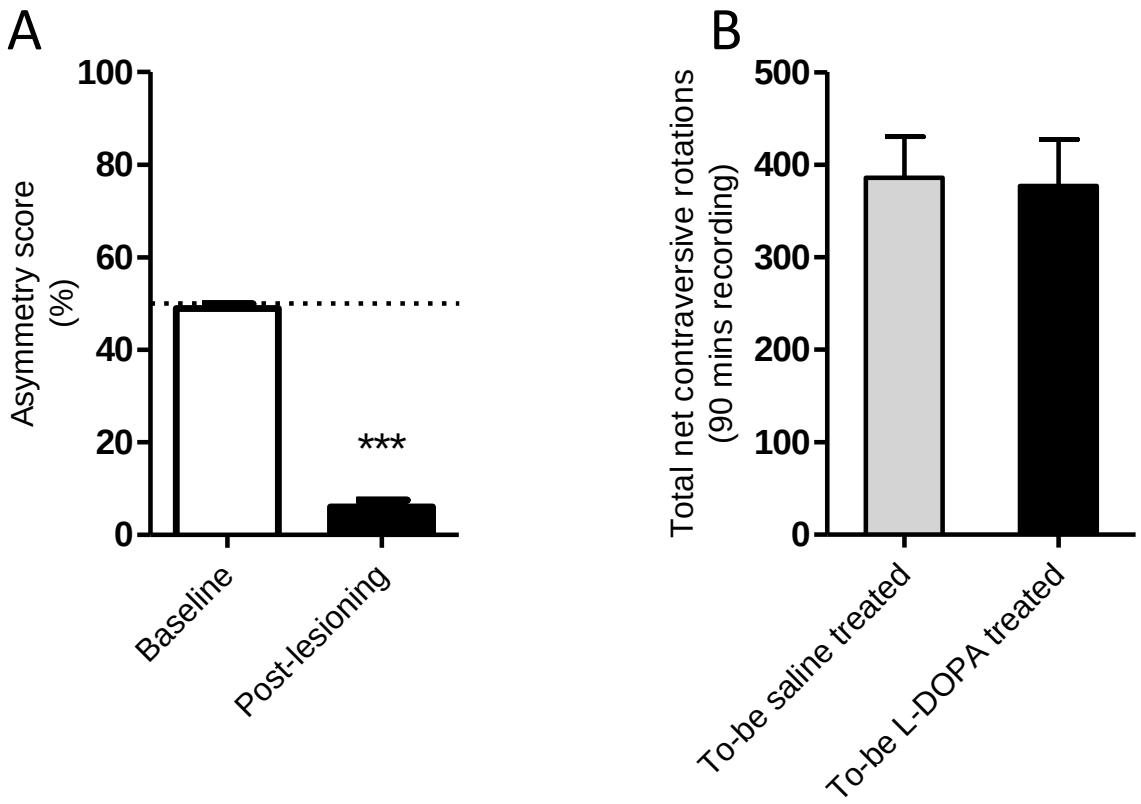


**Figure 53: Cylinder test and apomorphine-induced rotation assessment of parkinsonian phenotype on day 14 post-lesion.**

(A) At baseline, to-be lesioned rats presented no bias in asymmetry score. These same animals post-lesion, presented a significant decrease in asymmetry score indicating a loss in contralateral paw use. (B) Lesioned animals administered with apomorphine produced high counts of contraversive rotations, representative of a fully ablated SNc. Both the to-be saline treated and to-be L-DOPA treated rats displayed a similar level of net contraversive rotations. Panel A: Student's *t*-test; *** denotes $p<0.001$. 6-OHDA-lesioned n=20. Panel B: to-be saline treated: n=10; to-be L-DOPA treated: n=9. Data are mean ± SEM. Graphs were produced by myself from data obtained by Dr Clare Finlay.

### 5.4.2. Administration of L-DOPA induced significant, pharmacologically reversible dyskinesias in fully lesioned rats

To analyse the striatum for markers of dyskinesia, a sufficient degree of LID was first needed. Animals were therefore tested for their scale of dyskinesia severity in the 180 mins following administration of L-DOPA or saline (depending on their experimental group).

Using the aforementioned rodent ALO AIMs scale (Cenci *et al.*, 1998; Winkler *et al.*, 2002), scores for each treatment day during the three week dyskinesia *priming period* (days 21 - 42 post-lesion) were obtained for every animal (figure 53A). The L-DOPA-treated animals presented an instant increase in AIMs score that then balanced out after 11 days of treatment (day 31 post-lesion; 182 ± 13). The scores of the L-DOPA-treated animals were significantly higher ($p<0.001$; Two-Way repeat measures ANOVA with Bonferroni post hoc) at every time point when compared to the saline-treated controls. Saline-treated animals presented no AIMs score (0) on any day of treatment. When all of these data were averaged within their respective groups (figure 53B), L-DOPA-treated animals displayed significantly higher AIMs scores (160 ± 17.44; $p<0.001$; Student's *t*-test) to those of the saline group, which did not produce any AIMs whatsoever (0).

Of the 9 L-DOPA treated animals 2 were considered moderately dyskinetic (boxed points) whereas the remaining 7 were classed as severely dyskinetic. However, all animals were included in the analysis, as all were considered dyskinetic.

To confirm that the AIMs measured in figures 53A + B were representative of LID, an AIMs reversal test was conducted using the known anti-dyskinetic agent amantadine (figure 53C). The saline-treated animals did not express any reduction in AIMs with either saline- or amantadine-treatment as no AIMs had been previously established. This confirmed that amantadine did not induce any AIMs following a single dose. L-DOPA-treated animals presented a significant decline in AIMs score when administered with amantadine rather than saline (saline: 167 ± 17, L-DOPA: 113 ± 19; $p=0.04$; Two-Way ANOVA with Bonferroni post hoc). This indicated that the AIMs induced by L-DOPA represented a rodent correlate of dyskinesia as seen in NHPs.

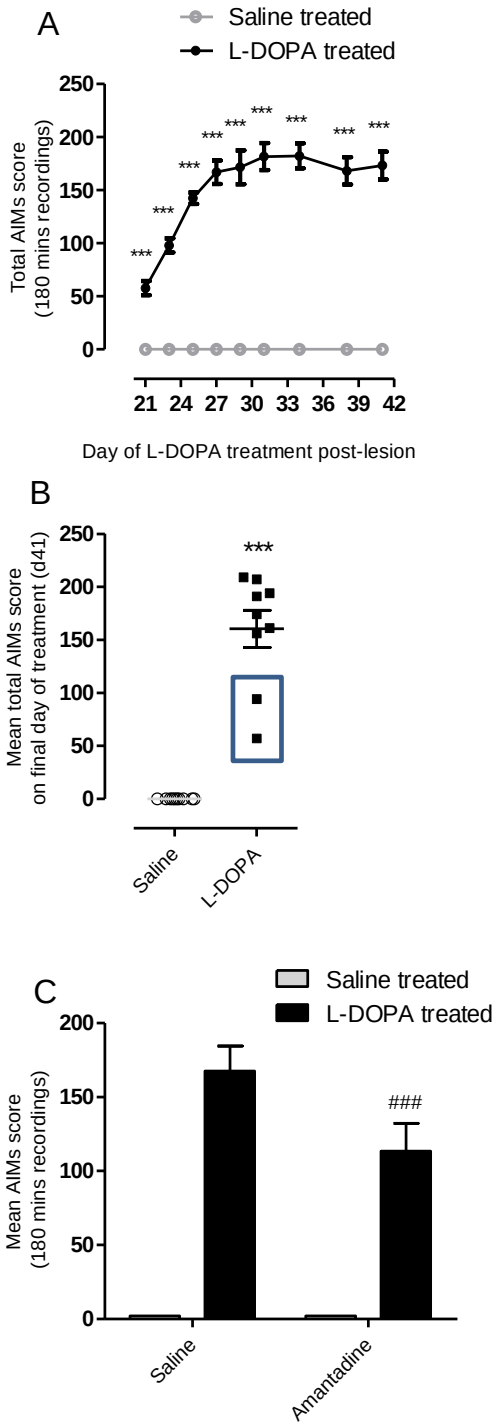


**Figure 54: Assessment of L-DOPA administration in rats presenting a full 6-OHDA lesion.**
(A) L-DOPA-treated animals displayed significantly higher AIMs scores on every day of treatment when compared to the saline-treated control group. (B) Every L-DOPA-treated animal displayed significantly higher AIMs scores on the final day of treatment (d41) when compared to the animals of the saline-treated control group. Blue rectangle: rats with moderate LID scores, still dyskinetic however. (C) Only the L-DOPA-treated animals presented a significant decrease in AIMs score when administered amantadine. Saline controls did not respond to amantadine. Panel A: Two-Way repeat measures ANOVA with Bonferroni post hoc, *** denotes $p<0.001$: between saline- and L-DOPA-treated animals on that day. Panel B: Student's *t*-test; *** denotes $p<0.001$. Panel C: Two-Way ANOVA with Bonferroni post hoc, ### denotes $p<0.001$: between AIMs scored following saline- and amantadine-treatment. Saline: n=10, L-DOPA n=9. Data are mean ± SEM. Graphs were produced by me from data obtained by Dr Clare Finlay.

### 5.4.3. Tensor-based morphometry MRI detected an increase in volume of the dorsal injured striatum in dyskinetic animals

To assess whether striatal volume changes had occurred within the dyskinetic striatum, structural tensor-based morphometry (TBM) MRI was conducted. A mean template image was created from the entire animal cohort (n=19), against which the L-DOPA-treated dyskinetic animals were compared. A heat map of voxel expansion or retraction of the L-DOPA-treated rat compared to the cohort template is shown in figure 54; this highlighted regions of increased or decreased volume. Figure 54 depicts 7 representative images of the striatum along the rostrocaudal axis of a L-DOPA-treated animal; the left hand hemisphere is the 6-OHDA-lesioned striatum whereas the right is the intact control hemisphere. The L-DOPA-treated animals present an increased volume of the dorsal striatum only in the lesioned hemisphere when compared to the template.

All data handling and analysis was performed by members of the Vernon laboratory based at the Institute of Psychiatry, Psychology and Neuroscience (King's College London) based at Denmark Hill, London.

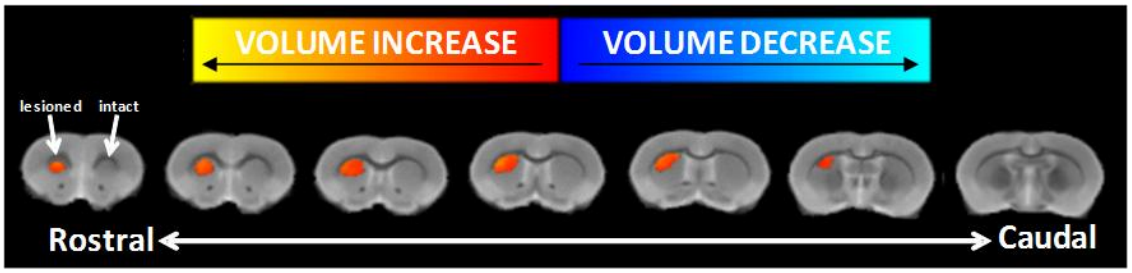


**Figure 55: Tensor-based morphometry MRI highlighted an increase in striatal volume in the L-DOPA-treated parkinsonian striatum when compared to the parkinsonian hemisphere of the saline controls.**
Orange region depicts a region of voxel expansion and thus increased volume. The parkinsonian 6-OHDA-lesioned striatum for both the L-DOPA and saline group was the left hand side.

### 5.4.4. Aggrecan optical densities were not altered in either the intact or lesioned striatum of dyskinetic rats

Using antibodies against aggrecan and versican, which have shown to stain well within the rodent striatum in Chapter 2, we assessed the CSPGs' optical densities for any alterations in the dorsal injured striatum of the dyskinetic striatum. These alterations may correlate with the volume increase detected in the MRI.

The optical densities of aggrecan were uniform across the striata of the dyskinetic and non-dyskinetic animals as previously seen in Chapter 2 (figure 55A). Aggrecan optical densities of the dorsal intact and dorsal lesioned striata of the non-dyskinetic (saline-treated) (Intact: 0.086 ± 0.004, Lesion: 0.077 ± 0.004) and of the dyskinetic (L-DOPA-treated) animals (Intact: 0.076 ± 0.004, Lesion: 0.077 ± 0.004) were not statistically significant (figure 55B). This lack of significance was also detected in the ventral intact and ventral lesioned striata optical densities (figure 55C) of the non-dyskinetic (saline-treated) (Intact: 0.114 ± 0.004, Lesion: 0.103 ± 0.004) and of the dyskinetic (L-DOPA-treated) animals (Intact: 0.104 ± 0.004, Lesion: 0.103 ± 0.004). All data presented above underwent Two-Way ANOVA with Bonferroni post hoc tests.

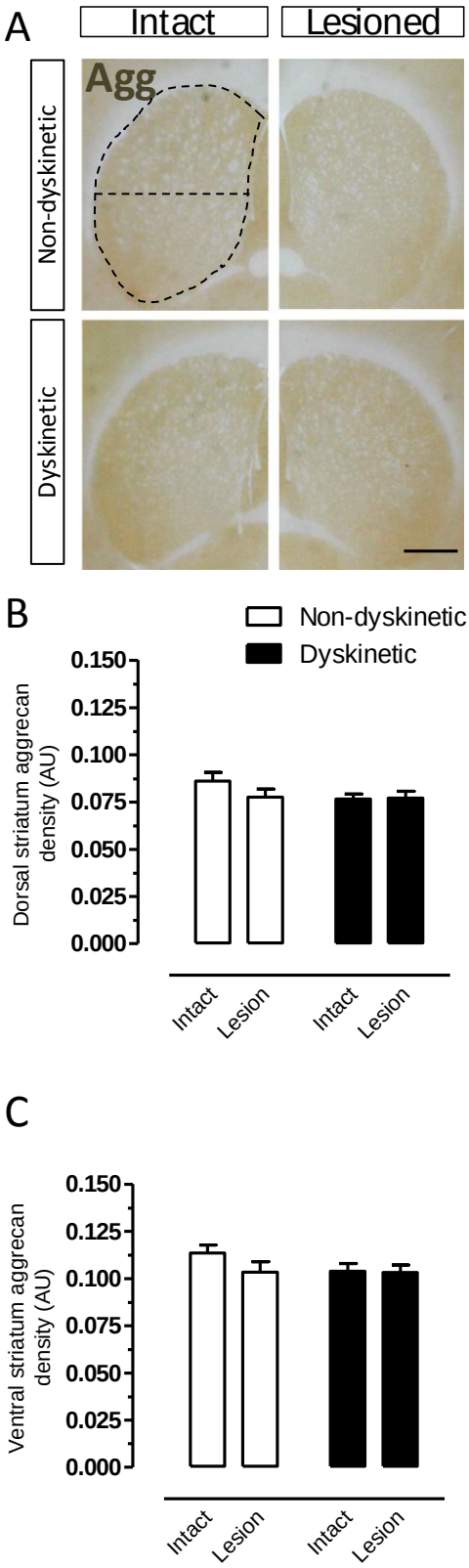


**Figure 56: Aggrecan marker optical densities measured within the dorsal and ventral striatum of non-dyskinetic saline-treated and dyskinetic L-DOPA-treated rats.**
(A) Photomicrographs (5X magnification) of aggrecan optical density within the medial-level intact and lesioned hemispheres of non-dyskinetic and dyskinetic rat striatum. Dashed lines divide the striatum into the dorsal and ventral regions taken for optical densities (B + C) No changes in aggrecan optical densities were detected within the dorsal or ventral striatum in either hemisphere or between experimental groups. Saline: n=10, L-DOPA n=9. Data are mean ± SEM. Data are averaged across all three levels of the rostrocaudal axis. Scale bar: 500 µm.

### 5.4.5. Versican optical densities were not increased in either the intact or lesioned striatum of dyskinetic rats

The optical densities of versican were uniform across the striata of the dyskinetic and non-dyskinetic animals as previously seen in Chapter 2 (figure 56A). Versican optical densities of the dorsal intact and dorsal lesioned striata of the non-dyskinetic (saline-treated) (Intact: 0.211 ± 0.006, Lesion: 0.197 ± 0.006) and of the dyskinetic (L-DOPA-treated) animals (Intact: 0.21 ± 0.004, Lesion: 0.208 ± 0.004) were not statistically significant (figure 56B). This lack of significance was also the case for the ventral intact and lesioned striata optical densities (figure 56C); non-dyskinetic (saline-treated) (Intact: 0.218 ± 0.006, Lesion: 0.206 ± 0.006) and of the dyskinetic (L-DOPA-treated) animals (Intact: 0.211 ± 0.004, Lesion: 0.214 ± 0.004). All data presented above underwent Two-Way ANOVA with Bonferroni post hoc tests.

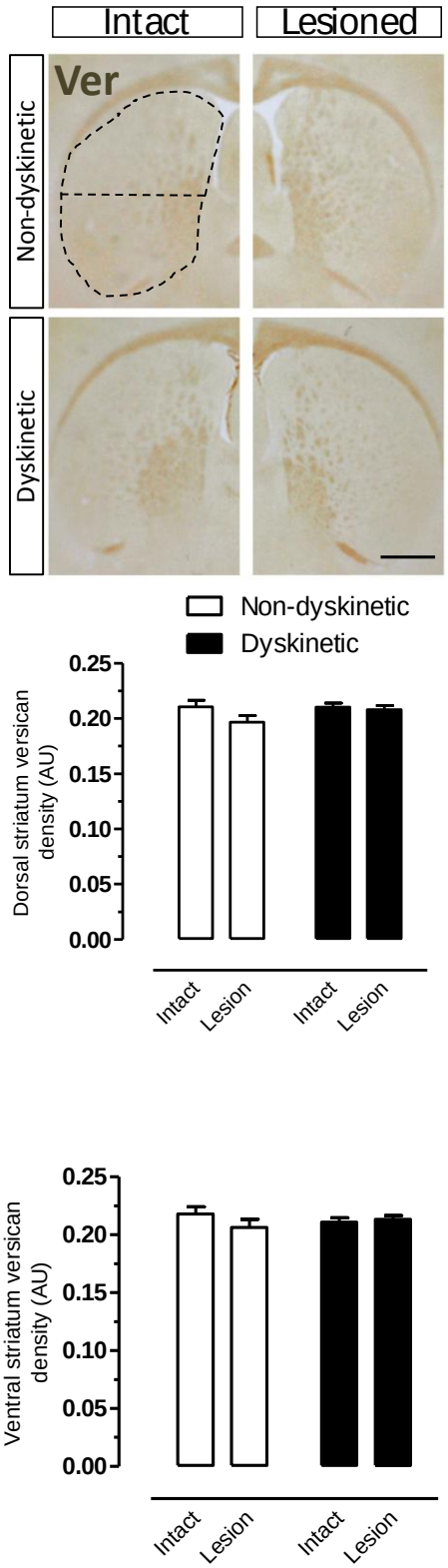


**Figure 57: Versican marker optical densities measured within the dorsal and ventral striatum of non-dyskinetic saline-treated and dyskinetic L-DOPA-treated rats.**

(A) Photomicrographs (5X magnification) of versican optical density within the medial-level intact and lesioned hemispheres of non-dyskinetic and dyskinetic rat striatum. Dashed lines divide the striatum into the dorsal and ventral regions taken for optical densities (B + C) No changes in versican optical densities were detected within the dorsal or ventral striatum between hemispheres or between experimental groups. Saline: n=10, L-DOPA n=9. Data are mean ± SEM. Data are averaged across all three levels of the rostrocaudal axis. Scale bar: 500 µm.

### 5.4.6. GFAP optical densities increased in the dorsal and ventral lesioned striata of both non-dyskinetic and dyskinetic rats

Representative photomicrographs of the GFAP-positive astrocytes within the dorsal striatum are displayed in figure 57A (magnification 20X; dorsal striatum). There was a significant difference between the optical densities of the dorsal intact and dorsal lesioned striata of the non-dyskinetic (saline-treated) animals (Intact: 0.249 ± 0.004, Lesion: 0.297 ± 0.007; $p<0.001$; Two-Way ANOVA with Bonferroni post hoc; figure 57B) and also the dorsal intact and dorsal lesioned striata of the dyskinetic (L-DOPA-treated) animals (Intact: 0.247 ± 0.005, Lesion: 0.302 ± 0.007; $p<0.001$; Two-Way ANOVA with Bonferroni post hoc).

As with the dorsal striatum, the ventral intact and ventral lesioned hemispheres of the non-dyskinetic (Intact: 0.225 ± 0.004, Lesion: 0.252 ± 0.004; $p<0.001$; Two-Way ANOVA with Bonferroni post hoc test) and of the dyskinetic animals (Intact: 0.226 ± 0.005, Lesion: 0.259 ± 0.005; $p<0.001$; Two-Way ANOVA with Bonferroni post hoc test; figure 57C) were significantly different.

Importantly, there was no difference in GFAP expression between dyskinetic and non-dyskinetic animals in any region of the striatum.

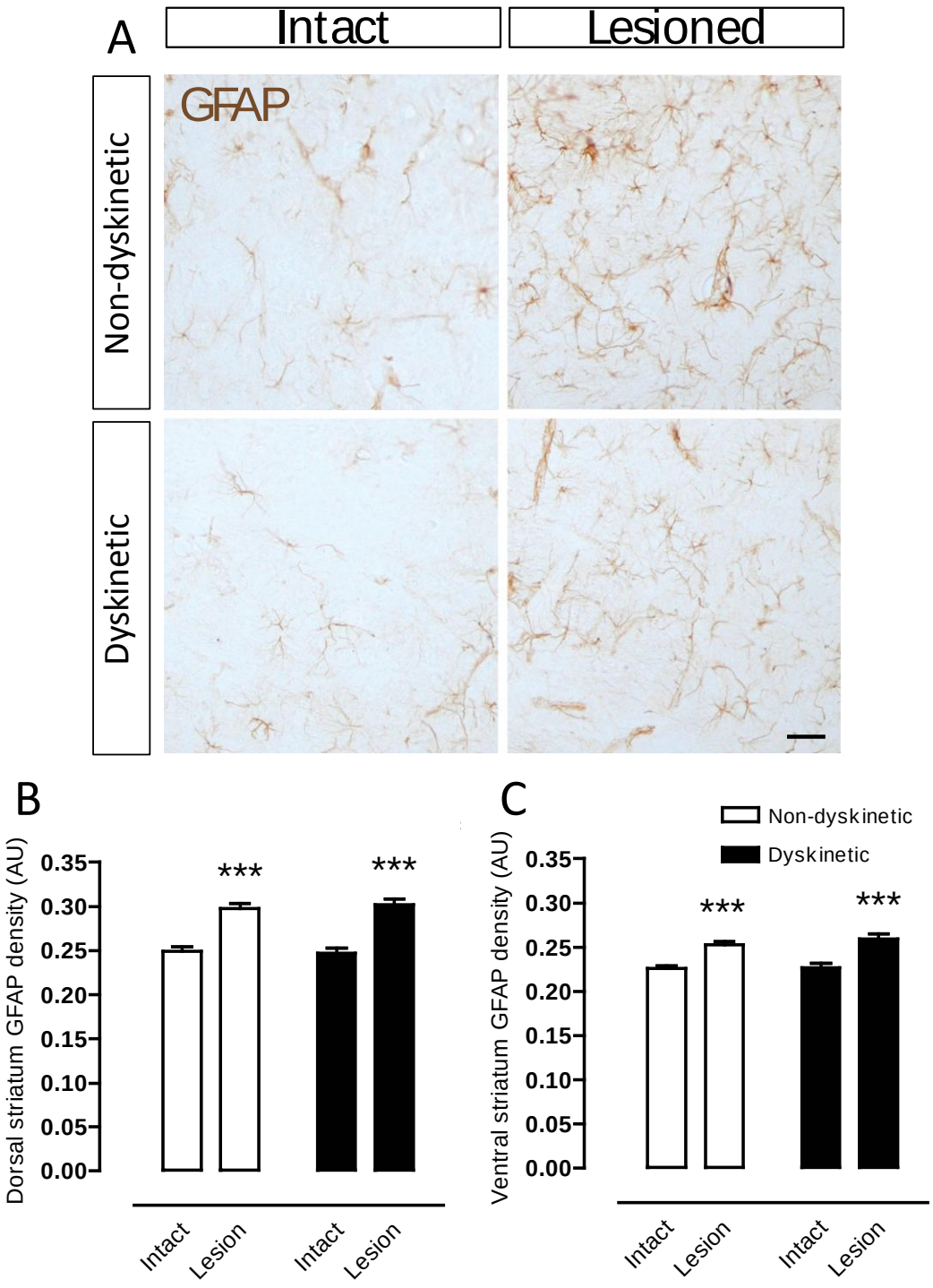


**Figure 58: Astrocytic marker optical densities measured within the dorsal and ventral striatum of non-dyskinetic saline-treated and dyskinetic L-DOPA-treated rats.**

(A) High magnification (20X) photomicrographs of GFAP optical density within the medial-level dorsal intact and lesioned hemispheres of non-dyskinetic and dyskinetic rat striatum. (B + C) A significant increase in GFAP optical density was detected between the intact and lesioned striata in both the dorsal and ventral regions of both the non-dyskinetic and dyskinetic groups. Panels B + C: Two-way ANOVA with Bonferroni post hoc; *** denotes $p<0.001$. Data are mean ± SEM. Data are averaged across all three levels of the rostrocaudal axis. Saline: n=10, L-DOPA n=9. GFAP, glial fibrillary acidic protein. Scale bar: 100 µm.

### 5.4.7. RECA1 optical density did not increase in the lesioned hemisphere of the dorsal and ventral striatum in either treatment group

Representative photomicrographs of the RECA1-positive endothelial cells within the dorsal striatum are displayed in figure 58A (magnification 20X; dorsal striatum). RECA1 optical densities of the dorsal intact and dorsal lesioned striata of the non-dyskinetic (saline-treated) (Intact: 0.039 ± 0.003, Lesion: 0.048 ± 0.003) and of the dyskinetic (L-DOPA-treated) animals (Intact: 0.043 ± 0.002, Lesion: 0.043 ± 0.004) were not significantly different (figure 58B). This lack of significance was also the case for the ventral intact and lesioned striata optical densities (figure 58C); non-dyskinetic (saline-treated) (Intact: 0.048 ± 0.005, Lesion: 0.063 ± 0.006) and of the dyskinetic (L-DOPA-treated) animals (Intact: 0.058 ± 0.003, Lesion: 0.06 ± 0.006). All data presented above underwent Two-Way ANOVA with Bonferroni post hoc tests.

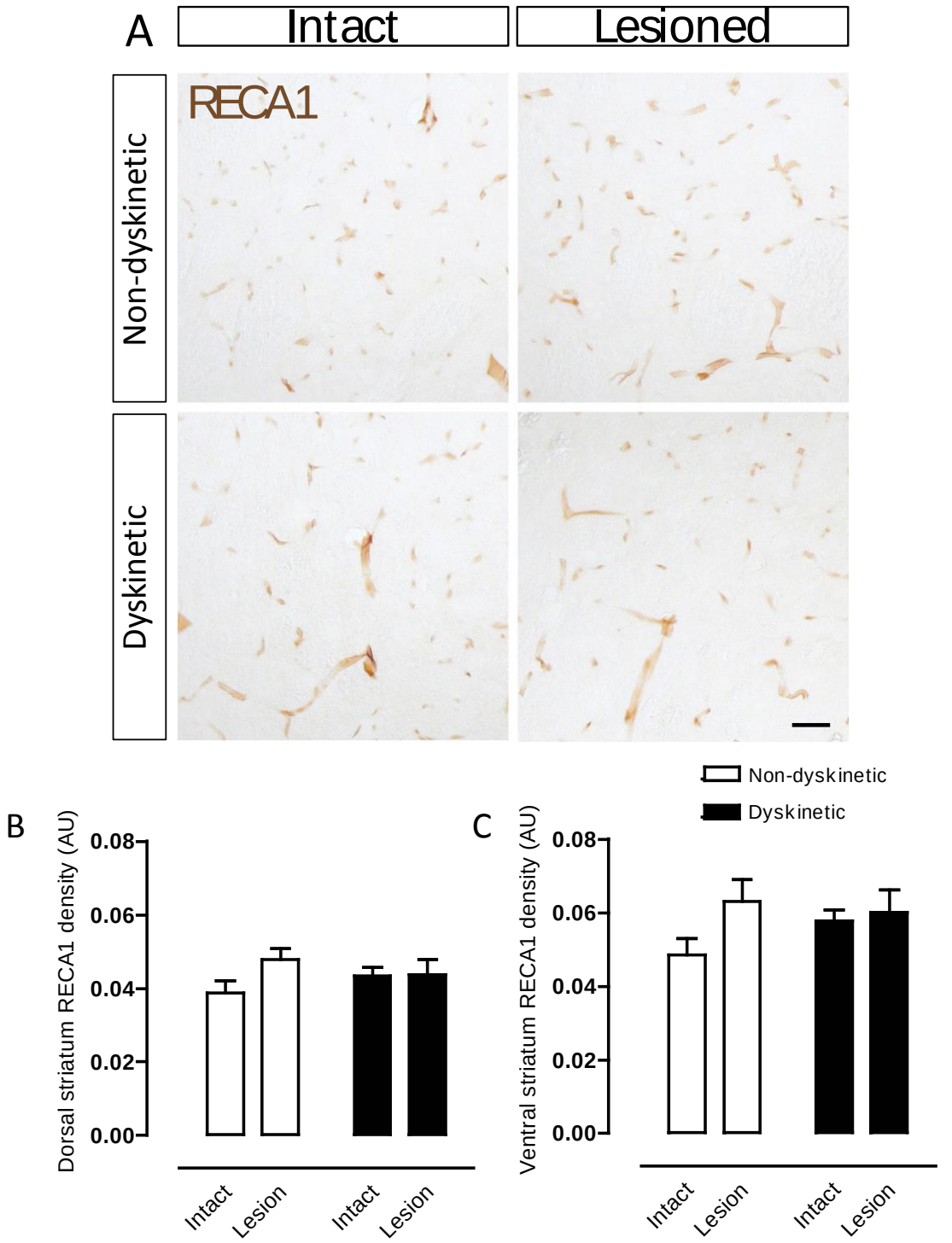


**Figure 59: Endothelial cell marker optical densities measured within the dorsal and ventral striatum of non-dyskinetic saline-treated and dyskinetic L-DOPA-treated rats.**
(A) High magnification (20X) photomicrographs of RECA1 optical density within the medial-level dorsal intact and dorsal lesioned hemispheres of non-dyskinetic and dyskinetic rat striatum. (B + C) No changes in versican optical densities were detected within the dorsal or ventral striatum in either hemisphere or between experimental groups. Saline: n=10, L-DOPA n=9. Data are mean ± SEM. Data are averaged across all three levels of the rostrocaudal axis. Scale bar: 100 µm.

### 5.4.8. Striatal Iba1-positive optical densities are significantly increased within the lesioned hemisphere of L-DOPA treated animals

Representative photomicrographs of the Iba1-positive mciroglia within the dorsal striatum are displayed in figure 59A (magnification 20X; dorsal striatum). There was a significant difference between the optical densities of the dorsal intact and dorsal lesioned striata of the non-dyskinetic (saline-treated) animals (Intact: 0.016 ± 0.003, Lesion: 0.034 ± 0.003; $p<0.001$; Two-Way ANOVA with Bonferroni post hoc; figure 59B). Significance was also detected between the optical densities of the dorsal intact and dorsal lesioned striata of the dyskinetic (L-DOPA-treated) animals (Intact: 0.024 ± 0.008, Lesion: 0.051 ± 0.004; $p<0.001$; Two-Way ANOVA with Bonferroni post).

Most importantly, a further increase in Iba1 optical density was detected between the two lesioned dorsal hemispheres of the non-dyskinetic and dyskinetic animals ($p=0.014$; Two-Way ANOVA with Bonferroni post hoc tests). This indicated a L-DOPA treatment effect.

The ventral striatum also presented significance but only between the intact and lesioned hemispheres of the non-dyskinetic (Intact: 0.026 ± 0.003, Lesion: 0.044 ± 0.004; $p<0.001$; Two-Way ANOVA with Bonferroni post hoc) and dyskinetic animals (Intact: 0.024 ± 0.003, Lesion: 0.057 ± 0.004; $p<0.001$; Two-Way ANOVA with Bonferroni post hoc; figure 59C). No significance was found between the lesioned hemispheres of the non-dyskinetic and dyskinetic animals.

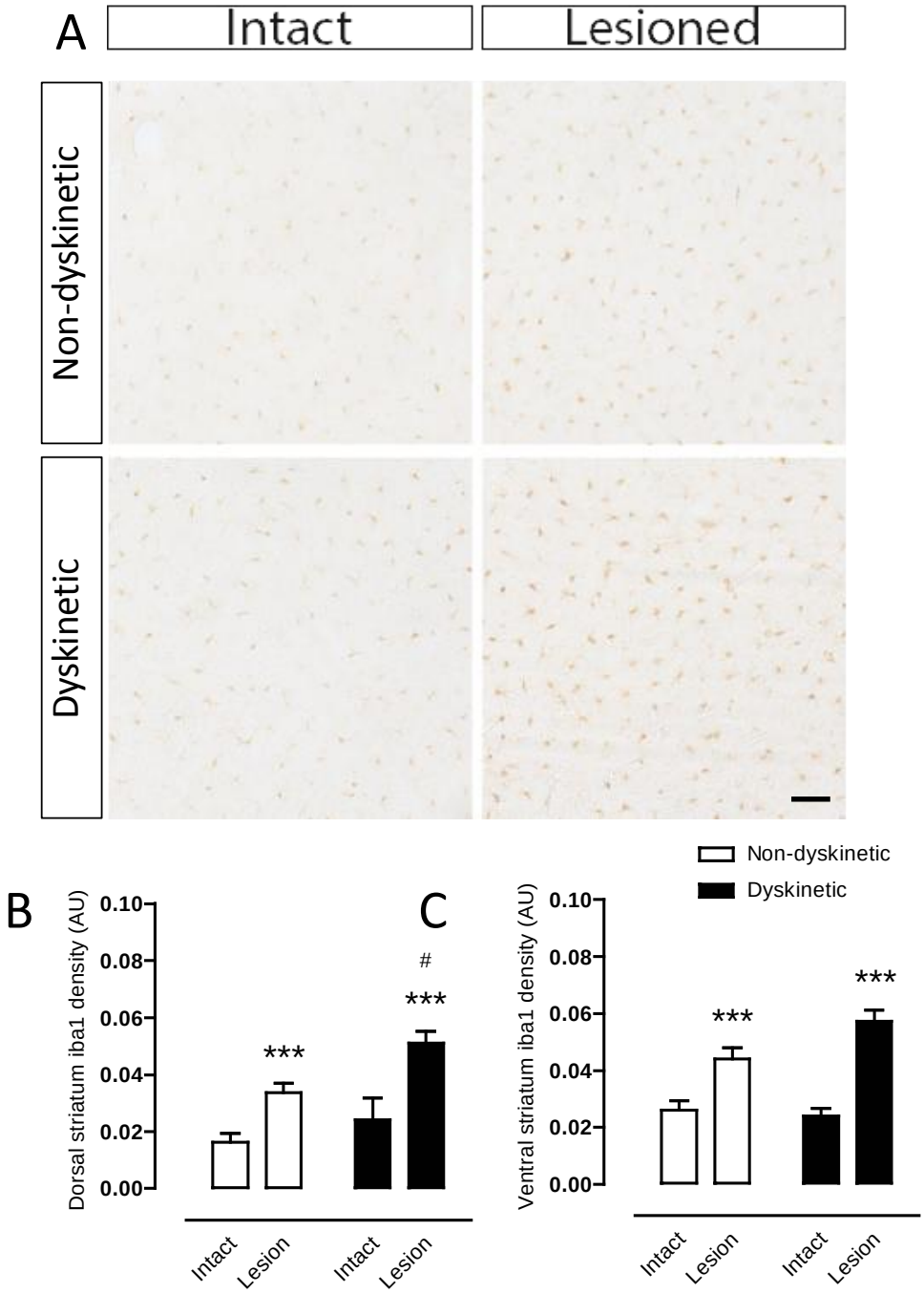


**Figure 60: Microglial marker optical densities measured within the dorsal and ventral striatum of non-dyskinetic saline-treated and dyskinetic L-DOPA-treated rats.**
(A) High magnification (20X) photomicrographs of Iba1 optical density within the medial-level dorsal intact and lesioned hemispheres of non-dyskinetic and dyskinetic rat striatum. (B) A significant increase in Iba1 optical density was detected between the intact and lesioned striata in both the dorsal and ventral regions of both the non-dyskinetic and dyskinetic groups. A further increase in Iba1 optical density was detected within the lesioned hemisphere of the dyskinetic animals compared to non-dyskinetic. (C) A significant increase in Iba1 optical density was detected between the intact and lesioned striata in both the dorsal and ventral regions of both the non-dyskinetic and dyskinetic groups. Panels B + C: Two-way ANOVA with Bonferroni post hoc; ***p<0.001: between intra-group hemispheres, $^{\#}$P<0.05: specific hemisphere between treatment groups. Data are mean ± SEM. Data are averaged across all three levels of the rostrocaudal axis. Saline: n=10, L-DOPA n=9. Iba1, ionized calcium-binding adapter molecule 1. Scale bar: 100 µm.

### 5.4.9. L-DOPA treatment does not affect the total microglial cell number within the lesioned striatum

To investigate the increased optical density of Iba1 within the dorsal lesioned dyskinetic striatum, counted the number of Iba1-positive microglia within the dorsal striatum.

Using the photomicrographs presented in figure 59A, the mean number of Iba1-positive microglia within the optical view was obtained. There was a significant difference between the number of Iba1-positive microglia in the dorsal intact and dorsal lesioned striata of the non-dyskinetic (saline-treated) animals (Intact: 82 ± 3 cells, Lesion: 104 ± 3 cells; P<0.001; Two-Way ANOVA with Bonferroni post hoc tests; figure 60A) and the dorsal intact and dorsal lesioned striata of the dyskinetic (L-DOPA-treated) animals (Intact: 87 ± 3 cells, Lesion: 106 ± 5 cells; p<0.001; Two-Way ANOVA with Bonferroni post hoc tests).

As with the dorsal striatum, the ventral striatum also presented significance between the intact and lesioned hemispheres of the non-dyskinetic (Intact: 83 ± 3, Lesion: 98 ± 5; p<0.001; Two-Way ANOVA with Bonferroni post hoc test) and dyskinetic animals (Intact: 81 ± 2, Lesion: 96 ± 3; p<0.001; Two-Way ANOVA with Bonferroni post hoc; figure 60B).

There was no significant effect of L-DOPA or dyskinesia enhancing Iba1-positive microglial proliferation in either the dorsal or ventral dyskinetic striatum.

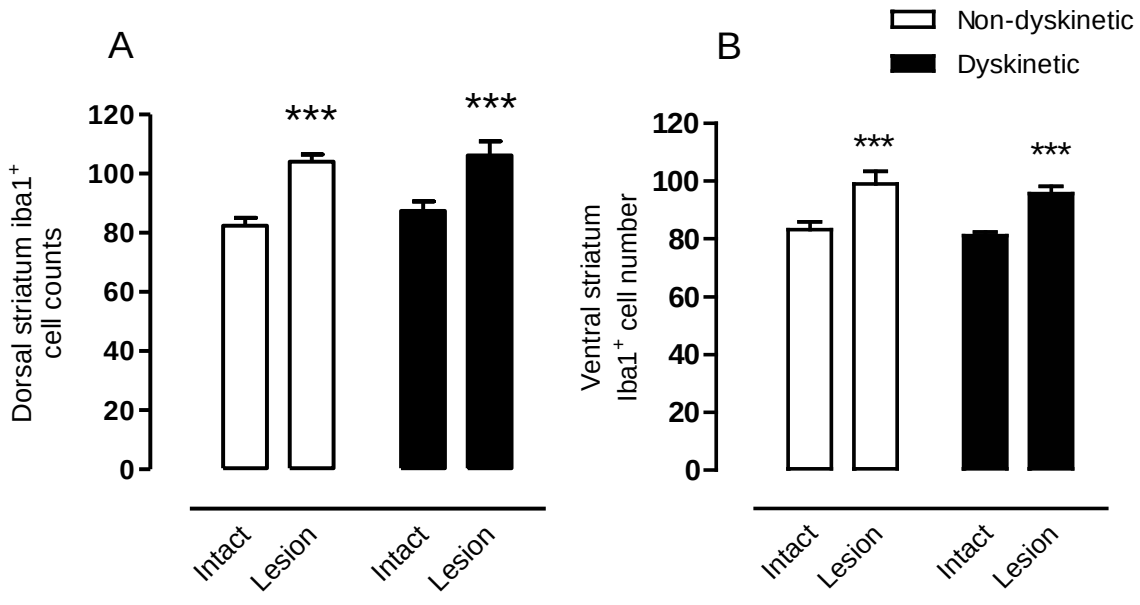


**Figure 61: Manually quantified Iba1-positive microglial cell counts within the dorsal and ventral striatum of non-dyskinetic saline-treated and dyskinetic L-DOPA-treated rats.**
(A + B) A significant increase in Iba1-positive microglia was detected between the intact and lesioned striata in both the dorsal and ventral regions of both the non-dyskinetic and dyskinetic groups. Two-way ANOVA with Bonferroni post hoc; *** denotes p<0.001. Data are mean ± SEM. Data are averaged across all three levels of the rostrocaudal axis. Saline: n=10, L-DOPA n=9. Iba1, ionized calcium-binding adapter molecule 1.

### 5.4.10. Iba-positive microglia of the dyskinetic lesioned striatum present a higher Iba1 intensity

Utilising higher magnification photomicrographs (63X oil immersion), Iba1 intensity of the microglial cell somas were analysed (figure 61A, dorsal stiatum).

There was a significant difference between the Iba1 intensity of the cell somas in the dorsal intact and dorsal lesioned striata of the non-dyskinetic (saline-treated) animals (Intact 0.153 ± 0.004, Lesion: 0.167 ± 0.004; $p<0.001$; Two-Way ANOVA with Bonferroni post hoc; figure 61B) and the dorsal intact and dorsal lesioned striata of the dyskinetic (L-DOPA-treated) animals (Intact: 0.15 ± 0.007, Lesion: 0.179 ± 0.004; $p<0.001$; Two-Way ANOVA with Bonferroni post hoc).

Furthermore, a further increase in Iba1 intensity of the cell somas were detected between the two lesioned dorsal hemispheres of the non-dyskinetic and dyskinetic animals ($p=0.014$; Two-Way ANOVA with Bonferroni post hoc tests).

The ventral striatum also presented significance between the intact and lesioned hemispheres of the non-dyskinetic animals (Intact: 0.144 ± 0.007, Lesion: 0.16 ± 0.008; $p<0.001$; Two-Way ANOVA with Bonferroni post hoc) and the dyskinetic animals (Intact: 0.142 ± 0.005, Lesion: 0.159 ± 0.007; $p<0.001$; Two-Way ANOVA with Bonferroni post hoc tests; figure 61C).

However, no significant difference between dyskinetic and non-dyskinetic animals was noted in either intact or lesioned hemispheres.

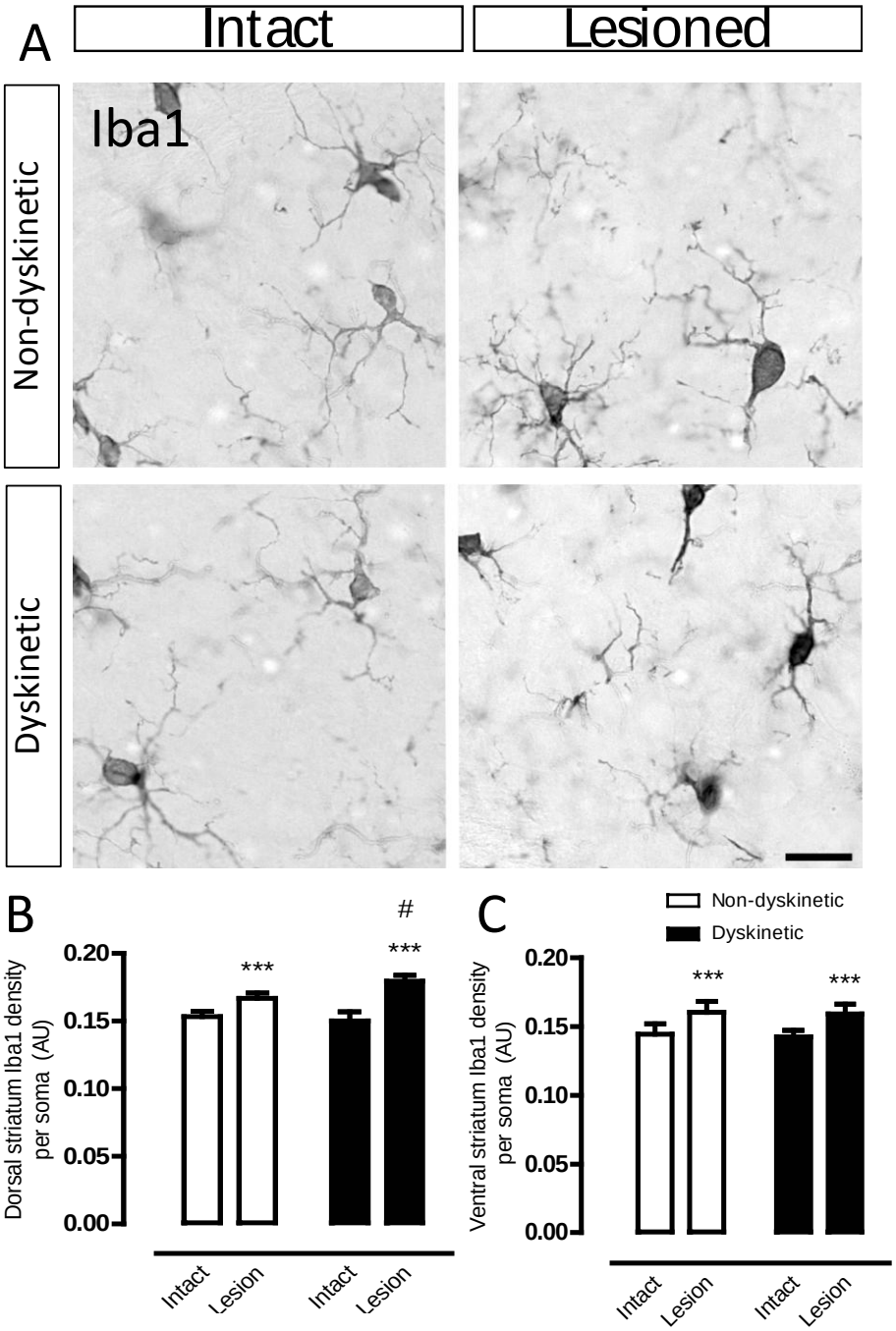


**Figure 62: Iba1 intensity per microglial cell soma measured within the dorsal and ventral striatum of non-dyskinetic saline-treated and dyskinetic L-DOPA-treated rats**.
(A) High magnification (63X, oil immersion) photomicrographs of Iba1 intensity per cell soma within the medial-level dorsal intact and lesioned hemispheres of non-dyskinetic and dyskinetic rat striatum. (B) A significant increase in Iba1 intensity per cell soma was detected between the dorsal intact and dorsal lesioned striata of both the non-dyskinetic and dyskinetic groups. A further increase in Iba1 intensity per cell soma was detected within the lesioned hemisphere of the dyskinetic animals compared to non-dyskinetic. (C) A significant increase in Iba1 optical density per cell soma was detected between the ventral intact and ventral lesioned striata of both the non-dyskinetic and dyskinetic groups. Panels B + C: Two-way ANOVA with Bonferroni post hoc; ***p<0.001: between intra-group hemispheres, $^{\#}$P<0.05: specific hemisphere between treatment groups. Iba1, ionized calcium-binding adapter molecule 1. Data are mean ± SEM. Two-Way ANOVA with Bonferroni post hoc. Saline: n=10, L-DOPA n=9. Scale bar: 20 µm

## 5.5. Discussion

This study examined whether, firstly, there were any structural or volumetric alterations found within the stratum of the rat 6-OHDA model of dyskinesia using T2-weighted MRI. Secondly, if the expression of aggrecan and versican had been altered in the striatum of the dyskinetic rat. Finally, if any structural changes could be correlated to cellular and extracellular modulators of plasticity (e.g. astrocytes, microglia). This was of particular interest due to the known correlation between brain functional activity and grey matter volume and shape (Fauvel *et al.*, 2014; Takeuchi *et al.*, 2010; Zatorre *et al.*, 2012).

### 5.5.1. MRI detected an increase in the volume of the dorsal striatum in dyskinetic rats

L-DOPA-treatment induced a high degree of AIMs in the unilaterally lesioned rats that were pharmacologically reversed by amantadine, the only known anti-dyskinetic agent in clinical use. Pharmacological reversal proved the validity of the rat model used and justified their use in the MRI investigations.

Dyskinetic rats presented significant volume expansions within the lesioned dorsal striatum when compared to the equivalent striatum in the non-dyskinetic parkinsonian animal. This volume increase therefore supports our first hypothesis that states that we would find structural changes in the striatum of the dyskinetic rats. This increase in dorsal striatum volume was potentially caused by a few factors, these being cell proliferation and expansion of the ECM. The most likely cells to contribute to enhanced proliferation would be the inflammatory cells (i.e. inflammatory astrocytes and microglia) and endothelial cells (i.e. markers of angiogenesis), both of which have been previously described as influential to dyskinesia (Bartels *et al.*, 2007; Bortolanza *et al.*, 2015a; Ohlin *et al.*, 2011). The most likely cause of ECM expansion would be the CSPGs, whereby increased CSPG expression would expand the interstitial space between neurones. Although not yet correlated with LID, CSPGs are known to increase in expression during CNS injury (Burnside *et al.*, 2014) therefore we believe they are a likely candidate of this expansion. On the other hand, if the CSPGs were found lowered within the dyskinetic striatum this could suggest that the lack of inhibition is promoting the sprouting of other cells. Perhaps measuring the optical density of dopaminergic terminals and GABAergic (GAD67-positive) cells for sprouting and plasticity would be a wise move for subsequent studies.

### 5.5.2. CSPGs are not upregulated in the striatum of dyskinetic rats and do not correlate with the increase in dorsal striatum volume

CSPGs are key regulators of plasticity in other CNS pathways and systems. Therefore, we examined whether their presence within the striatum was altered in the dyskinetic rats when compared to the non-dyskinetic. Although we know a wide range of CSPGs (primarily the lectican family) to be found within the mammalian striatum, only aggrecan and versican were found to be present within the adult brain (see Chapter 2). These were therefore the two CSPGs investigated.

No alterations in aggrecan or versican expression were found in the striatum of the dyskinetic animals. This was rather disappointing, as the previous two chapters of this thesis have identified CSPGs as a promising therapeutic target in PD. It is likely that these CSPGs do retain a significant function in the corticostriatal pathway but only during early development, as with neurocan (Charvet *et al.*, 1998). It may be worth applying ChABC to the same dyskinetic model as established within this chapter (during the same surgery as the MFB lesioning) to see whether CSPGs and PNNs have a say in LID manifestation. Unfortunately, due to the immunohistochemical embedding process, it was not possible to stain for PNNs within this study. This would have been of interest, as these structures surround the many GABAergic MSNs within the striatum that contribute to the corticostriatal pathway. Perhaps the removal of PNNs would lead to aberrant plasticity via the reopening of the critical period.

Additionally, lectican CPSGs that are expressed only during development (i.e. neurocan (Milev *et al.*, 1998)) may have been expressed within the dyskinetic rat striatum. These CSPGs would be wise to investigate in later studies as we know they have plastic effects within the corticostriatal pathway during development (Charvet *et al.*, 1998).

### 5.5.3. Only Iba1 was found to correlate with the expansion of the dorsal striatum. Neither RECA1 nor GFAP presented an increase.

For the aforementioned reasons stated in section 5.5.2., we analysed the expression of certain cellular markers in order to try to explain the volume increase within the striatum. Astrocytic (GFAP) and microglial (Iba1) optical densities were both increased within the lesioned hemisphere of both the dyskinetic and non-dyskinetic animals. However, only the Iba1 optical density was further enhanced within only the dorsal striatum of the dyskinetic animals. This correlates with the expansion found in the MRI. It is worth noting, that the astrocytic response found in the lesioned hemisphere of both groups was most likely the effect of 6-OHDA-induced cell death.

Our data suggest that the increase in Iba1-positive optical density was due to cell soma Iba1-positivity; indicating increased soma density or increased cell activity (i.e. an activated phenotype). To date there is no evidence that the Iba1 protein itself has any role in dyskinesia, therefore within this study we considered it merely a marker of microglial cells.

It was surprising that there was not an increase in vasculature in the striatum of the dyskinetic rats. It has been documented that angiogenesis occurs within the brains of dyskinetic PD patients and animal models. Studies have discovered the proliferation of blood vessel endothelial cells (Faucheux *et al.*, 1999; Ohlin *et al.*, 2011) and alterations in BBB permeability (Westin *et al.*, 2006) of the dyskinetic BG. These alterations are theorised to be due to enhanced energy consumption, altered neuronal firing and synaptic activity; factors that are present in regions of the striatum with the most prominent level of microvasculature (Westin *et al.*, 2006). However, in this work BBB permeability was detected in animals treated with much higher doses of L-DOPA (25 mg/kg; 10 mg/kg) (Ohlin *et al.*, 2011; Westin *et al.*, 2006), 4-fold and 2-fold higher than the dose used in this study. We argue that these alterations in striatal microvasculature are only observed in animals receiving higher doses of L-DOPA.

### 5.5.4. Microglia may play a role in L-DOPA-induced dyskinesia manifestation

Due to the subtlety of the detected histological change, it is most unlikely that the increased expression of Iba1-positive microglia account for the entirety of the increased dorsal striatum volume and, therefore, a direct cause of LID. However, these data do suggest that microglia play a role in the dyskinetic corticostriatal pathway. Be it a cause or effect, however, we do not know.

It is understood that microglia have a significant role in neuronal synapse plasticity such as remodelling and pruning. These activities are integral to the development of the brain and potentially the progression of neurodegenerative disease (Hong *et al.*, 2016; Paolicelli *et al.*, 2011a; Paolicelli *et al.*, 2011b). If the increased activity of microglia follows a similar pattern in the dyskinetic human, it may be possible that downstream remodelling such as neuronal arborisation, a known candidate for maladaptive plasticity in LID (Linazasoro, 2005; Morgante *et al.*, 2006), could have a role in the disorder. This theory becomes more pertinent with the recent discovery of inflammatory glia expressing DA receptors *de novo* following environmental stress. Studies have discovered reactive astrocytes expressing both D1 and D2 receptors (Kuric *et al.*, 2013; Ruscher *et al.*, 2012) whereas microglia were found expressing D2 (Huck *et al.*, 2015). In PD this could turn the striatum into a DA sensitive state, in which activated microglia may potentiate the effects of L-DOPA through direct DA agonism. Thus leading to a neuroinflammatory feedback mechanism, further activating more microglia and worsening the

effect of LID through increased plasticity and remodelling, or through the production of inflammatory mediators.

It has been previously shown that the typical loss of SNc neurons found in PD can be associated with the increased microglial response in the BG (Niranjan, 2014; Przedborski, 2010). However, it is uncertain whether these responses are a cause or effect of the disease and whether they have a significant role in LID. Studies investigating levels the microglial-derived inflammatory molecule, NO, and its neuronal production enzyme, nNOS, have shown increased levels of both within the BG of PD patients (Eve *et al.*, 1998; Gatto *et al.*, 2000) and the striatum of 6-OHDA lesioned rats (Czarnecka *et al.*, 2013; Padovan-Neto *et al.*, 2011). Recently, targeted inhibitors of nNOS such as 7-nitroindazole (7-NI) have been administered to lesioned rats alongside L-DOPA. These treatments saw no manifestation of AIMs, a result claimed to be associated with the inhibition of glial cell activation and the glial-expressed NOS, inducible nitric oxide synthase (iNOS) (Bortolanza *et al.*, 2016; Bortolanza *et al.*, 2015b; Del-Bel *et al.*, 2015). This indicates an indirect role for microglia in the worsening of LID. However, selective iNOS inhibition studies have yet been conducted and so it may be worthwhile to investigate the assumed downregulation of iNOS through 7-NI-inhibited nNOS.

Although our data suggest an increased density of microglia within the dyskinetic striatum, these data do not account for their activity phenotype. Activated microglia can adopt one of two phenotypes depending on environmental factors, the pro-inflammatory (M1) and pro-repair (M2) phenotype (Sica *et al.*, 2012). As opposed to the classical M1 macrophage, the M2 is seen as beneficial to injury in which they initiate tissue repair and the de-activation of the M1 response (Fiorentino *et al.*, 1989). Therefore, identifying levels of either the M1 or M2 phenotype by cytokine expression would be of interest. Nevertheless, it must be understood that the release of inflammatory cytokines does not indicate a damaging pro-inflammatory response entirely. The release of striatal tumour necrosis factor-α has been shown to be an adaptive response to the disease state and as a way of returning homeostasis to striatal synaptic function (Lewitus *et al.*, 2014).

In recent years, imaging techniques have been used to analyse inflammatory responses within patients *in vivo*. Through means of PET scanning PD patients (but not specifically dyskinetic), researchers have indirectly measured microglial activity by the expression of 18 kDa translocator protein (TSPO), a receptor site found on the outer mitochondrial membrane of activated macrophages. Although initially promising, the use of radioligands such as [$^{11}$C]-PK11195, [$^{18}$F]-FEPPA and [$^{11}$C]-PBR28 (Gerhard, 2013; Jucaite *et al.*, 2015; Koshimori *et al.*, 2015) to analyse microglial activity within the parkinsonian brain, have come under scrutiny

due to mixed results. While issues with radioligand sensitivity and binding are present, differences within the patient groups have most likely confused results. Despite these issues, TSPO PET scanning of the PD striatum between dyskinetic and non-dyskinetic patients could help identify mechanisms involved in LID development whilst avoiding the problems associated with post mortem tissue.

### 5.5.5. Study validity and future studies

As previously mentioned, a significant drawback to this study was the inability to reproduce dyskinetic controls, i.e. non-dyskinetic L-DOPA-treated 6-OHDA lesioned rats. As the prerequisites for LID development were met, dyskinesia was inevitable. The lack of this control made it impossible to distinguish the increases in dorsal striatal microglial optical density and volume as an effect of dyskinesia itself rather than purely L-DOPA treatment.

However, if these changes were purely due to L-DOPA treatment in the dyskinetic rats, these effects may be transient and could decline following a drug wash out period. If so, in future studies a *L-DOPA holiday* would be enforced to help differentiate plastic changes in response to the drug treatment or the dyskinetic state. The caveat to this is that we assume the dyskinetic state is permanent. Additionally, in future studies it may be of interest to lower the dose of L-DOPA to induce milder dyskinetic responses. A study with a cohort of rats with both mild and severe dyskinesia could help tease these volumetric and cellular changes from L-DOPA treatment and dyskinesia, whereby we would expect a higher striatal volume in the more severely dyskinetic rats. Interestingly in this study, two animals were considered moderately dyskinetic (section 5.4.2.). Although their striata were investigated, they were not significantly different to rats with more severe AIMs. However, as there were only two moderately dyskinetic animals we cannot use this data to support our hypothesis.

In future studies it would be wise to investigate this enhanced neuroinflammatory response in more detail. Utilising several Western blotting and ELISA techniques to detect inflammatory mediators (e.g. interleukin-6, -10, tumour necrosis factor-α) could further identify the source of microglial activation. Certain inflammatory mediators could also highlight the phenotype of the microglia within the dorsal striatum of the dyskinetic animals. Could the microglia resident to the dyskinetic rat lesioned striatum be associated with positive plasticity and repair (i.e. M2 microglia; expression of interleukin-4 and -13(Tang *et al.*, 2016))?

### 5.5.6. Chapter conclusions

The studies in this chapter revealed novel findings in the mechanisms underpinning LID. Tensor-based morphometry MRI detected an increase in dorsal striatal volume within

dyskinetic rats. Although previous investigations have correlated functional neuroimaging with LID, this is the first time structural changes been associated with the dyskinetic brain. This is also the first time cellular changes have been mapped to these alterations as well.

Aggrecan and versican expression was investigated in the dyskinetic rat striatum to identify whether CSPGs were potential mediators of LID and also whether they were the cause of the striatal volume increase (i.e. ECM expansion). However, neither CSPG was found up regulated in the dorsal or ventral striatum. This indicated that aggrecan and versican are unlikely to contribute to LID or indeed the volume change found in the dorsal striatum. As previously described, it may be of use to investigate other CSPGs not expressed in the adult rodent striatum. These CSPGs may be aberrantly expressed in the dyskinetic brain and so contribute to LID pathophysiology.

Although endothelial and astrocytic cells were theorised to be accountable for the striatal volume increase in the dyskinetic rats (i.e. angiogenesis and astrogliosis), only Iba1-positive microglia were seen to increase within the dorsal striatum of the dyskinetic rats. From our data, the number of resident microglia was not the cause of the detected optical density; rather it was the cell soma Iba1-positivity that had increased. Correlating inflammatory alterations in the dorsal striatum has highlighted a novel therapeutic target in LID research. It has also highlighted the importance of investigating anti-inflammatory agents to counter LID, as others have before (Teema *et al.*, 2016).

To date there is no epidemiological evidence to suggest anti-inflammatory agents decrease the risk of LID. However, this would be worth investigating to shed light on the potential link between neuroinflammation and dyskinesia.

# 6. General conclusions

Investigating novel approaches to address the two unmet clinical needs of PD was the ultimate target of the work presented in this thesis. These needs were, firstly, to discover new strategies that halt disease progression by increasing SNc cell survival. Secondly, to elucidate the mechanisms underpinning LID to support the search for better anti-dyskinetic agents.

It is nearly 200 years since PD was first discovered and yet there is still no effective way to tackle its associated cell pathology. Although treatments are available to counter the motor dysfunctions caused by SNc degeneration, they are not without their flaws. Perhaps the most successful therapeutic is L-DOPA but, as previously discussed, its chronic treatment induces dyskinesia.

In this thesis, we examined whether the CSPGs of the extracellular matrix may act as novel targets for achieving cellular recovery and act as contributors to LID manifestation. Previous studies have identified the digestion of these CSPGs, via the bacterial enzyme ChABC, permitted axonal regeneration following brain injury (Bradbury *et al.*, 2002; Moon *et al.*, 2001). Although ChABC's efficacy has been analysed as an agent to improve the success of homotopic dopaminergic cell grafting (Diaz-Martinez *et al.*, 2013), no study has assessed its efficacy in promoting cell survival in a validated model of PD (e.g. 6-OHDA lesion model). Here for the first time, we investigated the potential of ChABC as a therapeutic strategy to aid cellular recovery in PD.

The general aims of this thesis were therefore to firstly confirm the expression of CSPGs within the naive mouse BG, particularly the SNc, and to check whether this expression was still evident in the more PD-relevant aged brain. Next, we aimed to investigate the efficacy of ChABC as an agent of cell survival in a 6-OHDA mouse model of PD, and to explore whether promoting striatal NTF levels within the same model could enhance any effect caused by ChABC treatment. The final aim of this thesis was to investigate the mechanism underpinning LID; CSPGs were strong contenders in the manifestation and propagation of the dyskinetic state that is considered to reflect neuroplasticity.

## 6.1. CSPG and PNN distributions in the mouse basal ganglia

CSPGs as therapeutic targets are a novel venture in the field of PD. Because of this, the expression of various CSPGs in the mouse BG had not been well characterised. We believed that although CSPG presence had been detected within the mouse CNS, it was important to identify the level and pattern of expression of a select few lectican CSPGs within the BG. If we were to continue the investigation of CSPG manipulation in the mouse this characterisation would help identify which CSPGs were most expressed and thus integral to the ECM surrounding pertinent regions (i.e. the SNc).

In Chapter 2, although we observed a moderate expression of the CSPGs aggrecan and versican within the SNc, NG2 was present in very low levels. Expression of brevican and neurocan was negligible, with imaging not being possible. In the case of brevican, this low expression was contrary to the works of Milev *et al*. We therefore focused on aggrecan and versican in our subsequent studies. While only mounted sections of the SNc were investigated in these studies, characterisation of CSPGs within the striatum would have been of great interest as particular CSPGs may have been expressed additionally within this region. This information would have widened the CSPG search beyond aggrecan and versican in the LID studies discussed later.

We also assessed the distribution of PNNs within the mouse BG. As work by Bruckner *et al.* had already identified PNNs to be absent in almost all dopaminergic systems in the human BG, we had hypothesised that this pattern was reflected in the mouse. This was certainly the case, confirming our hypothesis. WFA-positive PNNs were absent from the SNc and appeared to be exclusive to the neighbouring GABAegic regions such as the SNr. In the future it would be interesting to examine whether these PNNs were indeed co-localised with GABAergic cells, as seen in other brain regions such as in the striatum (Bruckner *et al* 2008). Although not directly affecting our studies, our results raise an interesting point concerning the potential protective role for PNNs. As SNc cells are potentially more susceptible to cell death due to their increased metabolic rate and poor $Ca^{2+}$ homeostasis (e.g. low calbindin levels, large influxes of $Ca^{2+}$ (Chan *et al*., 2010; Liang *et al*., 1996)), the lack of PNN buffering in the SNc may therefore exacerbate cell susceptibility to excess $Ca^{2+}$. Although difficult to imagine how it may be achieved, if it was possible to induce PNN deposition in the SNc this may enforce neuroprotection against the intrinsic sensitivity to excess $Ca^{2+}$ ions.

Our final investigative study of Chapter 2 analysed CSPG distributions in the aged and young adult mouse BG. Aggrecan and CS56 were used to assess the CSPG and CS-GAG presence, respectively. Aggrecan and CS56 both displayed enhanced expression within the aged SNc and

aggrecan was further elevated within the dorsal striatum. This enhanced degree of CSPG expression was consistent with the lectican expression plots described in Chapter 2 (Milev *et al.*, 1998). As the aged mouse retained CSPG expression from the young adult, CSPG presence confirmed their use as therapeutic targets in age-related diseases such as PD. Although a small increase, this expression in the aged tissue suggested that young adult mice could be used to model PD. Additionally, this increase in aggrecan and CS56 expression indicated a potential role of these CSPGs in ageing.

This alteration in expression between the aged mouse and the young adult (a typical age for experimentation) raised the point of model validity when researching age-related diseases. However, it is unlikely that research groups will adopt older animals due to the many monetary and ethical considerations.

Within this investigation, we also assessed whether age was a factor in the number of SNc cells present and the density of TH-positive fibres within the striatum. The aged animals had far fewer TH-positive cells within the SNc than the young adult had but possessed significantly more TH-positive fibres in the striatum. Although the decline in cells was not surprising, as age correlates with lowered activity in several pro-survival systems and senescence (e.g. UPS (Tai et al., 2008)), the increase in TH-positive fibres was. This may be a form of compensatory terminal sprouting where the decline in SNc cells (~50% of the young adult) spurs plasticity in the striatum to counter the loss in DA release. Contrary to this theory, published evidence suggests that there is a loss in striatal dopaminergic markers in relation to age (Haycock *et al.*, 2003). Therefore, further investigation is required to clarify the exact nature of changes within the striatum in aged mouse brain.

Importantly, the studies in this chapter set the scene for subsequent Chapters by identifying at least two CSPGs present in the mouse BG and that the young adult mouse translates to the PD patient.

## 6.2. ChABC as a strategy for improving SNc cell survival

With the knowledge that CSPGs were expressed within the mouse BG, we next proceeded to investigate the effects of their digestion via ChABC in the 6-OHDA unilateral lesion model of PD. Due to the novelty of the strategy, initial studies were conducted to examine the pattern of digestion of CSPGs along the NS. At this point, we were not sure whether the cell terminals or SNc cell bodies were to be the target of CSPG digestion for cell survival effects, therefore the entire NS was digested. After a failed attempt of digesting the entire NS, whereby the injection sites were too far away from each other, the coordinates for the intracerebral administration of ChABC were readjusted. This new protocol ensured the entire digestion of CSPGs along the entire NS; a digestion pattern consistently reproduced throughout these studies.

ChABC did not provide any cell survival in the full lesion model. This was thought to be caused by the severity and speed at which this lesion developed. Perhaps the beneficial effects induced by ChABC were too slow to tackle the quick loss of SNc cells. In contrast, ChABC possessed a modest cell survival effect within the partial lesion model. Although we still do not know what underpins the efficacy of ChABC treatment post CSPG digestion, our work can argue in favour of either a neuroprotective or neuroreparative effect. However, this work cannot distinguish between these effects.

### *Neuroprotective*

A neuroprotective mechanism would be one that occurs in tandem with SNc cell degeneration. ChABC treatment induces pro-survival effects (e.g. NTF liberation, removal of physical contacts as discussed in Chapter 3) that counter the slow decline in SNc cell number. Unlike the partial lesion that takes ~2 weeks to develop, the full lesion model would have taken only 2 to 3 days. This is perhaps far too rapid or severe for the beneficial events brought about by ChABC to take effect within the *neuroprotective window*. See figure 40 in Chapter 3 representing this window.

### *Neuroreparative*

On the other hand, a neurorepair action is one that occurs after the initial damage to the SNc has occurred. Alternatively, ChABC-mediated digestion of the CSPGs requires some remaining cells for repair and plasticity. Therefore, in a fully ablated SNc no/very few cells remain to respond to the pro-repair events caused by ChABC treatment. In the partial lesion, the ~40-50% cells remaining is enough to benefit from CSPG digestion during the repair period following lesion development.

This debate of *protection or repair* has been discussed throughout this thesis. Although we did not set out to test whether ChABC had a neuroprotective or neuroreparative action, it is of importance to investigate this in the future. Fortunately, this can be conducted with relative ease. As described in Chapter 3, administering ChABC before lesioning would examine a protective effect and administrating ChABC after the lesion was stable (i.e. two weeks post lesion) would examine a repair effect. If we were to see beneficial effects from the protective examination, we could assign the effects to protection and repair. If the repair examination presented beneficial effects then this would be solely a result of a repair effect. Comparing cell survival between these two examinations may help dissect the protection from repair effects underlying CSPG digestion.

Inducing cell survival in the partial lesion model was a success. However, the lack of behavioural phenotype was a disappointing shortfall. The overall aim of this novel strategy was to induce cell survival in order to better the motor function in the animal model and, ultimately, PD itself. We therefore next set out to improve this modest cell survival effect by promoting NTF release in the striatum.

CSPGs have been previously described as *reservoirs for growth factors* (Bandtlow *et al.*, 2000). Although we had not assessed the liberation of NTFs from CSPG digestion, being reservoirs, CSPG digestion would therefore be predicted to liberate harboured NTFs which would activate pro-survival pathways (Wang *et al.*, 2012a). However, it was clear from data in Chapter 3 that the degree of increased survival was small, suggesting there was insufficient liberation of NTFs to have functional significance. Unfortunately, due to the preparation of the tissue (i.e. paraffin embedded fixed tissue) it was impossible to assess NTF levels following ChABC treatment.

In Chapter 4 we set out to examine whether, by enhancing NTF levels by other means, we could enhance the beneficial effects of ChABC on SNc cell survival and thereby reveal a behavioural improvement. We were keen not to complicate matters by delivering NTFs directly into the striatum. Therefore, we chose a pharmacological approach to promote intrinsic NTF expression instead. Selegiline had been previously confirmed to promote striatal GDNF and BDNF levels in mice following two weeks of once-a-day daily administration (Zhao *et al.*, 2013). We therefore wished to test selegiline's efficacy. Our pilot study found that once-a-day daily administration of selegiline for 7 days induced a significant increase in striatal GDNF and BDNF in naive mice. This level was then maintained until the end of the study (14 days). When a daily once-a-day treatment of selegiline was applied to our ChABC administered lesioned model from Chapter 3, no improved cell survival or even increases in NTF levels were found. Unexpectedly, selegiline rather negated the pro-survival effect of ChABC. The ChABC-only

group reproduced effects seen in Chapter 3, ChABC was concluded to still be in effect. We believe that these unaffected NTF levels may be due to selegiline desensitisation. This is due to the possible decline of GDNF and BDNF levels seen on day 14 following daily treatment in the selegiline pilot study, whereby there was a marked decrease in GDNF and BDNF levels compared to the levels seen at day 7 (NTF levels on day 14 were still significant however). Selegiline may therefore only induce an increase in the two NTFs over a small timeframe when daily dosed at 1 mg/kg. It may be worth investigating the levels of NTFs at regular time points following 1 to 2 months of daily selegiline treatment. If a clear maintained decrease in GDNF and BDNF were apparent at 2 weeks, a subsequent study investigating variations in selegiline treatment (e.g. lower dose, intermittent dosing times) may help establish a dosing regimen that would bypass the potential desensitisation to selegiline.

## 6.3. L-DOPA-induced dyskinesia

While Chapters 3 and 4 focussed on the unmet clinical need of improving SNc cell survival, Chapter 5 aimed to further our understanding of the mechanism behind LID in order to help tackle the need for improved anti-dyskinetic agents. LID is thought to involve several aberrant alterations within the striatum and the corticostriatal pathway that lead to a dysregulated BG. However, the exact nature of this corticostriatal plasticity remains unknown. We hypothesised that striatal plasticity may be reflected in structural changes within the striatum that may involve CSPG alterations. However, following the investigation of aggrecan and versican expression levels in the striatum of dyskinetic rats, no changes were found. We next investigated the structure and volume of the striatum in the dyskinetic rats. Using structural MRI, we detected an increase in volume within the dyskinetic animals' dorsal striatum. Several candidates were suggested to cause this increase such as the CSPGs, inflammatory cells and vasculature endothelial cells. As previously mentioned, no changes in aggrecan and versican expression were found in the dorsal striatum. Similarly, no alterations in vasculature (RECA1) or astrocytes (GFAP) optical densities were either observed. The latter two have been associated with LID in previous studies whereby BBB permeability and astrogliosis go hand-in-hand within the pathophysiology of PD and LID (Cabezas *et al.*, 2014; Ohlin *et al.*, 2011). However, only Iba1 optical density was found to increase within the dorsal striatum of the dyskinetic animals. This suggests an increased activation of Iba1-positive microglia in the dyskinetic state, a finding that raises several interesting points concerning the neuroinflammatory response in LID.

Published studies have identified glia to express D1 and D2 receptors *de novo* under stressed conditions (Huck *et al.*, 2015; Ruscher *et al.*, 2012). This work suggests a *de novo* expression of DA receptors on glia in the stroke-stressed brain, a possibility that may also occur in the PD-

stressed brain. If this were the case in PD, L-DOPA-metabolised DA may agonise and activate resident glia in the striatum furthering neuroinflammation and plasticity. In addition, other work has found the inhibition of NOS to halt the manifestation of dyskinesia, suggesting a significant role of microglial-derived NO in LID (Bortolanza *et al.*, 2016; Bortolanza *et al.*, 2015a). Moreover, other work has highlighted the importance of the NO/cyclic GMP pathway in the regulation of striatal signalling (Calabresi *et al.*, 1999) and in the release of glutamate (Neitz *et al.*, 2011). Therefore, it may be possible that activated microglia of the striatum mediate LID through the production of NO. If the works by Huck *et al*. were to apply to PD, the presence of *de novo* expressed microglial-DA receptors may potentiate resident microglia activity resulting in the promotion of NO. This increase in NO could therefore explain the aberrant glutamatergic transmission of the corticostriatal pathway as depicted in the schematic below (figure 62).

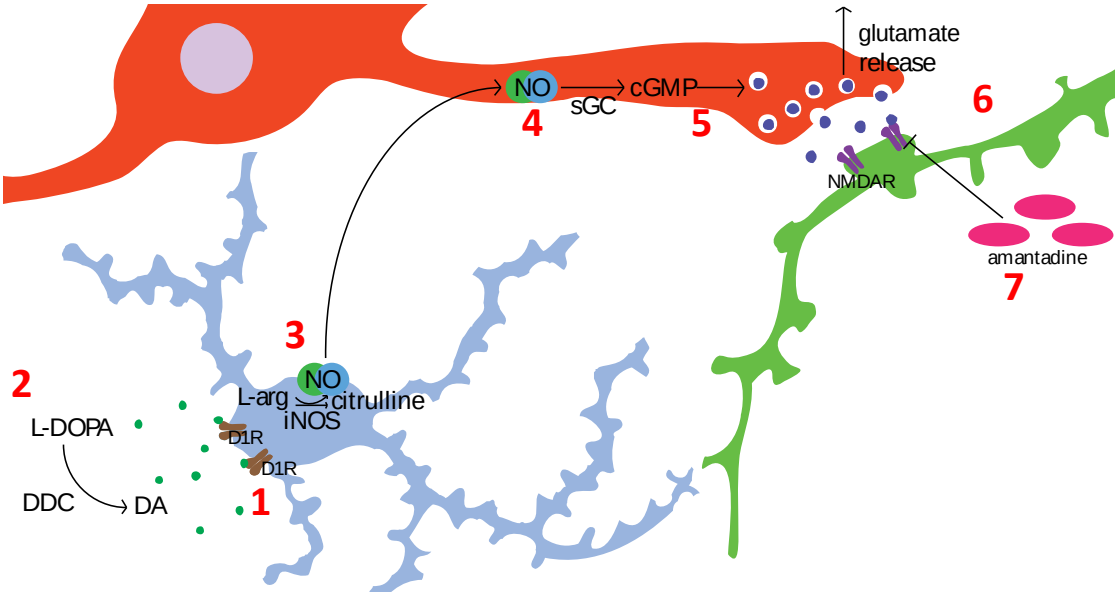


**Figure 63: Theorised mechanism of microglia in the manifestation of LID.**
(1) Under stressed conditions such as PD, striatal microglia express D1 receptors (DA receptor subtype known to modulate LID). (2) The increased level of L-DOPA-metabolised DA agonises the microglial D1 receptors. (3) Agonism increases activity of resident microglia that produce NO and citrulline as a result of L-arginine (L-arg) oxidation via the iNOS enzyme. (4) NO translocates to the glutamatergic afferents of the corticostriatal pathway. (5) NO stimulates the production of cyclic GMP (cGMP) via the binding to soluble guanylyl cyclase (sGC). (6) cGMP induces the increased release of glutamate transmission in the corticostriatal pathway. (7) Amantadine targets the post-synaptic NMDA receptors to reduce transmission. Red cell = cortical projection; green cell = medium spiny neurone; blue cell = microglia.

In subsequent studies, it would be of interest to test this theorised mechanism. A preliminary in-house immunofluorescent investigation (not shown) has suggested an increase in D1 receptor and Iba1 in the 6-OHDA-stressed striatum. Further investigations identifying the location of these receptors would be a wise next step in an attempt to confirm the *de novo*

microglial expression of DA receptors. If microglia were seen to express DA receptors in the 6-OHDA model tissue, further *in vivo* testing would be required. Utilising iNOS inhibitors in the established rat model of LID would be of interest as only nNOS inhibitors (e.g. 7-NI) have been tested as anti-dyskinetics so far.

## 6.4. Concluding remarks

The work presented in this thesis represents entirely novel ventures within the PD field and although previous work had suggested ChABC may induce axonal repair (Moon *et al.*, 2001), it was not guaranteed. Therefore, it was a significant discovery to find ChABC-treatment as a potential therapeutic strategy in the mouse model of PD. Although ChABC induced only a modest increase in SNc cell survival that did not provide a better behavioural phenotype, this discovery can be considered a starting point for further studies. Subsequent studies identifying ways to enhance ChABC-mediated cell survival will be invaluable, as behavioural benefits are desirable for PD therapeutics. However, in its current state, ChABC has potential use as an adjunct to L-DOPA where ChABC may halt disease progression whilst L-DOPA improves motor function. Despite this, ChABC's efficacy as a bolus or a mini-pump treatment may be inadequate due to its limiting enzymatic properties (e.g. denaturing under certain conditions). Furthering its use as a virally expressed enzyme is most likely the future for ChABC; a venture already spearheaded by the spinal cord injury field (Bartus *et al.*, 2014).

In lieu of a PD cure, addressing the problematic dyskinesias patients experience from the treatment of L-DOPA is required. We have shown that structural changes occur in the striatum of dyskinetic rats and that they are accompanied by an increase in Iba1 expression. As this expression may be integral to LID, investigating the suggested LID manifestation mechanism (figure 62) would be an interesting venture to pursue. Although we identified an increase in Iba1-positive microglia optical density within the striatum of dyskinetic animals, we believe that this does not account for the volume increase detected by MRI. This is because there was no increase in microglial cell number, and only a slight enhancement in Iba1 optical density. Therefore, further investigations into the true cause of this striatal expansion in LID would be an interesting next step.

In conclusion, whilst not producing any firm indication of how the unmet clinical needs in PD may be addressed, this work has paved the way for novel investigations in the use of ChABC as a PD therapeutic and in the mechanisms of the microglial response in LID manifestation.

# 7. References


*Aharon-Peretz J, Rosenbaum H, Gershoni-Baruch R (2004). Mutations in the glucocerebrosidase gene and Parkinson's disease in Ashkenazi Jews. N Engl J Med **351**(19): 1972-1977.*

*Ahlskog JE, Muenter MD (2001). Frequency of levodopa-related dyskinesias and motor fluctuations as estimated from the cumulative literature. Mov Disord **16**(3): 448-458.*

*Allen SJ, Watson JJ, Shoemark DK, Barua NU, Patel NK (2013). GDNF, NGF and BDNF as therapeutic options for neurodegeneration. Pharmacol Ther **138**(2): 155-175.*

*Anderson DG, Mariappan SV, Buettner GR, Doorn JA (2011). Oxidation of 3,4-dihydroxyphenylacetaldehyde, a toxic dopaminergic metabolite, to a semiquinone radical and an ortho-quinone. J Biol Chem **286**(30): 26978-26986.*

*Armando V, Antonio G, Giovanni F, Maurizio I, Ida RM, Andrea G, et al. (2016). Parkinson's Disease: Autoimmunity and Neuroinflammation. Autoimmun Rev.*

*Asher RA, Morgenstern DA, Fidler PS, Adcock KH, Oohira A, Braistead JE, et al. (2000). Neurocan is upregulated in injured brain and in cytokine-treated astrocytes. J Neurosci **20**(7): 2427-2438.*

*Asher RA, Morgenstern DA, Shearer MC, Adcock KH, Pesheva P, Fawcett JW (2002). Versican is upregulated in CNS injury and is a product of oligodendrocyte lineage cells. J Neurosci **22**(6): 2225-2236.*

*Ba M, Kong M, Yu G, Sun X, Liu Z, Wang X (2011). GluR1 phosphorylation and persistent expression of levodopa-induced motor response alterations in the Hemi-Parkinsonian rat. Neurochem Res **36**(6): 1135-1144.*

*Bandtlow CE, Zimmermann DR (2000). Proteoglycans in the developing brain: new conceptual insights for old proteins. Physiological reviews **80**(4): 1267-1290.*

*Bar-Am O, Weinreb O, Amit T, Youdim MB (2010). The neuroprotective mechanism of 1-(R)-aminoindan, the major metabolite of the anti-parkinsonian drug rasagiline. J Neurochem **112**(5): 1131-1137.*

*Barbacid M (1994). The Trk family of neurotrophin receptors. Journal of neurobiology **25**(11): 1386-1403.*

*Barker RA, Dunnett SB, Faissner A, Fawcett JW (1996). The time course of loss of dopaminergic neurons and the gliotic reaction surrounding grafts of embryonic mesencephalon to the striatum. Exp Neurol **141**(1): 79-93.*

*Barraud Q, Lambrecq V, Forni C, McGuire S, Hill M, Bioulac B, et al. (2009). Sleep disorders in Parkinson's disease: the contribution of the MPTP non-human primate model. Exp Neurol **219**(2): 574-582.*

*Barritt AW, Davies M, Marchand F, Hartley R, Grist J, Yip P, et al. (2006). Chondroitinase ABC promotes sprouting of intact and injured spinal systems after spinal cord injury. J Neurosci **26**(42): 10856-10867.*

*Bartels AL, Leenders KL (2007). Neuroinflammation in the pathophysiology of Parkinson's disease: evidence from animal models to human in vivo studies with [11C]-PK11195 PET. Mov*

*Disord **22**(13): 1852-1856.*

*Bartus K, James ND, Bosch KD, Bradbury EJ (2012). Chondroitin sulphate proteoglycans: key modulators of spinal cord and brain plasticity. Exp Neurol **235**(1): 5-17.*

*Bartus K, James ND, Didangelos A, Bosch KD, Verhaagen J, Yanez-Munoz RJ, et al. (2014). Large-scale chondroitin sulfate proteoglycan digestion with chondroitinase gene therapy leads to reduced pathology and modulates macrophage phenotype following spinal cord contusion injury. J Neurosci **34**(14): 4822-4836.*

*Ben-Shachar D, Eshel G, Finberg JP, Youdim MB (1991). The iron chelator desferrioxamine (Desferal) retards 6-hydroxydopamine-induced degeneration of nigrostriatal dopamine neurons. J Neurochem **56**(4): 1441-1444.*

*Benhamou L, Kehat O, Cohen D (2014). Firing pattern characteristics of tonically active neurons in rat striatum: context dependent or species divergent? J Neurosci **34**(6): 2299-2304.*

*Betarbet R, Porter RH, Greenamyre JT (2000a). GluR1 glutamate receptor subunit is regulated differentially in the primate basal ganglia following nigrostriatal dopamine denervation. J Neurochem **74**(3): 1166-1174.*

*Betarbet R, Sherer TB, MacKenzie G, Garcia-Osuna M, Panov AV, Greenamyre JT (2000b). Chronic systemic pesticide exposure reproduces features of Parkinson's disease. Nat Neurosci **3**(12): 1301-1306.*

*Bezard E, Ferry S, Mach U, Stark H, Leriche L, Boraud T, et al. (2003). Attenuation of levodopa-induced dyskinesia by normalizing dopamine D3 receptor function. Nat Med **9**(6): 762-767.*

*Bezard E, Przedborski S (2011). A tale on animal models of Parkinson's disease. Mov Disord **26**(6): 993-1002.*

*Bibbiani F, Oh JD, Kielaite A, Collins MA, Smith C, Chase TN (2005). Combined blockade of AMPA and NMDA glutamate receptors reduces levodopa-induced motor complications in animal models of PD. Exp Neurol **196**(2): 422-429.*

*Block G, Liss C, Reines S, Irr J, Nibbelink D (1997). Comparison of immediate-release and controlled release carbidopa/levodopa in Parkinson's disease. A multicenter 5-year study. The CR First Study Group. Eur Neurol **37**(1): 23-27.*

*Boger HA, Middaugh LD, Zaman V, Hoffer B, Granholm AC (2008). Differential effects of the dopamine neurotoxin MPTP in animals with a partial deletion of the GDNF receptor, GFR alpha1, gene. Brain Res **1241**: 18-28.*

*Bonifati V, Rizzu P, Squitieri F, Krieger E, Vanacore N, van Swieten JC, et al. (2003). DJ-1( PARK7), a novel gene for autosomal recessive, early onset parkinsonism. Neurol Sci **24**(3): 159-160.*

*Bonini NM, Giasson BI (2005). Snaring the function of alpha-synuclein. Cell **123**(3): 359-361.*

*Bortolanza M, Bariotto-Dos-Santos KD, Dos-Santos-Pereira M, da-Silva CA, Del-Bel E (2016). Antidyskinetic Effect of 7-Nitroindazole and Sodium Nitroprusside Associated with Amantadine in a Rat Model of Parkinson's Disease. Neurotox Res.*

*Bortolanza M, Cavalcanti-Kiwiatkoski R, Padovan-Neto FE, da-Silva CA, Mitkovski M, Raisman-Vozari R, et al. (2015a). Glial activation is associated with l-DOPA induced dyskinesia and*

*blocked by a nitric oxide synthase inhibitor in a rat model of Parkinson's disease. Neurobiol Dis* ***73:*** *377-387.*

*Bortolanza M, Padovan-Neto FE, Cavalcanti-Kiwiatkoski R, Dos Santos-Pereira M, Mitkovski M, Raisman-Vozari R, et al. (2015b). Are cyclooxygenase-2 and nitric oxide involved in the dyskinesia of Parkinson's disease induced by L-DOPA? Philos Trans R Soc Lond B Biol Sci* ***370****(1672).*

*Bosch C, Mailly P, Degos B, Deniau JM, Venance L (2012). Preservation of the hyperdirect pathway of basal ganglia in a rodent brain slice. Neuroscience* ***215:*** *31-41.*

*Braak H, Del Tredici K, Rub U, de Vos RA, Jansen Steur EN, Braak E (2003). Staging of brain pathology related to sporadic Parkinson's disease. Neurobiol Aging* ***24****(2)****:*** *197-211.*

*Bradbury EJ, Moon LD, Popat RJ, King VR, Bennett GS, Patel PN, et al. (2002). Chondroitinase ABC promotes functional recovery after spinal cord injury. Nature* ***416****(6881)****:*** *636-640.*

*Breckenridge CB, Berry C, Chang ET, Sielken RL, Jr., Mandel JS (2016). Association between Parkinson's Disease and Cigarette Smoking, Rural Living, Well-Water Consumption, Farming and Pesticide Use: Systematic Review and Meta-Analysis. PLoS One* ***11****(4)****:*** *e0151841.*

*Brooks DJ, Piccini P, Turjanski N, Samuel M (2000). Neuroimaging of dyskinesia. Ann Neurol* ***47****(4 Suppl 1)****:*** *S154-158; discussion S158-159.*

*Bruckner G, Hausen D, Hartig W, Drlicek M, Arendt T, Brauer K (1999). Cortical areas abundant in extracellular matrix chondroitin sulphate proteoglycans are less affected by cytoskeletal changes in Alzheimer's disease. Neuroscience* ***92****(3)****:*** *791-805.*

*Bruckner G, Morawski M, Arendt T (2008). Aggrecan-based extracellular matrix is an integral part of the human basal ganglia circuit. Neuroscience* ***151****(2)****:*** *489-504.*

*Burnside ER, Bradbury EJ (2014). Manipulating the extracellular matrix and its role in brain and spinal cord plasticity and repair. Neuropathol Appl Neurobiol* ***40****(1)****:*** *26-59.*

*Cabezas R, Avila M, Gonzalez J, El-Bacha RS, Baez E, Garcia-Segura LM, et al. (2014). Astrocytic modulation of blood brain barrier: perspectives on Parkinson's disease. Front Cell Neurosci* ***8:*** *211.*

*Cabungcal JH, Steullet P, Morishita H, Kraftsik R, Cuenod M, Hensch TK, et al. (2013). Perineuronal nets protect fast-spiking interneurons against oxidative stress. Proc Natl Acad Sci U S A* ***110****(22)****:*** *9130-9135.*

*Calabresi P, Di Filippo M, Ghiglieri V, Tambasco N, Picconi B (2010). Levodopa-induced dyskinesias in patients with Parkinson's disease: filling the bench-to-bedside gap. Lancet Neurol* ***9****(11)****:*** *1106-1117.*

*Calabresi P, Gubellini P, Centonze D, Sancesario G, Morello M, Giorgi M, et al. (1999). A critical role of the nitric oxide/cGMP pathway in corticostriatal long-term depression. J Neurosci* ***19****(7)****:*** *2489-2499.*

*Calabresi P, Picconi B, Tozzi A, Di Filippo M (2007). Dopamine-mediated regulation of corticostriatal synaptic plasticity. Trends Neurosci* ***30****(5)****:*** *211-219.*

*CALM-PD (2000). A randomized controlled trial comparing pramipexole with levodopa in early Parkinson's disease: design and methods of the CALM-PD Study. Parkinson Study Group. Clin Neuropharmacol **23**(1): 34-44.*

*Calon F, Rajput AH, Hornykiewicz O, Bedard PJ, Di Paolo T (2003). Levodopa-induced motor complications are associated with alterations of glutamate receptors in Parkinson's disease. Neurobiol Dis **14**(3): 404-416.*

*Carlsson T, Carta M, Winkler C, Bjorklund A, Kirik D (2007). Serotonin neuron transplants exacerbate L-DOPA-induced dyskinesias in a rat model of Parkinson's disease. J Neurosci **27**(30): 8011-8022.*

*Carta M, Carlsson T, Kirik D, Bjorklund A (2007). Dopamine released from 5-HT terminals is the cause of L-DOPA-induced dyskinesia in parkinsonian rats. Brain **130**(Pt 7): 1819-1833.*

*Carta M, Carlsson T, Munoz A, Kirik D, Bjorklund A (2008). Serotonin-dopamine interaction in the induction and maintenance of L-DOPA-induced dyskinesias. Prog Brain Res **172:** 465-478.*

*Carulli D, Pizzorusso T, Kwok JC, Putignano E, Poli A, Forostyak S, et al. (2010). Animals lacking link protein have attenuated perineuronal nets and persistent plasticity. Brain **133**(Pt 8): 2331-2347.*

*Carulli D, Rhodes KE, Brown DJ, Bonnert TP, Pollack SJ, Oliver K, et al. (2006). Composition of perineuronal nets in the adult rat cerebellum and the cellular origin of their components. J Comp Neurol **494**(4): 559-577.*

*Cenci MA, Lee CS, Bjorklund A (1998). L-DOPA-induced dyskinesia in the rat is associated with striatal overexpression of prodynorphin- and glutamic acid decarboxylase mRNA. Eur J Neurosci **10**(8): 2694-2706.*

*Cerasa A, Pugliese P, Messina D, Morelli M, Gioia MC, Salsone M, et al. (2012). Prefrontal alterations in Parkinson's disease with levodopa-induced dyskinesia during fMRI motor task. Mov Disord **27**(3): 364-371.*

*Chan CS, Gertler TS, Surmeier DJ (2010). A molecular basis for the increased vulnerability of substantia nigra dopamine neurons in aging and Parkinson's disease. Mov Disord **25 Suppl 1:** S63-70.*

*Chandra S, Chen X, Rizo J, Jahn R, Sudhof TC (2003). A broken alpha -helix in folded alpha -Synuclein. J Biol Chem **278**(17): 15313-15318.*

*Chao CC, Chiang CH, Ma YL, Lee EH (2006). Molecular mechanism of the neurotrophic effect of GDNF on DA neurons: role of protein kinase CK2. Neurobiol Aging **27**(1): 105-118.*

*Chao CC, Lee EH (1999). Neuroprotective mechanism of glial cell line-derived neurotrophic factor on dopamine neurons: role of antioxidation. Neuropharmacology **38**(6): 913-916.*

*Charvet I, Hemming FJ, Feuerstein C, Saxod R (1998). Transient compartmental expression of neurocan in the developing striatum of the rat. J Neurosci Res **51**(5): 612-618.*

*Chase TN, Oh JD, Konitsiotis S (2000). Antiparkinsonian and antidyskinetic activity of drugs targeting central glutamatergic mechanisms. J Neurol **247 Suppl 2:** II36-42.*

*Chesselet MF, Richter F (2011). Modelling of Parkinson's disease in mice. Lancet Neurol **10**(12):*

*1108-1118.*

*Chiu SC, Hung HS, Lin SZ, Chiang E, Liu DD (2009). Therapeutic potential of olfactory ensheathing cells in neurodegenerative diseases. J Mol Med (Berl)* ***87****(12):* *1179-1189.*

*Chung EK, Chen LW, Chan YS, Yung KK (2008). Downregulation of glial glutamate transporters after dopamine denervation in the striatum of 6-hydroxydopamine-lesioned rats. J Comp Neurol* ***511****(4):* *421-437.*

*Clement AM, Nadanaka S, Masayama K, Mandl C, Sugahara K, Faissner A (1998). The DSD-1 carbohydrate epitope depends on sulfation, correlates with chondroitin sulfate D motifs, and is sufficient to promote neurite outgrowth. J Biol Chem* ***273****(43):* *28444-28453.*

*Colotla VA, Flores E, Oscos A, Meneses A, Tapia R (1990). Effects of MPTP on locomotor activity in mice. Neurotoxicol Teratol* ***12****(4):* *405-407.*

*Cong L, Muir ER, Chen C, Qian Y, Liu J, Biju KC, et al. (2016). Multimodal MRI Evaluation of the MitoPark Mouse Model of Parkinson's Disease. PLoS One* ***11****(3):* *e0151884.*

*Cookson MR (2010). Unravelling the role of defective genes. Prog Brain Res* ***183:*** *43-57.*

*Cordero-Llana O, Houghton BC, Rinaldi F, Taylor H, Yanez-Munoz RJ, Uney JB, et al. (2015). Enhanced efficacy of the CDNF/MANF family by combined intranigral overexpression in the 6-OHDA rat model of Parkinson's disease. Mol Ther* ***23****(2):* *244-254.*

*Crum WR, Modo M, Vernon AC, Barker GJ, Williams SC (2013). Registration of challenging pre-clinical brain images. J Neurosci Methods* ***216****(1):* *62-77.*

*Curinga GM, Snow DM, Mashburn C, Kohler K, Thobaben R, Caggiano AO, et al. (2007). Mammalian-produced chondroitinase AC mitigates axon inhibition by chondroitin sulfate proteoglycans. J Neurochem* ***102****(1):* *275-288.*

*Czarnecka A, Lenda T, Domin H, Konieczny J, Smialowska M, Lorenc-Koci E (2013). Alterations in the expression of nNOS in the substantia nigra and subthalamic nucleus of 6-OHDA-lesioned rats: the effects of chronic treatment with l-DOPA and the nitric oxide donor, molsidomine. Brain Res* ***1541:*** *92-105.*

*d'Anglemont de Tassigny X, Pascual A, Lopez-Barneo J (2015). GDNF-based therapies, GDNF-producing interneurons, and trophic support of the dopaminergic nigrostriatal pathway. Implications for Parkinson's disease. Front Neuroanat* ***9:*** *10.*

*da Silva-Junior FP, Braga-Neto P, Sueli Monte F, de Bruin VM (2005). Amantadine reduces the duration of levodopa-induced dyskinesia: a randomized, double-blind, placebo-controlled study. Parkinsonism Relat Disord* ***11****(7):* *449-452.*

*Darmopil S, Martin AB, De Diego IR, Ares S, Moratalla R (2009). Genetic inactivation of dopamine D1 but not D2 receptors inhibits L-DOPA-induced dyskinesia and histone activation. Biol Psychiatry* ***66****(6):* *603-613.*

*DATATOP (1989). DATATOP: a multicenter controlled clinical trial in early Parkinson's disease. Parkinson Study Group. Arch Neurol* ***46****(10):* *1052-1060.*

*Dauer W, Przedborski S (2003). Parkinson's disease: mechanisms and models. Neuron* ***39****(6):* *889-909.*

*Davie CA (2008). A review of Parkinson's disease. Br Med Bull **86:** 109-127.*

*Dawson TM, Dawson VL (2010). The role of parkin in familial and sporadic Parkinson's disease. Mov Disord **25 Suppl 1:** S32-39.*

*de Lau LM, Breteler MM (2006). Epidemiology of Parkinson's disease. Lancet Neurol **5**(6)**:** 525-535.*

*de Rijk MC, Launer LJ, Berger K, Breteler MM, Dartigues JF, Baldereschi M, et al. (2000). Prevalence of Parkinson's disease in Europe: A collaborative study of population-based cohorts. Neurologic Diseases in the Elderly Research Group. Neurology **54**(11 Suppl 5)**:** S21-23.*

*de Winter F, Kwok JC, Fawcett JW, Vo TT, Carulli D, Verhaagen J (2016). The Chemorepulsive Protein Semaphorin 3A and Perineuronal Net-Mediated Plasticity. Neural plasticity **2016:** 3679545.*

*De Wit J, De Winter F, Klooster J, Verhaagen J (2005). Semaphorin 3A displays a punctate distribution on the surface of neuronal cells and interacts with proteoglycans in the extracellular matrix. Mol Cell Neurosci **29**(1)**:** 40-55.*

*Deepa SS, Carulli D, Galtrey C, Rhodes K, Fukuda J, Mikami T, et al. (2006). Composition of perineuronal net extracellular matrix in rat brain: a different disaccharide composition for the net-associated proteoglycans. J Biol Chem **281**(26)**:** 17789-17800.*

*Del-Bel E, Padovan-Neto FE, Bortolanza M, Tumas V, Aguiar AS, Jr., Raisman-Vozari R, et al. (2015). Nitric oxide, a new player in L-DOPA-induced dyskinesia? Front Biosci (Elite Ed) **7:** 168-192.*

*DeWitt DA, Richey PL, Praprotnik D, Silver J, Perry G (1994). Chondroitin sulfate proteoglycans are a common component of neuronal inclusions and astrocytic reaction in neurodegenerative diseases. Brain Res **656**(1)**:** 205-209.*

*Dexter DT, Carayon A, Vidailhet M, Ruberg M, Agid F, Agid Y, et al. (1990). Decreased ferritin levels in brain in Parkinson's disease. J Neurochem **55**(1)**:** 16-20.*

*Dexter DT, Carter CJ, Wells FR, Javoy-Agid F, Agid Y, Lees A, et al. (1989a). Basal lipid peroxidation in substantia nigra is increased in Parkinson's disease. J Neurochem **52**(2)**:** 381-389.*

*Dexter DT, Wells FR, Lees AJ, Agid F, Agid Y, Jenner P, et al. (1989b). Increased nigral iron content and alterations in other metal ions occurring in brain in Parkinson's disease. J Neurochem **52**(6)**:** 1830-1836.*

*Di Monte DA (2003). The environment and Parkinson's disease: is the nigrostriatal system preferentially targeted by neurotoxins? Lancet Neurol **2**(9)**:** 531-538.*

*Diao J, Burre J, Vivona S, Cipriano DJ, Sharma M, Kyoung M, et al. (2013). Native alpha-synuclein induces clustering of synaptic-vesicle mimics via binding to phospholipids and synaptobrevin-2/VAMP2. eLife **2:** e00592.*

*Diaz-Martinez NE, Tamariz E, Diaz NF, Garcia-Pena CM, Varela-Echavarria A, Velasco I (2013). Recovery From Experimental Parkinsonism by Semaphorin-guided Axonal Growth of Grafted Dopamine Neurons. Mol Ther.*

*Dick G, Tan CL, Alves JN, Ehlert EM, Miller GM, Hsieh-Wilson LC, et al. (2013). Semaphorin 3A binds to the perineuronal nets via chondroitin sulfate type E motifs in rodent brains. J Biol Chem **288**(38): 27384-27395.*

*Ding JB, Guzman JN, Peterson JD, Goldberg JA, Surmeier DJ (2010). Thalamic gating of corticostriatal signaling by cholinergic interneurons. Neuron **67**(2): 294-307.*

*Ding Y, Restrepo J, Won L, Hwang DY, Kim KS, Kang UJ (2007). Chronic 3,4-dihydroxyphenylalanine treatment induces dyskinesia in aphakia mice, a novel genetic model of Parkinson's disease. Neurobiol Dis **27**(1): 11-23.*

*Ding Y, Won L, Britt JP, Lim SA, McGehee DS, Kang UJ (2011). Enhanced striatal cholinergic neuronal activity mediates L-DOPA-induced dyskinesia in parkinsonian mice. Proc Natl Acad Sci U S A **108**(2): 840-845.*

*Dityatev A, Bruckner G, Dityateva G, Grosche J, Kleene R, Schachner M (2007). Activity-dependent formation and functions of chondroitin sulfate-rich extracellular matrix of perineuronal nets. Dev Neurobiol **67**(5): 570-588.*

*Domanskyi A, Saarma M, Airavaara M (2015). Prospects of Neurotrophic Factors for Parkinson's Disease: Comparison of Protein and Gene Therapy. Human gene therapy **26**(8): 550-559.*

*Dopeso-Reyes IG, Rico AJ, Roda E, Sierra S, Pignataro D, Lanz M, et al. (2014). Calbindin content and differential vulnerability of midbrain efferent dopaminergic neurons in macaques. Front Neuroanat **8:** 146.*

*Dorsey ER, Constantinescu R, Thompson JP, Biglan KM, Holloway RG, Kieburtz K, et al. (2007). Projected number of people with Parkinson disease in the most populous nations, 2005 through 2030. Neurology **68**(5): 384-386.*

*Dougherty KD, Milner TA (1999). p75NTR immunoreactivity in the rat dentate gyrus is mostly within presynaptic profiles but is also found in some astrocytic and postsynaptic profiles. J Comp Neurol **407**(1): 77-91.*

*Duty S, Jenner P (2011). Animal models of Parkinson's disease: a source of novel treatments and clues to the cause of the disease. Br J Pharmacol **164**(4): 1357-1391.*

*Earle KM (1968). Studies on Parkinson's disease including x-ray fluorescent spectroscopy of formalin fixed brain tissue. Journal of neuropathology and experimental neurology **27**(1): 1-14.*

*Ekstrand MI, Galter D (2009). The MitoPark Mouse - an animal model of Parkinson's disease with impaired respiratory chain function in dopamine neurons. Parkinsonism Relat Disord **15 Suppl 3:** S185-188.*

*Emanuele M, Chieregatti E (2015). Mechanisms of alpha-synuclein action on neurotransmission: cell-autonomous and non-cell autonomous role. Biomolecules **5**(2): 865-892.*

*Encarnacion EV, Hauser RA (2008). Levodopa-induced dyskinesias in Parkinson's disease: etiology, impact on quality of life, and treatments. Eur Neurol **60**(2): 57-66.*

*Erikson KM, Aschner M (2003). Manganese neurotoxicity and glutamate-GABA interaction.*

*Neurochem Int* ***43****(4-5)****:*** *475-480.*

*Eusebio A, Thevathasan W, Doyle Gaynor L, Pogosyan A, Bye E, Foltynie T, et al. (2011). Deep brain stimulation can suppress pathological synchronisation in parkinsonian patients. J Neurol Neurosurg Psychiatry* ***82****(5)****:*** *569-573.*

*Eve DJ, Nisbet AP, Kingsbury AE, Hewson EL, Daniel SE, Lees AJ, et al. (1998). Basal ganglia neuronal nitric oxide synthase mRNA expression in Parkinson's disease. Brain Res Mol Brain Res* ***63****(1)****:*** *62-71.*

*Factor SA, Molho ES, Podskalny GD, Brown D (1995). Parkinson's disease: drug-induced psychiatric states. Adv Neurol* ***65:*** *115-138.*

*Fahn S, Oakes D, Shoulson I, Kieburtz K, Rudolph A, Lang A, et al. (2004). Levodopa and the progression of Parkinson's disease. N Engl J Med* ***351****(24)****:*** *2498-2508.*

*Farhoudi M, Taheraghdam A, Farid GA, Talebi M, Pashapou A, Majidi J, et al. (2012). Serum iron and ferritin level in idiopathic Parkinson. Pakistan journal of biological sciences : PJBS* ***15****(22)****:*** *1094-1097.*

*Faucheux BA, Bonnet AM, Agid Y, Hirsch EC (1999). Blood vessels change in the mesencephalon of patients with Parkinson's disease. Lancet* ***353****(9157)****:*** *981-982.*

*Fauvel B, Groussard M, Chetelat G, Fouquet M, Landeau B, Eustache F, et al. (2014). Morphological brain plasticity induced by musical expertise is accompanied by modulation of functional connectivity at rest. Neuroimage* ***90:*** *179-188.*

*Fiorentino DF, Bond MW, Mosmann TR (1989). Two types of mouse T helper cell. IV. Th2 clones secrete a factor that inhibits cytokine production by Th1 clones. J Exp Med* ***170****(6)****:*** *2081-2095.*

*Fisher D, Xing B, Dill J, Li H, Hoang HH, Zhao Z, et al. (2011). Leukocyte common antigen-related phosphatase is a functional receptor for chondroitin sulfate proteoglycan axon growth inhibitors. J Neurosci* ***31****(40)****:*** *14051-14066.*

*Fitch MT, Silver J (1997). Activated macrophages and the blood-brain barrier: inflammation after CNS injury leads to increases in putative inhibitory molecules. Exp Neurol* ***148****(2)****:*** *587-603.*

*Fletcher AM, Kowalczyk TH, Padegimas L, Cooper MJ, Yurek DM (2011). Transgene expression in the striatum following intracerebral injections of DNA nanoparticles encoding for human glial cell line-derived neurotrophic factor. Neuroscience* ***194:*** *220-226.*

*Foffani G, Priori A, Egidi M, Rampini P, Tamma F, Caputo E, et al. (2003). 300-Hz subthalamic oscillations in Parkinson's disease. Brain* ***126****(Pt 10)****:*** *2153-2163.*

*Fornai F, Schluter OM, Lenzi P, Gesi M, Ruffoli R, Ferrucci M, et al. (2005). Parkinson-like syndrome induced by continuous MPTP infusion: convergent roles of the ubiquitin-proteasome system and alpha-synuclein. Proc Natl Acad Sci U S A* ***102****(9)****:*** *3413-3418.*

*Fowler JS, Volkow ND, Logan J, Wang GJ, MacGregor RR, Schyler D, et al. (1994). Slow recovery of human brain MAO B after L-deprenyl (Selegeline) withdrawal. Synapse* ***18****(2)****:*** *86-93.*

*Fox SH, Katzenschlager R, Lim SY, Ravina B, Seppi K, Coelho M, et al. (2011). The Movement Disorder Society Evidence-Based Medicine Review Update: Treatments for the motor symptoms of Parkinson's disease. Mov Disord* ***26 Suppl 3:*** *S2-41.*

*Francardo V, Cenci MA (2014). Investigating the molecular mechanisms of L-DOPA-induced dyskinesia in the mouse. Parkinsonism Relat Disord **20 Suppl 1:** S20-22.*

*Francardo V, Recchia A, Popovic N, Andersson D, Nissbrandt H, Cenci MA (2011). Impact of the lesion procedure on the profiles of motor impairment and molecular responsiveness to L-DOPA in the 6-hydroxydopamine mouse model of Parkinson's disease. Neurobiol Dis **42**(3)**:** 327-340.*

*Frim DM, Uhler TA, Galpern WR, Beal MF, Breakefield XO, Isacson O (1994). Implanted fibroblasts genetically engineered to produce brain-derived neurotrophic factor prevent 1-methyl-4-phenylpyridinium toxicity to dopaminergic neurons in the rat. Proc Natl Acad Sci U S A **91**(11)**:** 5104-5108.*

*Fukushima T, Tan X, Luo Y, Kanda H (2010). Relationship between blood levels of heavy metals and Parkinson's disease in China. Neuroepidemiology **34**(1)**:** 18-24.*

*Gage GJ, Stoetzner CR, Wiltschko AB, Berke JD (2010). Selective activation of striatal fast-spiking interneurons during choice execution. Neuron **67**(3)**:** 466-479.*

*Galtrey CM, Asher RA, Nothias F, Fawcett JW (2007). Promoting plasticity in the spinal cord with chondroitinase improves functional recovery after peripheral nerve repair. Brain **130**(Pt 4)**:** 926-939.*

*Galtrey CM, Kwok JC, Carulli D, Rhodes KE, Fawcett JW (2008). Distribution and synthesis of extracellular matrix proteoglycans, hyaluronan, link proteins and tenascin-R in the rat spinal cord. Eur J Neurosci **27**(6)**:** 1373-1390.*

*Gama CI, Hsieh-Wilson LC (2005). Chemical approaches to deciphering the glycosaminoglycan code. Curr Opin Chem Biol **9**(6)**:** 609-619.*

*Gatto EM, Riobo NA, Carreras MC, Chernavsky A, Rubio A, Satz ML, et al. (2000). Overexpression of neutrophil neuronal nitric oxide synthase in Parkinson's disease. Nitric Oxide **4**(5)**:** 534-539.*

*Genovese CR, Lazar NA, Nichols T (2002). Thresholding of statistical maps in functional neuroimaging using the false discovery rate. Neuroimage **15**(4)**:** 870-878.*

*Gerhard A (2013). Imaging of neuroinflammation in parkinsonian syndromes with positron emission tomography. Curr Neurol Neurosci Rep **13**(12)**:** 405.*

*Gibrat C, Saint-Pierre M, Bousquet M, Levesque D, Rouillard C, Cicchetti F (2009). Differences between subacute and chronic MPTP mice models: investigation of dopaminergic neuronal degeneration and alpha-synuclein inclusions. J Neurochem **109**(5)**:** 1469-1482.*

*Gil SJ, Park CH, Lee JE, Minn YK, Koh HC (2011). Positive association between striatal serotonin level and abnormal involuntary movements in chronic L-DOPA-treated hemiparkinsonian rats. Brain Res Bull **84**(2)**:** 151-156.*

*Gilbert RJ, McKeon RJ, Darr A, Calabro A, Hascall VC, Bellamkonda RV (2005). CS-4,6 is differentially upregulated in glial scar and is a potent inhibitor of neurite extension. Mol Cell Neurosci **29**(4)**:** 545-558.*

*Gill SS, Patel NK, Hotton GR, O'Sullivan K, McCarter R, Bunnage M, et al. (2003). Direct brain infusion of glial cell line-derived neurotrophic factor in Parkinson disease. Nat Med **9**(5)**:** 589-*

*595.*

*Glajch KE, Fleming SM, Surmeier DJ, Osten P (2012). Sensorimotor assessment of the unilateral 6-hydroxydopamine mouse model of Parkinson's disease. Behav Brain Res **230**(2): 309-316.*

*Glinka Y, Gassen M, Youdim MB (1997). Mechanism of 6-hydroxydopamine neurotoxicity. J Neural Transm Suppl **50:** 55-66.*

*Goldberg MS, Lansbury PT, Jr. (2000). Is there a cause-and-effect relationship between alpha-synuclein fibrillization and Parkinson's disease? Nat Cell Biol **2**(7): E115-119.*

*Goldstein DS, Jinsmaa Y, Sullivan P, Holmes C, Kopin IJ, Sharabi Y (2016). Comparison of Monoamine Oxidase Inhibitors in Decreasing Production of the Autotoxic Dopamine Metabolite 3,4-Dihydroxyphenylacetaldehyde in PC12 Cells. J Pharmacol Exp Ther **356**(2): 483-492.*

*Gorell JM, Johnson CC, Rybicki BA, Peterson EL, Kortsha GX, Brown GG, et al. (1999). Occupational exposure to manganese, copper, lead, iron, mercury and zinc and the risk of Parkinson's disease. Neurotoxicology **20**(2-3): 239-247.*

*Graham DG (1979). On the origin and significance of neuromelanin. Arch Pathol Lab Med **103**(7): 359-362.*

*Guillin O, Diaz J, Carroll P, Griffon N, Schwartz JC, Sokoloff P (2001). BDNF controls dopamine D3 receptor expression and triggers behavioural sensitization. Nature **411**(6833): 86-89.*

*Gunter TE, Gerstner B, Lester T, Wojtovich AP, Malecki J, Swarts SG, et al. (2010). An analysis of the effects of Mn2+ on oxidative phosphorylation in liver, brain, and heart mitochondria using state 3 oxidation rate assays. Toxicol Appl Pharmacol **249**(1): 65-75.*

*Halliwell B (1992). Reactive oxygen species and the central nervous system. J Neurochem **59**(5): 1609-1623.*

*Hascall VC, Morales TI, Hascall GK, Handley CJ, McQuillan DJ (1983). Biosynthesis and turnover of proteoglycans in organ culture of bovine articular cartilage. J Rheumatol Suppl **11:** 45-52.*

*Haycock JW, Becker L, Ang L, Furukawa Y, Hornykiewicz O, Kish SJ (2003). Marked disparity between age-related changes in dopamine and other presynaptic dopaminergic markers in human striatum. J Neurochem **87**(3): 574-585.*

*He Y, Le WD, Appel SH (2002). Role of Fcgamma receptors in nigral cell injury induced by Parkinson disease immunoglobulin injection into mouse substantia nigra. Exp Neurol **176**(2): 322-327.*

*Healy DG, Falchi M, O'Sullivan SS, Bonifati V, Durr A, Bressman S, et al. (2008). Phenotype, genotype, and worldwide genetic penetrance of LRRK2-associated Parkinson's disease: a case-control study. Lancet Neurol **7**(7): 583-590.*

*Hely MA, Morris JG, Reid WG, Trafficante R (2005). Sydney Multicenter Study of Parkinson's disease: non-L-dopa-responsive problems dominate at 15 years. Mov Disord **20**(2): 190-199.*

*Hendry IA (1975). The effects of axotomy on the development of the rat superior cervical ganglion. Brain Res **90**(2): 235-244.*

*Hernandez-Lopez S, Tkatch T, Perez-Garci E, Galarraga E, Bargas J, Hamm H, et al. (2000). D2*

*dopamine receptors in striatal medium spiny neurons reduce L-type Ca2+ currents and excitability via a novel PLC[beta]1-IP3-calcineurin-signaling cascade. J Neurosci **20**(24): 8987-8995.*

*Herrero MT, Levy R, Ruberg M, Luquin MR, Villares J, Guillen J, et al. (1996). Consequence of nigrostriatal denervation and L-dopa therapy on the expression of glutamic acid decarboxylase messenger RNA in the pallidum. Neurology **47**(1): 219-224.*

*Heuer A, Smith GA, Lelos MJ, Lane EL, Dunnett SB (2012). Unilateral nigrostriatal 6-hydroxydopamine lesions in mice I: motor impairments identify extent of dopamine depletion at three different lesion sites. Behav Brain Res **228**(1): 30-43.*

*Hirsch EC, Hunot S (2009). Neuroinflammation in Parkinson's disease: a target for neuroprotection? Lancet Neurol **8**(4): 382-397.*

*Ho SC, Woo J, Lee CM (1989). Epidemiologic study of Parkinson's disease in Hong Kong. Neurology **39**(10): 1314-1318.*

*Hong JY, Oh JS, Lee I, Sunwoo MK, Ham JH, Lee JE, et al. (2014). Presynaptic dopamine depletion predicts levodopa-induced dyskinesia in de novo Parkinson disease. Neurology **82**(18): 1597-1604.*

*Hong S, Dissing-Olesen L, Stevens B (2016). New insights on the role of microglia in synaptic pruning in health and disease. Curr Opin Neurobiol **36**: 128-134.*

*Howells DW, Porritt MJ, Wong JY, Batchelor PE, Kalnins R, Hughes AJ, et al. (2000). Reduced BDNF mRNA expression in the Parkinson's disease substantia nigra. Exp Neurol **166**(1): 127-135.*

*Huang WC, Kuo WC, Cherng JH, Hsu SH, Chen PR, Huang SH, et al. (2006). Chondroitinase ABC promotes axonal re-growth and behavior recovery in spinal cord injury. Biochem Biophys Res Commun **349**(3): 963-968.*

*Huck JH, Freyer D, Bottcher C, Mladinov M, Muselmann-Genschow C, Thielke M, et al. (2015). De novo expression of dopamine D2 receptors on microglia after stroke. J Cereb Blood Flow Metab **35**(11): 1804-1811.*

*Iancu R, Mohapel P, Brundin P, Paul G (2005). Behavioral characterization of a unilateral 6-OHDA-lesion model of Parkinson's disease in mice. Behav Brain Res **162**(1): 1-10.*

*Ilg R, Wohlschlager AM, Gaser C, Liebau Y, Dauner R, Woller A, et al. (2008). Gray matter increase induced by practice correlates with task-specific activation: a combined functional and morphometric magnetic resonance imaging study. J Neurosci **28**(16): 4210-4215.*

*Ito K, Enomoto H (2016). Retrograde transport of neurotrophic factor signaling: implications in neuronal development and pathogenesis. Journal of biochemistry **160**(2): 77-85.*

*Jankovic J (2008). Parkinson's disease: clinical features and diagnosis. J Neurol Neurosurg Psychiatry **79**(4): 368-376.*

*Jankovic J, Aguilar LG (2008). Current approaches to the treatment of Parkinson's disease. Neuropsychiatr Dis Treat **4**(4): 743-757.*

*Jenkinson M, Bannister P, Brady M, Smith S (2002). Improved optimization for the robust and*

*accurate linear registration and motion correction of brain images. Neuroimage **17**(2): 825-841.*

*Jenkinson M, Smith S (2001). A global optimisation method for robust affine registration of brain images. Med Image Anal **5**(2): 143-156.*

*Jenner P (2008a). Functional models of Parkinson's disease: a valuable tool in the development of novel therapies. Ann Neurol **64 Suppl 2:** S16-29.*

*Jenner P (2008b). Molecular mechanisms of L-DOPA-induced dyskinesia. Nat Rev Neurosci **9**(9): 665-677.*

*Jenner P (1996). Oxidative stress in Parkinson's disease and other neurodegenerative disorders. Pathol Biol (Paris) **44**(1): 57-64.*

*Jucaite A, Svenningsson P, Rinne JO, Cselenyi Z, Varnas K, Johnstrom P, et al. (2015). Effect of the myeloperoxidase inhibitor AZD3241 on microglia: a PET study in Parkinson's disease. Brain **138**(Pt 9): 2687-2700.*

*Kadoguchi N, Kimoto H, Yano R, Kato H, Araki T (2008). Failure of acute administration with proteasome inhibitor to provide a model of Parkinson's disease in mice. Metab Brain Dis **23**(2): 147-154.*

*Kalb RG, Hockfield S (1994). Electrical activity in the neuromuscular unit can influence the molecular development of motor neurons. Dev Biol **162**(2): 539-548.*

*Kannan K, Jain SK (2000). Oxidative stress and apoptosis. Pathophysiology **7**(3): 153-163.*

*Kaplan DR, Miller FD (1997). Signal transduction by the neurotrophin receptors. Current opinion in cell biology **9**(2): 213-221.*

*Kaplan S, Tarsy D (2013). Initial Treatment of Parkinson's Disease: An Update. Curr Treat Options Neurol.*

*Karumbaiah L, Enam SF, Brown AC, Saxena T, Betancur MI, Barker TH, et al. (2015). Chondroitin Sulfate Glycosaminoglycan Hydrogels Create Endogenous Niches for Neural Stem Cells. Bioconjugate chemistry **26**(12): 2336-2349.*

*Katzenschlager R, Sampaio C, Costa J, Lees A (2003). Anticholinergics for symptomatic management of Parkinson's disease. Cochrane Database Syst Rev(2): CD003735.*

*Kauhausen JA, Thompson LH, Parish CL (2015). Chondroitinase improves midbrain pathway reconstruction by transplanted dopamine progenitors in Parkinsonian mice. Mol Cell Neurosci **69:** 22-29.*

*Kiani C, Chen L, Wu YJ, Yee AJ, Yang BB (2002). Structure and function of aggrecan. Cell Res **12**(1): 19-32.*

*Kitada T, Asakawa S, Hattori N, Matsumine H, Yamamura Y, Minoshima S, et al. (1998). Mutations in the parkin gene cause autosomal recessive juvenile parkinsonism. Nature **392**(6676): 605-608.*

*Klein RL, Lewis MH, Muzyczka N, Meyer EM (1999). Prevention of 6-hydroxydopamine-induced rotational behavior by BDNF somatic gene transfer. Brain Res **847**(2): 314-320.*

*Kohno R, Sawada H, Kawamoto Y, Uemura K, Shibasaki H, Shimohama S (2004). BDNF is induced by wild-type alpha-synuclein but not by the two mutants, A30P or A53T, in glioma cell line. Biochem Biophys Res Commun **318**(1): 113-118.*

*Kordower JH, Bjorklund A (2013). Trophic factor gene therapy for Parkinson's disease. Mov Disord **28**(1): 96-109.*

*Kordower JH, Kanaan NM, Chu Y, Suresh Babu R, Stansell J, 3rd, Terpstra BT, et al. (2006). Failure of proteasome inhibitor administration to provide a model of Parkinson's disease in rats and monkeys. Ann Neurol **60**(2): 264-268.*

*Koshimori Y, Ko JH, Mizrahi R, Rusjan P, Mabrouk R, Jacobs MF, et al. (2015). Imaging Striatal Microglial Activation in Patients with Parkinson's Disease. PLoS One **10**(9): e0138721.*

*Kouti L, Noroozian M, Akhondzadeh S, Abdollahi M, Javadi MR, Faramarzi MA, et al. (2013). Nitric oxide and peroxynitrite serum levels in Parkinson's disease: correlation of oxidative stress and the severity of the disease. Eur Rev Med Pharmacol Sci **17**(7): 964-970.*

*Kramer ER, Aron L, Ramakers GM, Seitz S, Zhuang X, Beyer K, et al. (2007). Absence of Ret signaling in mice causes progressive and late degeneration of the nigrostriatal system. PLoS Biol **5**(3): e39.*

*Kruger R, Kuhn W, Muller T, Woitalla D, Graeber M, Kosel S, et al. (1998). Ala30Pro mutation in the gene encoding alpha-synuclein in Parkinson's disease. Nat Genet **18**(2): 106-108.*

*Kuhn AA, Kupsch A, Schneider GH, Brown P (2006). Reduction in subthalamic 8-35 Hz oscillatory activity correlates with clinical improvement in Parkinson's disease. Eur J Neurosci **23**(7): 1956-1960.*

*Kumar N, Van Gerpen JA, Bower JH, Ahlskog JE (2005). Levodopa-dyskinesia incidence by age of Parkinson's disease onset. Mov Disord **20**(3): 342-344.*

*Kumar R, Riddle L, Griffin SA, Grundt P, Newman AH, Luedtke RR (2009). Evaluation of the D3 dopamine receptor selective antagonist PG01037 on L-dopa-dependent abnormal involuntary movements in rats. Neuropharmacology **56**(6-7): 944-955.*

*Kumari U, Tan EK (2009). LRRK2 in Parkinson's disease: genetic and clinical studies from patients. FEBS J **276**(22): 6455-6463.*

*Kunikowska G, Jenner P (2001). 6-Hydroxydopamine-lesioning of the nigrostriatal pathway in rats alters basal ganglia mRNA for copper, zinc- and manganese-superoxide dismutase, but not glutathione peroxidase. Brain Res **922**(1): 51-64.*

*Kuric E, Wieloch T, Ruscher K (2013). Dopamine receptor activation increases glial cell line-derived neurotrophic factor in experimental stroke. Exp Neurol **247**: 202-208.*

*Kwok JC, Afshari F, Garcia-Alias G, Fawcett JW (2008). Proteoglycans in the central nervous system: plasticity, regeneration and their stimulation with chondroitinase ABC. Restor Neurol Neurosci **26**(2-3): 131-145.*

*Lander AD (1993). Proteoglycans in the nervous system. Curr Opin Neurobiol **3**(5): 716-723.*

*Lang AE, Gill S, Patel NK, Lozano A, Nutt JG, Penn R, et al. (2006). Randomized controlled trial of*

*intraputamenal glial cell line-derived neurotrophic factor infusion in Parkinson disease. Ann Neurol **59**(3): 459-466.*

*Langston JW, Ballard P, Tetrud JW, Irwin I (1983). Chronic Parkinsonism in humans due to a product of meperidine-analog synthesis. Science **219**(4587): 979-980.*

*Lau YS, Trobough KL, Crampton JM, Wilson JA (1990). Effects of probenecid on striatal dopamine depletion in acute and long-term 1-methyl-4-phenyl-1,2,3,6-tetrahydropyridine (MPTP)-treated mice. Gen Pharmacol **21**(2): 181-187.*

*Lee H, Leamey CA, Sawatari A (2008). Rapid reversal of chondroitin sulfate proteoglycan associated staining in subcompartments of mouse neostriatum during the emergence of behaviour. PLoS One **3**(8): e3020.*

*Lee H, McKeon RJ, Bellamkonda RV (2010). Sustained delivery of thermostabilized chABC enhances axonal sprouting and functional recovery after spinal cord injury. Proc Natl Acad Sci U S A **107**(8): 3340-3345.*

*Lees AJ (2007). Unresolved issues relating to the shaking palsy on the celebration of James Parkinson's 250th birthday. Mov Disord **22 Suppl 17:** S327-334.*

*Lees AJ, Head J, Shlomo YB (1997). Selegiline and mortality in Parkinson's disease: another view. Ann Neurol **41**(2): 282-283.*

*Lei W, Jiao Y, Del Mar N, Reiner A (2004). Evidence for differential cortical input to direct pathway versus indirect pathway striatal projection neurons in rats. J Neurosci **24**(38): 8289-8299.*

*Leroy E, Boyer R, Auburger G, Leube B, Ulm G, Mezey E, et al. (1998). The ubiquitin pathway in Parkinson's disease. Nature **395**(6701): 451-452.*

*Lesage S, Brice A (2009). Parkinson's disease: from monogenic forms to genetic susceptibility factors. Hum Mol Genet **18**(R1): R48-59.*

*Lev N, Barhum Y, Pilosof NS, Ickowicz D, Cohen HY, Melamed E, et al. (2013). DJ-1 protects against dopamine toxicity: implications for Parkinson's disease and aging. J Gerontol A Biol Sci Med Sci **68**(3): 215-225.*

*Levin J, Hogen T, Hillmer AS, Bader B, Schmidt F, Kamp F, et al. (2011). Generation of ferric iron links oxidative stress to alpha-synuclein oligomer formation. J Parkinsons Dis **1**(2): 205-216.*

*Levine JM (1994). Increased expression of the NG2 chondroitin-sulfate proteoglycan after brain injury. J Neurosci **14**(8): 4716-4730.*

*Levy R, Ashby P, Hutchison WD, Lang AE, Lozano AM, Dostrovsky JO (2002). Dependence of subthalamic nucleus oscillations on movement and dopamine in Parkinson's disease. Brain **125**(Pt 6): 1196-1209.*

*Lewitus E, Kelava I, Kalinka AT, Tomancak P, Huttner WB (2014). An adaptive threshold in mammalian neocortical evolution. PLoS Biol **12**(11): e1002000.*

*Lewy FH (1912). Paralysis agitans. I. Pathologische Anatomie **3:** 920-933.*

*Liang CL, Sinton CM, Sonsalla PK, German DC (1996). Midbrain dopaminergic neurons in the*

*mouse that contain calbindin-D28k exhibit reduced vulnerability to MPTP-induced neurodegeneration. Neurodegeneration : a journal for neurodegenerative disorders, neuroprotection, and neuroregeneration* ***5****(4):* *313-318.*

*Lin LF, Doherty DH, Lile JD, Bektesh S, Collins F (1993). GDNF: a glial cell line-derived neurotrophic factor for midbrain dopaminergic neurons. Science* ***260****(5111):* *1130-1132.*

*Lin R, Rosahl TW, Whiting PJ, Fawcett JW, Kwok JC (2011). 6-Sulphated chondroitins have a positive influence on axonal regeneration. PLoS One* ***6****(7):* *e21499.*

*Linazasoro G (2005). New ideas on the origin of L-dopa-induced dyskinesias: age, genes and neural plasticity. Trends Pharmacol Sci* ***26****(8):* *391-397.*

*Lindahl M, Saarma M, Lindholm P (2016). Unconventional neurotrophic factors CDNF and MANF: Structure, physiological functions and therapeutic potential. Neurobiol Dis.*

*Lindholm P, Saarma M (2010). Novel CDNF/MANF family of neurotrophic factors. Dev Neurobiol* ***70****(5):* *360-371.*

*Liou HH, Tsai MC, Chen CJ, Jeng JS, Chang YC, Chen SY, et al. (1997). Environmental risk factors and Parkinson's disease: a case-control study in Taiwan. Neurology* ***48****(6):* *1583-1588.*

*Litchfield DW (2003). Protein kinase CK2: structure, regulation and role in cellular decisions of life and death. Biochem J* ***369****(Pt 1):* *1-15.*

*Liu B, Gao HM, Hong JS (2003). Parkinson's disease and exposure to infectious agents and pesticides and the occurrence of brain injuries: role of neuroinflammation. Environ Health Perspect* ***111****(8):* *1065-1073.*

*Liu H, Iacono RP, Szalay AA (2001). Detection of GDNF secretion in glial cell culture and from transformed cell implants in the brains of live animals. Mol Genet Genomics* ***266****(4):* *614-623.*

*Lohr KM, Chen M, Hoffman CA, McDaniel MJ, Stout KA, Dunn AR, et al. (2016). Vesicular monoamine transporter 2 (VMAT2) level regulates MPTP vulnerability and clearance of excess dopamine in mouse striatal terminals. Toxicol Sci.*

*Lotia M, Jankovic J (2016). New and Emerging Medical Therapies in Parkinson's Disease. Expert Opin Pharmacother: 1-15.*

*Lundblad M, Andersson M, Winkler C, Kirik D, Wierup N, Cenci MA (2002). Pharmacological validation of behavioural measures of akinesia and dyskinesia in a rat model of Parkinson's disease. Eur J Neurosci* ***15****(1):* *120-132.*

*Luthman J, Fredriksson A, Sundstrom E, Jonsson G, Archer T (1989). Selective lesion of central dopamine or noradrenaline neuron systems in the neonatal rat: motor behavior and monoamine alterations at adult stage. Behav Brain Res* ***33****(3):* *267-277.*

*Maeda T, Nagata K, Yoshida Y, Kannari K (2005). Serotonergic hyperinnervation into the dopaminergic denervated striatum compensates for dopamine conversion from exogenously administered l-DOPA. Brain Res* ***1046****(1-2):* *230-233.*

*Mandel S, Grunblatt E, Riederer P, Amariglio N, Jacob-Hirsch J, Rechavi G, et al. (2005). Gene expression profiling of sporadic Parkinson's disease substantia nigra pars compacta reveals impairment of ubiquitin-proteasome subunits, SKP1A, aldehyde dehydrogenase, and chaperone*

*HSC-70. Ann N Y Acad Sci **1053:** 356-375.*

*Manning-Bog AB, Reaney SH, Chou VP, Johnston LC, McCormack AL, Johnston J, et al. (2006). Lack of nigrostriatal pathology in a rat model of proteasome inhibition. Ann Neurol **60**(2): 256-260.*

*Marchitti SA, Deitrich RA, Vasiliou V (2007). Neurotoxicity and metabolism of the catecholamine-derived 3,4-dihydroxyphenylacetaldehyde and 3,4-dihydroxyphenylglycolaldehyde: the role of aldehyde dehydrogenase. Pharmacol Rev **59**(2): 125-150.*

*Martin D, Miller G, Fischer N, Diz D, Cullen T, Russell D (1996). Glial cell line-derived neurotrophic factor: the lateral cerebral ventricle as a site of administration for stimulation of the substantia nigra dopamine system in rats. Eur J Neurosci **8**(6): 1249-1255.*

*Maruyama W, Naoi M (2013). ''70th Birthday Professor Riederer'' induction of glial cell line-derived and brain-derived neurotrophic factors by rasagiline and (-)deprenyl: a way to a disease-modifying therapy? J Neural Transm (Vienna) **120**(1): 83-89.*

*Maruyama W, Nitta A, Shamoto-Nagai M, Hirata Y, Akao Y, Yodim M, et al. (2004). N-Propargyl-1 (R)-aminoindan, rasagiline, increases glial cell line-derived neurotrophic factor (GDNF) in neuroblastoma SH-SY5Y cells through activation of NF-kappaB transcription factor. Neurochem Int **44**(6): 393-400.*

*Massey JM, Hubscher CH, Wagoner MR, Decker JA, Amps J, Silver J, et al. (2006). Chondroitinase ABC digestion of the perineuronal net promotes functional collateral sprouting in the cuneate nucleus after cervical spinal cord injury. J Neurosci **26**(16): 4406-4414.*

*Masuda-Suzukake M, Nonaka T, Hosokawa M, Oikawa T, Arai T, Akiyama H, et al. (2013). Prion-like spreading of pathological alpha-synuclein in brain. Brain **136**(Pt 4): 1128-1138.*

*Matsuda N, Sato S, Shiba K, Okatsu K, Saisho K, Gautier CA, et al. (2010). PINK1 stabilized by mitochondrial depolarization recruits Parkin to damaged mitochondria and activates latent Parkin for mitophagy. J Cell Biol **189**(2): 211-221.*

*McCormack AL, Di Monte DA, Delfani K, Irwin I, DeLanney LE, Langston WJ, et al. (2004). Aging of the nigrostriatal system in the squirrel monkey. J Comp Neurol **471**(4): 387-395.*

*McNaught KS, Belizaire R, Isacson O, Jenner P, Olanow CW (2003). Altered proteasomal function in sporadic Parkinson's disease. Exp Neurol **179**(1): 38-46.*

*McNaught KS, Bjorklund LM, Belizaire R, Isacson O, Jenner P, Olanow CW (2002). Proteasome inhibition causes nigral degeneration with inclusion bodies in rats. Neuroreport **13**(11): 1437-1441.*

*McNaught KS, Jenner P (2001). Proteasomal function is impaired in substantia nigra in Parkinson's disease. Neurosci Lett **297**(3): 191-194.*

*McNaught KS, Perl DP, Brownell AL, Olanow CW (2004). Systemic exposure to proteasome inhibitors causes a progressive model of Parkinson's disease. Ann Neurol **56**(1): 149-162.*

*Mehanna R, Moore S, Hou JG, Sarwar AI, Lai EC (2014). Comparing clinical features of young onset, middle onset and late onset Parkinson's disease. Parkinsonism Relat Disord **20**(5): 530-534.*

*Mela F, Millan MJ, Brocco M, Morari M (2010). The selective D(3) receptor antagonist, S33084, improves parkinsonian-like motor dysfunction but does not affect L-DOPA-induced dyskinesia in 6-hydroxydopamine hemi-lesioned rats. Neuropharmacology **58**(2): 528-536.*

*Meredith GE, Totterdell S, Potashkin JA, Surmeier DJ (2008). Modeling PD pathogenesis in mice: advantages of a chronic MPTP protocol. Parkinsonism Relat Disord **14 Suppl 2:** S112-115.*

*Meyer-Puttlitz B, Junker E, Margolis RU, Margolis RK (1996). Chondroitin sulfate proteoglycans in the developing central nervous system. II. Immunocytochemical localization of neurocan and phosphacan. J Comp Neurol **366**(1): 44-54.*

*Mi R, Chen W, Hoke A (2007). Pleiotrophin is a neurotrophic factor for spinal motor neurons. Proc Natl Acad Sci U S A **104**(11): 4664-4669.*

*Micieli G, Martignoni E, Cavallini A, Pacchetti C, Rossi F, Horowski R, et al. (1996). Lisuride and bromocryptine in L-Dopa stable-responder parkinsonian patients: a comparative, double-blind evaluation of cardiopressor and neurochemical effects. Funct Neurol **11**(6): 317-325.*

*Mikami T, Yasunaga D, Kitagawa H (2009). Contactin-1 is a functional receptor for neuroregulatory chondroitin sulfate-E. J Biol Chem **284**(7): 4494-4499.*

*Milatovic D, Zaja-Milatovic S, Gupta RC, Yu Y, Aschner M (2009). Oxidative damage and neurodegeneration in manganese-induced neurotoxicity. Toxicol Appl Pharmacol **240**(2): 219-225.*

*Milev P, Maurel P, Chiba A, Mevissen M, Popp S, Yamaguchi Y, et al. (1998). Differential regulation of expression of hyaluronan-binding proteoglycans in developing brain: aggrecan, versican, neurocan, and brevican. Biochem Biophys Res Commun **247**(2): 207-212.*

*Miyata S, Komatsu Y, Yoshimura Y, Taya C, Kitagawa H (2012). Persistent cortical plasticity by upregulation of chondroitin 6-sulfation. Nat Neurosci **15**(3): 414-422, S411-412.*

*Mizuta I, Ohta M, Ohta K, Nishimura M, Mizuta E, Hayashi K, et al. (2000). Selegiline and desmethylselegiline stimulate NGF, BDNF, and GDNF synthesis in cultured mouse astrocytes. Biochem Biophys Res Commun **279**(3): 751-755.*

*Molho ES, Factor SA, Weiner WJ, Sanchez-Ramos JR, Singer C, Shulman L, et al. (1995). The use of pramipexole, a novel dopamine (DA) agonist, in advanced Parkinson's disease. J Neural Transm Suppl **45:** 225-230.*

*Monnier PP, Sierra A, Schwab JM, Henke-Fahle S, Mueller BK (2003). The Rho/ROCK pathway mediates neurite growth-inhibitory activity associated with the chondroitin sulfate proteoglycans of the CNS glial scar. Mol Cell Neurosci **22**(3): 319-330.*

*Montgomery EB, Jr. (1995). Heavy metals and the etiology of Parkinson's disease and other movement disorders. Toxicology **97**(1-3): 3-9.*

*Moon LD, Asher RA, Rhodes KE, Fawcett JW (2001). Regeneration of CNS axons back to their target following treatment of adult rat brain with chondroitinase ABC. Nat Neurosci **4**(5): 465-466.*

*Moon LD, Asher RA, Rhodes KE, Fawcett JW (2002). Relationship between sprouting axons, proteoglycans and glial cells following unilateral nigrostriatal axotomy in the adult rat.*

*Neuroscience **109**(1): 101-117.*

*Moos T (2002). Brain iron homeostasis. Dan Med Bull **49**(4): 279-301.*

*Morano A, Jimenez-Jimenez FJ, Molina JA, Antolin MA (1994). Risk-factors for Parkinson's disease: case-control study in the province of Caceres, Spain. Acta Neurol Scand **89**(3): 164-170.*

*Morawski M, Bruckner G, Arendt T, Matthews RT (2012). Aggrecan: Beyond cartilage and into the brain. Int J Biochem Cell Biol **44**(5): 690-693.*

*Morawski M, Bruckner MK, Riederer P, Bruckner G, Arendt T (2004). Perineuronal nets potentially protect against oxidative stress. Exp Neurol **188**(2): 309-315.*

*Moreau C, Delval A, Tiffreau V, Defebvre L, Dujardin K, Duhamel A, et al. (2013). Memantine for axial signs in Parkinson's disease: a randomised, double-blind, placebo-controlled pilot study. J Neurol Neurosurg Psychiatry **84**(5): 552-555.*

*Morgante F, Espay AJ, Gunraj C, Lang AE, Chen R (2006). Motor cortex plasticity in Parkinson's disease and levodopa-induced dyskinesias. Brain **129**(Pt 4): 1059-1069.*

*Morgenstern DA, Asher RA, Fawcett JW (2002). Chondroitin sulphate proteoglycans in the CNS injury response. Prog Brain Res **137:** 313-332.*

*Morissette M, Dridi M, Calon F, Hadj Tahar A, Meltzer LT, Bedard PJ, et al. (2006). Prevention of levodopa-induced dyskinesias by a selective NR1A/2B N-methyl-D-aspartate receptor antagonist in parkinsonian monkeys: implication of preproenkephalin. Mov Disord **21**(1): 9-17.*

*Moro E, Lang AE (2006). Criteria for deep-brain stimulation in Parkinson's disease: review and analysis. Expert Rev Neurother **6**(11): 1695-1705.*

*Mountney A, Zahner MR, Sturgill ER, Riley CJ, Aston JW, Oudega M, et al. (2013). Sialidase, chondroitinase ABC, and combination therapy after spinal cord contusion injury. J Neurotrauma **30**(3): 181-190.*

*Muthane UB, Swamy HS, Satishchandra P, Subhash MN, Rao S, Subbakrishna D (1994). Early onset Parkinson's disease: are juvenile- and young-onset different? Mov Disord **9**(5): 539-544.*

*Nambu A, Tokuno H, Takada M (2002). Functional significance of the cortico-subthalamo-pallidal 'hyperdirect' pathway. Neurosci Res **43**(2): 111-117.*

*Naoi M, Maruyama W (2010). Monoamine oxidase inhibitors as neuroprotective agents in age-dependent neurodegenerative disorders. Current pharmaceutical design **16**(25): 2799-2817.*

*Neitz A, Mergia E, Eysel UT, Koesling D, Mittmann T (2011). Presynaptic nitric oxide/cGMP facilitates glutamate release via hyperpolarization-activated cyclic nucleotide-gated channels in the hippocampus. Eur J Neurosci **33**(9): 1611-1621.*

*Neve KA, Seamans JK, Trantham-Davidson H (2004). Dopamine receptor signaling. J Recept Signal Transduct Res **24**(3): 165-205.*

*Niederost BP, Zimmermann DR, Schwab ME, Bandtlow CE (1999). Bovine CNS myelin contains neurite growth-inhibitory activity associated with chondroitin sulfate proteoglycans. J Neurosci **19**(20): 8979-8989.*

*Niranjan R (2014). The role of inflammatory and oxidative stress mechanisms in the pathogenesis of Parkinson's disease: focus on astrocytes. Mol Neurobiol **49**(1): 28-38.*

*Nutt JG (1990). Levodopa-induced dyskinesia: review, observations, and speculations. Neurology **40**(2): 340-345.*

*Nutt JG, Woodward WR, Carter JH, Gancher ST (1992). Effect of long-term therapy on the pharmacodynamics of levodopa. Relation to on-off phenomenon. Arch Neurol **49**(11): 1123-1130.*

*Oberlander U, Pletinckx K, Dohler A, Muller N, Lutz MB, Arzberger T, et al. (2011). Neuromelanin is an immune stimulator for dendritic cells in vitro. BMC Neurosci **12:** 116.*

*Obeso JA, Marin C, Rodriguez-Oroz C, Blesa J, Benitez-Temino B, Mena-Segovia J, et al. (2008). The basal ganglia in Parkinson's disease: current concepts and unexplained observations. Ann Neurol **64 Suppl 2:** S30-46.*

*Ogawa T, Hagihara K, Suzuki M, Yamaguchi Y (2001). Brevican in the developing hippocampal fimbria: differential expression in myelinating oligodendrocytes and adult astrocytes suggests a dual role for brevican in central nervous system fiber tract development. J Comp Neurol **432**(3): 285-295.*

*Ohlin KE, Francardo V, Lindgren HS, Sillivan SE, O'Sullivan SS, Luksik AS, et al. (2011). Vascular endothelial growth factor is upregulated by L-dopa in the parkinsonian brain: implications for the development of dyskinesia. Brain **134**(Pt 8): 2339-2357.*

*Olanow CW (2000). Tolcapone and hepatotoxic effects. Tasmar Advisory Panel. Arch Neurol **57**(2): 263-267.*

*Olanow CW, Kieburtz K, Odin P, Espay AJ, Standaert DG, Fernandez HH, et al. (2014). Continuous intrajejunal infusion of levodopa-carbidopa intestinal gel for patients with advanced Parkinson's disease: a randomised, controlled, double-blind, double-dummy study. Lancet Neurol **13**(2): 141-149.*

*Olanow CW, Obeso JA, Stocchi F (2006). Continuous dopamine-receptor treatment of Parkinson's disease: scientific rationale and clinical implications. Lancet Neurol **5**(8): 677-687.*

*Oliveri RL, Annesi G, Zappia M, Civitelli D, Montesanti R, Branca D, et al. (1999). Dopamine D2 receptor gene polymorphism and the risk of levodopa-induced dyskinesias in PD. Neurology **53**(7): 1425-1430.*

*Olney JW, Ho OL, Rhee V (1971). Cytotoxic effects of acidic and sulphur containing amino acids on the infant mouse central nervous system. Exp Brain Res **14**(1): 61-76.*

*Onyango IG, Tuttle JB, Bennett JP, Jr. (2005). Brain-derived growth factor and glial cell line-derived growth factor use distinct intracellular signaling pathways to protect PD cybrids from H2O2-induced neuronal death. Neurobiol Dis **20**(1): 141-154.*

*Oohira A, Matsui F, Katoh-Semba R (1991). Inhibitory effects of brain chondroitin sulfate proteoglycans on neurite outgrowth from PC12D cells. J Neurosci **11**(3): 822-827.*

*Oohira A, Matsui F, Watanabe E, Kushima Y, Maeda N (1994). Developmentally regulated expression of a brain specific species of chondroitin sulfate proteoglycan, neurocan, identified with a monoclonal antibody IG2 in the rat cerebrum. Neuroscience **60**(1): 145-157.*

*Orrenius S, Zhivotovsky B, Nicotera P (2003). Regulation of cell death: the calcium-apoptosis link. Nat Rev Mol Cell Biol **4**(7): 552-565.*

*Ouattara B, Gasparini F, Morissette M, Gregoire L, Samadi P, Gomez-Mancilla B, et al. (2010). Effect of L-Dopa on metabotropic glutamate receptor 5 in the brain of parkinsonian monkeys. J Neurochem **113**(3): 715-724.*

*Padovan-Neto FE, Echeverry MB, Chiavegatto S, Del-Bel E (2011). Nitric Oxide Synthase Inhibitor Improves De Novo and Long-Term l-DOPA-Induced Dyskinesia in Hemiparkinsonian Rats. Front Syst Neurosci **5:** 40.*

*Pahwa R, Tanner CM, Hauser RA, Sethi K, Isaacson S, Truong D, et al. (2015). Amantadine extended release for levodopa-induced dyskinesia in Parkinson's disease (EASED Study). Mov Disord **30**(6): 788-795.*

*Pal PK, Samii A, Calne DB (1999). Manganese neurotoxicity: a review of clinical features, imaging and pathology. Neurotoxicology **20**(2-3): 227-238.*

*Paolicelli RC, Bolasco G, Pagani F, Maggi L, Scianni M, Panzanelli P, et al. (2011a). Synaptic pruning by microglia is necessary for normal brain development. Science **333**(6048): 1456-1458.*

*Paolicelli RC, Gross CT (2011b). Microglia in development: linking brain wiring to brain environment. Neuron Glia Biol **7**(1): 77-83.*

*Parkin SG, Gregory RP, Scott R, Bain P, Silburn P, Hall B, et al. (2002). Unilateral and bilateral pallidotomy for idiopathic Parkinson's disease: a case series of 115 patients. Mov Disord **17**(4): 682-692.*

*Parkinson J. (2002). An essay on the shaking palsy. 1817. J Neuropsychiatry Clin Neurosci **14**(2): 223-36.*

*Patel NK, Bunnage M, Plaha P, Svendsen CN, Heywood P, Gill SS (2005). Intraputamenal infusion of glial cell line-derived neurotrophic factor in PD: a two-year outcome study. Ann Neurol **57**(2): 298-302.*

*Paulus W, Baur I, Dours-Zimmermann MT, Zimmermann DR (1996). Differential expression of versican isoforms in brain tumors. Journal of neuropathology and experimental neurology **55**(5): 528-533.*

*Penc SF, Pomahac B, Winkler T, Dorschner RA, Eriksson E, Herndon M, et al. (1998). Dermatan sulfate released after injury is a potent promoter of fibroblast growth factor-2 function. J Biol Chem **273**(43): 28116-28121.*

*Perl DP, Olanow CW (2007). The neuropathology of manganese-induced Parkinsonism. Journal of neuropathology and experimental neurology **66**(8): 675-682.*

*Petrova P, Raibekas A, Pevsner J, Vigo N, Anafi M, Moore MK, et al. (2003). MANF: a new mesencephalic, astrocyte-derived neurotrophic factor with selectivity for dopaminergic neurons. J Mol Neurosci **20**(2): 173-188.*

*Pisani A, Centonze D, Bernardi G, Calabresi P (2005). Striatal synaptic plasticity: implications for motor learning and Parkinson's disease. Mov Disord **20**(4): 395-402.*

*Pizzorusso T, Medini P, Berardi N, Chierzi S, Fawcett JW, Maffei L (2002). Reactivation of ocular dominance plasticity in the adult visual cortex. Science **298**(5596)**:** 1248-1251.*

*Pont-Sunyer C, Hotter A, Gaig C, Seppi K, Compta Y, Katzenschlager R, et al. (2015). The onset of nonmotor symptoms in Parkinson's disease (the ONSET PD study). Mov Disord **30**(2)**:** 229-237.*

*Postuma RB, Aarsland D, Barone P, Burn DJ, Hawkes CH, Oertel W, et al. (2012). Identifying prodromal Parkinson's disease: pre-motor disorders in Parkinson's disease. Mov Disord **27**(5)**:** 617-626.*

*Pouly S, Becher B, Blain M, Antel JP (1999). Expression of a homologue of rat NG2 on human microglia. Glia **27**(3)**:** 259-268.*

*Przedborski S (2010). Inflammation and Parkinson's disease pathogenesis. Mov Disord **25 Suppl 1:** S55-57.*

*Quinn N (1995). Drug treatment of Parkinson's disease. BMJ **310**(6979)**:** 575-579.*

*Quinn N, Critchley P, Marsden CD (1987). Young onset Parkinson's disease. Mov Disord **2**(2)**:** 73-91.*

*Rakovic A, Grunewald A, Kottwitz J, Bruggemann N, Pramstaller PP, Lohmann K, et al. (2011). Mutations in PINK1 and Parkin impair ubiquitination of Mitofusins in human fibroblasts. PLoS One **6**(3)**:** e16746.*

*Rascol O, Brooks DJ, Korczyn AD, De Deyn PP, Clarke CE, Lang AE (2000). A five-year study of the incidence of dyskinesia in patients with early Parkinson's disease who were treated with ropinirole or levodopa. N Engl J Med **342**(20)**:** 1484-1491.*

*Reichardt LF (2006). Neurotrophin-regulated signalling pathways. Philos Trans R Soc Lond B Biol Sci **361**(1473)**:** 1545-1564.*

*Reichmann H, Bilsing A, Ehret R, Greulich W, Schulz JB, Schwartz A, et al. (2006). Ergoline and non-ergoline derivatives in the treatment of Parkinson's disease. J Neurol **253 Suppl 4:** IV36-38.*

*Remple MS, Bradenham CH, Kao CC, Charles PD, Neimat JS, Konrad PE (2011). Subthalamic nucleus neuronal firing rate increases with Parkinson's disease progression. Mov Disord **26**(9)**:** 1657-1662.*

*Rhodes KE, Fawcett JW (2004). Chondroitin sulphate proteoglycans: preventing plasticity or protecting the CNS? J Anat **204**(1)**:** 33-48.*

*Riachi NJ, LaManna JC, Harik SI (1989). Entry of 1-methyl-4-phenyl-1,2,3,6-tetrahydropyridine into the rat brain. J Pharmacol Exp Ther **249**(3)**:** 744-748.*

*Rich KM (1992). Neuronal death after trophic factor deprivation. J Neurotrauma **9 Suppl 1:** S61-69.*

*Rieck M, Schumacher-Schuh AF, Altmann V, Francisconi CL, Fagundes PT, Monte TL, et al. (2012). DRD2 haplotype is associated with dyskinesia induced by levodopa therapy in Parkinson's disease patients. Pharmacogenomics **13**(15)**:** 1701-1710.*

*Rieck M, Schumacher-Schuh AF, Callegari-Jacques SM, Altmann V, Schneider Medeiros M,*

*Rieder CR, et al. (2015). Is there a role for ADORA2A polymorphisms in levodopa-induced dyskinesia in Parkinson's disease patients? Pharmacogenomics **16**(6): 573-582.*

*Riederer P, Laux G (2011). MAO-inhibitors in Parkinson's Disease. Experimental neurobiology **20**(1): 1-17.*

*Riederer P, Sofic E, Rausch WD, Schmidt B, Reynolds GP, Jellinger K, et al. (1989). Transition metals, ferritin, glutathione, and ascorbic acid in parkinsonian brains. J Neurochem **52**(2): 515-520.*

*Ritchie CW, Bush AI, Mackinnon A, Macfarlane S, Mastwyk M, MacGregor L, et al. (2003). Metal-protein attenuation with iodochlorhydroxyquin (clioquinol) targeting Abeta amyloid deposition and toxicity in Alzheimer disease: a pilot phase 2 clinical trial. Arch Neurol **60**(12): 1685-1691.*

*Rodriguez-Pallares J, Parga JA, Munoz A, Rey P, Guerra MJ, Labandeira-Garcia JL (2007). Mechanism of 6-hydroxydopamine neurotoxicity: the role of NADPH oxidase and microglial activation in 6-hydroxydopamine-induced degeneration of dopaminergic neurons. J Neurochem **103**(1): 145-156.*

*Rogers CJ, Clark PM, Tully SE, Abrol R, Garcia KC, Goddard WA, 3rd, et al. (2011). Elucidating glycosaminoglycan-protein-protein interactions using carbohydrate microarray and computational approaches. Proc Natl Acad Sci U S A **108**(24): 9747-9752.*

*Ruoslahti E (1988). Structure and biology of proteoglycans. Annu Rev Cell Biol **4**: 229-255.*

*Ruscher K, Kuric E, Wieloch T (2012). Levodopa treatment improves functional recovery after experimental stroke. Stroke **43**(2): 507-513.*

*Saint-Pierre M, Tremblay ME, Sik A, Gross RE, Cicchetti F (2006). Temporal effects of paraquat/maneb on microglial activation and dopamine neuronal loss in older rats. J Neurochem **98**(3): 760-772.*

*Salvatore MF, Ai Y, Fischer B, Zhang AM, Grondin RC, Zhang Z, et al. (2006). Point source concentration of GDNF may explain failure of phase II clinical trial. Exp Neurol **202**(2): 497-505.*

*Salvatore MF, Davis RW, Arnold JC, Chotibut T (2012). Transient striatal GLT-1 blockade increases EAAC1 expression, glutamate reuptake, and decreases tyrosine hydroxylase phosphorylation at ser(19). Exp Neurol **234**(2): 428-436.*

*Sanberg PR (1980). Haloperidol-induced catalepsy is mediated by postsynaptic dopamine receptors. Nature **284**(5755): 472-473.*

*Sanchez G, Rodriguez MJ, Pomata P, Rela L, Murer MG (2011). Reduction of an afterhyperpolarization current increases excitability in striatal cholinergic interneurons in rat parkinsonism. J Neurosci **31**(17): 6553-6564.*

*Sathyanarayana Rao TS, Yeragani VK (2009). Hypertensive crisis and cheese. Indian J Psychiatry **51**(1): 65-66.*

*Sawada H, Ibi M, Kihara T, Urushitani M, Nakanishi M, Akaike A, et al. (2000). Neuroprotective mechanism of glial cell line-derived neurotrophic factor in mesencephalic neurons. J Neurochem **74**(3): 1175-1184.*

*Scalzo P, Kummer A, Bretas TL, Cardoso F, Teixeira AL (2010). Serum levels of brain-derived neurotrophic factor correlate with motor impairment in Parkinson's disease. J Neurol **257**(4): 540-545.*

*Schallert T, Fleming SM, Leasure JL, Tillerson JL, Bland ST (2000). CNS plasticity and assessment of forelimb sensorimotor outcome in unilateral rat models of stroke, cortical ablation, parkinsonism and spinal cord injury. Neuropharmacology **39**(5): 777-787.*

*Schneider JS (1990). Chronic exposure to low doses of MPTP. II. Neurochemical and pathological consequences in cognitively-impaired, motor asymptomatic monkeys. Brain Res **534**(1-2): 25-36.*

*Schrag A (2005). Entacapone in the treatment of Parkinson's disease. Lancet Neurol **4**(6): 366-370.*

*Segal RA (2003). Selectivity in neurotrophin signaling: theme and variations. Annual review of neuroscience **26:** 299-330.*

*Shen Y, Tenney AP, Busch SA, Horn KP, Cuascut FX, Liu K, et al. (2009). PTPsigma is a receptor for chondroitin sulfate proteoglycan, an inhibitor of neural regeneration. Science **326**(5952): 592-596.*

*Sica A, Mantovani A (2012). Macrophage plasticity and polarization: in vivo veritas. J Clin Invest **122**(3): 787-795.*

*Singh S, Ahmad R, Mathur D, Sagar RK, Krishana B (2006). Neuroprotective effect of BDNF in young and aged 6-OHDA treated rat model of Parkinson disease. Indian J Exp Biol **44**(9): 699-704.*

*Singleton AB, Farrer M, Johnson J, Singleton A, Hague S, Kachergus J, et al. (2003). alpha-Synuclein locus triplication causes Parkinson's disease. Science **302**(5646): 841.*

*Sivak WN, White JD, Bliley JM, Tien LW, Liao HT, Kaplan DL, et al. (2014). Delivery of chondroitinase ABC and glial cell line-derived neurotrophic factor from silk fibroin conduits enhances peripheral nerve regeneration. J Tissue Eng Regen Med.*

*Sivasankaran R, Pei J, Wang KC, Zhang YP, Shields CB, Xu XM, et al. (2004). PKC mediates inhibitory effects of myelin and chondroitin sulfate proteoglycans on axonal regeneration. Nat Neurosci **7**(3): 261-268.*

*Slevin JT, Gash DM, Smith CD, Gerhardt GA, Kryscio R, Chebrolu H, et al. (2006). Unilateral intraputaminal glial cell line-derived neurotrophic factor in patients with Parkinson disease: response to 1 year each of treatment and withdrawal. Neurosurg Focus **20**(5): E1.*

*Smidt MP (2009). Specific vulnerability of substantia nigra compacta neurons. J Neural Transm Suppl(73): 39-47.*

*Smith Y, Galvan A, Ellender TJ, Doig N, Villalba RM, Huerta-Ocampo I, et al. (2014). The thalamostriatal system in normal and diseased states. Front Syst Neurosci **8:** 5.*

*Snow BJ, Macdonald L, McAuley D, Wallis W (2000). The effect of amantadine on levodopa-induced dyskinesias in Parkinson's disease: a double-blind, placebo-controlled study. Clin Neuropharmacol **23**(2): 82-85.*

*Solis O, Garcia-Montes JR, Gonzalez-Granillo A, Xu M, Moratalla R (2015). Dopamine D3 Receptor Modulates l-DOPA-Induced Dyskinesia by Targeting D1 Receptor-Mediated Striatal Signaling. Cereb Cortex.*

*Soto-Otero R, Mendez-Alvarez E, Hermida-Ameijeiras A, Munoz-Patino AM, Labandeira-Garcia JL (2000). Autoxidation and neurotoxicity of 6-hydroxydopamine in the presence of some antioxidants: potential implication in relation to the pathogenesis of Parkinson's disease. J Neurochem **74**(4): 1605-1612.*

*Spina MB, Squinto SP, Miller J, Lindsay RM, Hyman C (1992). Brain-derived neurotrophic factor protects dopamine neurons against 6-hydroxydopamine and N-methyl-4-phenylpyridinium ion toxicity: involvement of the glutathione system. J Neurochem **59**(1): 99-106.*

*Spira PJ, Sharpe DM, Halliday G, Cavanagh J, Nicholson GA (2001). Clinical and pathological features of a Parkinsonian syndrome in a family with an Ala53Thr alpha-synuclein mutation. Ann Neurol **49**(3): 313-319.*

*Sprenger F, Poewe W (2013). Management of motor and non-motor symptoms in Parkinson's disease. CNS Drugs **27**(4): 259-272.*

*Staal RG, Sonsalla PK (2000). Inhibition of brain vesicular monoamine transporter (VMAT2) enhances 1-methyl-4-phenylpyridinium neurotoxicity in vivo in rat striata. J Pharmacol Exp Ther **293**(2): 336-342.*

*Stenslik MJ, Potts LF, Sonne JW, Cass WA, Turchan-Cholewo J, Pomerleau F, et al. (2015). Methodology and effects of repeated intranasal delivery of DNSP-11 in a rat model of Parkinson's disease. J Neurosci Methods **251**: 120-129.*

*Stokes AH, Hastings TG, Vrana KE (1999). Cytotoxic and genotoxic potential of dopamine. J Neurosci Res **55**(6): 659-665.*

*Sun M, Kong L, Wang X, Lu XG, Gao Q, Geller AI (2005). Comparison of the capability of GDNF, BDNF, or both, to protect nigrostriatal neurons in a rat model of Parkinson's disease. Brain Res **1052**(2): 119-129.*

*Surmeier DJ, Guzman JN, Sanchez-Padilla J (2010). Calcium, cellular aging, and selective neuronal vulnerability in Parkinson's disease. Cell Calcium **47**(2): 175-182.*

*Suttkus A, Rohn S, Jager C, Arendt T, Morawski M (2012). Neuroprotection against iron-induced cell death by perineuronal nets - an in vivo analysis of oxidative stress. Am J Neurodegener Dis **1**(2): 122-129.*

*Suttkus A, Rohn S, Weigel S, Glockner P, Arendt T, Morawski M (2014). Aggrecan, link protein and tenascin-R are essential components of the perineuronal net to protect neurons against iron-induced oxidative stress. Cell Death Dis **5**: e1119.*

*Tai HC, Schuman EM (2008). Ubiquitin, the proteasome and protein degradation in neuronal function and dysfunction. Nat Rev Neurosci **9**(11): 826-838.*

*Takada W, Fukushima M, Pothacharoen P, Kongtawelert P, Sugahara K (2013). A sulfated glycosaminoglycan array for molecular interactions between glycosaminoglycans and growth factors or anti-glycosaminoglycan antibodies. Anal Biochem **435**(2): 123-130.*

*Takeuchi H, Sekiguchi A, Taki Y, Yokoyama S, Yomogida Y, Komuro N, et al. (2010). Training of*

*working memory impacts structural connectivity. J Neurosci **30**(9): 3297-3303.*

*Tanaka H, Kannari K, Maeda T, Tomiyama M, Suda T, Matsunaga M (1999). Role of serotonergic neurons in L-DOPA-derived extracellular dopamine in the striatum of 6-OHDA-lesioned rats. Neuroreport **10**(3): 631-634.*

*Tang Y, Le W (2016). Differential Roles of M1 and M2 Microglia in Neurodegenerative Diseases. Mol Neurobiol **53**(2): 1181-1194.*

*Teema AM, Zaitone SA, Moustafa YM (2016). Ibuprofen or piroxicam protects nigral neurons and delays the development of L-dopa induced dyskinesia in rats with experimental Parkinsonism: influence on angiogenesis. Neuropharmacology.*

*Tester NJ, Plaas AH, Howland DR (2007). Effect of body temperature on chondroitinase ABC's ability to cleave chondroitin sulfate glycosaminoglycans. J Neurosci Res **85**(5): 1110-1118.*

*Thiele SL, Warre R, Nash JE (2012). Development of a unilaterally-lesioned 6-OHDA mouse model of Parkinson's disease. J Vis Exp(60).*

*Thiruchelvam M, McCormack A, Richfield EK, Baggs RB, Tank AW, Di Monte DA, et al. (2003). Age-related irreversible progressive nigrostriatal dopaminergic neurotoxicity in the paraquat and maneb model of the Parkinson's disease phenotype. Eur J Neurosci **18**(3): 589-600.*

*Timar J (1989). Recovery of MAO-B enzyme activity after (-)deprenyl (selegiline) pretreatment, measured in vivo. Acta Physiol Hung **74**(3-4): 259-266.*

*Tom VJ, Sandrow-Feinberg HR, Miller K, Santi L, Connors T, Lemay MA, et al. (2009). Combining peripheral nerve grafts and chondroitinase promotes functional axonal regeneration in the chronically injured spinal cord. J Neurosci **29**(47): 14881-14890.*

*Ugarte SD, Lin E, Klann E, Zigmond MJ, Perez RG (2003). Effects of GDNF on 6-OHDA-induced death in a dopaminergic cell line: modulation by inhibitors of PI3 kinase and MEK. J Neurosci Res **73**(1): 105-112.*

*Uitti RJ, Rajput AH, Ahlskog JE, Offord KP, Schroeder DR, Ho MM, et al. (1996). Amantadine treatment is an independent predictor of improved survival in Parkinson's disease. Neurology **46**(6): 1551-1556.*

*Um JW, Im E, Lee HJ, Min B, Yoo L, Yoo J, et al. (2010). Parkin directly modulates 26S proteasome activity. J Neurosci **30**(35): 11805-11814.*

*Ungerstedt U (1968). 6-Hydroxy-dopamine induced degeneration of central monoamine neurons. Eur J Pharmacol **5**(1): 107-110.*

*Valente EM, Abou-Sleiman PM, Caputo V, Muqit MM, Harvey K, Gispert S, et al. (2004). Hereditary early-onset Parkinson's disease caused by mutations in PINK1. Science **304**(5674): 1158-1160.*

*Van Den Eeden SK, Tanner CM, Bernstein AL, Fross RD, Leimpeter A, Bloch DA, et al. (2003). Incidence of Parkinson's disease: variation by age, gender, and race/ethnicity. Am J Epidemiol **157**(11): 1015-1022.*

*Vekrellis K, Xilouri M, Emmanouilidou E, Rideout HJ, Stefanis L (2011). Pathological roles of alpha-synuclein in neurological disorders. Lancet Neurol **10**(11): 1015-1025.*

*Verhagen Metman L, Del Dotto P, Natte R, van den Munckhof P, Chase TN (1998). Dextromethorphan improves levodopa-induced dyskinesias in Parkinson's disease. Neurology **51**(1): 203-206.*

*Vernon AC, Modo M (2011). Non-invasive MR imaging of neurodegeneration in a rodent model of Parkinson's disease. Methods Mol Biol **711:** 487-510.*

*Vidailhet M, Bonnet AM, Marconi R, Durif F, Agid Y (1999). The phenomenology of L-dopa-induced dyskinesias in Parkinson's disease. Mov Disord **14 Suppl 1:** 13-18.*

*Vidyadhara DJ, Yarreiphang H, Abhilash PL, Raju TR, Alladi PA (2016). Differential expression of calbindin in nigral dopaminergic neurons in two mice strains with differential susceptibility to 1-methyl-4-phenyl-1,2,3,6-tetrahydropyridine. J Chem Neuroanat.*

*Vijverman AC, Fox SH (2014). New treatments for the motor symptoms of Parkinson's disease. Expert review of clinical pharmacology **7**(6): 761-777.*

*Visanji NP, Fox SH, Johnston T, Reyes G, Millan MJ, Brotchie JM (2009). Dopamine D3 receptor stimulation underlies the development of L-DOPA-induced dyskinesia in animal models of Parkinson's disease. Neurobiol Dis **35**(2): 184-192.*

*Vo T, Carulli D, Ehlert EM, Kwok JC, Dick G, Mecollari V, et al. (2013). The chemorepulsive axon guidance protein semaphorin3A is a constituent of perineuronal nets in the adult rodent brain. Mol Cell Neurosci **56:** 186-200.*

*Wallace DC (2005). A mitochondrial paradigm of metabolic and degenerative diseases, aging, and cancer: a dawn for evolutionary medicine. Annual review of genetics **39:** 359-407.*

*Wang D, Fawcett J (2012a). The perineuronal net and the control of CNS plasticity. Cell and tissue research **349**(1): 147-160.*

*Wang D, Ichiyama RM, Zhao R, Andrews MR, Fawcett JW (2011). Chondroitinase combined with rehabilitation promotes recovery of forelimb function in rats with chronic spinal cord injury. J Neurosci **31**(25): 9332-9344.*

*Wang H, Katagiri Y, McCann TE, Unsworth E, Goldsmith P, Yu ZX, et al. (2008). Chondroitin-4-sulfation negatively regulates axonal guidance and growth. Journal of cell science **121**(Pt 18): 3083-3091.*

*Wang L, Muramatsu S, Lu Y, Ikeguchi K, Fujimoto K, Okada T, et al. (2002). Delayed delivery of AAV-GDNF prevents nigral neurodegeneration and promotes functional recovery in a rat model of Parkinson's disease. Gene Ther **9**(6): 381-389.*

*Wang Y, Jia H, Li WY, Tong XJ, Liu GB, Kang SW (2012b). Synergistic effects of bone mesenchymal stem cells and chondroitinase ABC on nerve regeneration after acellular nerve allograft in rats. Cell Mol Neurobiol **32**(3): 361-371.*

*Wang Z, Kai L, Day M, Ronesi J, Yin HH, Ding J, et al. (2006). Dopaminergic control of corticostriatal long-term synaptic depression in medium spiny neurons is mediated by cholinergic interneurons. Neuron **50**(3): 443-452.*

*Weinreb O, Mandel S, Bar-Am O, Yogev-Falach M, Avramovich-Tirosh Y, Amit T, et al. (2009). Multifunctional neuroprotective derivatives of rasagiline as anti-Alzheimer's disease drugs.*

*Neurotherapeutics **6**(1): 163-174.*

*Weintraub D, Koester J, Potenza MN, Siderowf AD, Stacy M, Voon V, et al. (2010). Impulse control disorders in Parkinson disease: a cross-sectional study of 3090 patients. Arch Neurol **67**(5): 589-595.*

*Werner-Allen JW, DuMond JF, Levine RL, Bax A (2016). Toxic Dopamine Metabolite DOPAL Forms an Unexpected Dicatechol Pyrrole Adduct with Lysines of alpha-Synuclein. Angew Chem Int Ed Engl.*

*Westin JE, Lindgren HS, Gardi J, Nyengaard JR, Brundin P, Mohapel P, et al. (2006). Endothelial proliferation and increased blood-brain barrier permeability in the basal ganglia in a rat model of 3,4-dihydroxyphenyl-L-alanine-induced dyskinesia. J Neurosci **26**(37): 9448-9461.*

*Winkler C, Kirik D, Bjorklund A, Cenci MA (2002). L-DOPA-induced dyskinesia in the intrastriatal 6-hydroxydopamine model of parkinson's disease: relation to motor and cellular parameters of nigrostriatal function. Neurobiol Dis **10**(2): 165-186.*

*Winkler C, Sauer H, Lee CS, Bjorklund A (1996). Short-term GDNF treatment provides long-term rescue of lesioned nigral dopaminergic neurons in a rat model of Parkinson's disease. J Neurosci **16**(22): 7206-7215.*

*Wirdefeldt K, Adami HO, Cole P, Trichopoulos D, Mandel J (2011). Epidemiology and etiology of Parkinson's disease: a review of the evidence. Eur J Epidemiol **26 Suppl 1:** S1-58.*

*Wirdefeldt K, Odin P, Nyholm D (2016). Levodopa-Carbidopa Intestinal Gel in Patients with Parkinson's Disease: A Systematic Review. CNS Drugs.*

*Wolf OT, Dyakin V, Vadasz C, de Leon MJ, McEwen BS, Bulloch K (2002). Volumetric measurement of the hippocampus, the anterior cingulate cortex, and the retrosplenial granular cortex of the rat using structural MRI. Brain Res Brain Res Protoc **10**(1): 41-46.*

*Xie W, Li X, Li C, Zhu W, Jankovic J, Le W (2010). Proteasome inhibition modeling nigral neuron degeneration in Parkinson's disease. J Neurochem **115**(1): 188-199.*

*Xu M, Koeltzow TE, Santiago GT, Moratalla R, Cooper DC, Hu XT, et al. (1997). Dopamine D3 receptor mutant mice exhibit increased behavioral sensitivity to concurrent stimulation of D1 and D2 receptors. Neuron **19**(4): 837-848.*

*Yamada H, Fredette B, Shitara K, Hagihara K, Miura R, Ranscht B, et al. (1997a). The brain chondroitin sulfate proteoglycan brevican associates with astrocytes ensheathing cerebellar glomeruli and inhibits neurite outgrowth from granule neurons. J Neurosci **17**(20): 7784-7795.*

*Yamada M, Ohnishi H, Sano S, Nakatani A, Ikeuchi T, Hatanaka H (1997b). Insulin receptor substrate (IRS)-1 and IRS-2 are tyrosine-phosphorylated and associated with phosphatidylinositol 3-kinase in response to brain-derived neurotrophic factor in cultured cerebral cortical neurons. J Biol Chem **272**(48): 30334-30339.*

*Yushkevich PA, Piven J, Hazlett HC, Smith RG, Ho S, Gee JC, et al. (2006). User-guided 3D active contour segmentation of anatomical structures: significantly improved efficiency and reliability. Neuroimage **31**(3): 1116-1128.*

*Zappia M, Annesi G, Nicoletti G, Arabia G, Annesi F, Messina D, et al. (2005). Sex differences in clinical and genetic determinants of levodopa peak-dose dyskinesias in Parkinson disease: an*

*exploratory study. Arch Neurol **62**(4):* 601-605.

*Zarranz JJ, Alegre J, Gomez-Esteban JC, Lezcano E, Ros R, Ampuero I, et al. (2004). The new mutation, E46K, of alpha-synuclein causes Parkinson and Lewy body dementia. Ann Neurol **55**(2):* 164-173.

*Zatorre RJ, Fields RD, Johansen-Berg H (2012). Plasticity in gray and white: neuroimaging changes in brain structure during learning. Nat Neurosci **15**(4):* 528-536.

*Zawada WM, Banninger GP, Thornton J, Marriott B, Cantu D, Rachubinski AL, et al. (2011). Generation of reactive oxygen species in 1-methyl-4-phenylpyridinium (MPP+) treated dopaminergic neurons occurs as an NADPH oxidase-dependent two-wave cascade. Journal of neuroinflammation **8:*** 129.

*Zhang J, Perry G, Smith MA, Robertson D, Olson SJ, Graham DG, et al. (1999). Parkinson's disease is associated with oxidative damage to cytoplasmic DNA and RNA in substantia nigra neurons. Am J Pathol **154**(5):* 1423-1429.

*Zhang Y, Gu Z, Qiu G, Song Y (2013). Combination of chondroitinase ABC, glial cell line-derived neurotrophic factor and Nogo A antibody delayed-release microspheres promotes the functional recovery of spinal cord injury. J Craniofac Surg **24**(6):* 2153-2157.

*Zhao Q, Cai D, Bai Y (2013). Selegiline rescues gait deficits and the loss of dopaminergic neurons in a subacute MPTP mouse model of Parkinson's disease. International journal of molecular medicine **32**(4):* 883-891.